INVESTIGATION OF TURBULENT CHARACTERISTICS WITHIN SURFACE LAYER DURING THUNDERSTORM

Ph. D. Thesis

BY

TASHMITA BOSE SINHA

(University Registration NO. - 46/16/Maths./24

JADAVPUR UNIVERSITY KOLKATA

THESIS SUBMITTED FOR THE DEGREE OF

DOCTOR OF PHILOSOPHY OF (SCIENCE) OF JADAVPUR UNIVERSITY

2024

Under the Guidance of :

Prof. Goutam Kumar Sen

DEPARTMENT OF MATHEMATICS

JADAVPUR UNIVERSITY

KOLKATA - 700032

WEST BENGAL, INDIA

JADA VPUR UNIVERSITY

KOLKATA - 700032, INDIA

SCHOOL OF OCEANOGRAPHIC STUDIES

CERTIFICATE FROM THE SUPERVISOR

This is to certify that the thesis entitled as **"Investigation of turbulent characteristics within surface layer during thunderstorm"** submitted by Smt. **Tashmita Bose Sinha** who got his name registered on **19th April, 2016 (Index No.: 46/16/Maths./24)for** the award of Ph.D. (Science) degree of Jadavpur University, is absolutely based upon his own work under the supervision of **Prof. Goutam Kumar Sen** and that neither this thesis nor any part of it has been submitted for either any degree/ diploma or any other academic award anywhere before.

Goutam Kumar Sen

(Signature of the Supervisor(S))
SCHOOL OF OCEANOGRAPHIC STUDIES

Retired Professor
School of Oceanographic Studies
Jadavpur University
Kolkata-700032, India

ACKNOWLEDGEMENT

I express my heartfelt gratitude to my Supervisor ***Prof. Goutam Kumar Sen****, Ex Jt. Director, School of Oceanographic Studies, Jadavpur University who was also the Ex Coordinator of the School of Environmental Studies without whose eagerness and untiring help it would not have been possible to enroll in the Ph. D. Course and to complete this thesis.*

I would like to express my gratitude to ***Dr. Parthasarathi Mukhopadhyay****, FASc Scientist- F, Indian Institute of Tropical Meteorolgy, Dr. Homi Bhabha Road, Pashan Pune 411008, Maharashtra, India who was also the Associate Editor, Journal of Earth System Sciences, Indian Academy of Sciences. He took a lot of keen interest in completing my dissertation.*

I would also like to present my sincere thanks to Co-guide ***Late Dr. Meenakshi Chatterjee****, Ex Reader and Head of the Department of Mathematics, Basanti Devi College, 147/B Rash Behari Avenue, Kolkata 700029 whose encouragement, support and kind attention have enabled me to prepare this Thesis.*

I would also like to present my sincere thanks to the Chief Editor ***Dr. Om Prakash Pandey*** *for his comments and suggestions that have helped to improve the quality of the Thesis.*

I would also like to present my sincere thanks to ***Dean of Science Dr. Asish Kumar Sarkar, Ex Dean of Science Dr. Subenoy Chakraborty, HOD of the Maths Department, Super Manoranjan Adhikari and Staff Members*** *associated with the Ph.D. Science section for their encouragement, support and kind attention have enabled me to prepare this Thesis.*

I express my heartfelt gratitude to the ***Mathematics Department****, Jadavpur University, Kolkata, West Bengal for supporting me in my Ph. D. registration and coursework. I would like to present my sincere thanks to express my gratitude to the* ***Indian Institute of Tropical Meteorology****, Pune, India for encouragement, support and kind attention to prepare this paper by giving me bulletin of thunderstorm days and providing the link of data source.*

I offer my sincere and special thanks to Dr. Saranya Chakraborti, Sarojini Naidu College For Women, Siddhartha Chatterjee, Principal, Gosaba Green College, Rituparna Sarkar, Indian Institute of Tropical Meteorology and Dr. Tanaya for their precious co-operation and assistance in conducting the observations required for this study.

My heartiest thanks go to my husband, Suvajit Sinha and my daughter, Swarnali Sinha for their constant encouragement and forbearance. My sister, Parna Bose always tried to help me in carrying out this research work. My daughter helped me in computer operating.

Dedicated to my late parents for their blessings,

which have enabled me to complete the thesis

Abstract

In the present work, we use thermodynamic indices to analyze thunderstorm episodes over the Kolkata region by using sounding data for the pre-monsoon period of April to May, 2022. We examine how well indices distinguish between days with and without thunder. The predicted values of these indices show how thunderstorm activity varies in kind.

Different types of indices used are, the Surface Lifted Index (SLI), K Index (KI), Convective Available Potential Energy (CAPE), Convective Inhibition (CIN), Severe Weather Threat Index (SWEAT), Total Totals Index (TTI), Bulk Richardson Number (BRN), Deep Convection Index (DCI), Humidity Index (HI), Boyden Index (BI), Showalter Index (SI), Dew point temperature at 500 hpa, 700 hpa and 850 hpa (DEW) and height, 700 hpa and 1000 hpa (H). Probability distribution curves are represented to identify the ability of the indices to differentiate between thunder and without thunder days. We have estimated the mean, standard deviations, and Z scores. Z scores of 75% or more are considered significant for further analysis, and the rest are rejected. It is not possible to forecast the occurrence of thunderstorm activity depending on only one index. This study suggests that the indexes with excellent skills for thunder forecasting are, BI, SLI and DCI, while the forecasting ability is deficient for other observed values. Observed values of these indices also reveal that different types of thunder were possible over Kolkata during the studied pre-monsoon months of April and May, 2022. The study's conclusion offers important new information about enhancing index forecasting abilities for more accurate prediction.

The current study focuses on the local thunderstorms in Kolkata. 9 thunderstorm days are considered in this study. The mixing ratio ranges at 00 and 12 UTC varies between 16.23g/kg to 23.67g/kg at 1000 hPa. This indicates a significant presence of moisture near the surface. In the occurrence of local severe storms in Kolkata, the relative humidity at 00 and 12 UTC ranges from 52% to 100%, indicating a substantial amount of moisture near the surface. The mean mixed layer mixing ratio in Kolkata the occurrence of thunderstorms varies from 13 g/kg to 22.17 g/kg, showing a significant amount of moisture in the mixed layer of the troposphere. The amount of Precipitable water in Kolkata during local storms at 00 and 12 UTC varies from 36.70 mm to 56.58 mm. It is worth noting that the Precipitable water in Kolkata was significantly higher during local storms at 00 UTC compared to days when no storms occurred. DRCT varies from 45 deg to 290 deg and SKNT varies from 1 to 8 knot at 00 and 12 UTC.

The present study is an attempt to investigate the variations of potential temperature, equivalent potential temperature and virtual potential temperature, both vertically over Kolkata on the dates of occurrence of 5 local severe storms. It has been found that the Potential temperature over Kolkata increases with height, becoming maximum at the top of the troposphere. The gradient of potential temperature between 1000 hPa and 500 hPa over Kolkata is relatively higher on the dates of occurrence in most cases ranging from 21.1 K to 29.2 K. The difference in potential temperature i.e. gradient of equivalent temperature

between 1000 hPa and 500 hPa over Kolkata ranges from -17.3 K to -39.6 K. The difference in virtual potential temperature between 1000 hPa and 500 hPa over Kolkata on the dates of occurrence of local storms is more than 17.8 K ranging from 17.8 K to 26.4 K.

The present study is an attempt to investigate observation studies with the help of Skew-t-Log P diagram and imaginaries study of NCMRWF Model and also observed high value of Reynolds number during thunderstorm days which indicate turbulent characteristics exist during thunderstorm days.

The future scope of thunderstorm studies in Kolkata should consider the development of more accurate and reliable forecasting models, the role of environmental factors and the implications of climate change on thunderstorm dynamics. Continued validation of predictive models with real-time data and the exploration of new methodologies will be crucial for enhancing the predictability and understanding of thunderstorms in this region.

CONTENTS

Chapter - 1

INTRODUCTION OF NOR'WESTER

General

Nor'wester is a subject of universal interest for several reasons. It gives relief after mid-day heat and the weather becomes comfortable. Its nature is unique and the causes are really interesting. During the hot weather period like from March to May the eastern and North-eastern states of the Indian subcontinent like West Bengal, Bihar, Assam, Orissa (parts), and Bangladesh experience dramatic appearance of a special type of violent thunderstorms known as Nor'wester.

In Bengal, it is known as 'KalBaisakhi' or Nor'westers of the month of Baisakh (April,15 - May,15). Apart from its calamitous effects like an unexpected rise in wind speed, lightning, thunder, and hail the rainfall associated with the storm although small in amount, is extremely helpful for the pre-Kharif crops like jute, Aush paddy, summer till, and a large number of vegetables and fruits and the sudden drop in temperature gives relief after unbearable mid-day heat. Kolkata region is shown in **Figure 1.1** and Nor'wester is shown in **Figure 1.2**.

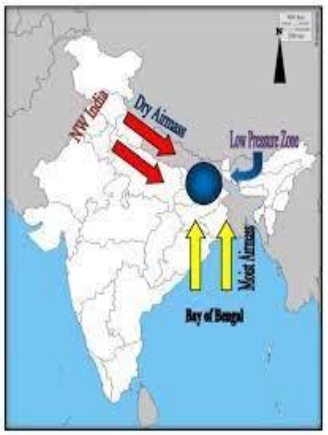

Figure 1.1 Kolkata **Figure 1.2** Nor'wester

These storms are more persistent in the late afternoon, although they are known to occur also at other times of the day. A nor'wester is always related to a thunderstorm, and the precursory signs of its approach are the same as those that signal the coming of an aggressive thunderstorm. Air that becomes buoyant gets up and is cooled down by adiabatic expansion until it eventually arrives at saturation point and causes a cumulus cloud. If the atmosphere is unstable further, the cumulus cloud increases in size vertically to form a cumulonimbus cloud and afterward a thunderstorm, commonly known as Nor'wester.Kolkata cloud chasers is shown in **Figure 1.3** and Storms with Kolkata cloud chasers is shown in **Figure 1.4**

Figure 1.3 Kolkata cloud chasers

Figure 1.4 Storms with Kolkata cloud chasers

Nor'westers or the Kalbaishakhi is a local precipitation and rainstorm that occurs in India and Bangladesh. The direction of blows is mainly from the northwest and they are called Nor'westers (Storm – an unexpected, aggressive gusty wind).

Kalbaishakhi

The hot weather condition in India is distinguished by the presence of localized thunderstorms. They cause severe rain, strong wind, and hailstorms. These thunderstorms are known by different names in different locations. In West Bengal, they are well known as Kalbaishakhi.

Chhota Nagpur Plateau

Kalbaishakhi or Nor'westers begin in the Chhota Nagpur Plateau. Strong thunderstorms in the Gangetic plains of India are nearby known as KalBaisakhi or Nor'westers. These localized occurrences are generally related to thunderstorms that occur with violent squally winds and heavy rainfall.

Formation of Thunderstorm

Thunderstorms that form at night happen in the absence of heating on the ground by the sun. Consequently, the storms that form at night are usually "uplifted," meaning that they form aloft above the cooler air near the ground, rather than near the ground, which only during the day can get warmer. Thunderstorm formation occurs when hot, moist air gets up into cold air. The hot air becomes cooler, which originates moisture, called water vapor, to form small water droplets — the procedure called condensation. The cooled air drops lower in the atmosphere, warms, and gets up again. The developing, grown-up, and dissipating stages of a thunderstorm. Most thunderstorms form in three stages: the developing stage, when storm clouds grown-up form; the fully grown-up stage, when the storm is fully formed; and the dissipating stage, when the storm weakens and breaks apart. The 4 Types of Thunderstorms - The single-cell, The multi-cell, The squalene, The supercell. Lighter, positively charged particles appear at the top of the cloud. Large, negatively charged particles fall to the lowest point of the cloud. When the positive and negative charges increase in size large enough, a giant spark - lightning - occurs between the two charges within the cloud. Thunderstorms are local-scale convective storms each time produced by a cumulonimbus cloud and always occur with lightning and thunder (AMS, 2015). These weather systems usually generate strong wind gusts, heavy rain, and sometimes hail. Severe nor'westers are sometimes associated with Mamatocumulus cloud in **Figure 1.6** especially near the anvils of the Cumulonimbus cloud.

Figure 1.6 Mamatocumulus cloud

Classification of local severe storms

In the study, thunderstorms are the local severe storms, which have been classified as follows:

Local severe storms	Maximum gusty wind (km/hr)
(a) Thunderstorms with gusty winds	31- 40
(b) Thunderstorms with squally winds/light Nor'westers	41- 60
(c) Moderate Nor'westers	61- 90
(d) Severe Nor'westers	91- 120
(e) Very Severe Nor'westers	121- 150
(f) Tornado	≥ 151

Life cycle of thunderstorms

The life cycle of a thunderstorm has three stages: (a) Cumulus stage, (b) Mature stage and (c) Dissipating stage. The three stages of the life cycle of a thunderstorm are shown in **Figure 1.5**.

(i) Developing stage

The first stage of a thunderstorm is the cumulus stage, or developing stage. In this stage, masses of moisture are lifted upwards into the atmosphere. The trigger for this lift can be Insolation heating the ground producing thermals, areas where two winds converge forcing air upwards, or where winds blow over terrain of increasing elevation. The moisture rapidly cools into liquid drops of water due to the cooler temperatures at high altitude, which appears

as cumulus clouds. As the water vapor condenses into liquid, latent heat is released which warms the air, causing it to become less dense than the surrounding dry air. The air tends to rise in an updraft through the process of convection (hence the term convective precipitation). This creates a low-pressure zone beneath the forming thunderstorm. In a typical thunderstorm, approximately 5×108 kg of water vapor are lifted into the Earth's atmosphere.

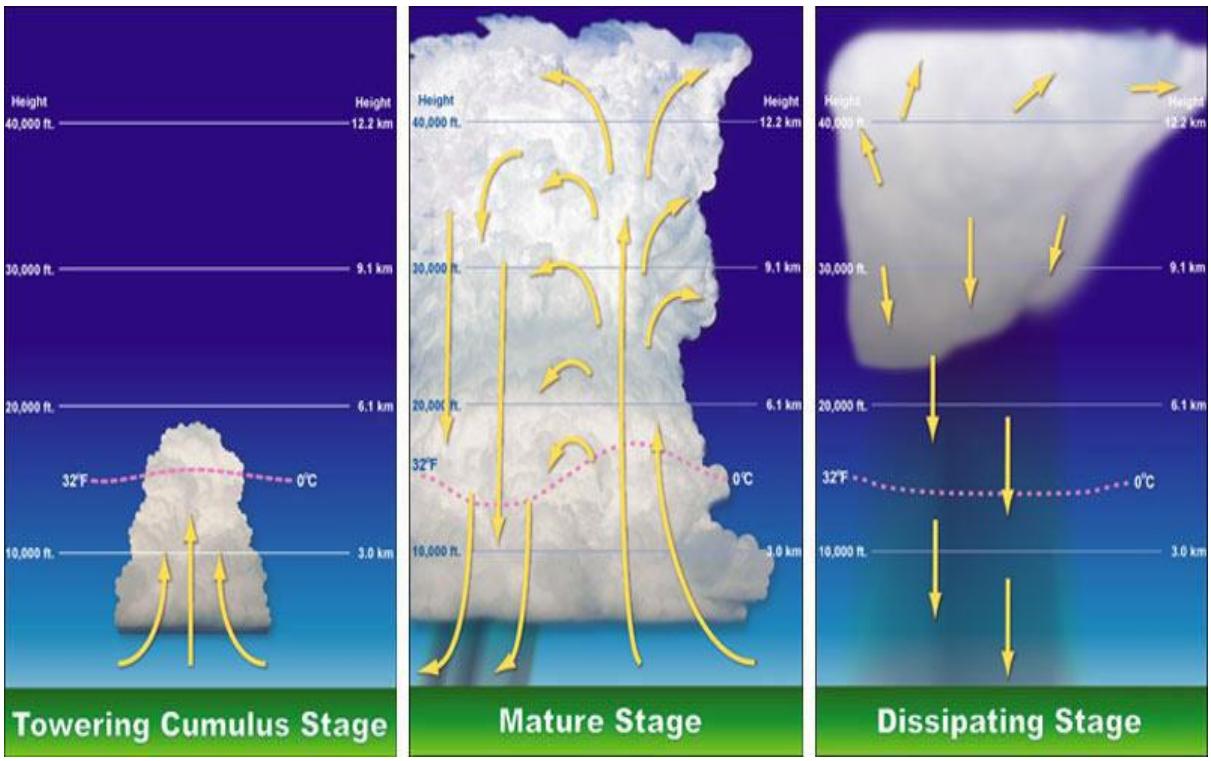

Figure 1.5 Three stages of the life cycle of a thunderstorm

(ii) Mature stage

In the mature stage of a thunderstorm, the warmed air continues to rise until it reaches existing air which is warmer, and the air can rise no further. Often this 'cap' is the tropopause. The air is instead forced to spread out, giving the storm a characteristic anvil shape. The resulting cloud is called cumulonimbus incus. The water droplets coalasce into larger and heavier droplets and freeze to become ice particles. As these fall they melt to become rain. If the updraft is strong enough, the droplets are held aloft long enough to be so large that they do not melt completely and fall as hail. While updrafts are still present, the falling rain creates downdrafts as well. The simultaneous presence of both an updraft and downdrafts marks the mature stage of the storm, and produces Cumulonimbus clouds. During this stage, considerable internal turbulence can occur in the storm system, which sometimes manifests as strong winds, severe lightning, and even tornadoes. Typically, if there is little wind shear, the storm will rapidly enter the dissipating stage and 'rain itself out', but if there is sufficient change in wind speed and/or direction the downdraft will be separated from the updraft, and the storm may become a supercell, and the mature stage can sustain itself for several hours.

(iii) Dissipating stage

In the dissipation stage, the thunderstorm is dominated by the downdraft. If atmospheric conditions do not support super cellular development, this stage occurs rather quickly, approximately 20–30 minutes into the life of the thunderstorm. The downdraft will push down out of the thunderstorm, hit the ground and spread out. This phenomenon is known as a downburst. The cool air carried to the ground by the downdraft cuts off the inflow of the thunderstorm, the updraft disappears and the thunderstorm will dissipate. Thunderstorms in an atmosphere with virtually no vertical wind shear weaken as soon as they send out an outflow boundary in all directions, which then quickly cuts off its inflow of relatively warm, moist air and kills the thunderstorm. The downdraft hitting the ground creates an outflow boundary, which can cause downbursts, a potential hazardous condition for aircraft flying through it as a substantial change in wind speed and direction occurs, resulting in decrease of lift of the aircraft. The stronger the outflow boundary is, the stronger the resultant vertical wind shear will become.

Effect of Thunderstorm

Lightning can heat the air it transects to 50,000 degrees Fahrenheit (5 times hotter than the surface of the sun). When lightning acts on a tree, the heat vaporizes any water in its path possibly causing the tree to detonate or a strip of bark to be blown off. Lightning is much warmer than lava. Lightning is 70,000 degrees Fahrenheit, different from Lava at 2,240 degrees. Near the source, the sound pressure level of thunder is usually 165 to 180 dB but can transcend 200 dB in some cases. Griggs says if a person is attacked by lightning, it can cause cardiac arrest, which stops a person's body from circulating blood and causes direct injury to the brain and nervous system, preventing the brain from being able to send the proper signals to tell the body to carry on with breathing. Most people survive a lightning attack but can face serious health issues. Tall objects, or objects that are good for conducting electricity will strike lightning. Stay away from them. Inside your home, stay away from anything attached to wires or piping (TVs, lights, appliances, faucets, etc.).

Like trees, houses, and people, anything outside is at risk of being attacked by lightning when thunderstorms are in the area, including cars. The good news though is that the outer metal shell of hard-topped metal vehicles does keep those inside a vehicle with the windows closed. Effect of Nor'westers is shown in **Figure 1.6** and Tree fall down after Nor'westers is shown in **Figure 1.7.**

Figure 1.6 Effect of Nor'westers

Figure 1.7 Tree fall down after Nor'westers

Lightning can enter through windows, so keep a safe distance from them during thunderstorms! The second way lightning can go into a building is through pipes or wires. If the lightning affects utility infrastructure, it can travel through those pipes or wires and cross the threshold of your home that way. Because electrical charges can linger in clouds after a thunderstorm has passed, experts agree that people should wait at least 30 minutes after the last thunderstorm before starting outdoor activities. Storms can be associated with all sorts of potential dangers, like flooded streets or homes, fallen trees, fires, and roofs being blown off houses. Lightning can also be intimidating to people. No one knows how many people are causing the death of every year by lightning, but it would be up to tens of thousands worldwide. It is frequently held that the maximum temperature at which humans can remain alive is 108.14 degrees Fahrenheit or 42.3 degrees Celsius. A higher temperature may attenuate proteins and cause critical damage to the brain. During a thunderstorm, keep away from open vehicles such as convertibles, motorcycles, and golf carts. Be sure to stay away from open structures such as porches, gazebos, baseball dugouts, and sports arenas. Avoid open spaces such as golf courses, parks, playgrounds, ponds, lakes, swimming pools, and beaches.

Research Review of Nor'westers

Thunderstorms are one of the natural threats that deliver huge damage to life and property and cause serious socio-economic impacts in the affected regions. Early forecasting of thunderstorms is essential to safeguard and prevent the damages resulting from these violent thunderstorms. During before rainstorm season, the eastern and north-eastern (NE) parts of India, that is Assam, Orissa, Gangetic West Bengal, Jharkhand, Bihar, and other parts of NE states, are affected by the higher frequency of severe thunderstorms locally named Kalbaishakhi or Nor'westers. These thunderstorms are predominantly from a northwest (NW) direction and are hence called Nor'westers **(**Desai 1950; Kessler 1982). These Nor'westers are not local heat storms. The southerly low-level warm and moist airflow from the Bay of Bengal and a cool, dry, westerly, or NW upper-level flow existing over the region gives rise to a favorable synoptic setting for the formation of Nor'westers. These have mesoscale structures with a very rapid development often associated with moderate/severe squalls achieving a speed in the range of 130–150 km/h, which may even reach tornadic severity causing significant damage to property and loss of life **(**Ghosh et al**.** 2008**).** Very few studies are described leading to the forecasting of these thunderstorms due to the scarcity of meso-network of observational platforms over the

region. To fill this gap and to understand the genesis, development, and upgrade of forecast skills of these thunderstorms, the Department of Science and Technology and the Ministry of Earth Sciences, Government of India, launched a multi-institutional program named ‘‘Severe Thunderstorms—Observations and Regional Modelling (STORM)’’ over Gangetic West Bengal and NE parts of India (STORM Science Plan 2005). Meteorologists use stability indices and skill scores to quickly asses the occurrence of thunderstorms. Stability indices are a measure of atmospheric static stability **(**Peppier 1988**).** Ravi et al. (1999) presented two objective methods based on stability indices to forecast the phenomenon of thunderstorms in Delhi. Mukhopadhyay et al. (2003) worked on the objective forecast of thundery/non-thundery days using conventional indices over three NE Indian stations. Haklander and Delden (2003) reported the thunderstorm predictors and their forecast skills for the Netherlands. Kunz (2007) investigated the skill of convective parameters and indices to predict isolated and severe thunderstorms over southwest (SW) Germany. Dhawan et al. (2008) have suggested statistical techniques for forecasting pre-monsoon thunderstorms for NW India. Litta and Mohanty (2008) have used the few thermodynamic indices values given in the literature to identify the occurrence of thunderstorm activity in their modeling study of a thunderstorm event. Sanchez et al. (2008) studied the pre-convective conditions leading to thunderstorm activity over SW Argentina and developed a short-term forecast model. In many regions, the efficiency of the various indices has been studied but such kinds of efforts are missing in Kolkata. Stability indices have been a keystone in the forecasting of convection for many decades and are often applied in the research literature as well. Studies on the efficiency of different stability indices for thunderstorm prediction have been made by several authors 17 – 19. Advection of hot air in the lower levels and cold air in the upper levels (generally related to deep troughs in the upper tropospheric westerlies) will increase the conditional instability in the atmosphere and favor the outbreak of severe thunderstorms 20–22. Srinivasan et al. (1973) have given a detailed account of severe thunderstorms in India and described several case studies. An attempt has been made to simulate the thunderstorm event that occurred on 20 May 2006 at Kolkata (22.52°N, 88.37°E) during the field experiment of Severe Thunderstorm Observation and Regional Modelling (STORM) program 2006, using Non-hydrostatic Mesoscale Model (NMM) core of the Weather Research and Forecasting (WRF) system with different initial conditions and validate the model results with STORM field experiment data. This model was expanded by the National Oceanic and Atmospheric Administration (NOAA)/National Centers for Environment Prediction (NCEP). In the past, short-term forecasts of convective activities are usually done using reflectivity echoes of impending storms using space-borne and weather radars (Browning, 1982; Cluckie and Collier, 1991; Mecklenburg et al., 2000; Wang et al., 2009). However, there has not been much success in this regard because the less period and localized nature of these activities make it difficult to predict them much in advance. Hermida et al. (2013) have studied the spatial variation and related climatological implications of hail storms which are accompanied by convective precipitation using a widely distributed network of 443 hailpads (ANELFA) covering various regions of France. Knowledge-based systems including radar, satellite, boundary layer profiler; lightning detectors, and upper air soundings are also being used for nowcasting intense convective activities. According to Kobler and Tafferner (2009), three parameters are important to recognize the occurrence of convection, namely, moisture, convective instability, and lifting mechanism. Atmospheric humidity profiles and temperature

and instability indices obtained from atmospheric soundings like radiosondes can be very useful in nowcasting rain and thunderstorms (McCann, 1994; Geerts, 2001; Manzato, 2003; Midya et al., 2011; Midya and Saha, 2011; Saha et al., 2012; Chakraborty et al., 2015). However, radiosonde measurements suffer from poor temporal resolution. A microwave radiometer can generate humidity and temperature profiles of the atmosphere up to 10 km with a high temporal resolution of 5 min and hence solve the problem faced by radiosondes. According to Chan and Lee (2011), alerting of wind shear can be concluded either by monitoring the stability of the boundary layer or by the standard deviations in the brightness temperature (BT) established from the microwave radiometer during both clear and cloudy skies at rear elevation. The atmospheric water vapor and brightness temperatures around the water vapor absorption line regulated by a radiometer are used for such purposes (Won et al., 2009). The use of BT of oxygen absorption lines along with water vapor can also predict rain with high accuracies (Chakraborty et al., 2014). In the case of radiometric weather forecasting, two types of parameters are widely used — (1) utilization of level 0 products such as brightness temperatures and (2) parameters obtained from BT computations like Integrated Water Vapor (IWV), Liquid Water Content (LWC), Cloud Base Height (CBH) and instability indices (Koffi et al. 2007; Won et al.,2009). These types of measurements are announced from different temperate regions; however, limited performance estimation of such techniques is available for tropical regions (Wilson et al., 1998). Won et al. (2009) acquired that an increase in Brightness Temperature (BT) is observed in water vapor channels (22–30 GHz) at about two hours (2 h) before rain. Güldner and Spänkuch (1999) have also acquired similar observations for an increase in the LWC and Precipitable Water Vapor (PWV) at about two hours (2 h) before the rain. According to Chan (2009), the average values of the K-index acquired from temperature and humidity profiles have a reasonable correlation with the tropospheric instability indicated by the radiometer located about 10-40 km by the number of lightning flashes within regions. Clifford et al. (2009) and Won et al. (2009) have studied the atmospheric conditions at the boundary layer using radar, lidar, wind profiler, and Radiometer. Many efforts have been made to forecast convective activities using instability indices from atmospheric profilers (Faubush et al., 1951; Showalter, 1953; Galway, 1956; Darkow, 1968; Chowdhury and Karmakar, 1986; Madhulatha et al., 2013; Saha et al., 2014, 2015). In the last few years, many efforts have been made to forecast precipitation-related activities. Dotzek and Forster (2011) employed the Cb-TRAM prediction algorithm with the ESWD dataset for six severe weather days in Europe from 2007 to 2008 to detect storms in advance. The maximum prediction efficiency obtained for a 30–60 min forecast was around 58%. Kohn et al. (2011) employed the WDSS-II algorithm to nowcast thunderstorms using one-year lightning data over the Mediterranean region. The technique was successful in forecasting thousands of thunderstorms about 30 min in advance with a minimal False Alarm Rate (FAR) of 0.03 but with a very low Probability of Detection (POD) of 0.46. Dvorak et al. (2012) devised a technique to detect precipitation and cloudiness using brightness temperature observations at 10 GHz from a microwave radiometer with a prediction efficiency of 80% and a false alarm rate of around 15%. Later, Merino et al. (2014) established a technique to identify hailstorms using MSG data acquired from the MEV valley in Spain from 2006 to 2010. The established technique called HDT employs two detection algorithms, namely convective mask and hail mask algorithms to find hailstorms. This technique has established an accuracy of 76.9% with a false alarm rate of 16.7%. As an extension of the previous work, Gascón et al. (2015) have designed

another technique using forward stepwise regression algorithms on five major instability parameters. This system has a high POD of 0.94 but the FAR calculated was 0.22 which is quite high. However, it may be noted that most of the above-said techniques have provided prediction efficiency of less than 80% or a false alarm rate greater than 20%. Recently, Chakraborty et al. (2014) attempted to predict convective heavy rain using the fluctuations in BT of 22 and 58 GHz. A high prediction efficiency of 90% was obtained; however, the obtained lead time was low. This work is an improvement to the previous attempt where instability indices have been used along with the previously used BT at 22 GHz to predict convective rain in terms of increasing convective strength marked by high values of Convective Available Potential Energy (CAPE). The present technique also provides a better understanding of the changing atmospheric conditions before convective events. The reason for this is that convective activities are generally associated with unstable lapse rates and high moisture contents at three important pressure levels of the lower atmosphere, namely, 850 mbar, 700 mbar, and 500 mbar pressures. BT at 58 GHz could manifest a decrease in ambient temperatures, but only in lower heights (generally b 2 km). Quadratic regression techniques are used to modify brightness temperature values into several atmospheric parameters like profiles of temperature and humidity, IWV, and a series of instability indices, namely Lifted Index (LI), K-Index (KI), Totals Total Index (TTI), and Showalter Index (SI). The brightness temperature and instability index observations from the Radiometer for 18 convective events during 12 convective days and 58 non-convective days of March–May, 2011 have been used. For validation of the forecast technique, radiometric data of 40 convective events during 28 days of March–May 2012 and 2013 has been used. A set of four parameters has been utilized to develop an algorithm to nowcast convective activities. They are LI, KI, BT standard deviation, and HI. The brightness temperature at 22 GHz indicates the amount of vapor in the atmosphere. Strong convective activities usually require a bulk concentration of atmospheric water vapor. These changes in the large values of BT at 22 GHz. However, BT values show strong seasonal and diurnal variation; hence a change in this parameter related to atmospheric vapor density before the event can be indicated convection can be recommended by an increase in its standard deviation value. For this reason, a 30-minute standard deviation of BT at 22 GHz has been included in the analysis instead of its absolute value. The Lifting Index (LI) indicates the stability of air parcels. When an air parcel is lifted adiabatically to a height of 500 bar pressure then the parcel temperature and the environmental temperatures at that height are compared. The negative or near negative value of LI reflects the condensation of saturated vapor parcel to liquid indicating instability and severe weather conditions. The K-Index measures the thunderstorm potential in terms of the vertical temperature lapse rate between 850 and 500 mbar pressure levels, the moisture content at 850 mbar pressure, and the depth of the moist layer at 700 mbar pressure level (George, 1960). KI values close to 30 K denote severe weather conditions (Haklander and van Delden, 2003). The Humidity index shows the difference between the dew point and environment temperature at various pressure levels of the atmosphere. These temperature differences at each level denote the degree of saturation of vapor and the extent of condensation at those layers. Lower values (HI b 30 K) indicate instability at all three pressure levels of the lower atmosphere (850, 700, and 500 mbar pressure levels) thereby indicating severe weather conditions (Litynska et al., 1976). In this study, various instability indices have been used to predict convective activities. However, the strength of these activities can best be quantified by their convective available

potential energy (CAPE). According to Emmanuel (1994), CAPE indicates the buoyant energy available to accelerate an air parcel vertically. It can be calculated using the summation of positive buoyant energy from the level of free convection (height where the parcel temperature N environment temperature) to the Equilibrium Level (height where parcel temperature = environment temperature). Higher CAPE provides more energy for convective growth; hence CAPE should be high in convective conditions and less in normal conditions. Rasmussen and Wilhelmson (1983) have mentioned that values of CAPE N 1500 J kg−1 are suitable for supercell formation. Hence the occurrence of CAPE values greater than 1500 J kg−1 is considered to be an indicator of the impending convective rain. To have a quality check of the data, the brightness temperatures and retrieved instability indices and CAPE obtained from the radiometer are compared with co-located radiosonde observations (taken at 00:00 h from IMD Kolkata, located b 10 km from the research facility) for 80 days during March to May 2011. Five parameters from both the instruments have been compared. They are the ground temperature and relative humidity, PWV, KI, and CAPE. The comparison between the parameters obtained from both instruments shows that the radiometric results have a good correlation with radiosonde measurements. Reasonably high correlation coefficients have been obtained between the two instruments in all five parameters. It has been found that there are some small errors in the relative humidity profiles. These errors are due to wet bias errors which are generally widespread in the height range of 1–6 km. Many researchers have described the existence of such types of biases (Chan, 2009; Xu et al., 2014). However, it has been established that the biases given by the radiometer are comparable to other studies as announced earlier (Chan, 2009; Chakraborty et al., 2014; Xu et al., 2014). Sánchez et al. (2013) differentiated vertical profiles of temperature and water vapor from multi-channel microwave radiometer observations with thousands of radiosonde profiles and acquired an error bias of 0.2– 1.2 K in temperature and 0.05– 0.5 g m−3 in water vapor figures. In addition to all this, an impact-type disdrometer (RD-80, Waldgovel type) has also been utilized for rain rate measurements. The rain events having a minimum duration of 10 min with a maximum instantaneous rain rate magnitude greater than 20 mm h−1 have been considered for the study. A set of 18 convective events and 58 non-convective events from 2011 have been used for testing the proposed model, while 40 convective events from 2012 have been utilized for validation purposes. The conclusion of whether an event is convective or not has been established on the criterion of the absence of bright band structures in the radar reflectivity profiles noticed with a collocated MRR at our research facility as already debated in previous studies (Das et al., 2012; Maitra et al., 2014; Sarkar et al., 2015).

An effective early warning system is essential to reduce the disaster risk. However, the forecasting of thunderstorms is a challenging task as it belongs to the cloud scale or mesoscale. Besides, the event is extremely convoluted, distinct, and highly unstable. As a result, accurate forecasting with sufficient lead time is a primary responsibility of the meteorological community. Synoptic weather chart analysis, thermodynamic diagram studies (T– ϕ gram), satellite imagery, Doppler Radar observations, and statistical and numerical models are used to forecast thunderstorms daily. Predicting thunderstorms by numerical weather prediction (NWP) models using the atmospheric variables determined by past conditions, means forecasting thunderstorms is based on the initial condition of the atmosphere. In reality, one of

the drawbacks of NWP models is the regularity of a chaotic atmosphere, and this increases intrinsic model error (Collins and Tissot 2016). Over the past few decades, numerous machine learning (ML) algorithms have been established to solve various problems arising in real-life implementations (Jiang et al. 2021, Maddalena et al. 2020; Nie et al. 2018; Mc Govern et al. 2017; Pal and Pal 2017; Pal et al. 2015; Pal and Sen 2010; Pal and Pathak 1986). Since the 1990s, the use of artificial intelligence in atmospheric sciences has been accepted for improvement. As there is no local network of observatories, traditional procedures for forecasting small-scale weather events have some limitations and may separate from accurate forecasts. In addition to the traditional approaches, machine-learning techniques have been widely accepted to synthesize large amounts of atmospheric data due to their capability to capture complex relationships in data and deliver correct forecasts without clear prediction assumptions (Jergensen et al. 2019, 2020). ML models map a set of inputs to a certain output by optimizing the model's structure so that the inconsistency between the ML predictions and the output observations, or "ground truth," is as small as possible. ML models enhance the prediction accuracy of forecasts, often established as a substitute for NWP with post-processing and interpretation of predictions (McGovern et al. 2017; Rasp and Lerch 2018; Schultz et al. 2021). Many researchers have established machine learning techniques to nowcast the occurrences of lightning (Mostajabi et al. 2019; Zhou et al. 2020; Shrestha et al. 2021). In the present study, Logistic Regression (LR) and Extreme Gradient Boosting (XGBoost), the two mostly used data-driven approaches, are established to assess and predict the occurrences of thunderstorms. Logistic regression analysis is utilized to examine the association (categorical or continuous) of independent variable(s) with one dichotomous dependent variable. Sánchez et al. (1998) established logistic regression to the short-term forecast of hail risk in the province of Leon in the northwestern Iberian Peninsula of Spain. Dasgupta and De (2007) explained binary logistic regression models for the prediction of convective developments from a prior knowledge of the values of certain dynamic and thermodynamic parameters. Lee et al. (2020) described logistic regression for convective detection in Korea. However, Logistic Regression is a summarized linear model (McCullagh and Nelder 1989). As an alternative, Gradient Boosting (GB) is a machine learning algorithm that utilizes decision trees that are trained iteratively with each successive tree rectifying the errors of the previous trees. Leinonen et al. 2022 used LightGBM, an implementation of the GB algorithm for nowcasting thunderstorm hazards in an area in the Northeastern United States. XGBoost is an algorithm that has recently been in control of applied machine learning. It has emerged as a potential tool for short-term forecasting, not only because of its capacity to describe complicated nonlinear systems flexibly but also because of its ability to directly map input variables to output variables. Although more non-linear regression algorithms such as neural networks have been explained to predict thunderstorms and convective weather systems (McCann1992; Litta et al. 2013; Tissot and Collins 2016; Zhou et al. 2019; Kamangir et al. 2020; Stankova et al. 2021), XGBoost and Logistic Regression are explained to be effective methods in data-driven weather forecasting. These ML models are like ‘Black Boxes’, constructed directly from the data by an algorithm. That means the users, or even those who develop them have no idea how variables are combined or interact to make predictions, given a list of input variables. For the task of model interpretation (explanation), we propose to apply Shapley Additive explanations (SHAP) to quantify the contributions of different predictor variables. It is based on the game-theoretic

approach that quantifies the contribution of each predictor variable to the prediction in terms of Shapley values, which can explain how predictions are made from any machine learning algorithm. It also correctly identifies the ranking of the importance of the predictor variables in terms of their contributions to the model output. In this paper, we focus on both the two approaches, viz., global explanations and local explanations. Local explanations attempt to interpret individual predictions at the single statistical unit level, whereas global explanations characterize the model as a whole in terms of which the explanatory variables mostly established their predictions for all statistical units. The Shapley value technique, first proposed by Shapley (1953) and applied by Lundberg and Lee (2017a, b), and Strumbelj and Kononenko (2010), is gaining a lot of attention among local explanation approaches because of its significant advantages. Shapley-based XAI methods may be used to assess the contribution of each explanatory variable to each point prediction of a machine learning model, regardless of the underlying model or principle. Their interpretation tools are not restricted to their specific model classes or data, allowing for greater applicability and nationalization of their findings. In this study, we emphasize the concept of "Explainable artificial intelligence" (XAI) for short-term predictions of pre-monsoon thunderstorms over Kolkata (22°33′N and 88°20′E) during the pre-monsoon season (March, April, and May). This is unique. Here, SHAP is used as a unifying framework to quantify the contributions and relevance of different predictor variables of an ML model; thereby providing the interpretation of the model's decision toward thunderstorm prediction. In terms of the said explainability, we have compared two machine learning models viz., XGBoost and Logistic Regression, with the thermodynamic indices and parameters as input variables. Besides, different performance metrics, namely, relative operating characteristic (ROC) curve, area under the curve (AUC), Matthews-correlation coefficient (MCC), root mean square error (RMSE), mean absolute error (MAE), and R2 (coefficient of determination) have been used to quantify the prediction capability of these models for evaluation and comparison. Finally, using the SHAP-based most important variables, the validity of the models is tested with domain knowledge.

In the present study, an attempt has been made to understand the efficiency of several stability indices and thermodynamic parameters in forecasting the occurrence of thunderstorms over Kolkata (in the Gangetic West Bengal Region) during the pre-monsoon period (April – May) during STORM experimental period 2022. The main objective of the present study is to assess the skill of various thermodynamic indices and to propose suitable threshold values for indices to predict the occurrence of thunderstorm activity during the pre-monsoon months of Kolkata.

Synoptic and other features of Kolkata

Study area Kolkata is the capital city of the East Indian state of West Bengal and one of the largest metropolitan areas of India. Kolkata is in eastern India in the Ganges Delta at 22°33′N and 88°20′E, along the east bank of the Hooghly River. The Chota Nagpur Plateau is in the western/SW section of the study zone, and the Bay of Bengal is in the southern part. This area connects to the tropical monsoon climate. There is a transition from winter monsoon to summer monsoon circulations during the pre-monsoon season, and the region receives highly intense insolation, resulting in the development of a heat flow. The season is characterized by high

surface temperatures and severe convective activity. Over the West Bengal region, two distinct air accumulations coexist land-based west-to-northwest winds and moist winds from the Bay of Bengal. During this time, a low-pressure system is present over the Chota Nagpur Plateau region, West Bengal, Assam, Bangladesh, and the surrounding areas, and a seasonal high-pressure system develops over the Bay of Bengal (Lohar and Pal 1995; Tyagi et al. 2011). During this time, a shallow layer of wet southerlies or south-westerlies from the Bay of Bengal near the ground and dry westerlies aloft characterized the upper airflow over Gangetic West Bengal and the surrounding areas. The atmosphere becomes potentially unstable in the pre-monsoon months of March, April, and May due to a weak surface pressure field, weak surface and lower atmospheric winds, and intense daytime heating. However, thunderstorms may not occur daily, even though the conditions are ideal for them to occur practically every day throughout these months. Synoptic systems or features provide the trigger for the occurrences of thunderstorms.

Research Review on Thunderstorm

During the last two decades, remote sensing techniques have become more prominent as high-resolution spatial imaginaries are available. Both the polar-orbiting (MODIS) and geostationary (INSAT) satellites are now providing imaginaries in the visible and infrared ranges along with deductible vertical profiles of temperature and humidity at high spatial and temporal resolutions. Polar-orbiting satellites provide data at 50 km resolution twice a day for any nearby region, whereas INSAT provides data at 15-minute intervals and 10 km resolution. The utilization of satellite data products gave a considerable advantage in forecasting thunderstorm events. Das et al. (2014) and Yadava et al. (2020) observed the importance of TRMM-LIS data in the analysis of thunderstorms and lightning activity over India. Jayakrishnan and Babu (2014) used the MODIS satellite data for calculating three stability indices, namely K-index (KI), LIFTED INDEX (LI), TOTAL TOTALS INDEX (TTI), and identified their threshold value as – 4 for LI, 35 to 40 for KI, 50 to 55 for TTI for the formation of thunderstorms over south peninsular India. The implementation of MODIS data has the restriction that it takes about 1–2 days to view the same point on the earth, which obstructs its application for real-time detection of convection. In contrast, geostationary satellites provide atmospheric data as imaginaries and Sounder at frequent time intervals and high spatial resolution, and their continuous monitoring of the three-dimensional atmosphere helps to detect the generation of convective activity. The Indian National Satellite System INSAT-3D, and INSAT-3DR geostationary satellites, which were launched on 26th July 2013 and 8th September 2016, respectively, provide data as imaginaries and Sounder at every 30-min-intervals and 10 km spatial resolution covering the Indian subcontinent. Recent studies by Kalsi (2002), Purdom (2003), Ivanova (2019), Lee et al. (2019), and Umakanth et al. (2019, 2020a, b, c) revealed the importance of satellites in thunderstorm identification and prediction. Lee et al. (2019) have shown the usage of the geostationary Meteosat Second Generation (MSG) satellite in the detection and tracking of rapidly developing thunderstorms over southern Africa. Purdom (2003) observed the usage of satellite data in nowcasting the severe storm occurrence, and their intensity over South Florida, USA. Kalsi (2002) demonstrated the use of satellite data in nowcasting severe storms in the identification of large-scale convective precipitation

systems such as monsoon depressions and tropical cyclones over the Indian region. The INSAT-3D satellite has become helpful for nowcasting the mesoscale convective systems with the assistance of Sounder and Imager products. Dineshkumar et al. (2020) studied the impact of the assimilation of high-resolution atmospheric motion vectors from INSAT-3DR satellite data and reported significant improvement in short-range weather forecasting. Jayakrishnan and Babu (2014) used the MODIS satellite data for calculating the stability indices like K-index (KI), lifted index (LI), and total totals index (TTI), which are the indicators of detection of the genesis of thunderstorms, and identified their thresholds as \–4 for LI, 35–40 for KI, 50–55 for TTI for convection to form over south peninsular India. The research works by (Jayakrishnan and Babu 2014; Dinesh Kumar et al. 2020) are the major motivation works for our current research study. Apart from conventional thermodynamic stability methodology, rapid developments in data assimilation have made it possible to use high-resolution mesoscale weather prediction models for the simulation and prediction of high-impact severe local convective storms. A few studies have been conducted for the simulation of thunderstorms over the Indian region (Litta and Mohanty 2008; Litta et al. 2012; Leena et al. 2019). Leena et al. (2019) imitated a pre-monsoon thunderstorm that occurred over Pune with the ARW model and reported that the model could simulate the storm development, structure, and evolution satisfactorily as verified by observations. Litta and Mohanty (2008) reproduced a thunderstorm over the Kolkata region using ARW-NMM (Non-hydrostatic Mesoscale Model core) and described that the model could broadly propagate several features of the thunderstorm event, such as temporal variability and spatial pattern. Litta et al. (2012) studied four thunderstorms of the pre-monsoon season over Kolkata with the ARW-NMM model, and their results show that the model could predict the thunderstorm occurrence with 6 – 12hour lead time and with good acceptance in spatial patterns, but with undervalue of precipitation intensity. Sandeep et al. (2020) simulated the lightning flows of Cash using the National Centre for Medium-Range Weather Forecasting regional UNIBED model (NCUM-R) and reported that an increase of graupel water path value as 200 g/m3 and with the inclusion of snow-rain collision process the model yielded escalation of lightning counts by 50% that were closer to the observations. Choudhury et al. (2020) simulated a thunderstorm event of the pre-monsoon season over northeast India using the ARW model and reported that the number of lightning flows of Cash yielded with the Morrison microphysical and cloud top height-based dynamical lightning parameterization scheme was in better agreement with the corresponding observations from TRMM- Lightning Imaging Sensor. Prediction of thunderstorms using weather prediction models is a complex task due to the nonlinearity of dynamics and microphysics of the system. A few studies are using the ARW model to simulate severe thunderstorms and to understand the cloud microphysics and dynamics over the Indian subcontinent and elsewhere (Litta and Mohanty 2008; Litta et al. 2012; Das et al.2015, Murthy et al. 2018; Sarkar et al. 2019; Choudhury et al. 2020).

Thunderstorms are short-lived mesoscale deep convective weather phenomena that are manifested in the form of squally winds, thunders, lightning, hail, and heavy precipitation. The severe thunderstorms cause damage to crops, damage to structures, and loss of life by extreme winds, lightning, and hail leading to severe socio-economic impacts in affected regions (Tyagi 2007). Thunderstorms occur in different parts of India during different seasons, but with

widespread and peak activity all over the country during the hot weather period, also known as the summer or pre-monsoon season, from March to May. Severe thunderstorms form and move generally from northwest to southeast over the eastern and northeastern states of India during the pre-monsoon season, they are locally called ‘‘Kalbaishakhi" or ‘‘Nor’westers’’. Strong heating of landmass during mid-day takes action on convection over the Chota Nagpur Plateau, which develops southeast and gets set up by mixing with warm moist air mass from the head Bay of Bengal (Kessler, 1982; Ghosh et al. 2008; Someshwar et al. 2014). Over the Gangetic West Bengal (GWB) region, comprehensive data sets are not available to understand the thermodynamic features of the atmosphere to upgrade the forecasting skill of the occurrence of thunderstorm activity. Keeping this in view, the Department of Science and Technology of the Government of India started a multi-institutional program named ‘‘Severe Thunderstorms Observations and Regional Modelling (STORM)’’ over Gangetic West Bengal and North East parts of India (Storm Science Plan 2005).

Few observational studies have been described on pre-monsoon thunderstorms over the GWB region to understand and delineate the characteristic signatures in the development of these events (Mukhopadhyay et al. 2009; Chaudhuri 2011; Tyagi et al. 2011, 2013a, b; Someshwar et al. 2014). Mukhopadhyay et al. (2009) studied the formation of severe thunderstorms over the Kolkata region by using Doppler radar and satellite observations and concluded that severe thunderstorms occur mainly due to the interaction of large-scale and mesoscale environments. Chaudhuri (2011) suggested that Convective Inhibition (CIN) (0–150 Jkg-1) and warm air (surface temperature 30–38 C) are the most significant parameters for the prevalence of severe thunderstorms over the Kolkata region during the pre-monsoon season. Tyagi et al. (2011) proposed the threshold values of the thermo-dynamical indices such as convective available potential energy (CAPE), lifted index (LI), K index (KI), humidity index (HI) on the days of thunderstorm activity using larger data set over Kolkata region. Observed values of these indices revealed that the occurrence of scattered, multi-cellular thunderstorms is possible over the Kolkata region during pre-monsoon months. Tyagi et al. (2013a, b) studied the thermo-dynamical structure of atmosphere and surface energy fluxes during the pre-monsoon season over Kharagpur using STORM data sets. It has been concluded that significant moisture availability in the lower troposphere in the presence of convective instability conditions leads to thunderstorm development at Kharagpur during pre-monsoon season. Field experiments have been conducted (Someshwar 2014) to gather comprehensive observations on severe thunderstorms over the South Asian Region for understanding their genesis and regional modeling. Short-range prediction of severe weather such as thunderstorms is an important aspect of the regional weather in the northeastern states of India. An accurate, location-specific (2009), and timely prediction is required to avoid loss of lives and properties due to strong winds and heavy precipitation associated with such weather systems. Prediction of thunderstorms is one of the most difficult tasks in weather prediction, due to rather smaller spatial, and temporal scales and inherent non-linearity of their dynamics and physics and due to the problem of prescribing precise initial conditions. Few modeling studies have been reported for pre-monsoon thunderstorm analysis over the GWB region in an attempt to predict the development of these events (Chatterjee et al. 2015; Someshwar et al. 2014; Kiran Prasad et al. 2014; Dawn and Mandal 2014; Srikanth et al. 2015; Litta et al. 2012a, b;). Litta et al.

(2012a) used a high-resolution (3 km) WRF non-hydrostatic mesoscale model (WRFNMM) model to simulate severe thunderstorm events over the east and northeast Indian region. With physics sensitivity experiments, they explained that the NMM model with the Ferrier microphysics scheme has well recorded the instability of the atmosphere for the occurrence of severe thunderstorms in the above regions. Litta et al. (2012b) studied the performance of WRF-NMM for a few thunderstorm cases during the STORM field experiments in 2007, 2009, and 2010 and explained that WRF-NMM with 3-km resolution predicted the events with appropriate accuracy over east and northeast Indian region. Srikanth et al. (2015) explained the performance of convective parameterization schemes (Kain–Fritsch, Grell– Devenyi and Betts–Miller–Janjic) of WRF-ARW for simulating pre-monsoon thunderstorm events around Kharagpur and predicted that Grell–Devenyi performed better than the other tested schemes in representing the thermo-dynamical state of atmosphere during the thunderstorm events over Kharagpur region. Kiran Prasad et al. (2014) studied the impact of Doppler weather radar (DWR) data on thunderstorm simulation during the STORM pilot phase over eastern and northeastern parts of India. They reported significant improvements in the mesoscale model results after combing DWR fields. Dawn and Mandal (2014) studied the WRF model-simulated surface mesoscale features associated with pre-monsoon convective episodes over the GWB, India by using STORM data sets. Prosenjit et al. (2015) studied the three pre-monsoon season convective episodes over the GWB, India by using the mesoscale model MM5. They have observed that mesoscale models have the capability of restoring temperature drop, rainfall, and regions of pressure rise and drop that occur during the thunderstorm period. Someshwar et al. (2014) simulated 15 severe thunderstorms using the WRF model that formed over northeast India during the pre-monsoon season of 2008. They simulated all the storms though they were slightly shifted in position and time. Boundary Layer (PBL) encompasses 2–3 km of the atmosphere of the lower troposphere and plays an important role in the transportation of energy such as momentum, heat, and moisture into the upper layers of the atmosphere (STULL 1988) and acts as a feedback mechanism in the generation and sustenance of thunderstorms. The intensity of convective thunderstorms is determined by the supply of heat and moisture from the surface. The PBL determines the amount of convectively available potential energy of the atmosphere that determines the genesis of thunderstorms. In numerical models, various approaches are used to parameterize the vertical turbulent mixing in the PBL. Consequently, the characteristics of the simulated storms may depend on the specific parameterizations to some extent. Studies were described in the literature regarding the sensitivity of PBL schemes to meteorological modeling (e.g., Bright and Mullen 2002; Srinivas et al. 2007a, b, 2013, 2015; XIE et al. 2012; Ramakrishna et al. 2012; Li and Pu 2008; Miao et al. 2009; Hu et al. 2010; Hariprasad et al. 2014; Srikanth et al. 2015). Hu et al. (2010) described the ability of three PBL schemes in WRF (MYJ, YSU, and ACM2) to simulate the PBL features for fair weather conditions over Texas. With the comparison of surface and boundary layer observations, they suggested that the ACM2 scheme produced better simulations than the other two. Srikanth et al. (2015) studied severe thunderstorm events using the WRF-ARW model over Gadanki in southern peninsular India using five PBL and three cumulus parameterization schemes. In simulating, they reported that the MYJ with Grell–Devenyi ensemble (GD) combination better simulated the boundary layer parameters, thermodynamic structure and vertical velocity profiles, and the characteristics of severe thunderstorm events. From the literature review, PBL

parameterization observed over India is mostly limited to cyclones and fair-weather conditions, and relatively few studies are available on thunderstorms. In particular, studies related to PBL parameterizations for meteorological modeling of thunderstorms are limited to the GWB region. The model simulations are validated with the available observations and statistical analysis performed to assess the efficiency of different PBL schemes for reproducing storm events.

Thunderstorms are characterized as temporary phenomena over-viewed by heavy rain, thunder, and lightning (Sahu et al., 2020 a, b). The correlated precipitation may be a heavy downpour of rain, snow, hail, or perhaps no precipitation at all (Williams, 2004, 2005). Severe thunderstorms have been described globally (Goliger and Milford, 1998), and tropical areas are mostly affected (Mahanta and Yamane, 2020). These storms crash infrastructure, buildings, the aviation industry, and, most significantly, the natural ecology. Early warnings and forecasts for both intensity and possible danger across any region can benefit from knowledge regarding the development of any natural hazard including high-intensity rainfall (Kursinski et al., 2008; Das et al., 2014). Because of its potentially hazardous nature, researchers made an effort to understand the life cycle, characteristics, and severity of these convective storms in different regions of the world (e.g., Risanto et al., 2019; Cecil and Blankenship, 2012; Rasmussen and Houze, 2011; Sánchez et al., 2008; Bissolli et al., 2007; Niall and Walsh, 2005; Dotzek, 2003; Kuleshov et al., 2002; De Coning and Adam, 2000;).
The Indian subcontinent experiences recurrent thunderstorms during the pre-monsoon season (March–May), especially over eastern and north-eastern regions (Rao and Raman, 1961; STORM, 2005). The spatial coverage of these pre-monsoon thunderstorms is expanded over parts of Bihar, Jharkhand, Odisha, West Bengal in eastern India and Assam, Meghalaya, Manipur, Mizoram, and Tripura in north-eastern India (Roy 2019). These thunderstorms are also known as Nor'westers as they pass from north-west to south-east, and locally as 'Kal-Baishakhi' in the Bengal region (Gupta, 1952), and 'Bordoichila or Bordoisila' in Assam (Chaudhuri et al., 2013). The hazardous nature of these pre-monsoon thunderstorms over eastern and north-eastern India makes them a priority research area of meteorologists working in the region for more than a century.

The yearly mean of thunderstorms over north-eastern India exceeds 100 days (Tyagi, 2007). There are various kinds of research for the Indian region dealing with thunderstorm observations and modeling to understand their genesis and dissipation for better forecasting (e.g., Awadesh, 1992; Kumar and Mohapatra, 2017; Santhosh et al., 2001; Tyagi et al., 2012; Tyagi and Satyanarayana, 2013a; Satyanarayana and Tyagi, 2013b; Tyagi et al., 2013; Tyagi et al., 2014; Satyanarayana and Tyagi, 2014a; Satyanarayana and Tyagi, 2014b; Sahu et al., 2020a; Sahu et al., 2020b). The researchers find the existence of troughs over northern India, with moisture transportation over north-eastern regions from the Bay of Bengal (Mohapatra and Kumar, 2006). The published works associated with pre-monsoon thunderstorms over northeast India observed to understand the characteristic features with synoptic analysis, frequency of occurrence, point observation (in-situ) based analysis of thunderstorm events, or model performance analysis for simulating these thunderstorms (e.g., Madala et al., 2014; Madala et al., 2016; Tyagi and Satyanarayana, 2015). Thermodynamic indices emerged as a successful approach for dealing with these thunderstorms forecasting on a short scale due to

correlated change detection in thermodynamical parameters (Sahu et al., 2020 a; Samanta et al., 2020).

Moreover, the studies correlated to spatial variations of atmospheric variables and thermodynamic indices over these regions are limited. Mahanta and Yamane (2020) designed the spatial distribution of thunderstorms over Assam; with the primary purpose of determining the frequency of these events. Collecting spatial information and collecting it for a regional picture of seasonal variation of thunderstorms over north-eastern India is an uphill task due to lack of data and limited information availability. Understanding the variation of thermodynamic indices over an area will help identify and understand the index predicting thunderstorm development and follow the direction related to climate change in response to thunderstorms.

Spatio-temporal variability of rainfall has a great impact on the earth's hydrological cycle, circulation model as well and global climatic change (Rao et al., 2020; Ochoa-Rodriguez et al., 2015; Nischitha et al., 2013). The characteristics and development probability of natural disasters like floods, droughts, and tropical cyclones are profoundly managed by the space-time diversity of global rainfall patterns (Huang et al., 2018). Diurnal variability of rainfall over a location is predominantly supervised by atmospheric parameters, processes, and geographical characteristics of that region (Singh and Kumar, 1997; Basu, 2007; Singh and Nakamura, 2009; Varikoden et al., 2013; Zhao et al., 2019). Consequently, scientific knowledge about the temporal variance of rainfall is outstanding for short-term weather forecasting. Diurnal cycles of rainfall over different portions of the world have already been estimated in several studies (Hara et al., 2014; Deshpande and Goswami, 2014; Tabari and Talaee, 2011; Hara et al., 2009; Buytaert et al., 2006; Bechtold et al., 2004; Collier and Bowman, 2004; Li et al., 2004; Barros and Lang, 2003; Hu, 2003; Gao et al., 2002; Dai, 2001; Ueno et al., 1998, 2001 a, b, 2008). Yu et al. 2007 recommended that the early morning peak mainly corresponds to long-duration rainfall events lasting longer than 6 h, whereas the late afternoon peak was mainly due to rainfall events lasting less than 3 h . Terrain-induced local circulations are established to be one of the causes of late-night and early-morning rainfalls (Singh and Nakamura, 2010, 2012; Bhatt and Nakamura, 2005, 2006; Singh et al., 2005; Barros et al., 2004; Lang and Barros, 2002, 2003, 2004; Kuwagata et al., 2001; Barros et al., 2000). However, an afternoon to early evening rainfall is quite common and more likely than a late night to early morning peak (Ueno et al., 2001; Ohsawa et al., 2001; Barros et al., 2000). The research on diurnal rainfall variations over India found a few decades back (Bhattacharya and Bhattacharyy, 1994; Harlar et al., 1991; Bhatt and Nakamura, 2005; Sahany et al., 2010; Singh and Nakamura, 2009; Subrahmanyam et al., 2015). However, most of these studies described the monsoon rainfall features from central India or the Himalayan foothill region within the Indian territory. Heavy rainfall during the night and early morning hours in the monsoon period has been described (Bhattacharya and Bhattacharyya, 1994) over North Bengal. Halder et al. (2023) explained that the effects of the mesoscale topography and the drift of thunderstorms are the reasons for the diurnal variation of precipitation over central India during the monsoon period. The diurnal precipitation characteristics around the Indian Himalayan region were investigated using Level 3, 3B42/TMPA precipitation product obtained from Tropical Rainfall Measuring Mission (TRMM) satellite data (Bhatt and Nakamura, 2005). Afternoon to evening precipitation was found as embedded convection over the location. Sahany et al., 2010, also distinguished the diurnal variation using TRMM data. They established three peaks of diurnal rainfall at 11:30, 14:30, and 17:30 IST over the Bay of Bengal, which

is placed very close to Kolkata and its surrounding region. Singh and Nakamura noticed the peak of diurnal variation of rainfall during the afternoon period (15–18 IST) from TRMM observations. Subrahmanyam et al. (2015), announced a positive relationship between the diurnal variation of convective available potential energy (CAPE) and precipitation over the Indian summer monsoon region. It has been explained by several authors that maximum rainfall occurs during the late afternoon hours of the Indian summer monsoon over the Indian land mass (Nesbitt and Zipser, 2003; Basu, 2007; Sen Roy and Sen Roy, 2011; Rajeevan et al., 2012).

The precipitation characteristics study is very much important in India, as it shows significant seasonal and inter-annual variations. The monsoon rainfall is mainly characterized by stratiform rain. There are many studies on the characteristics of monsoon rainfall in India as mentioned earlier. On the other hand, pre-monsoon rainfall is mostly associated with localized convective phenomena, and predominantly connected to local variabilities of atmospheric parameters. The pre-monsoon rainfall plays a significant role in determining the total rainfall of the year (Bera, 2017). Pre-monsoon rainfall is also a determining factor in the inter-annual variation of monsoon rainfall (Ghosh et al., 2018). Kolkata is located near the land-ocean boundary, on the verge of the tropics. As a consequence of the flow of land-sea breeze, convective phenomena are very likely over Kolkata during the pre-monsoon period (Sadhukhan et al., 2000). Over a tropical urban location, like Kolkata and its surroundings, the study of pre-monsoon rainfall characteristics is thus quite significant. Most of the studies of diurnal variation of precipitation over India have been performed using TRMM data products. In the present study, the diurnal precipitation characteristics and association with atmospheric parameters have been investigated, using two ground-based instruments, a disdrometer, and a radiometer. The level 3, 3B42/TMPA precipitation product derived from TRMM satellite data of spatial precipitation patterns encompassing the Kolkata region has also been evidenced. Kolkata (22°34́N, 88°29́E) experiences appreciable rainfall during the monsoon (June-September) and the pre-monsoon (April-May) seasons of the year. Though the monsoon rainfall has a major contribution to the annual rainfall occurring in Kolkata, pre-monsoon rainfall still plays a significant role in determining the total rainfall of the year (Chakraborty and Das, 2021). The convective rainfall during the pre-monsoon period in Kolkata is known as Nor'westers, which are localized thunderstorms along with medium to heavy precipitation. A previous study reported that maximum pre-monsoon rainfall occurs during the afternoon period over the tropical land masses (Hirose and Nakamura, 2009). However, the observation was based upon TRMM PR satellite of a few convective events over India from March to May of the years 1998–2003. The spatio-temporal variation of Asian precipitation systems had been investigated through the diurnal rainfall variability to identify the topographical impact on the rainfall-regime determination. The lack of accurate precipitation records often acts as a hindrance to carry out such studies on an elaborate basis. In the present study, atmospheric conditions and parameters associated with Nor'westers have been investigated to analyze their comparable and contrasting patterns in connection with the temporal shifting of the rainfall events from afternoon to late evening period during the pre-monsoon days over the tropical urban location, Kolkata. The urban agglomeration of Kolkata at the verge of the tropics in the Indian state of West Bengal kindled the scope of diurnal precipitation research at the particular locus. The diurnal cycle of rainfall not only exhibits distinguishable characteristics over the tropical lands and oceans but is also found to be more prominent over the landmass (Gray and Jacobson, 1977). Kolkata, being located near the land-ocean boundary, becomes a specialized location for the investigation of diurnal precipitation variability.

Chapter 2

Meteorological Variables Explanation and Data Details of Thunderstorms and Non-Thunderstorms Days Over Kolkata Region, West Bengal

Description of Sounding Columns

Parameter	Description	Units
PRES:	Atmospheric Pressure	[hPa]
HGHT:	Geo-potential Height	[meter]
TEMP:	Temperature	[celsius]
DWPT:	Dew point Temperature	[celsius]
FRPT:	Frost Point Temperature	[celsius]
RELH:	Relative Humidity	[%]
RELI:	Relative Humidity with respect to Ice	[%]
MIXR:	Mixing Ratio	[gram/kilogram]
DRCT:	Wind Direction	[degrees true]
SKNT:	Wind Speed	[knot]
THTA:	Potential Temperature	[kelvin]
THTE:	Equivalent Potential Temperature	[kelvin]
THTV:	Virtual Potential Temperature	[kelvin]

Meteorological Variables

Skew-t Structure

The skew-t – log P diagram is the most commonly used thermodynamic diagram within the United States. A large number of meteorological variables, indices, and atmospheric conditions can be found directly or through simple analytical procedures. Typically, the environmental temperature, dew point temperature, wind speed and wind direction at various pressure levels are plotted on the diagram. This plot is commonly called a 'sounding'. Sounding data come from weather balloons that are launched around the country at 00Z and 12Z, as well as various special situations in which they are used in field experiments and other campaigns. **Figure 2.1** is an example skew-t-log P diagram.

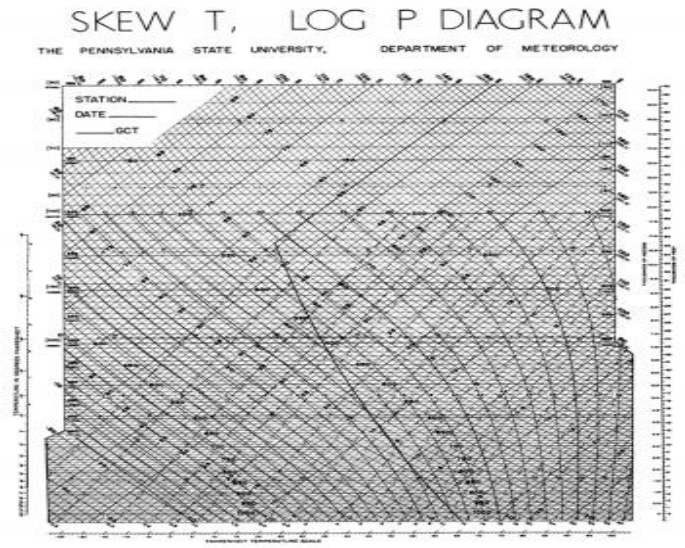

***F*igure 2.1 S**kew-T - Log P Thermodynamic Diagram

Let's take a closer look at **Figure 2.1** and identify the lines on the skew-t diagram. **Figure 2.2** is a close up of the lower right corner of the diagram in **Figure 2.1**. Each line is labeled accordingly. The solid diagonal lines are isotherms, lines of constant temperature. Temperatures are in degrees Celsius, and a Fahrenheit scale is also at the bottom of the diagram. The dashed lines are mixing ratios. The dry adiabats on the diagram are the curved lines with the lesser slope and are drawn at 2° intervals. Moist adiabats have a much greater slope and follow much more vertical path on the skew-t diagram. Two height scales are located on the right side of the diagram. The left scale is the height in meters and the right scale is height in thousands of feet. Pressure levels are in millibars (mb)/ hectopascals (hPa).

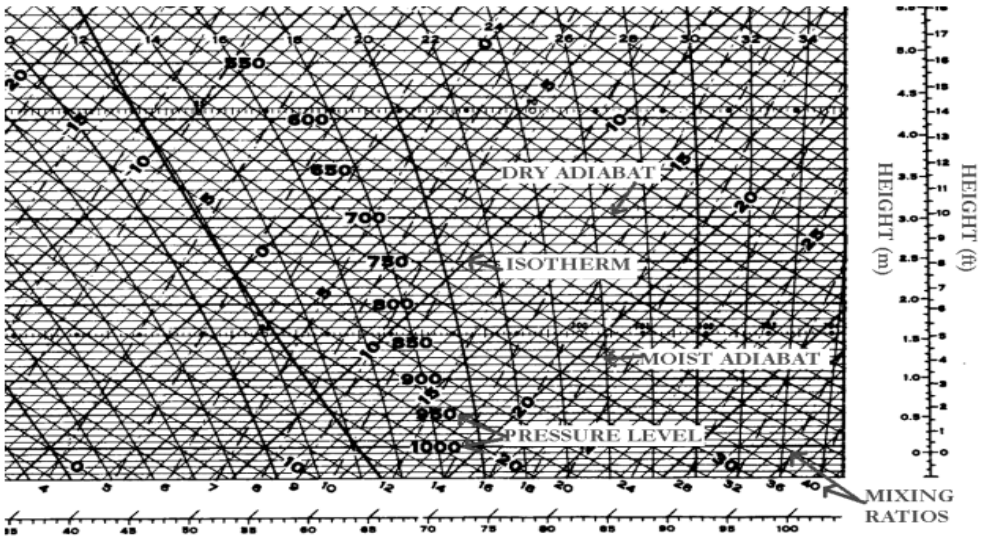

Figure 2.2 A close-up of a skew-t diagram presents the various definitions of lines

Levels

a. Lifting Condensation Level (LCL): The level at which a parcel of air first becomes saturated when lifted dry adiabatically. This level can be found by finding the intersection of the dry adiabats through the temperature at the pressure level of interest, and the mixing ratio through the dew point temperature at the pressure level of interest (**Figure 2.3**).

b. Convective Condensation Level (CCL): The level that a parcel, if heated sufficiently from below, will rise adiabatically until it is saturated. This is a good estimate for a cumuliform cloud base from surface heating. To find the convective condensation level, find the intersection of the mixing ratio through the dew point temperature at the pressure level of interest and the temperature sounding (**Figure 2.3**).

c. Level of Free Convection (LFC): The level in which a parcel first becomes positively buoyant. To find the level of free convection, find the lifting condensation for the level of interest, and find the intersection of the moist adiabats that goes through the LCL, and the temperature curve (**Figure 2.3**).

d. Equilibrium Level (EL): The point at which a positively buoyant parcel becomes negatively buoyant, which typically will occur in the upper troposphere. To find this level, find the level of free convection, follow the moist adiabats through this level of free convection up until it intersects the temperature sounding again. This point is the equilibrium level (**Figure 2.3**).

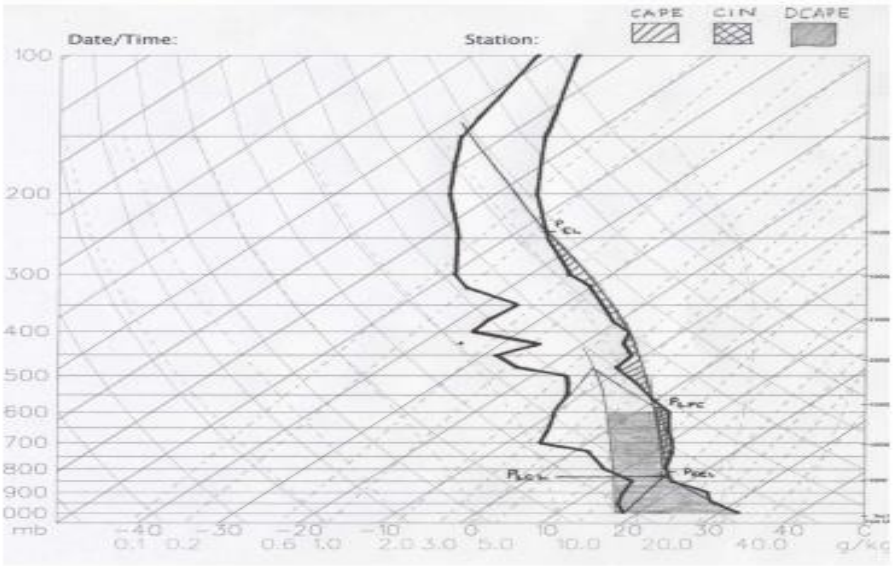

Figure 2.3 An example skew-t showing the levels and energies

Meteorological Variables

As stated before, a sounding can allow the user determine values of many meteorological variables, making it one of the most useful resources for meteorologists. A variety of temperatures, mixing ratios, vapor pressures, stability indices, and conditions can be derived from temperature and dew point temperature soundings on a skew-t.

Temperatures

1. Potential Temperature (Θ): Potential temperature is the temperature a parcel of air would have it were lifted (expanded) or sunk (compressed) adiabatically to 1000mb. The value of the potential temperature is the temperature of the dry adiabats that runs through the temperature at the pressure level of interest, at 1000mb (**Figure 2.4**).

2. Equivalent Temperature (Te): The equivalent temperature is the temperature of a parcel if, via a moist adiabatic process, all moisture was condensed into the parcel. Finding the equivalent temperature is slightly more difficult. To find Te, follow the moist adiabats that runs through the lifting condensation level at the pressure level of interest to a pressure level in which the moist adiabats and dry adiabats have similar slopes, then go down the dry adiabats at this point back down to the original pressure level of interest; this temperature is the equivalent temperature. If the dry adiabats continues beyond the boundary of the skew-t in which it can not be determined, an alternative is to read off the temperature scale that runs diagonally in the middle of the skew-t (**Figure 2.4**).

3. Equivalent Potential Temperature (Θe): The equivalent potential temperature is similar to the equivalent temperature however after the moisture has been condensed out of the parcel, the parcel is brought down dry adiabatically to 1000mb. The process to find the equivalent potential temperature is the same as the regular equivalent temperature however when the parcel is brought down the dry adiabats it continues past the original pressure level and is brought down to 1000mb. The temperature at this intersection is the equivalent potential temperature.

4. Saturated Equivalent Potential Temperature (Θes): The temperature at which an unsaturated parcel would have if it were saturated. To find the saturated equivalent potential temperature, use a similar process used for determining the equivalent potential temperature however one must follow the moist adiabats through the environmental temperature at the necessary pressure level, unlike using the lifting condensation level for equivalent potential temperature (**Figure 2.4**).

5. Wet-bulb Temperature (Tw): The minimum temperature at which a parcel of air can obtain by cooling via the process of evaporating water into it at constant pressure. To find the wet-bulb temperature follow the moist adiabats through the lifting condensation level and find the temperature of the intersection of this moist adiabats with the original pressure level of interest (**Figure 2.4**).

6. **Wet-bulb Potential Temperature (Θw)**: Similar to the wet-bulb temperature, however the parcel is then brought down dry adiabatically to 1000mb. To find the wet-bulb temperature, use similar means as the regular potential temperature, however continue down the moist adiabats through the lifting condensation level through the original pressure level to 1000mb and read the temperature at the intersection of the moist adiabats and the 1000mb pressure level (**Figure 2.4**).

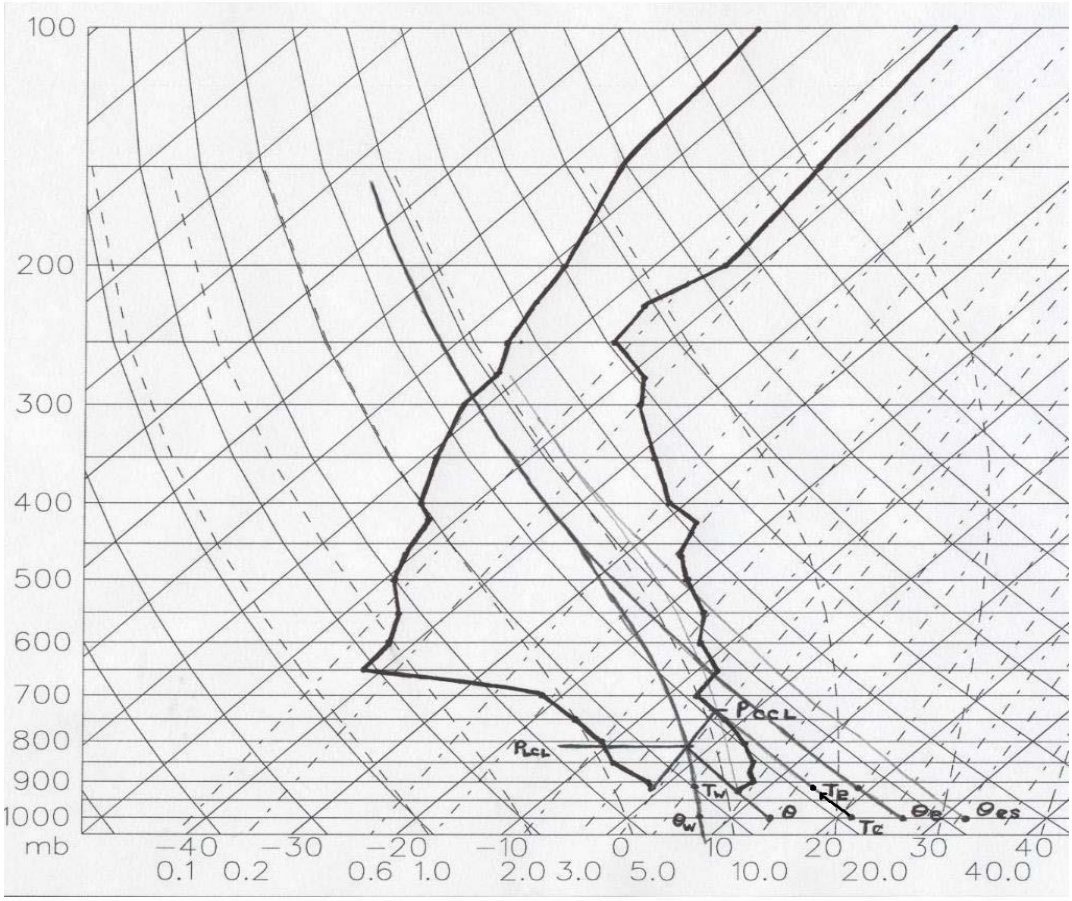

Figure 2.4 This figure shows the methods of finding the temperatures

Vapor Pressures

1. **Vapor Pressure (e):** The amount of atmospheric pressure that is a result of the pressure from water vapor in the atmosphere. To find the vapor pressure follow an isotherm (a line parallel to an isotherm) through the dew point temperature at the pressure level of interest, up to 622mb. The value of the mixing ratio at this intersection is the vapor pressure in millibars.

2. **Saturated Vapor Pressure (es):** The amount of atmospheric pressure that is a result of the pressure of water vapor in saturated air. This quantity can be found using similar means as the vapor pressure however one must follow a parallel isotherm through the temperature at the pressure level of interest.

Mixing Ratios

1. **Mixing Ratio (w):** The mixing ratio is the ratio of the mass of water vapor in the air over the mass of dry air. This quantity is found by reading the mixing ratio line that goes through the dew point temperature at the pressure level of interest.

2. **Saturated Mixing Ratio (ws**): A similar mixing ratio as above, however it is the mixing ratio of a saturated parcel of air at a given temperature and pressure. It can be found by finding the value of the mixing ratio through the temperature at a pressure level of interest.

Stability Indices

a. K-index: Used for determining what the probability and spatial coverage of ordinary

thunderstorms would be based on temperature and dew point temperature.

$$K = (T + T_d)_{850} - T_{500} - (T_{700} - T_{d700})$$

For K > 35, numerous thunderstorms are likely. For K values between 31 and 35, scattered thunderstorms may occur. For K values between 26 and 30 widely scattered thunderstorms are probable. For K values between 20 and 25, isolated thunderstorms are probable, and below 20, thunderstorm will only have a small chance to develop. A summary of these values are in **Table 2.**

b. Lifted Index (LI): If storms form, this is an index that indicates the severity of the storms.

$$LI = T_{500} - T_{sfc8500}$$

T_p is the temperature of a parcel of air lifted to 500mb moist adiabatically from the surface lifting condensation level. T500 is the environmental temperature at this level. LI > - 2 is only a slight severity, LI from -3 to -5 has a much strong severity, and the strongest severity are values with LI < -5. A summary of these values are in **Table 2.**

c. Showalter Index (SI): This is similar to the LI however the level of interest is the 850mb pressure level.

SI = T (500 mb envir) – T (500 mb parcel) in degrees C (weather.gov/lmk/indices)

This index is good for indicating elevated thunderstorms which are not picked up by the lifted index.

d. Total Totals Index (TT): This gives an indication for the probability of seeing severe

thunderstorm activity.

$$TT = 2(T_{850} - T_{500}) - (T_{850} - T_{d850})$$

Values of TT above 52 indicate a high probability of thunderstorms, in which many of the

thunderstorms will become severe. Values between 48 and 52 indicate the possibility exists for severe thunderstorms. Values between 44 and 48 indicate the probability for scattered thunderstorms with only a low probability of severe thunderstorms. Finally, values lower than that 44 indicate that only normal thunderstorms will occur.

e. Convective Available Potential Energy (CAPE): The amount of potential energy that a parcel can obtain from environmental conditions. Mathematically, it is the area between the level of free convection and the equilibrium level. In order to identify CAPE on a sounding, find the level of free convection and follow the moist adiabats through this level up to the equilibrium level. The area between this curve and the temperature curve is positive area, CAPE (**Figure 2.1**) .

f. Convective Inhibition (CIN): Amount of energy from the environmental conditions that are required for a parcel to reach the level of free convection. This is considered to be opposite that of the CAPE, whereas it is called negative area. It is a requirement for strong thunderstorms to occur. The CIN is proportional to the area between the temperature curve and a parcels ascent via both a dry and moist adiabatically lapse rates (**Figure 2.1**).

g. Downdraft Convective Available Potential Energy (DCAPE): This is proportional to the amount of energy that a saturated downdraft would have while falling to the surface. It is found by finding the lifting condensation level at 600mb, descending the moist adiabats through this level down to the surface, and is proportional to the area that is between this line and the temperature curve (**Figure 2.1**).

h. Cap Strength: The cap strength and can measure thunderstorm initiation. It is defined as the maximum temperature deficit within the levels below the level of free convection. Values > 2K would be considered large, and thunderstorm initiation unlikely.

Cloud Layers

Skew-t – Log P diagrams readily allow the user to determine possible cloud layers in the atmosphere. Cloud layers are indicated by locations in which the dew point temperature is very close to the regular temperature. This means that the air is near saturation and a cloud may exist. A shallow cloud layer is seen when the two temperature curves are only near each other for a short vertical layer. Deep cloud layers can be identified by locations in which the dew point temperature and regular temperature curves are near the same magnitude for deep vertical layers in the atmosphere. Furthermore, one can identify cloud cover by noticing a sudden drop in the dew point temperature. This represents the condensation of water vapor into cloud drops. Another way to look at it is that a cloud is located in a region in which there is a significant drop in mixing ratio as well. One will recall that the mixing ratio is defined to be the ratio of the mass of water vapor to the mass of dry air. As water condenses into cloud drops, the mass of water vapor decreases, and thus the mixing ratio decreases.

Atmospheric Mixing

In the morning, when solar radiation warms the Earth, warm pockets of air become positively buoyant and rise, and upon reaching a level aloft, will eventually become negatively buoyant and fall. This process is called turbulence and one of the consequences of turbulence in the atmosphere is mixing. During the afternoon, typically mixing will reach a peak, and when this occurs many meteorological variables become constant. Using a skew-t – Log P diagram, one can determine just how well mixed the atmosphere is using two methods. When the atmosphere has reached a point in which mixing is at a maximum, the mixing ratio and potential temperature will be relatively constant with height. A dew-point curve that runs parallel to a mixing ratio line (typically dashed on a skew-t) is considered constant mixing ratio. Constant potential temperature occurs when the temperature sounding is close to that of slope of the dry adiabats. An example of a well-mixed atmosphere can be seen in Figure 5. Notice the constant potential temperature (the temperature sounding almost parallels the dry adiabats) and the mixing ratio is constant with height. This indicates that the atmosphere is very well mixed, particularly the atmosphere up to 650mb. This sounding is from Amarillo, Texas during July. To see a profile with this ideal look is not uncommon during the summer months when strong daytime heating causes a very large amount of turbulence in the atmosphere. A second approach to determining how well mixed the atmosphere is for a particular sounding is to find the lifting condensation level for the surface temperature and surface dew point temperature and compare it to the actual observed cloud base at that time. If these two levels compare to each other, then the atmosphere is very well mixed. Large variations in these two levels indicate only a moderate mixing in the atmosphere.

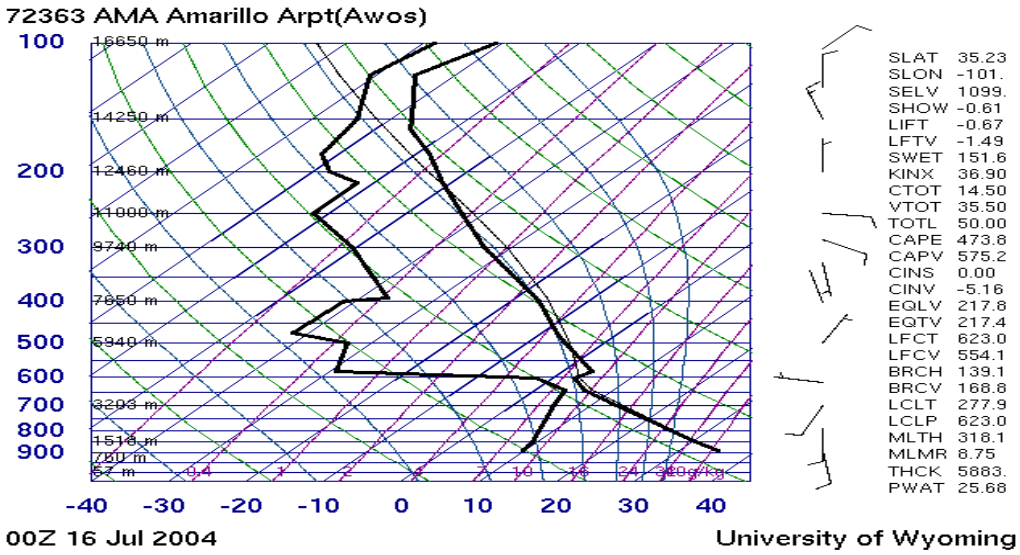

Figure 5. A well-mixed atmosphere in the levels from the surface to 650mb.

Atmospheric Static Stability

Identification of layers that are unstable, stable, or neutrally stable is important for identifying how high buoyant parcels of air will rise in the atmosphere. Unstable layers will promote and enhance positive buoyancy and stable layers will tend to cease lifting and cause parcels to be come negatively buoyant. A neutrally stable layer will have no net effect on the buoyancy of a parcel of air. A conditionally unstable layer, depending on the environment can have a positive or negative affect on a parcel's buoyancy. There are a few methods for determining the stability of a layer in the atmosphere, using lapse rates, using potential temperature, and or the saturated equivalent potential temperature.

a. **Using Lapse Rates**: The necessary lapse rates for determining stability are the moist adiabatic lapse rate, the dry adiabatic lapse rate, and the environmental lapse rate of the layer of interest. The following are the conditions for stability by comparing the environmental lapse rates to the dry and moist adiabatic lapse rate.

   $\Gamma > \Gamma_w$ Absolutely Stable

   $\Gamma_d > \Gamma > \Gamma_w$ Conditionally Unstable

   $\Gamma > \Gamma_d$ Absolutely Stable

b. **Using Potential Temperature:** The conditions for stability using the change in potential temperature with height are as follows:

$$\frac{\partial \Theta}{\partial z} > 0 \quad \text{Stable} \qquad \frac{\partial \Theta}{\partial z} = 0 \quad \text{Neutral} \qquad \frac{\partial \Theta}{\partial z} < 0 \quad \text{Unstable}$$

c. **Using Saturation Equivalent Potential Temperature**: The conditions for static stability using the change in saturation equivalent potential temperature with height are the following:

$$\frac{\partial \Theta es}{\partial z} > 0 \ \text{Stable} \qquad \frac{\partial \Theta es}{\partial z} < 0 \quad \text{Conditionally Unstable}$$

Wind Shear

Often times the wind speed and direction are plotted on a skew-t diagram on the left edge of the diagram, near the height axis. This plot can be used to determine levels of strong wind shear. Wind shear has two components: speed shear and directional shear. Speed shear is defined as an abrupt increase or decrease in wind speed in a relatively short distance, and directional shear is defined as an abrupt change in wind direction over a relatively short distance. One determines these conditions by interpreting the wind plots on the skew-t diagram. The amount of shear in the atmosphere is critical for the development of strong thunderstorms, and is producers of waves in the atmosphere.

Closing Remarks

The use of the skew-t is a very important resource to understand the current state of the atmosphere and, in addition, the forecasted state of the atmosphere. A forecasted skew-t can be just as good as a spatial model that is typically viewed when making a forecast. Various critical meteorological variables can be determined, cloud layer depth and height can be found, and severe weather probabilities and coverage can be derived from the skew-t diagram. Likewise, wind shear and static stabilities can be calculated from the skew-t diagram.

(**Source**: file:///D:/Skew-T-Manual.pdf)

For the year 2022, the total number of 11 days with thunder and 14 days without thunder is taken into account. The total number of thunderstorm and non-thunderstorm 00 UTC and 12 UTC data are given in **Table 2.1** to **Table 2.53** in this study over the Kolkata region, West Bengal (India).

Table 2.1 00 UTC Sounding Data during TS and NTD days

Data	T_{500}	T_{700}	T_{850}	T_{d500}	T_{d700}	T_{d850}	R_{H700}	R_{H1000}	H_{700}	H_{1000}
16.04.22	-7.9	11.4	25.6	-40.9	0.4	11.6	47	89	312.6	1.1
17.04.22(T)	-8.1	10.8	25.2	-32.1	2.8	11.2	58	80	313.0	2.2
18.04.22	-6.9	11.2	24.6	-45.9	-2.8	9.6	37	86	314.9	4.4
19.04.22	-8.5	10.8	26.4	-28.5	-2.2	-3.6	40	83	316.5	6.4
20.04.22	-7.7	11.4	25	-31.7	-1.6	13	40	83	315.1	4.7
21.04.22(T)	-5.1	11.2	18	-42.1	-0.8	16.5	43	83	313.4	6.3
22.04.22(T)	-5.5	10	21.6	-14.5	6.7	18	80	79	314.4	5.9
23.04.22	-4.7	8.6	23.2	-22.7	5.3	10.2	80	94	314.8	6.1
28.04.22	-7.1	11.6	26.8	-47.1	-1.4	6.8	40	85	315.9	4.5
29.04.22(T)	-7.1	11.8	27.4	-54.1	-3.2	2.4	35	84	316.6	5.0
30.04.22	-11.9	12.4	24	-15.3	0.4	11	44	65	314.1	4.7
01.05.22(T)	-11.5	11.6	24.2	-13.2	-1.4	6.2	40	100	312.9	3.4
02.05.22	-7.9	7.6	17.8	-22.9	1.6	13	66	89	312.1	5.6
03.05.22(T)	-9.1	11	23.4	-16.1	1	11.4	50	87	312.3	3.6
04.05.22	-6.1	10.4	21.4	-27.1	5.4	11.4	71	8	312.5	5.4
12.05.22	-3.9	12.2	21	-5.9	5.2	13	62	83	311.6	3.4
13.05.22(T)	-2.7	12.2	21.8	-7.7	8	16.8	76	85	310.0	0.6
16.05.22	-4.9	14.6	27.6	-7.9	-11.4	3.6	15	79	313.7	2.0
17.05.22(T)	-7.3	14.2	26	-14.3	-2.8	10	31	81	312.5	1.6
18.05.22	-5.9	13.2	25.4	-10.9	-10.9	14.4	54	84	313.5	2.6
19.05.22(T)	-4.3	13	25	-11.3	3	10	51	84	314.3	3.5
20.05.22(T)	-7.3	12.8	24.2	-29.3	2.8	14.2	51	84	313.0	2.7
21.05.22(T)	-5.3	13.6	27	-8.9	3.6	7	51	-	309.8	-3.1
22.05.22	-8.3	11.8	25	-11.4	2.8	10	54	-	308.4	-2.2
23.05.22	-3.9	10.6	22.2	-51.9	3.6	10.2	62	-	306.1	-2.3

Table 2.2 00 UTC Sounding Data during TS and NTD days

Data	SLI	KI	CAPE	CIN	SWEAT	TTI	BRN	DCI	HI	BI	SI
16.04.22	-8.29	34.10	3232.04	-263.17	281.20	53	92.63	45.99	58	100.1	-2.91
17.04.22(T)	-7.26	36.50	2558.06	-292.37	275.40	52.6	61.57	43.66	46	100	-2.61
18.04.22	-6.70	27.10	3072.1	-206.38	164.19	48	96.25	40.9	68	99.3	0.11
19.04.22	-7.15	18.30	2293.18	-291.06	38.01	39.8	59.81	29.95	63	99.3	5.23
20.04.22	-7.17	32.70	2648.19	-249.61	317	53.4	43.6	45.17	49	99	-3.59
21.04.22(T)	-1.81	27.60	1030.54	-146.86	249.98	44.7	18.57	36.31	50.5	95.9	-1.06
22.04.22(T)	-4.75	41.80	2418.84	-74.17	273.99	50.6	52.23	44.35	15.9	98.5	-4.52
23.04.22	-4.36	34.80	2784.52	-129.71	179.41	42.8	56.14	37.76	34.3	101.1	2.53
28.04.22	-8.07	27.70	3480.92	-228.85	120.61	47.8	287.5	41.67	73	99.8	0.83
29.04.22(T)	-7.83	21.90	3262.42	-255.80	69.79	44	154.67	37.63	87	99.8	3.20
30.04.22	-5.62	34.90	476.78	-571.48	538.11	58.8	5.66	40.62	28.4	97	-5.69
01.05.22(T)	-4.11	28.90	226.53	-624.27	210.40	53.4	41.76	34.51	32.7	97.9	-1.86
02.05.22	-2.15	32.70	530.63	-74.03	192.99	46.6	13.56	32.95	25.8	98.9	-0.38
03.05.22(T)	-9.44	33.90	2521.08	-6.44	416.25	53	136.26	44.24	29	97.7	-2.93
04.05.22	9.57	33.90	0	0	193.81	45	0	23.23	36	96.7	1.04
12.05.22	-3.46	30.90	938.58	-32.41	225	41.8	50.01	37.46	17	96	2.05
13.05.22(T)	-3.89	37.10	1965.90	-17.62	410.35	44	97.38	42.49	14.2	97.2	-0.63
16.05.22	-4.47	10.10	1213.43	-294.36	231.45	41	35.42	35.67	53	97.1	4.62
17.05.22(T)	-8.28	26.30	2091.06	-135.39	365.44	50.6	84.83	44.28	40	96.7	-1.26
18.05.22	-7.31	36.70	2487.88	-2.94	403.56	51.6	311.25	47.11	40.1	97.7	-3.16
19.05.22(T)	-5.84	29.30	2717.73	-93.79	166.99	43.6	202.65	40.84	32	97.8	2.22
20.05.22(T)	-8.41	35.70	2479.43	-0.15	301.41	53	156.57	46.81	42	97.5	-3.87
21.05.22(T)	-3.02	29.30	501.94	-372.72	162.01	44.6	9.25	37.02	33.6	99.3	2.40
22.05.22	-4.55	34.30	428.34	-392.82	230.02	51.6	41.25	39.55	27.1	98.8	-1.78
23.05.22	-3.04	29.30	1049.66	-89.29	164.40	40.2	120.8	35.44	67	97.8	3.82

Table 2.3 12 UTC Sounding Data during TS and NTD days

Data	T_{500}	T_{700}	T_{850}	T_{d500}	T_{d700}	T_{d850}	R_{H700}	R_{H1000}	H_{700}	H_{1000}
16.04.22	-8.1	12.8	26.2	-35.1	-4.2	1.2	30	53	312	0.6
17.04.22(T)	-7.7	12.6	25.4	-39.7	-3.4	8.4	33	59	313.1	0.6
18.04.22	-6.5	11.6	27.4	-42.5	-2.4	-5.6	38	63	314.1	2.9
19.04.22	-8.5	12.8	25.6	-30.5	-7.2	11.6	24	56	315.4	4.0
20.04.22	-6.9	11.4	20.6	-35.9	-1.6	18	40	52	313.2	3.7
21.04.22(T)	-4.9	11.8	20.4	-38.9	0.8	16.4	47	59	313.5	3.7
22.04.22(T)	-5.9	12	22.4	-15.9	-3.0	15.4	35	52	313.6	3.4
23.04.22	-4.3	10	24.8	-41.3	5	1.8	71	31	314.6	3.3
28.04.22	-6.1	12.6	28	-43.1	-4.4	4	30	26	315.8	3.1
29.04.22(T)	-6.9	13.2	28.6	-53.9	-7.8	-4.4	22	53	314.4	1.3
30.04.22	-7.5	14	20.4	-44.5	-4.0	18	28	56	312.6	1.5
01.05.22(T)	-9.3	12.8	21.4	-18.3	0.8	13.4	60	63	311.4	1.3
02.05.22	-7.5	9	19	-13.5	-9.0	12	27	28	312.4	4.0
03.05.22(T)	-7.5	8.4	19.2	-12.5	6.1	16	85	70	311.5	4.3
04.05.22	-7.9	11.8	19.4	-24.9	0.8	17.1	47	22	313.1	4.3
12.05.22	-2.1	11.8	20.4	-7	9.9	17.8	88	59	309.6	0.6
13.05.22(T)	-0.9	13	22	-49.9	-2.0	19.3	35	-	309.1	-1.6
16.05.22	-4.5	14.6	25.4	-16.5	-1.4	14.4	33	-	312.4	0.1
17.05.22(T)	-4.9	12.8	24.6	-12.9	6.8	15.6	67	-	313.3	-0.4
18.05.22	-4.1	13.4	25	-11.1	-1.6	13	35	63	312.6	1.1
19.05.22(T)	-3.7	13.2	23.8	-11.7	1.2	18.8	44	71	312.1	0.6
20.05.22(T)	-2.3	13.2	22.8	-43.3	1.2	15.8	44	-	310.8	-0.8
21.05.22(T)	-	-	-	-	-	-	-	-	-	-
22.05.22	-6.3	11.8	23.8	-10.6	3.8	9.8	58	-	306.5	-3.5
23.05.22	-4.5	11	21	-24.5	3.0	17.2	58	-	307.6	-2.2

Table 2.4 12 UTC Sounding Data during TS and NTD days

Data	SLI	KI	CAPE	CIN	SWEAT	TTI	BRN	DCI	HI	BI	SI
16.04.22	-9.75	18.50	3710.68	-92.95	50.38	43.60	167.93	37.15	69	98.6	3.48
17.04.22(T)	-9.61	25.50	4175.20	-87.25	149.81	49.20	137.10	43.41	65	99.9	-0.19
18.04.22	-8.78	14.30	4645.42	-117.75	40	34.80	96.19	30.58	83	99.9	7.45
19.04.22	-9.43	25.70	3329.02	-143.80	54.20	299.18	62.22	46.63	56	98.6	-3.51
20.04.22	-7.84	32.50	3293.21	-11.57	321.98	52.40	29.47	46.44	44.6	98.1	-5.50
21.04.22(T)	-5.84	30.70	3249.63	-1.01	234.81	46.60	92.50	42.64	49	98	-1.84
22.04.22(T)	-7.37	28.70	3511.15	-29.01	252.78	49.60	51.30	45.17	32	98.2	-2.76
23.04.22	-1.62	25.90	1084.85	-31.34	51.59	35.20	39.83	28.22	65	101.3	7.71
28.04.22	-7.83	21.10	3728.91	-171.40	76.01	44.20	203.49	39.83	78	100.1	2.99
29.04.22(T)	-7.43	10.10	2508.69	-267.97	37	38	42.82	31.63	101	99.9	5.93
30.04.22	-7.28	27.90	1894.94	-157.79	346.02	53.40	45.56	45.68	57.4	97.1	-6.02
01.05.22(T)	-10.67	32.10	3126.71	-2.04	453.27	53.40	88.39	45.47	29	97.3	-3.89
02.05.22	0.37	20.50	74.01	-56.01	193.01	46	4.20	30.63	31	99.4	0.32
03.05.22(T)	-4.11	40.40	582.64	-96.43	272.99	50.20	12.97	39.31	10.5	98.8	-3.51
04.05.22	-3.93	33.40	619.32	-214.91	303.21	52.30	11.89	40.43	30.3	97	-5.09
12.05.22	-2.13	38.40	955.90	-13.92	376.30	42.40	62.90	40.33	9.4	97.2	-0.42
13.05.22(T)	-3.43	27.20	2777.81	-18.47	425	43.10	78.41	44.73	66.7	97.7	-1.38
16.05.22	-6.25	28.30	2451.0	-124.97	219.79	48.80	80.84	46.05	39	97.7	-1.76
17.05.22(T)	-7.25	39.10	2916.78	-81.91	251.22	50	82.53	47.45	23	100.9	-2.89
18.05.22	-6.28	27.10	2780.35	-69.41	205.01	46.20	81.57	44.28	34	98.1	0.01
19.05.22(T)	-7.42	34.30	4067.39	-35.66	292.61	50	179.60	50.02	25	98.3	-4.38
20.05.22(T)	-5.85	28.90	3846.89	0	245.60	43.20	60.49	44.45	60	98.4	0.29
21.05.22(T)	-	-	-	-	-	-	-	-	-	-	-
22.05.22	-4.72	31.90	866.88	-177.93	149.57	46.20	37.78	38.32	26.3	98.2	0.95
23.05.22	-5.97	34.70	2377.95	-1.09	247.41	47.20	89.78	44.17	31.8	98.8	-2.48

Table 2.5 42809 VECC Kolkata Observations (TS) at 00Z on 17 April 2022

PRES hPa	HGHT M	TEMP C	DWPT C	RELH %	MIXR g/kg	DRCT Deg	SKNT Knot	THTA k	THTE k	THTV K
1000.0	22	27.6	23.8	80	18.98	175	4	300.8	356.8	304.1
925.0	714	31.4	14.4	36	11.27	255	15	311.4	346.4	313.5
850.0	1466	25.2	11.2	41	9.92	255	21	312.5	343.5	314.4
700.0	3130	10.8	2.8	58	6.73	260	14	314.4	335.9	315.7
600	4388	-0.9	-5.4	72	4.29	275	19	315.0	329.0	315.9
500	5820	-8.1	-32.1	13	0.52	260	27	323.1	325.1	323.2
400	7520	-18.7	-47.7	6	0.13	260	41	330.6	331.1	330.6
300	9600	-32.7	-37.4	63	0.51	250	68	339.2	341.2	339.3
200	12360	-49.7	-69.7	8	0.02	265	58	353.9	354.0	353.9
100	16590	-77.1	-89.1	13	0.00	235	31	378.5	378.5	378.5

Table 2.6 42809 VECC Kolkata Observations (TS) at 12Z on 17 April 2022

PRES hPa	HGHT m	TEMP C	DWPT C	RELH %	MIXR g/kg	DRCT Deg	SKNT knot	THTA k	THTE K	THTV K
1000.0	17	32.8	23.8	59	18.98	180	6	305.9	363.3	309.4
925.0	714	25.4	22.7	85	19.20	185	10	305.3	363.0	308.8
850.0	1460	25.4	8.4	34	8.20	225	8	312.7	338.5	314.3
700.0	3131	12.6	-3.4	33	4.27	275	13	316.4	330.4	317.2
600	4395	0.6	-7.4	55	3.67	260	15	316.8	328.9	317.5
500	5830	-7.7	-39.7	6	0.24	280	29	323.6	324.6	323.6
400	7540	-18.7	-45.7	7	0.16	265	38	330.6	331.3	330.6
300	9620	-32.5	-36.0	71	0.59	255	66	339.4	341.8	339.6
200	12380	-49.3	-71.3	6	0.01	260	58	354.5	354.6	354.5
100	16610	-76.5	-89.5	11	0.00	265	31	379.7	379.7	379.7

Table 2.7 42809 VECC Kolkata Observations (TS) at 00Z on 21 April 2022

PRES hPa	HGHT M	TEMP C	DWPT C	RELH %	MIXR g/kg	DRCT Deg	SKNT knot	THTA k	THTE k	THTV K
1000.0	63	24.4	21.3	83	16.23	45	5	297.6	344.8	300.4
925.0	749	23.4	22.3	94	18.72	200	10	303.2	359.1	306.6
850.0	1485	18.0	16.5	91	14.09	220	11	305.0	347.3	307.6
700.0	3134	11.2	-0.8	43	5.18	310	27	314.9	331.6	315.8
600	4393	-0.5	-6.5	64	3.94	300	34	315.5	328.4	316.2
500	5840	-5.1	-42.1	4	0.19	325	30	326.8	327.5	326.8
400	7560	-16.7	-32.7	24	0.61	310	31	333.2	335.6	333.3
300	9650	-31.9	-47.9	19	0.17	275	60	340.3	341.0	340.3
200	12390	-52.9	-67.9	15	0.02	270	46	348.8	348.9	348.8
100	16600	-79.3	-89.3	18	0.0	260	13	374.3	374.3	374.3

Table 2.8 42809 VECC Kolkata Observations (TS) at 12Z on 21 April 2022

PRES hPa	HGHT M	TEMP C	DWPT C	RELH %	MIXR g/kg	DRCT Deg	SKNT knot	THTA k	THTE k	THTV K
1000.0	37	32.0	23.0	59	18.05	190	6	305.1	359.5	308.4
925.0	733	25.2	21.9	82	18.26	180	12	305.1	359.9	308.4
850.0	1472	20.4	16.4	78	14.00	205	8	307.5	350.0	310.1
700.0	3135	11.8	0.8	47	5.83	280	17	315.5	334.3	316.6
600	4402	4.2	-25.8	9	0.78	315	31	320.9	323.8	321.1
500	5860	-4.9	-38.9	5	0.26	310	22	327.0	328.1	327.1
400	7580	-17.5	-30.5	31	0.76	285	30	332.2	335.1	332.3
300	9670	-31.9	-45.9	24	0.21	275	53	340.3	341.2	340.3
200	12410	-51.7	-66.7	15	0.02	275	58	350.7	350.9	350.71
100	16620	-78.3	-89.3	16	0.00	270	16	376.2	376.2	376.2

Table 2.9 42809 VECC Kolkata Observations (TS) at 00Z on 22 April 2022

PRES hPa	HGHT M	TEMP C	DWPT C	RELH %	MIXR g/kg	DRCT Deg	SKNT knot	THTA k	THTE k	THTV k
1000.0	59	28	24	79	19.21	205	7	301.1	358	304.6
925.0	748	23.2	20.5	85	16.71	215	25	303	352.8	306.1
850.0	1486	21.6	18	80	15.53	245	7	308.8	356.1	311.6
700.0	3144	10	6.7	80	8.87	295	19	313.5	341.4	315.2
600	4409	1.6	-6.4	55	3.97	315	27	317.9	331	318.7
500	5860	-5.5	-14.5	49	2.50	300	12	326.3	335	326.8
400	7570	-18.5	-23.5	65	1.45	300	21	330.9	336.1	331.1
300	9650	-32.1	-34.9	76	0.66	240	44	340	342.6	340.1
200	12390	-50.7	-54.5	64	0.12	245	56	352.3	352.9	352.4
100	16600	-77.9	-81.5	56	0.01	275	9	377	377	377

Table 2.10 42809 VECC Kolkata Observations (TS) at 12Z on 22 April 2022

PRES hPa	HGHT M	TEMP C	DWPT C	RELH %	MIXR g/kg	DRCT Deg	SKNT knot	THTA k	THTE k	THTV K
1000.0	34	32.8	21.8	52	16.75	170	6	305.9	356.5	309
925.0	734	26.8	22.5	77	18.96	205	8	306.7	364.1	310.2
850.0	1477	22.4	15.4	65	13.11	290	11	309.6	349.8	312
700.0	3136	12	-3	35	4.40	300	18	315.7	330.1	316.6
600	4411	4.2	-6.8	45	3.85	265	15	320.9	333.8	321.7
500	5870	-5.9	-15.9	45	2.23	280	34	325.8	333.6	326.2
400	7580	-17.1	-22.1	65	1.64	255	46	332.7	338.7	333
300	9670	-31.5	-38.5	50	0.46	265	37	340.9	342.7	341
200	12420	-50.7	-64.7	17	0.03	265	49	352.3	352.5	352.3
100	16630	-80.1	-87.1	31	0.00	245	18	372.7	372.7	372.7

Table 2.11 42809 VECC Kolkata Observations (TS) at 00Z on 29 April 2022

PRES hPa	HGHT M	TEMP C	DWPT C	RELH %	MIXR g/kg	DRCT Deg	SKNT knot	THTA k	THTE k	THTV k
1000.0	50	28.2	25.2	84	20.69	170	4	301.4	362.7	305.1
925.0	745	30.2	15.2	40	11.88	230	10	310.2	346.8	312.4
850.0	1496	27.4	2.4	20	5.38	250	11	314.8	332.2	315.9
700.0	3166	11.8	-3.2	35	4.34	265	14	315.5	329.7	316.4
600	4457	1.6	-6.4	55	3.97	290	19	317.9	331	318.7
500	5930	-7.1	-54.1	1	0.05	285	19	324.3	324.5	324.3
400	7630	-19.7	-45.7	8	0.16	265	25	329.3	330	329.3
300	9700	-31.7	-50.7	14	0.12	255	60	340.6	341.1	340.6
200	12470	-49.7	-77.7	2	0.00	265	47	353.9	353.9	353.9
100	16710	-78.5	-90.5	13	0.00	245	17	375.8	375.8	375.8

Table 2.12 42809 VECC Kolkata Observations (TS) at 12Z on 29 April 2022

PRES hPa	HGHT M	TEMP C	DWPT C	RELH %	MIXR g/kg	DRCT Deg	SKNT knot	THTA k	THTE k	THTV K
1000.0	13	34.6	23.6	53	18.74	180	8	307.8	364.8	311.2
925.0	713	26.6	23.1	81	19.68	195	17	306.5	366.1	310.1
850.0	1468	28.6	-4.4	11	3.26	255	8	316.1	326.9	316.7
700.0	3144	13.2	-7.8	22	3.05	310	19	317.1	327.3	317.7
600	4414	1.0	-13.0	34	2.35	295	22	317.2	325.2	317.7
500	5860	-6.9	-53.9	1	0.05	285	21	324.6	324.8	324.6
400	7560	-19.9	-40.9	14	0.27	275	29	329.0	330.1	329.1
300	9660	-26.5	-64.5	1	0.02	285	39	347.9	348	347.9
200	12460	-48.7	-78.7	2	0.0	280	44	355.5	355.5	355.5
100	16690	-77.5	-92.5	8	0.0	295	18	377.7	377.7	377.7

Table 2.13 42809 VECC Kolkata Observations (TS) at 00Z on 01 May 2022

PRES hPa	HGHT M	TEMP C	DWPT C	RELH %	MIXR g/kg	DRCT Deg	SKNT knot	THTA k	THTE k	THTV k
1000.0	34	24.8	24.8	100	20.19	290	3	297.9	356.8	301.5
925.0	721	24.6	15.6	57	12.19	225	15	304.5	341.1	306.7
850.0	1464	24.2	6.2	31	7.04	240	8	311.5	333.6	312.8
700.0	3129	11.6	-1.4	40	4.96	310	8	315.3	331.4	316.2
600	4395	0.6	-3.0	77	5.14	300	20	316.8	333.5	317.8
500	5830	-11.5	-13.2	87	2.78	295	32	318.9	328.3	319.5
400	7520	-18.3	-40.3	13	0.29	255	31	331.1	332.3	331.2
300	96 40	-28.3	-60.3	3	0.04	255	44	345.4	345.6	345.4
200	12430	-49.5	-72.5	5	0.01	255	40	354.2	354.3	354.2
100	16660	-77.7	-87.7	19	0.00	310	4	377.4	377.4	377.4

Table 2.14 42809 VECC Kolkata Observations (TS) at 12Z on 01 May 2022

PRES hPa	HGHT M	TEMP C	DWPT C	RELH %	MIXR g/kg	DRCT Deg	SKNT knot	THTA k	THTE k	THTV K
1000.0	13	32.4	24.4	63	19.69	135	2	305.6	365	309.1
925.0	710	25.8	21.9	79	18.26	180	14	305.7	360.7	309
850.0	1450	21.4	13.4	60	11.49	225	19	308.6	343.7	310.7
700.0	3114	12.8	0.8	44	5.83	260	11	316.6	335.5	317.7
600	4383	1.0	-4.0	69	4.77	295	17	317.2	332.8	318.1
500	5820	-9.3	-18.3	48	1.82	295	24	321.6	328	322
400	7510	-17.3	-46.3	6	0.15	270	30	332.4	333	332.4
300	9640	-26.7	-64.7	1	0.02	265	52	347.6	347.7	347.6
200	12430	-48.9	-74.9	3	0.01	265	44	355.2	355.2	355.2
100	16660	-77.7	-89.7	13	0.00	280	18	377.4	377.4	377.4

Table 2.15 42809 VECC Kolkata Observations (TS) at 00Z on 03 May 2022

PRES hPa	HGHT M	TEMP C	DWPT C	RELH %	MIXR g/kg	DRCT Deg	SKNT knot	THTA k	THTE k	THTV K
1000.0	36	27.6	25.3	87	20.82	175	3	300.8	362.3	304.5
925.0	726	23.6	21.4	87	17.69	200	21	303.4	356.2	306.6
850.0	1465	23.4	11.4	47	10.05	205	17	310.6	341.8	312.5
700.0	3123	11	1	50	5.91	250	12	314.6	333.6	315.8
600	4385	1.2	-8.8	47	3.29	270	22	317.5	328.4	318.1
500	5820	-9.1	-16.1	57	2.19	275	23	321.9	329.5	322.3
400	7540	-15.3	-29.3	29	0.85	285	47	335	338.3	335.2
300	9660	-28.9	-49.9	11	0.13	265	63	344.5	345.1	344.6
200	12430	-50.5	-75.5	4	0.01	270	58	352.6	352.7	352.6
100	16670	-75.1	-88.1	12	0.00	305	22	382.4	382.4	382.4

Table 2.16 42809 VECC Kolkata Observations (TS) at 12Z on 03 May 2022

PRES hPa	HGHT M	TEMP C	DWPT C	RELH %	MIXR g/kg	DRCT Deg	SKNT knot	THTA k	THTE k	THTV K
1000.0	43	28.4	22.4	70	17.39	140	3	301.6	353	304.7
925.0	732	24.6	18.6	69	14.80	120	17	304.5	348.8	307.2
850.0	1468	19.2	16	82	13.64	140	15	306.2	347.4	308.8
700.0	3115	8.4	6.1	85	8.51	290	24	311.8	338.3	313.4
600	4378	1.4	-3.5	70	4.95	315	32	317.7	333.9	318.6
500	5820	-7.5	-12.5	67	2.94	310	27	323.8	333.9	324.4
400	7540	-14.5	-51.5	3	0.08	265	24	336.1	336.4	336.1
300	9660	-27.7	-50.7	9	0.12	260	62	346.2	346.8	346.2
200	12450	-49.7	-74.7	4	0.01	255	50	353.9	353.9	353.9
100	16680	-77.3	-92.3	8	0.00	335	26	378.1	378.1	378.1

Table 2.17 42809 VECC Kolkata Observations (TS) at 00Z on 13 May 2022

PRES hPa	HGHT M	TEMP C	DWPT C	RELH %	MIXR g/kg	DRCT Deg	SKNT knot	THTA k	THTE K	THTV K
1000.0	6	28.8	26	85	21.73	180	6	301.9	366.6	305.9
925.0	698	24.0	21.5	86	17.80	210	33	303.8	357	307.1
850.0	1437	21.8	16.8	73	14.37	220	31	309	352.9	311.6
700.0	3100	12.2	8.0	76	9.71	265	13	316.0	346.7	317.8
600	4375	4.2	0.6	77	6.71	270	15	320.9	342.8	322.2
500	5840	-2.7	-7.7	68	4.31	270	26	329.7	344.5	330.5
400	7580	-12.3	-27.3	27	1.02	265	27	338.9	342.9	339.1
300	9720	-26.1	-56.1	4	0.06	280	13	348.5	348.8	348.5
200	12520	-48.1	-65.1	12	0.03	20	13	356.4	356.6	356.4
100	16730	-79.7	-88.7	22	0.00	35	18	373.5	373.5	373.5

Table 2.18 42809 VECC Kolkata Observations (TS) at 12Z on 13 May 2022

PRES hPa	HGHT M	TEMP C	DWPT C	RELH %	MIXR g/kg	DRCT Deg	SKNT knot	THTA k	THTE K	THTV K
1000.0	-16									
998	6	32.8	25.8	67	21.51	225	8	306.1	371.3	310
925.0	682	25.8	22.3	81	18.72	190	25	305.7	362.1	309.1
850.0	1424	22	19.3	85	16.88	210	18	309.2	360.8	312.3
700.0	3091	13.0	-2.0	35	4.74	250	17	316.9	332.3	317.8
600	4373	6.2	-14.8	21	2.03	260	27	323.2	330.4	323.6
500	5850	-0.9	-49.9	1	0.08	265	30	331.9	332.2	331.9
400	7590	-12.5	-36.5	12	0.42	280	36	338.6	340.4	338.7
300	9720	-26.3	-43.3	19	0.28	275	17	348.2	349.4	348.3
200	12530	-48.5	-64.5	14	0.03	0	16	355.8	356	355.8
100	16750	-80.7	-83.8	60	0.0	40	22	371.6	371.6	371.6

Table 2.19 42809 VECC Kolkata Observations (TS) at 00Z on 17 May 2022

PRES hPa	HGHT M	TEMP C	DWPT C	RELH %	MIXR g/kg	DRCT Deg	SKNT knot	THTA k	THTE K	THTV K
1000.0	16	29.0	25.5	81	21.08	185	8	302.1	364.9	305.9
925.0	707	24	21.8	88	18.14	205	33	303.8	358.1	307.1
850.0	1451	26	10	37	9.15	225	26	313.4	342.1	315.1
700.0	3125	14.2	-2.8	31	4.47	260	16	318.2	332.9	319
600	4401	3.4	-7.6	44	3.62	275	18	320	332.1	320.7
500	5850	-7.3	-14.3	57	2.54	295	19	324.1	332.9	324.6
400	7570	-12.5	-30.5	21	0.76	290	22	338.6	341.6	338.8
300	9710	-26.5	-38.5	31	0.46	290	14	347.9	349.8	348
200	12510	-48.7	-57.7	34	0.08	130	6	355.5	355.9	355.5
100	16720	-81.1	-84.3	59	0.00	145	7	370.8	370.8	370.8

Table 2.20 42809 VECC Kolkata Observations (TS) at 12Z on 17 May 2022

PRES hPa	HGHT m	TEMP C	DWPT C	RELH %	MIXR g/kg	DRCT Deg	SKNT knot	THTA k	THTE K	THTV k
1000.0	-4									
999	6	34	25	59	20.46	180	6	307.2	369.4	311
925.0	695	26	22.8	83	19.32	195	17	305.9	364.2	309.4
850.0	1442	24.6	15.6	57	13.29	255	10	311.9	353	314.4
700.0	3113	12.8	6.8	67	8.93	300	11	316.6	345	318.3
600	4385	3.4	-4.6	56	4.55	265	19	320	335.1	320.9
500	5840	-4.9	-12.9	53	2.85	295	24	327	336.9	327.6
400	7580	-11.9	-25.9	30	1.16	260	25	339.4	343.9	339.7
300	9720	-28.1	-38.1	38	0.48	245	21	345.7	347.6	345.8
200	12510	-47.7	-64.7	12	0.03	215	17	357.1	357.2	357.1
100	16740	-79.9	-86.9	31	0.00	75	11	373.1	373.1	373.1

Table 2.21 42809 VECC Kolkata Observations (TS) at 00Z on 19 May 2022

PRES hPa	HGHT m	TEMP C	DWPT C	RELH %	MIXR g/kg	DRCT deg	SKNT knot	THTA k	THTE K	THTV k
1000.0	35	29	26.1	84	21.87	180	4	302.1	367.3	306.1
925.0	727	25.2	21.4	79	17.69	220	28	305.1	358.2	308.3
850.0	1471	25	10.0	39	9.15	245	13	312.3	340.9	314.0
700.0	3143	13	3.0	51	6.83	320	9	316.9	338.8	318.1
600	4411	2.4	-2.3	71	5.42	295	9	318.9	336.5	319.9
500	5860	-4.3	-11.3	58	3.24	270	21	327.7	339.0	328.4
400	7590	-12.7	-54.7	2	0.06	270	23	338.4	338.6	338.4
300	9720	-27.9	-62.9	2	0.03	265	17	345.9	346.1	345.9
200	12510	-49.7	-59.7	30	0.06	275	23	353.9	354.2	353.9
100	16740	-78.7	-84.7	37	0.00	145	9	375.4	375.4	375.4

Table 2.22 42809 VECC Kolkata Observations (TS) at 12Z on 19 May 2022

PRES hPa	HGHT m	TEMP C	DWPT C	RELH %	MIXR g/kg	DRCT deg	SKNT knot	THTA k	THTE k	THTV K
1000.0	6	33.4	27.4	71	23.67	180	8	306.6	378.6	310.9
925.0	702	26.0	23.1	84	19.68	185	18	305.9	365.3	309.5
850.0	1450	23.8	18.8	74	16.35	220	6	311.1	361.4	314.1
700.0	3121	13.2	1.2	44	6.00	240	7	317.1	336.5	318.2
600	4393	2.4	-5.6	56	4.22	270	8	318.9	332.8	319.7
500	5850	-3.7	-11.7	54	3.14	265	35	328.5	339.4	329.1
400	7570	-9.3	-40.3	6	0.29	275	32	342.8	344.0	342.9
300	9730	-26.1	-40.1	26	0.39	270	21	348.5	350.1	348.6
200	12530	-48.3	-62.3	18	0.04	270	27	356.1	356.3	356.1
100	16760	-79.5	-85.5	37	0.0	330	8	373.9	373.9	373.9

Table 2.23 42809 VECC Kolkata Observations (TS) at 00Z on 20 May 2022

PRES hPa	HGHT m	TEMP C	DWPT C	RELH %	MIXR g/kg	DRCT deg	SKNT knot	THTA k	THTE K	THTV K
1000.0	27	28.8	25.9	84	21.60	200	1	301.9	366.2	305.8
925.0	718	25.2	21.9	82	18.26	230	13	305.1	359.9	308.4
850.0	1463	24.2	14.2	54	12.12	250	16	311.5	349.0	313.8
700.0	3130	12.8	2.8	51	6.73	290	13	316.6	338.2	317.9
600	4398	2.2	-2.8	70	5.22	305	12	318.6	335.7	319.6
500	5840	-7.3	-29.3	15	0.68	320	19	324.1	326.6	324.2
400	7570	-12.5	-55.5	1	0.05	295	17	338.6	338.9	338.7
300	9710	-28.3	-61.3	3	0.03	275	19	345.4	345.5	345.4
200	12490	-49.3	-61.3	23	0.05	250	30	354.5	354.8	354.6
100	16720	-77.3	-85.3	27	0.00	235	6	378.1	378.1	378.1

Table 2.24 42809 VECC Kolkata Observations (TS) at 12Z on 20 May 2022

PRES hPa	HGHT m	TEMP C	DWPT C	RELH %	MIXR g/kg	DRCT deg	SKNT knot	THTA k	THTE K	THTV k
1000.0	-8									
999	6	34.8	25.8	60	21.49	180	4	308	373.7	312.0
925.0	694	26.8	23.0	80	19.56	185	14	306.7	365.9	310.3
850.0	1437	22.8	15.8	65	13.46	205	12	310.0	351.4	312.5
700.0	3108	13.2	1.2	44	6.00	305	24	317.1	336.5	318.2
600	4381	3.0	-13.0	30	2.35	330	32	319.5	327.6	320.0
500	5840	-2.3	-43.3	3	0.17	285	32	330.2	330.9	330.2
400	7570	-11.5	-50.5	2	0.09	255	19	339.9	340.4	340.0
300	9710	-26.5	-60.5	3	0.04	260	34	347.9	348.1	347.9
200	12510	-48.9	-68.9	8	0.02	240	38	355.2	355.3	355.2
100	16750	-78.1	-91.1	11	0.00	90	9	376.6	376.6	376.6

Table 2.25 42809 VECC Kolkata Observations (TS) at 00Z on 21 May 2022

PRES hPa	HGHT m	TEMP C	DWPT C	RELH %	MIXR g/kg	DRCT deg	SKNT knot	THTA k	THTE k	THTV K
1000.0	-31									
996	6	29.4	25.7	81	21.43	180	6	302.9	366.9	306.8
925.0	667	29.2	13.2	37	10.41	265	24	309.2	341.2	311.1
850.0	1421	27.0	7.0	28	7.44	280	27	314.4	338.1	315.8
700.0	3098	13.6	3.6	51	7.13	310	17	317.5	340.4	318.9
600	4370	3.0	-12.0	32	2.55	320	39	319.5	328.2	320.0
500	5820	-5.3	-8.9	76	3.92	295	24	326.5	339.9	327.3
400	7550	-14.1	-16.8	80	2.58	265	28	336.6	345.9	337.1
300	9680	-27.3	-30.5	74	1.01	275	23	346.8	350.8	347.0
200	12480	-48.3	-65.3	12	0.03	255	35	356.1	356.3	356.1
100	16700	-78.7	-83.1	49	0.00	355	12	375.4	375.4	375.4

Non-Thunderstorm Data

Table 2.26 42809 VECC Kolkata Observations (NTS) at 00Z on 16 April 2022

PRES hPa	HGHT m	TEMP C	DWPT C	RELH %	MIXR g/kg	DRCT deg	SKNT knot	THTA k	THTE K	THTV K
1000.0	11	27.8	25.8	89	21.47	180	6	300.9	364.5	304.8
925.0	707	32.0	16.0	38	12.51	235	20	312.0	350.9	314.4
850.0	1460	25.6	11.6	42	10.19	260	19	312.9	344.8	314.9
700.0	3126	11.4	0.4	47	5.66	260	16	315.1	333.3	316.1
600	4389	-0.3	-8.3	55	3.42	290	20	315.7	327	316.4
500	5830	-7.9	-40.9	5	0.22	260	24	323.3	324.2	323.4
400	7530	-18.3	-27.3	45	1.02	260	40	331.1	334.9	331.3
300	9620	-31.9	-36.9	61	0.54	245	58	340.3	342.5	340.4
200	12370	-51.5	-67.5	13	0.02	255	66	351.1	351.2	351.1
100	16590	-76.7	-86.7	19	0.00	265	40	379.3	379.3	379.3

Table 2.27 42809 VECC Kolkata Observations (NTS) at 12Z on 16 April 2022

PRES hPa	HGHT m	TEMP C	DWPT C	RELH %	MIXR g/kg	DRCT deg	SKNT knot	THTA k	THTE k	THTV K
1000.0	6	35.8	24.8	53	20.19	180	4	308.9	370.8	312.7
925.0	703	27.8	21.8	70	18.14	165	8	307.7	362.9	311.1
850.0	1452	26.2	1.2	20	4.93	345	3	313.6	329.5	314.5
700.0	3120	12.8	-4.2	30	4.02	280	14	316.6	329.9	317.4
600	4385	1.0	-8.0	51	3.51	260	22	317.2	328.9	317.9
500	5820	-8.1	-35.1	9	0.39	270	30	323.1	324.6	323.2
400	7520	-17.7	-37.7	16	0.37	255	42	331.9	333.4	332.0
300	9620	-30.5	-42.5	30	0.30	245	73	342.3	343.5	342.3
200	12380	-49.5	-69.5	8	0.02	260	64	354.2	354.3	354.2
100	16610	-77.3	-89.3	13	0.00	270	34	378.1	378.1	378.1

Table 2.28 42809 VECC Kolkata Observations (NTS) at 00Z on 18 April 2022

PRES hPa	HGHT m	TEMP C	DWPT C	RELH %	MIXR g/kg	DRCT deg	SKNT knot	THTA k	THTE k	THTV K
1000.0	44	27.4	24.8	86	20.19	170	3	300.6	360.1	304.2
925.0	735	29.2	18.2	52	14.43	250	18	309.2	353.3	311.8
850.0	1484	24.6	9.6	39	8.90	280	15	311.9	339.7	313.6
700.0	3149	11.2	-2.8	37	4.47	300	13	314.9	329.4	315.7
600	4407	-0.9	-6.9	64	3.82	285	15	315.0	327.5	315.8
500	5840	-6.9	-45.9	3	0.13	280	19	324.6	325.1	324.6
400	7540	-19.5	-51.5	4	0.08	260	22	329.6	329.9	329.6
300	9610	-34.3	-36.8	78	0.55	245	48	336.9	339.1	337
200	12370	-50.1	-73.1	5	0.01	260	48	353.3	353.3	353.3
100	16590	-78.3	-88.3	19	0.00	260	25	376.2	376.2	376.2

Table 2.29 42809 VECC Kolkata Observations (NTS) at 12Z on 18 April 2022

PRES hPa	HGHT m	TEMP C	DWPT C	RELH %	MIXR g/kg	DRCT deg	SKNT knot	THTA k	THTE k	THTV k
1000.0	29	33.0	25.0	63	20.44	170	5	306.1	368.0	309.9
925.0	727	25.8	23.0	85	19.56	185	11	305.7	364.7	309.2
850.0	1477	27.4	-5.6	11	2.98	285	9	314.8	324.7	315.4
700.0	3144	11.6	-2.4	38	4.60	310	20	315.3	330.3	316.2
600	4406	0.0	-16.0	29	1.84	325	20	316.1	322.4	316.4
500	5850	-6.5	-42.5	4	0.18	285	22	325.1	325.8	325.1
400	7550	-20.3	-53.3	4	0.07	270	22	328.5	328.8	328.5
300	9630	-32.3	-62.3	3	0.03	270	47	339.7	339.9	339.7
200	12390	-51.1	-75.1	4	0.01	265	55	351.7	351.7	351.7
100	16610	-77.1	-90.1	11	0.00	240	23	378.5	378.5	378.5

Table 2.30 42809 VECC Kolkata Observations (NTS) at 00Z on 19 April 2022

PRES hPa	HGHT m	TEMP C	DWPT C	RELH %	MIXR g/kg	DRCT deg	SKNT knot	THTA k	THTE k	THTV K
1000.0	64	27.0	23.9	83	19.09	140	6	300.1	356.4	303.6
925.0	753	28.0	15.0	45	11.72	210	17	307.9	343.7	310.1
850.0	1502	26.4	-3.6	14	3.46	230	12	313.8	325.2	314.4
700.0	3165	10.8	-2.2	40	4.67	255	10	314.4	329.5	315.3
600	4426	-0.9	-8.9	55	3.27	300	16	315.0	325.8	315.6
500	5860	-8.5	-28.5	18	0.73	310	14	322.6	325.3	322.8
400	7540	-21.5	-41.5	15	0.25	280	23	327.0	328.0	327.0
300	9630	-30.9	-61.9	3	0.03	265	63	341.7	341.9	341.7
200	12390	-50.7	-71.7	7	0.01	280	52	352.3	352.4	352.3
100	16600	-77.1	-89.1	13	0.00	290	27	378.5	378.5	378.5

Table 2.31 42809 VECC Kolkata Observations (NTS) at 12Z on 19 April 2022

PRES hPa	HGHT m	TEMP C	DWPT C	RELH %	MIXR g/kg	DRCT deg	SKNT knot	THTA k	THTE k	THTV K
1000.0	40	32.2	22.2	56	17.17	185	6	305.4	357.1	308.5
925.0	737	25.2	22.6	86	19.08	195	16	305.1	362.4	308.5
850.0	1482	25.6	11.6	42	10.19	265	15	312.9	344.8	314.9
700.0	3154	12.8	-7.2	24	3.20	300	19	316.6	327.3	317.2
600	4421	1.8	-11.2	37	2.72	320	27	318.2	327.3	318.7
500	5860	-8.5	-30.5	15	0.61	310	26	322.6	324.9	322.7
400	7560	-20.1	-45.1	9	0.17	300	23	328.8	329.5	328.8
300	9660	-29.5	-65.5	2	0.02	285	61	343.7	343.8	343.7
200	12420	-50.3	-71.3	7	0.01	275	43	352.9	353	353
100	16630	-77.9	-90.9	11	0.00	285	19	377	377	377

Table 2.32 42809 VECC Kolkata Observations (NTS) at 00Z on 20 April 2022

PRES hPa	HGHT m	TEMP C	DWPT C	RELH %	MIXR g/kg	DRCT deg	SKNT knot	THTA k	THTE k	THTV K
1000.0	47	27.8	24.6	83	19.94	190	7	300.9	359.9	304.5
925.0	737	28.4	15.4	45	12.03	215	30	308.3	345.1	310.6
850.0	1486	25.0	13.0	47	11.19	255	23	312.3	347.1	314.4
700.0	3151	11.4	-1.6	40	4.89	290	19	315.1	330.9	316
600	4410	-0.3	-7.3	59	3.70	295	34	315.7	327.9	316.4
500	5840	-7.7	-31.7	13	0.54	295	27	323.6	325.6	323.7
400	7540	-18.7	-46.7	7	0.14	305	51	330.6	331.2	330.6
300	9640	-32.3	-45.3	26	0.22	295	59	339.7	340.7	339.8
200	12400	-50.9	-69.9	9	0.02	280	48	352	352.1	352
100	16600	-78.3	-87.3	22	0.00	280	19	376.2	376.2	376.2

Table 2.33 42809 VECC Kolkata Observations (NTS) at 12Z on 20 April 2022

PRES hPa	HGHT m	TEMP C	DWPT C	RELH %	MIXR g/kg	DRCT deg	SKNT knot	THTA k	THTE k	THTV K
1000.0	37	31.8	20.8	52	15.73	140	6	304.9	352.2	307.8
925.0	732	25.2	22.5	85	18.96	150	11	305.1	362.1	308.5
850.0	1472	20.6	18.0	85	15.53	145	3	307.7	354.9	310.6
700.0	3132	11.4	-1.6	40	4.89	325	33	315.1	330.9	316.0
600	4397	1.4	-15.6	27	1.90	310	35	317.7	324.2	318.1
500	5840	-6.9	-35.9	8	0.36	320	32	324.6	325.9	324.6
400	7550	-15.5	-36.5	15	0.42	315	49	334.8	336.4	334.8
300	9650	-31.7	-44.7	26	0.24	290	62	340.6	341.6	340.6
200	12400	-51.9	-66.9	15	0.02	265	43	350.4	350.5	350.4
100	16620	-77.5	-87.5	19	0.00	265	20	377.7	377.8	377.7

Table 2.34 42809 VECC Kolkata Observations (NTS) at 00Z on 23 April 2022

PRES hPa	HGHT m	TEMP C	DWPT C	RELH %	MIXR g/kg	DRCT deg	SKNT knot	THTA k	THTE k	THTV K
1000.0	61	27	26	94	21.73	175	6	300.1	364.3	304
925.0	752	27.2	16.2	51	12.68	205	21	307.1	345.6	309.4
850.0	1497	23.2	10.2	44	9.27	265	16	310.4	339.2	312.2
700.0	3148	8.6	5.3	80	8.04	305	15	312	337.1	313.5
600	4407	1.6	-6.4	55	3.97	280	27	317.9	331	318.7
500	5860	-4.7	-22.7	23	1.24	270	25	327.2	331.8	327.5
400	7570	-18.1	-29.1	38	0.87	275	39	331.4	334.6	331.6
300	9660	-32.7	-39.7	50	0.41	250	49	339.2	340.8	339.2
200	12390	-51.3	-66.3	15	0.03	255	47	351.4	351.5	351.4
100	16600	-77.3	-87.3	19	0.00	245	32	378.1	378.1	378.1

Table 2.35 42809 VECC Kolkata Observations (NTS) at 12Z on 23 April 2022

PRES hPa	HGHT m	TEMP C	DWPT C	RELH %	MIXR g/kg	DRCT deg	SKNT knot	THTA k	THTE k	THTV K
1000.0	33	37	17	31	12.34	220	1	310.1	348.2	312.4
925.0	738	30.4	16.4	43	12.84	230	2	310.4	349.9	312.8
850.0	1487	24.8	1.8	22	5.15	160	2	312.1	328.6	313.1
700.0	3146	10	5	71	7.87	285	19	313.5	338.4	315
600	4406	2.2	-15.8	25	1.87	295	34	318.6	325.1	319
500	5860	-4.3	-41.3	4	021	270	26	327.7	328.6	327.8
400	7580	-18.1	-40.1	13	0.29	265	39	331.4	332.6	331.4
300	9670	-30.7	-44.7	24	0.24	265	66	342	343	342
200	12420	-51.7	-60.7	33	0.05	265	62	350.7	351.0	350.8
100	16630	-77.3	-86.3	23	0.00	270	17	378.1	378.1	378.1

Table 2.36 42809 VECC Kolkata Observations (NTS) at 00Z on 28 Apr 2022

PRES hPa	HGHT m	TEMP C	DWPT C	RELH %	MIXR g/kg	DRCT deg	SKNT knot	THTA k	THTE k	THTV K
1000.0	45	28.6	25.8	85	21.47	205	1	301.8	365.5	305.6
925.0	738	30.2	14.2	38	11.12	240	13	310.2	344.5	312.3
850.0	1490	26.8	6.8	28	7.34	270	8	314.2	337.5	315.6
700.0	3159	11.6	-1.4	40	4.96	285	9	315.3	331.4	316.2
600	4419	-0.7	-6.7	64	3.88	300	14	315.3	328.0	316.0
500	5860	-7.1	-47.1	2	0.11	300	23	324.3	324.8	324.3
400	7570	-18.5	-59.5	1	0.03	265	27	330.9	331	330.9
300	9650	-32.5	-40.5	45	0.37	245	58	339.4	341	339.5
200	12400	-50.5	-70.5	8	0.01	260	65	352.6	352.7	352.6
100	16640	-77.3	-93.3	6	0.00	300	21	378.1	378.1	378.1

Table 2.37 42809 VECC Kolkata Observations (NTS) at 12Z on 28 April 2022

PRES hPa	HGHT m	TEMP C	DWPT C	RELH %	MIXR g/kg	DRCT deg	SKNT knot	THTA k	THTE k	THTV K
1000.0	31	34.2	12.2	26	9.0	220	6	307.4	335	309
925.0	733	27.8	24.1	80	20.95	180	10	307.7	371.5	311.6
850.0	1485	28	4	22	6.03	250	6	315.5	334.9	316.6
700.0	3158	12.6	-4.4	30	3.96	290	14	316.4	329.4	317.2
600	4423	1.6	-19.4	19	1.38	310	15	317.9	322.8	318.2
500	5870	-6.1	-43.1	4	0.17	285	16	325.5	326.2	325.6
400	7570	-18.9	-43.9	9	0.20	280	25	330.3	331.1	330.4
300	9660	-31.5	-49.5	15	0.14	250	58	340.9	341.5	340.9
200	12420	-49.1	-77.1	2	0.01	270	49	354.9	354.9	354.9
100	16670	-76.3	-95.3	4	0.00	345	17	380.1	380.1	380.1

Table 2.38 42809 VECC Kolkata Observations (NTS) at 00Z on 30 April 2022

PRES hPa	HGHT m	TEMP C	DWPT C	RELH %	MIXR g/kg	DRCT deg	SKNT knot	THTA k	THTE k	THTV K
1000.0	47	25.6	18.6	65	13.67	115	7	298.8	338.8	301.2
925.0	735	24.4	20.2	77	16.40	130	16	304.2	353.3	307.2
850.0	1476	24	11	44	9.79	220	18	311.3	341.7	313.1
700.0	3141	12.4	0.4	44	5.66	250	19	316.2	334.5	317.3
600	4408	1.4	-7.6	51	3.62	280	23	317.7	329.7	318.4
500	5840	-11.9	-15.3	76	2.34	300	26	318.5	326.4	318.9
400	7530	-19.7	-45.7	8	0.16	275	22	329.3	330	329.3
300	9640	-27.5	-59.5	3	0.04	260	42	346.5	346.7	346.5
200	12430	-48.7	-77.7	2	0.0	275	37	355.5	355.5	355.5
100	16650	-76.9	-90.9	9	00	345	32	378.9	378.9	378.9

Table 2.39 42809 VECC Kolkata Observations (NTS) at 12Z on 30 Apr 2022

PRES hPa	HGHT m	TEMP C	DWPT C	RELH %	MIXR g/kg	DRCT deg	SKNT knot	THTA k	THTE k	THTV K
1000.0	15	33.2	23.2	56	18.28	180	6	306.4	361.6	309.7
925.0	712	25.4	22.4	83	18.84	160	13	305.3	361.9	308.7
850.0	1451	20.4	18	86	15.53	210	10	307.5	354.6	310.4
700.0	3126	14	-4	28	4.08	285	16	318	331.4	318.7
600	4400	2	-7	51	3.79	280	19	318.4	331	319.1
500	5840	-7.5	-44.5	3	0.15	285	22	323.8	324.4	323.9
400	7530	-18.1	-46.1	7	0.15	285	26	331.4	332	331.4
300	9660	-27.9	-62.9	2	0.03	280	39	345.9	346.1	345.9
200	12450	-48.7	-75.7	3	0.01	265	37	355.5	355.5	355.5
100	16690	-76.3	-90.3	10	0.00	10	11	380.1	380.1	380.1

Table 2.40 42809 VECC Kolkata Observations (NTS) at 00Z on 02 May 2022

PRES hPa	HGHT m	TEMP C	DWPT C	RELH %	MIXR g/kg	DRCT deg	SKNT knot	THTA k	THTE k	THTV K
1000.0	41	22.8	20.1	85	15.05	65	1	295.9	339.4	298.6
925.0	728	27.4	10.4	35	8.63	195	13	307.3	333.8	308.9
850.0	1469	22	8	41	7.98	170	9	309.2	333.9	310.7
700.0	3126	11	1	50	5.91	265	16	314.6	333.6	315.8
600	4391	1.6	-9.4	44	3.14	305	24	317.9	328.4	318.5
500	5830	-9.9	-12.3	83	2.99	265	34	320.9	331	321.5
400	7530	-16.1	-18.6	81	2.22	270	19	334	342	334.4
300	9640	-30.7	-37.7	50	0.50	280	39	342	344	342.1
200	12400	-49.3	-55.3	49	0.11	255	45	354.5	355	354.6
100	16650	-77.1	-79.5	69	0.01	320	16	378.5	378.6	378.5

Table 2.41 42809 VECC Kolkata Observations (NTS) at 12Z on 02 May 2022

PRES hPa	HGHT m	TEMP C	DWPT C	RELH %	MIXR g/kg	DRCT deg	SKNT knot	THTA k	THTE k	THTV K
1000.0	20	32	22	56	16.96	130	4	305.1	356.2	308.2
925.0	715	25.2	21.2	79	17.47	130	9	305.1	357.6	308.2
850.0	1454	21.0	16	73	13.64	195	12	308.1	349.7	310.6
700.0	3114	12.2	2.2	50	6.45	270	18	316	336.7	317.2
600	4380	1.8	-7.2	51	3.73	270	17	318.2	330.5	318.9
500	5820	-7.9	-12.9	67	2.85	290	30	323.3	333.1	323.9
400	7530	-16.1	-35.1	18	0.49	265	33	334	335.9	334.1
300	9660	-28.7	-50.7	10	0.12	260	54	344.8	345.4	344.8
200	12430	-49.7	-67.7	10	0.02	265	51	353.9	354	353.9
100	16660	-75.7	-86.7	17	0.00	265	22	381.2	381.2	381.2

Table 2.42 42809 VECC Kolkata Observations at 00Z on 04 May 2022

PRES hPa	HGHT m	TEMP C	DWPT C	RELH %	MIXR g/kg	DRCT deg	SKNT knot	THTA k	THTE k	THTV K
1000.0	54	22.6	-13.4	8	1.37	65	1	295.8	300.1	296
925.0	735	22.2	17.4	74	13.70	235	8	302	342.7	304.5
850.0	1472	21.4	11.4	53	10.05	230	24	308.6	339.4	310.4
700.0	3125	10.4	5.4	71	8.1	325	15	314	339.5	315.5
600	4386	0.4	-7.6	55	3.62	325	39	316.5	328.5	317.2
500	5830	-6.1	-27.1	17	0.83	320	9	325.5	328.6	325.7
400	7540	-17.1	-23.1	60	1.50	275	33	332.7	338.2	333
300	9650	-28.9	-42.9	25	0.29	255	54	344.5	345.8	344.6
200	12430	-48.7	-70.7	6	0.01	270	55	355.5	355.6	355.5
100	16670	-76.9	-91.9	8	0.00	255	4	378.9	378.9	378.9

Table 2.43 42809 VECC Kolkata Observations (NTS) at 12Z on 04 May 2022

PRES hPa	HGHT m	TEMP C	DWPT C	RELH %	MIXR g/kg	DRCT deg	SKNT knot	THTA k	THTE K	THTV K
1000.0	43	31.2	7.2	22	6.41	85	4	304.4	324	305.5
925.0	737	25.2	20.8	77	17.03	140	7	305.1	356.2	308.2
850.0	1475	19.4	17.1	87	14.65	225	8	306.4	350.7	309.1
700.0	3131	11.8	0.8	47	5.83	305	22	315.5	334.3	316.6
600	4396	1	-17	25	1.69	315	29	317.2	323.1	317.6
500	5840	-7.9	-24.9	24	1.02	295	16	323.3	327.1	323.5
400	7540	-17.1	-58.1	2	0.04	300	30	332.7	332.8	332.7
300	9660	-27.5	-64.5	2	0.02	295	44	346.5	346.6	346.5
200	12460	-47.9	-78.9	2	0.0	305	44	356.8	356.8	356.8
100	16700	-77.1	-91.1	9	0.0	320	17	378.5	378.5	378.5

Table 2.44 42809 VECC Kolkata Observations (NTS) at 00Z on 12 May 2022

PRES hPa	HGHT m	TEMP C	DWPT C	RELH %	MIXR g/kg	DRCT deg	SKNT knot	THTA k	THTE k	THTV k
1000.0	34	27.6	24.5	83	19.82	170	1	300.8	359.3	304.3
925.0	724	24.2	20.5	80	16.71	215	21	304.1	354	307.1
850.0	1461	21	13	60	11.19	220	27	308.1	342.3	310.2
700.0	3116	12.2	5.2	62	7.98	235	15	316	341.4	317.5
600	4393	4.8	-0.2	70	6.33	250	13	321.6	342.4	322.9
500	5860	-3.9	-5.9	86	4.95	275	15	328.2	345.1	329.2
400	7590	-11.3	-43.3	5	0.21	285	23	340.2	341.1	340.3
300	9720	-26.5	-46.5	13	0.20	305	20	347.9	348.8	348
200	12520	-48.3	-79.3	2	0.0	350	16	356.1	356.1	356.1
100	16750	-77.9	-90.9	11	0.0	55	17	377	377	377

Table 2.45 42809 VECC Kolkata Observations (NTS) at 12Z on 12 May 2022

PRES hPa	HGHT m	TEMP C	DWPT C	RELH %	MIXR g/kg	DRCT deg	SKNT knot	THTA k	THTE K	THTV k
1000.0	6	32.8	23.8	59	18.98	225	8	305.9	363.3	309.4
925.0	699	25.6	20.9	75	17.14	205	18	305.5	357.1	308.6
850.0	1439	20.4	17.8	85	15.33	215	21	307.5	354	310.3
700.0	3096	11.8	9.9	88	11.06	240	20	315.5	350.3	317.6
600	4377	6.2	1.2	70	7.01	255	21	323.2	346.3	324.6
500	5850	-2.1	-7	69	4.55	250	24	330.4	346.1	331.3
400	7590	-12.1	-40.1	8	0.29	285	23	339.2	340.4	339.2
300	9720	-25.7	-59.7	3	0.04	320	18	349.0	349.2	349.1
200	12530	-47.9	-69.9	6	0.02	350	15	356.8	356.8	356.8
100	16760	-77.9	-89.9	13	00	30	22	377	377	377

Table 2.46 42809 VECC Kolkata Observations (NTS) at 00Z on 16 May 2022

PRES hPa	HGHT m	TEMP C	DWPT C	RELH %	MIXR g/kg	DRCT deg	SKNT knot	THTA k	THTE k	THTV k
1000.0	20	28	24	79	19.21	180	1	301.1	358	304.6
925.0	711	24.2	21.6	85	17.91	215	32	304.1	357.6	307.3
850.0	1457	27.6	3.6	21	5.86	230	17	315	333.9	316.2
700.0	3137	14.6	-11.4	15	2.30	315	4	318.6	326.5	319.1
600	4412	3	-10	38	3	330	25	319.5	329.7	320.1
500	5860	-4.9	-7.9	79	4.24	290	21	327	341.5	327.8
400	7590	-13.1	-16.2	78	2.72	265	15	337.9	347.7	338.4
300	9730	-26.9	-37.9	35	0.49	205	10	347.4	349.4	347.5
200	12520	-49.1	-52.8	65	0.14	270	8	354.9	355.5	354.9
100	16730	-81.9	-83.1	82	0.00	80	6	369.2	369.3	369.2

Table 2.47 42809 VECC Kolkata Observations (NTS) at 12Z on 16 May 2022

PRES hPa	HGHT m	TEMP C	DWPT C	RELH %	MIXR g/kg	DRCT deg	SKNT knot	THTA k	THTE k	THTV K
1000.0	1									
999	6	34	26	63	21.76	180	8	307.2	373.5	311.2
925.0	699	25.8	22.7	83	19.20	185	20	305.7	363.6	309.2
850.0	1445	25.4	14.4	51	12.28	230	15	312.7	350.9	315.1
700.0	3124	14.6	-1.4	33	4.96	260	12	318.6	334.9	319.6
600	4400	3.6	-13.4	28	2.28	325	20	320.2	328.1	320.7
500	5850	-4.5	-16.5	39	2.12	285	17	327.5	335	327.9
400	7590	-12.3	-19.3	56	2.09	255	21	338.9	346.6	339.3
300	9730	-26.7	-36.7	38	0.55	260	17	347.6	349.9	347.8
200	12530	-49.1	-60.1	27	0.06	255	11	354.9	355.1	354.9
100	16740	-80.3	-85.1	45	0.0	30	24	372.3	372.4	372.3

Table 2.48 42809 VECC Kolkata Observations (NTS) at 00Z on 18 May 2022

PRES hPa	HGHT m	TEMP C	DWPT C	RELH %	MIXR g/kg	DRCT deg	SKNT knot	THTA k	THTE k	THTV K
1000.0	26	29	26	84	21.73	185	6	302.1	366.9	306.1
925.0	717	24	22	89	18.37	215	29	303.8	358.8	307.2
850.0	1460	25.4	14.4	51	12.28	200	17	312.7	350.9	315.1
700.0	3135	13.2	4.2	54	7.44	245	6	317.1	340.9	318.5
600	4409	3.2	-3.8	60	4.84	275	13	319.8	335.7	320.7
500	5860	-5.9	-10.9	68	3.35	250	24	325.8	337.3	326.4
400	7580	-13.7	-35.7	14	0.46	265	25	337.1	338.9	337.2
300	9710	-27.1	-49.1	11	0.15	265	25	347.1	347.7	347.1
200	12500	-49.5	-57.5	39	0.08	205	14	354.2	354.6	354.2
100	16730	-78.9	-85.9	31	0.0	95	10	375	375.1	375

Table 2.49 42809 VECC Kolkata Observations (NTS) at 12Z on 18 May 2022

PRES hPa	HGHT m	TEMP C	DWPT C	RELH %	MIXR g/kg	DRCT deg	SKNT knot	THTA k	THTE K	THTV K
1000.0	11	33.4	25.4	63	20.95	180	6	306.6	370.1	310.4
925.0	709	25.6	22.8	85	19.32	190	16	305.5	363.7	309
850.0	1453	25	13	47	11.19	230	12	312.3	347.1	314.4
700.0	3126	13.4	-1.6	35	4.89	300	13	317.3	333.2	318.2
600	4398	2.6	-4.4	60	4.62	265	14	319.1	334.3	320
500	5850	-4.1	-11.1	58	3.29	265	25	328	339.4	328.6
400	7590	-12.5	-22.5	43	1.58	240	21	338.6	344.6	339
300	9720	-27.5	-42.5	23	0.30	265	20	346.5	347.8	346.6
200	12510	-48.1	-59.1	27	0.07	245	32	356.4	356.8	356.4
100	16750	-79.3	-87.3	26	0.00	195	3	374.3	374.3	374.3

Table 2.50 42809 VECC Kolkata Observations (NTS) at 00Z on 22 May 2022

PRES hPa	HGHT m	TEMP C	DWPT C	RELH %	MIXR g/kg	DRCT deg	SKNT knot	THTA k	THTE K	THTV K
1000.0	-22									
997	6	26.2	22	78	17.01	0	0	299.6	349.5	302.6
925.0	671	28.6	14.6	42	11.42	225	25	308.6	343.5	310.7
850.0	1419	25	10	39	9.15	265	20	312.3	340.9	314
700.0	3084	11.8	2.8	54	6.73	275	8	315.5	337.1	316.8
600	4355	2.6	-5.4	56	4.29	315	8	319.1	333.2	319.9
500	5800	-8.3	-11.4	78	3.22	315	18	322.9	333.8	323.5
400	7510	-15.1	-17.1	85	2.52	235	29	335.3	344.4	335.8
300	9640	-26.3	-59.3	3	0.04	275	36	348.2	348.4	348.2
200	12430	-49.1	-65.1	14	0.03	255	29	354.9	355	354.9
100	16670	-75.5	-79	58	0.01	250	2	381.6	381.6	381.6

Table 2.51 42809 VECC Kolkata Observations (NTS) at 12Z on 22 May 2022

PRES hPa	HGHT m	TEMP C	DWPT C	RELH %	MIXR g/kg	DRCT deg	SKNT knot	THTA k	THTE k	THTV K
1000.0	-25									
996	6	31	23	62	18.13	0	0	304.5	358.9	307.8
925.0	659	27.2	16.2	51	12.68	30	3	307.1	345.6	309.4
850.0	1402	23.8	9.8	41	9.02	210	3	311.1	339.1	312.8
700.0	3065	11.8	3.8	58	7.23	255	14	315.5	338.6	316.9
600	4337	3.0	-5.0	56	4.42	220	12	319.5	334.2	320.4
500	5790	-6.3	-10.6	72	3.43	270	26	325.3	337	326
400	7510	-14.7	-15.9	91	2.78	220	28	335.8	345.8	336.4
300	9630	-25.7	-44.7	15	0.24	250	41	349	350.1	349.1
200	12440	-47.9	-65.9	11	0.03	225	38	356.8	356.9	356.8
100	16680	-77.5	-82.5	45	0.00	110	7	377.7	377.8	377.7

Table 2.52 42809 VECC Kolkata Observations (NTS) at 00Z on 23 May 2022

PRES hPa	HGHT m	TEMP C	DWPT C	RELH %	MIXR g/kg	DRCT deg	SKNT knot	THTA k	THTE k	THTV K
1000.0	-23									
997	6	25.8	24.3	91	19.63	0	0	299.2	356.8	302.7
925.0	665	24.2	18.2	69	14.43	225	15	304.1	347.2	306.7
850.0	1405	22.2	10.2	46	9.27	225	13	309.4	338	311.1
700.0	3061	10.6	3.6	62	7.13	275	13	314.2	336.8	315.5
600	4326	1.2	-6.8	55	3.85	280	8	317.5	330.2	318.2
500	5780	-3.9	-51.9	1	0.06	310	16	328.2	328.5	328.2
400	7500	-13.5	-22.5	47	1.58	270	21	337.4	343.2	337.7
300	9650	-26.5	-37.5	35	0.51	245	16	347.9	350	348
200	12450	-48.9	-59.9	27	0.06	225	43	355.2	355.4	355.2
100	16660	-79.1	-83.6	48	0.0	170	5	374.6	374.7	374.6

Table 2.53 42809 VECC Kolkata Observations (NTS) at 12Z on 23 May 2022

PRES hPa	HGHT m	TEMP C	DWPT C	RELH %	MIXR g/kg	DRCT deg	SKNT knot	THTA k	THTE k	THTV k
1000.0	-22									
997	6	34.2	25.2	60	20.75	135	4	307.6	370.8	311.4
925.0	678	27	22	74	18.37	155	9	306.9	362.6	310.3
850.0	1420	21	17.2	79	14.75	170	12	308.1	353	310.9
700.0	3076	11	3	58	6.83	300	17	314.6	336.4	315.9
600	4344	4	-9.0	38	3.24	295	22	320.7	331.6	321.3
500	5800	-4.5	-24.5	19	1.06	270	17	327.5	331.4	327.7
400	7530	-13.1	-34.1	15	0.54	315	12	337.9	340	338
300	9670	-26.9	-54.9	5	0.07	215	23	347.4	347.7	347.4
200	12470	-47.7	-67.7	8	0.02	210	33	357.1	357.2	357.1
100	16700	-78.5	-87.5	22	0.0	160	21	375.8	375.8	375.8

Chapter - 3

Observation based studies with the help of Skew T– Log P diagram and Parameters of thunderstorm and non -thunderstorm days over Kolkata region, West Bengal

Skew-T Parameters

The Skew-T Log-P offers an almost instantaneous snapshot of the atmosphere from the surface to about the 100 millibar level. The advantages and disadvantages of the Skew-T are given below:

Advantages of Skew-T Log-P diagrams

1. Can assess the stability of the atmosphere.

2. Can see weather elements at every layer in the atmosphere.

3. Determine cap strength, convective temperature, forecasting temperatures.

4. Determine character of severe weather.

5. This is the data used to produce the synoptic scale forecast models.

Disadvantages of the Skew-T Log-P diagrams

1. Available generally twice a day (00Z and 12Z), character of weather can change dramatically between soundings.

2. Sounding does not give a true vertical dimension since wind blows balloon downstream.

3. Sounding does not give true instantaneous measurements since it takes several minutes to travel from the surface to the upper troposphere.

Below are all the basics lines that make up the Skew-T Log-P diagrams in **Figure 3.1**

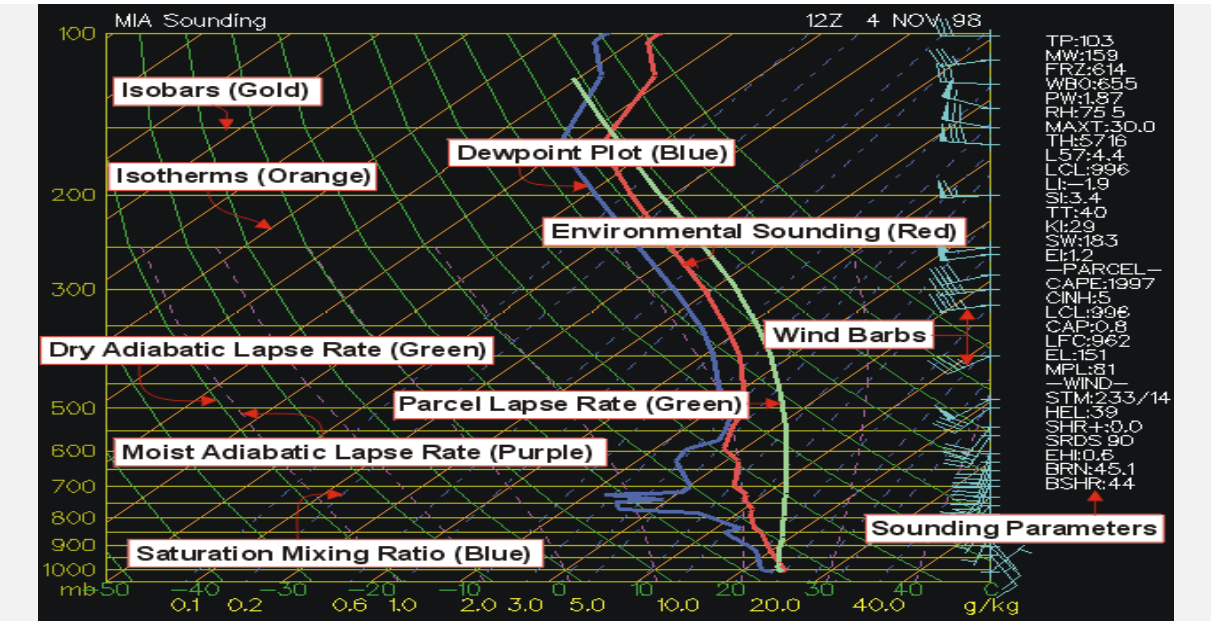

Figure 3.1 Skew-T Log-P diagrams

Isobars - Lines of equal pressure. They run horizontally from left to right and are labelled on the left side of the diagram. Pressure is given in increments of 100 mb and ranges from 1050 to 100 mb. Notice the spacing between isobars increases in the vertical (thus the name Log P).

Isotherms - Lines of equal temperature. They run from the southwest to the northeast (thus the name skew) across the diagram and are SOLID. Increments are given for every 10 degrees in units of Celsius. They are labelled at the bottom of the diagram.

Saturation mixing ratio lines - Lines of equal mixing ratio (mass of water vapour divided by mass of dry air -- grams per kilogram). These lines run from the southwest to the northeast and are DASHED. They are labelled on the bottom of the diagram.

Wind barbs - Wind speed and direction given for each plotted barb. Plotted on the right of the diagram.

Dry adiabatic lapse rate - Rate of cooling (10 degrees Celsius per kilometre) of a rising unsaturated parcel of air. These lines slope from the southeast to the northwest and are SOLID. Lines gradually arc to the North with height.

Moist adiabatic lapse rate - Rate of cooling (depends on moisture content of air) of a rising saturated parcel of air. These lines slope from the south toward the northwest. The MALR increases with height since cold air has less moisture content that warm air.

Environmental sounding - Same as the actual measured temperatures in the atmosphere. This is the jagged line running south to north on the diagram. This line is always to the right of the dew point plot.

Dew point plot - This is the jagged line running south to north. It is the vertical plot of dew point temperature. This line is always to the left of the environmental sounding.

Parcel lapse rate - The temperature path a parcel would take if raised from the Planetary Boundary Layer. The lapse rate follows the DALR until saturation, then follows the MALR. This line is used to calculate the LI, CAPE, CINH, and other thermodynamic indices.

Below shows thermodynamic diagram area proportional to energy vertical profiles of the troposphere and stratosphere in **Figure 3.2.**

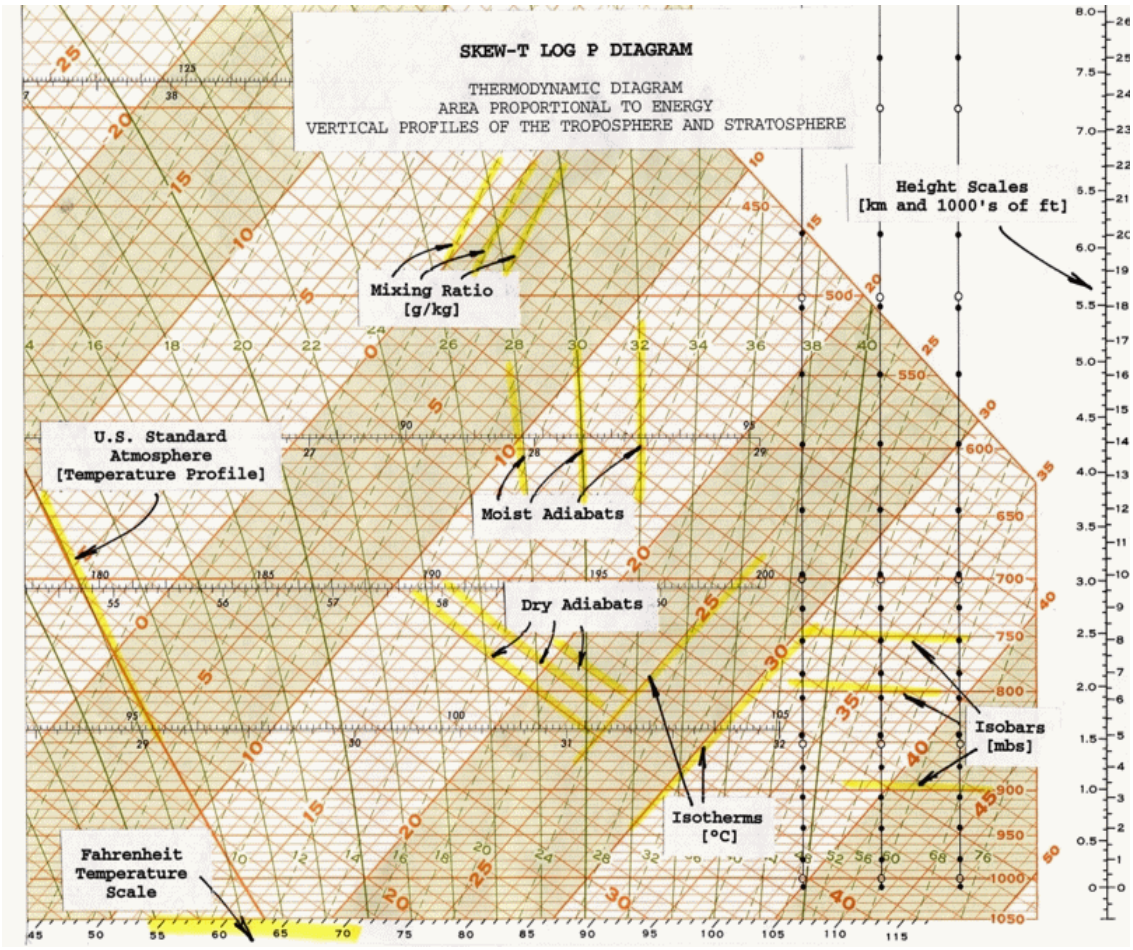

Figure 3.2 thermodynamic diagram area proportional to energy vertical profiles of the troposphere and stratosphere

Skew-T Derived Parameters

This section interprets most of those values and gives operational significance to the values. Each parameter or indices will be broken down one by one. In a severe weather situations and during inclement weather, these indices come in handy. The indices should be used as guides. Often, indices will contradict each other and can change rapidly in the course of a couple of hours. An experienced meteorologist is well informed to how a sounding will change throughout the day and why some sounding indices are better than others in certain situations. Soundings are most notably changed through thermal advection, moisture advection, and evaporational cooling. Modified soundings should be studied along with the standard 12Z and 00Z sounding.

Below shows CAPE and CIN in **Figure 3.3**

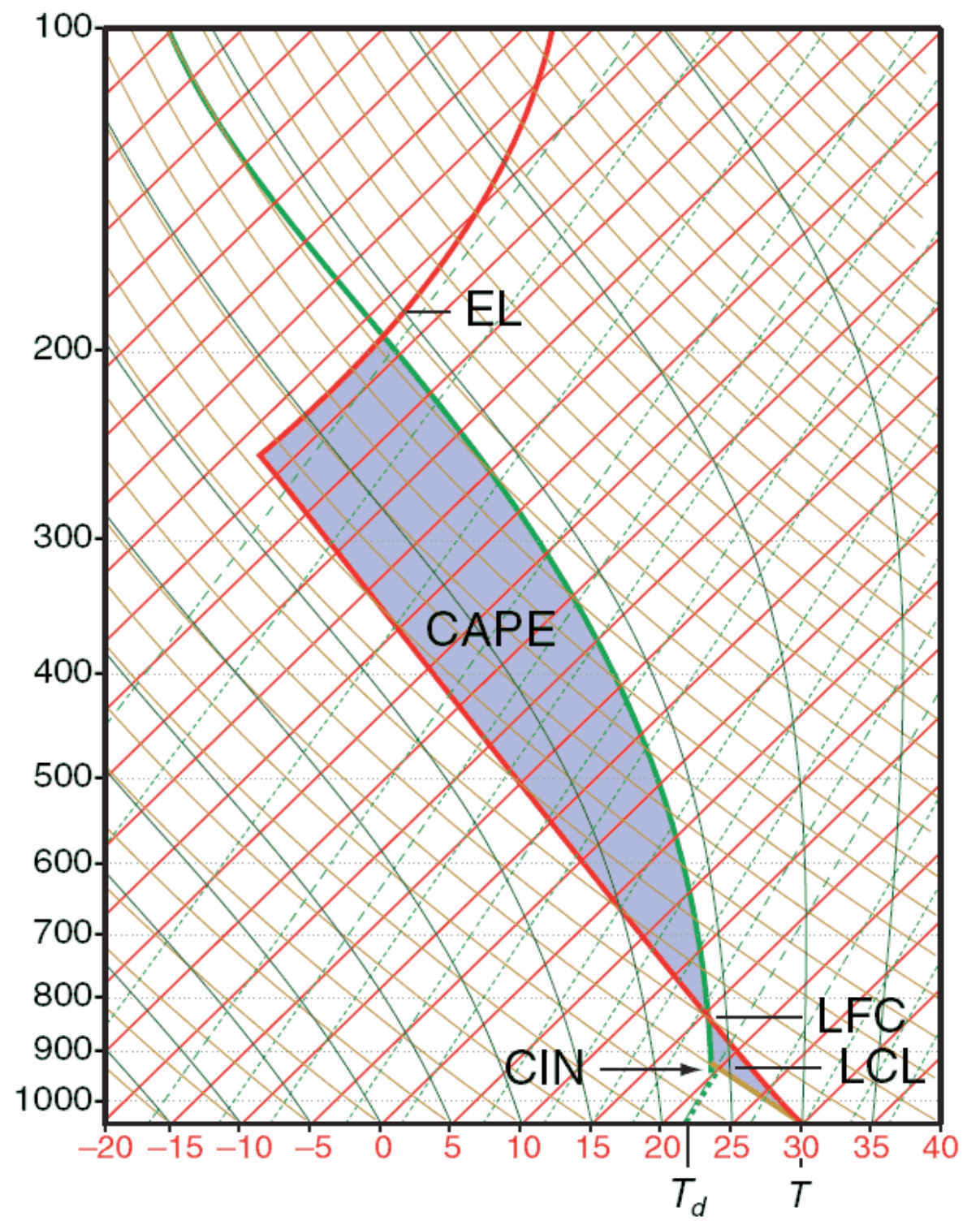

Figure 3.3 represents CAPE and CIN

Below shows EL, LFC, LCL in **Figure 3.4**

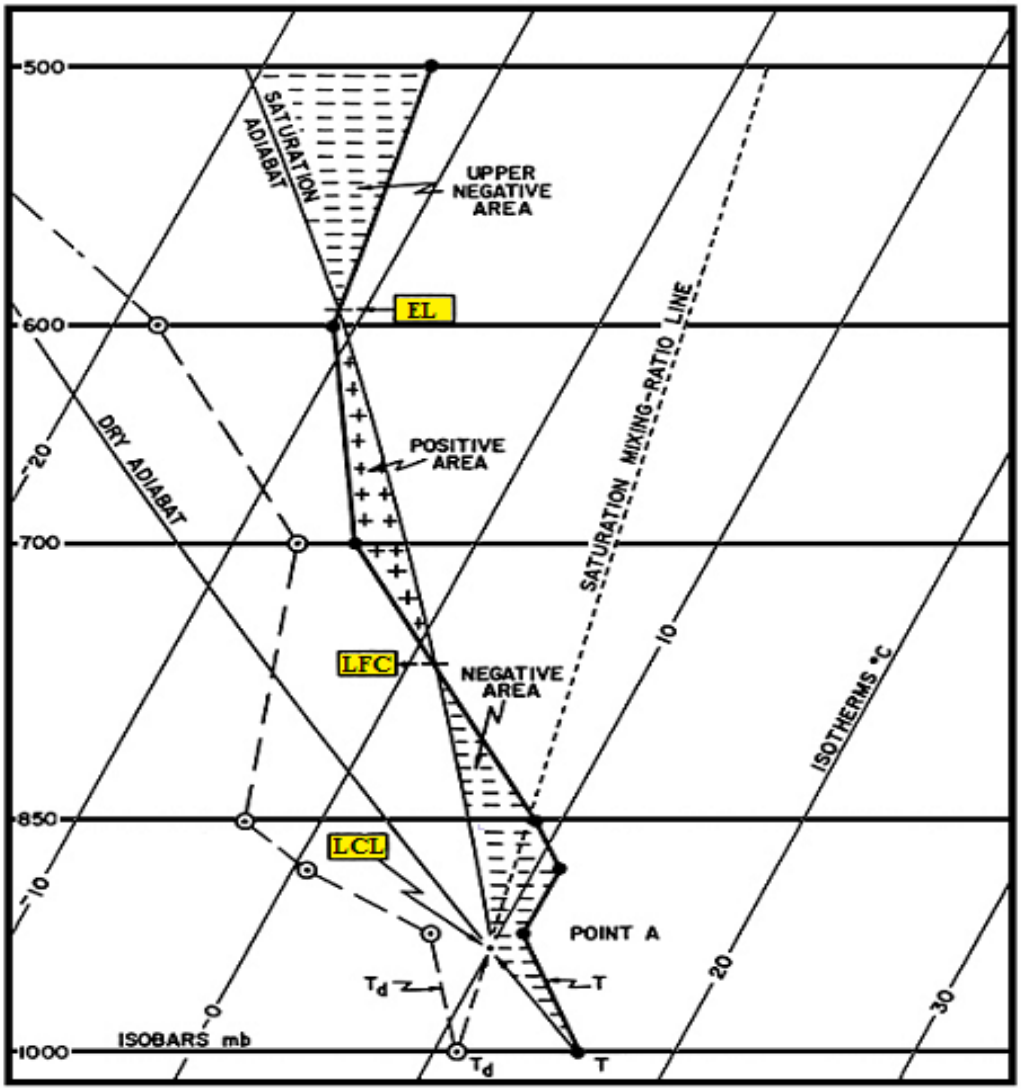

Figure 3.4 represents EL, LFC, LCL

BRN (**Bulk Richardson Number**)

EQUATION: (CAPE / 0-6km shear)

less than 45 (Super cells)

less than 10 (Environment too sheared)

Teens (Optimum for severe storms, good balance of CAPE and shear)

BSHR (**Bulk shear value**) - magnitude of shear over layer.

CAP(**Cap strength in degrees Celsius**) - Values above 2 indicate convection will not occur within at least the next couple of hours. Cap needs to be less than 2 in general before it can be broken.

CAPE (**Convective Available Potential Energy**) - This is the positive area on a sounding (the area between the parcel and environmental temperature).

1 to 1,500 (Positive CAPE)

1,500 to 2,500 (Large CAPE)

2,500+ (Extreme CAPE)
Max upward vertical velocity = (2*CAPE)^1/2, does not take into consideration water loading, entrainment. Largest CAPE will occur in the warm sector of a mid-latitude cyclone High values of CAPE will result in high values of upward vertical velocity in the updraft region of a thunderstorm. CAPE is increased by low level warm air advection, daytime heating, low level moisture advection (high low level dew point), upper level cold air advection (cooling temperature in mid-levels) CAPE values tend to be highest in the warm season (especially late Spring).

CCL (**Convective Condensation Level**) - Level at which condensation will occur if sufficient afternoon heating causes rising parcels of air to reach saturation. The CCL is greater than or equal in height (lower or equal pressure level) than the LCL. The CCL and the LCL are equal when the atmosphere is saturated. Found at the intersection of the saturation mixing ratio line (through the surface dew point) and the environmental temperature.

CIN (**Convective Inhibition**) - This is the negative area on a sounding. A large cap or a dry planetary boundary layer will lead to high values of CIN and stability.

Convective instability - Occurs when a dry layer overlays a warm and humid layer. Lifting of atmosphere causes the lapse rate to increase since the lower layer cool at the WALR while the dry layer cools at the DALR.

Convective Temperature - The approximate temperature that the air near the ground must warm to in order for surface-based convection to develop, based on analysis of a sounding. Calculation involves many assumptions, such that thunderstorms sometimes develop well before or well after the convective temperature is reached (or may not develop at all). However, in some cases the convective temperature is a useful parameter for forecasting the onset of convection. Also-the convective temperature is found on a Skew-T Log-P diagram by dropping a parcel of air dry adiabatically from the CCL (Convective Condensation Level) to the surface and reading off the new temperature once the parcel reaches the surface.

Think of the convective temperature as the temperature the surface of the earth must warm to in order for thunderstorms to occur in the absence of synoptic scale forcing mechanism (i.e., development of afternoon "air-mass" thunderstorms). The convective temperature is most likely to be reached in the late afternoon hours due to cumulative solar heating. The strength of the "cap" determines if the convective temperature will be reached. When the cap is very strong, the convective temperature will be higher than the high temperature for that day and thus no storms develop. The amount of low-level moisture also determines if the convective temperature will be reached. The CCL increases in height as the average PBL dew point decreases. A higher CCL results in a higher convective temperature. Dynamic upward forcing lowers the theoretical convective temperature since parcels of air can be "forced" or brought closer to the CCL by lifting mechanisms such as fronts, low level WAA and low level

convergence.

EHI (**Energy helicity index**) - Combines CAPE and Helicity into a single index. EHI increases as CAPE and/or Helicity increases. Tornadic development often initiates in region of EHI max (especially if EHI max is 5 or greater).

EQUATION: (SR HEL * CAPE) / 160,000

EHI > 1 (Supercells likely)

EHI from 1 to 5 (F2, F3 tornadoes possible)

EHI 5+ (F4, F5 tornadoes possible)

(**EI**) - Energy Index

EL (**Equilibrium level)** - The pressure value at the top of the positive CAPE area In extreme situation's, EHI max will be near 10.

Equivalent Potential Temperature - Also known as THETA-E. Temperature of a parcel after all latent heat energy is released in a parcel then brought to the 1000 mb level. From pressure of interest (typically the surface) find the LCL, lift the parcel wet adiabatically to 100 mb. Next, descend the parcel dry.

FRZ - Pressure level at which the environmental sounding is exactly zero degrees Celsius. Find intersection of 0-degree isotherm with environmental sounding.

HEL - Helicity Amount of stream-wise Vorticity available for ingestion into a storm. Stream-wise Vorticity is a function of low level inflow and horizontal Vorticity generated by speed shear with height or directional shear with height in the PBL.

150 to 300 (possible super cell)

300 to 400 (super cell severe storms)

400+ (Tornadic super cells possible)

Low level inflow, speed shear and directional shear maximize helicity values

Helicity values tend to be highest ahead of cold fronts and near warm fronts within the warm sector of a mid-latitude cyclone

The Low Level Jet can amplify low level inflow. Higher winds lead to a more rapid rotation of air if shear exists

Differential advection and surface friction cause speed and directional shear
Hydro lapse - Rapid increase or decrease in dew point with height.

K (K Index) - The K Index is primarily applicable in the prediction of air mass thunderstorms. Low values of the K Index in the presence of other strong thunderstorms indicators (sharp

trough, high level jet, etc.) may suggest a severe thunderstorm potential. For example, a low K value might result from a 700 mb dry tongue. Limitations: Favours non severe convection. This index is a measure of thunderstorm potential but has nothing to do with severity of storms cannot be used in mountain areas. The K value may not be representative of the air mass if the 850mb level is near the surface.

EQUATION: $(T_{850} - T_{500}) + (T_{d850} - T_{d700})$

Lapse rate + available moisture

-or-

EQUATION: $(T_{850} - T_{500}) + (T_{d850}) - (T_{700} - T_{d700})$

(Lapse rate) + (low-level moisture) - (extent of moist layer)

<15 (Convection not likely)

15 to 25 (Small potential for convection)

26 to 39 (Moderate potential for convection)

40+ (High potential for convection)

LFC (Level of Free Convection) - The level at the bottom of the area of positive CAPE. If a parcel reaches this level it will begin to accelerate in the vertical.

LI (**Lifted Index**) - This is the temperature difference between the environmental and parcel temperatures at the 500 mb level. In theory, the LI is computed by taking parcel 25 mb above the surface and lifting it dry-adiabatically to saturation; then moist adiabatically to 500 mb. The difference between the sounding temperature and the parcel temperature yields the LI. In practice, the following method is employed.

A. Determine the mean temperature and mean dew point temperature in the lowest 50 mb of the sounding. These values are considered representative of the level 25 mb above the surface.
B. From approximately 25 mb above the surface, lift the estimated mean temperature until it intersects the mixing ratio line which passes through the mean dew point temperature, this determines the LCL.
C. Lift the parcel moist adiabatically to 500 mb.
D. The difference between the ambient air temperature at 500 mb and the parcel temperature is the LI.

EQUATION: 500 mb environmental temperature - 500 mb parcel temperature

0 or greater (stable)

-1 to -4 (marginal instability)

-5 to -7 (large instability)

-8 to -10 (extreme instability)

-11 or less (ridiculous instability)

(**Potential Temperature**) - Temperature found by lifting or descending a parcel to the 1000 mb level from the pressure level of interest.

(**PW**) - Value of precipitable water in inches. This is the amount of liquid water on the surface after all water in all three phases is brought to the surface. Greater than 1.75 inches represents a water loaded sounding. Less than 0.75 inches represents a fairly dry sounding.

RH (**Relative Humidity**) - Found by dividing the mixing ratio by the saturation mixing ratio or the vapour pressure divided by the saturation vapour pressure. Find the saturation mixing ratio value that runs through the dew point and the temperature. Next, divide the dew point mixing ratio by the temperature mixing ratio. The average relative humidity between the surface and 500 millibars. Relative humidity is a good measure of the evaporational drying power of the air and how close the atmosphere is to saturation. It does not, however, tell you how much moisture mass there is in the air. Adiabatically to the 1000 mb level. The temperature at 1000 mb of this parcel is the THETA-E.

0 to 40% (very low)

41 to 60% (low)

61 to 80% (moderate)

81 to 100% (moist)

SHR - Positive shear in the 0 to 3000m above ground level. Units are in time to the negative 1. Dividing the change in vertical wind speed by the change in the distance derives these units. Km/hr divided by km = hr-1. Value is found by finding the change in wind speed from the surface to 3000m and dividing that value by 3000m (3 km).

0 to 3 (weak)

4 to 5 (moderate)

6 to 8 (large)

9+ (very large)

SI (**Showalter Index**) - Same as LI, except parcel is lifted from 850 mb. Use SI instead of LI in the cool season especially when surface is capped by a cool front.

EQUATION: 500 mb environmental temperature - 500 mb parcel temperature

A. Lift the 850 mb temperature dry adiabatically until it intersects the mixing ratio line which passes through the 850 mb dew point.
B. Lift the parcel moist adiabatically to 500 mb.
C. The difference between the ambient air temperature at 500 mb and the parcel temperature determines the SI.

SRDS (**Storm relative directional shear**).

STM (**Estimated storm motion**) - Storm will be moving from X and X knots.

(**SWEAT**) - Severe Weather Threat Index. Indices combining many thermodynamic and wind values. The SWEAT Index was developed by AWS to identify areas of potentially severe convective activity. The terms in the index refer to low level moisture, convective potential, low and midlevel winds, and wind shear. Empirically, the threshold for severe thunderstorms is 300 and the threshold for tornadoes is 400. It should be stressed that the above statistics were derived from known severe weather cases; nothing can be inferred above the false alarm ratio. Also, the SWEAT Index gives severe weather potential; a trigger is still needed to realize this potential. this SWI should not be used to predict ordinary thunderstorms. Since this index can change dramatically in a short period of time, it should be computed at both 12Z and 00Z during severe weather situations. Formula covers: low level moisture, instability, low level jet, upper level jet, warm air advection.

150 to 300 (Slight severe)

300 to 400 (Severe storms possible)

400+ (Tornadic severe storms possible)

TP (**Tropopause Level**) - Location in millibars of the tropopause, generally near 150 millibars.

TT (**Total Totals Index**) - The Total Totals Index was first introduced by Miller for use in identifying potential areas of thunderstorm development. The Vertical Totals measures the vertical lapse rate, while the Cross Totals incorporates low level moisture. the VT and CT thresholds for potential convective activity vary widely from one region to another. Inspection of the Total Totals equation shows a strong dependence on the 500 mb temperature. Very cold 500 mb temperatures, without corresponding convective support in the lower levels, may produce artificially high index values. This might be the case in a cold deep trough. Limitations: large lapse rates can produce large TT values with little low level moisture TT is region specific.

EQUATION: (T850 - T500) + (Td850 - T500) (Vertical Totals + Cross Totals)
<44 (convection not likely)

44 to 50 (convection likely)

51 - 52 (isolated severe storms)

53 - 56 (widely scattered severe storms)

>56 (scattered severe storms)

WBO (**Wet bulb zero temperature**) - Value at which the sounding is at zero degrees Celsius due to evaporational cooling. Value is given as a pressure level. This value will always be at a higher pressure (closer to the surface) than the FRZ level unless the sounding is saturated. Value found through computer algorithms (once the wet bulb is found for every pressure level, the wet bulb zero can then be located.) Wet bulb temperature can be found by the following sequence:
1. Pick a pressure level
2. Find LCL from that pressure level
3. From LCL go back down the sounding at the wet adiabatic lapse rate to the original pressure
4. This temperature is the wet bulb temperature

(**Wet Bulb potential temperature**) - Found the same as the wet bulb. When the wet bulb value is found, keep descending wet adiabatically to the 1000 mb level.

Source:
https://www.weather.gov/source/zhu/ZHU_Training_Page/convective_parameters/skewt/skewtinfo.html#SKEW3

1st case on 17th April 2022 over Kolkata region, West Bengal , India of thunderstorm day

At 00Z Skew T - Log P diagram on 17th April 2022 is shown in **Figure 3.5** over Kolkata region of thunderstorm day

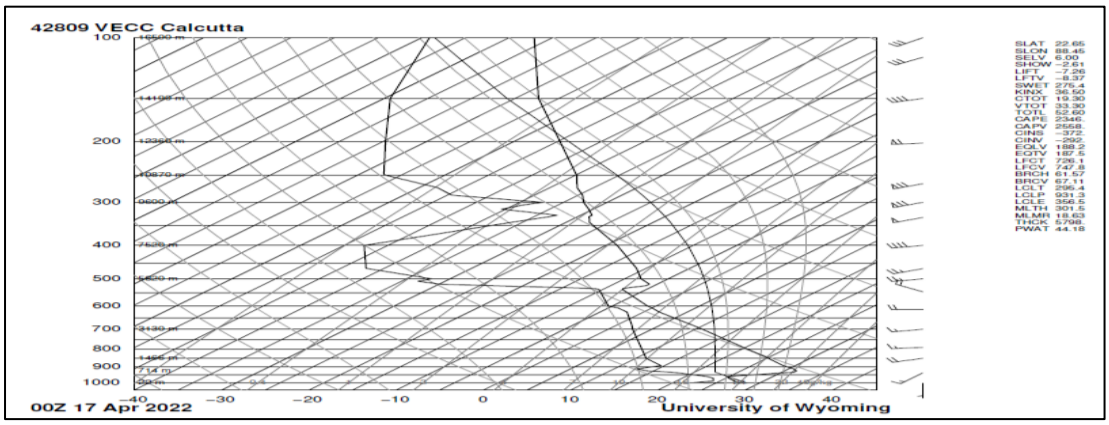

Figure 3.5 At 00Z Skew T - Log P diagram on 17th April 2022 over Kolkata region of thunderstorm day.

Station identifier: VECC
Station number: 42809
Observation time: 220417/0000
Station latitude: 22.65
Station longitude: 88.45
Station elevation: 6.0
Showalter index: -2.61
Lifted index: -7.26
LIFT computed using virtual temperature: -8.37
SWEAT index: 275.40
K index: 36.50
Cross totals index: 19.30
Vertical totals index: 33.30
Totals totals index: 52.60
Convective Available Potential Energy: 2346.74
CAPE using virtual temperature: 2558.06
Convective Inhibition: -372.39
CINS using virtual temperature: -292.37
Equilibrium Level: 188.27
Equilibrium Level using virtual temperature: 187.51
Level of Free Convection: 726.16
LFCT using virtual temperature: 747.81
Bulk Richardson Number: 61.57
Bulk Richardson Number using CAPV: 67.11
Temp [K] of the Lifted Condensation Level: 295.45
Pres [hPa] of the Lifted Condensation Level: 931.38
Equivalent potential temp [K] of the LCL: 356.52
Mean mixed layer potential temperature: 301.53
Mean mixed layer mixing ratio: 18.63
1000 hPa to 500 hPa thickness: 5798.00
Precipitable water [mm] for entire sounding: 44.18

At 12Z on 17th April Skew T - Log P diagram of thunderstorm day is shown in **Figure 3.6** over Kolkata region.

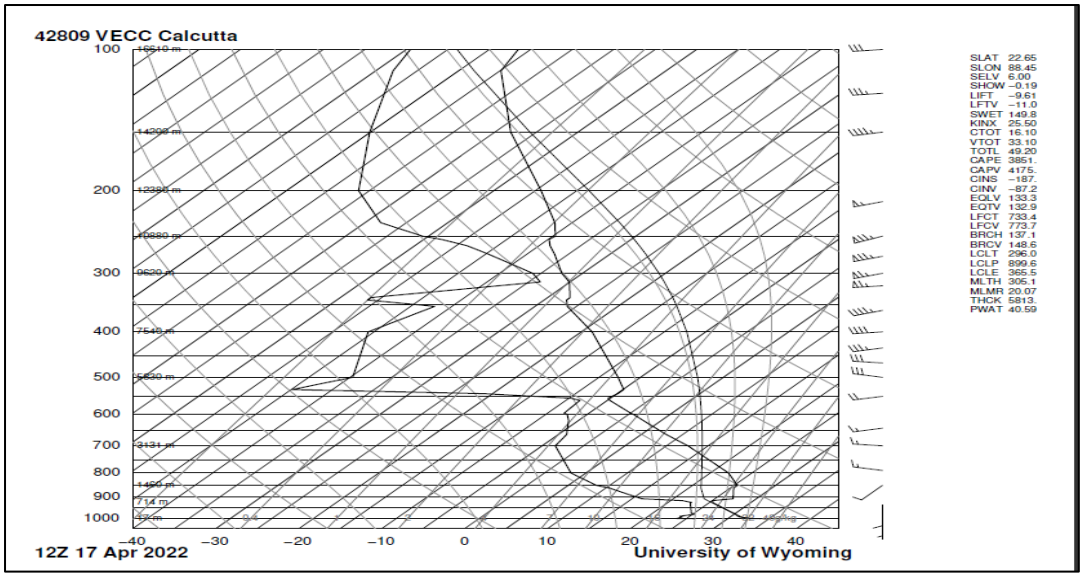

Figure 3.6 At 12 Z Skew T - Log P diagram on 17th April 2022 over Kolkata region of thunderstorm day.

Station identifier: VECC
Station number: 42809
Observation time: 220417/1200
Station latitude: 22.65
Station longitude: 88.45
Station elevation: 6.0
Showalter index: -0.19
Lifted index: -9.61
LIFT computed using virtual temperature: -11.04
SWEAT index: 149.81
K index: 25.50
Cross totals index: 16.10
Vertical totals index: 33.10
Totals totals index: 49.20
Convective Available Potential Energy: 3851.23
CAPE using virtual temperature: 4175.20
Convective Inhibition: -187.59
CINS using virtual temperature: -87.25
Equilibrium Level: 133.30
Equilibrium Level using virtual temperature: 132.91
Level of Free Convection: 733.45
LFCT using virtual temperature: 773.78
Bulk Richardson Number: 137.10
Bulk Richardson Number using CAPV: 148.63
Temp [K] of the Lifted Condensation Level: 296.09
Pres [hPa] of the Lifted Condensation Level: 899.65
Equivalent potential temp [K] of the LCL: 365.50
Mean mixed layer potential temperature: 305.18
Mean mixed layer mixing ratio: 20.07
1000 hPa to 500 hPa thickness: 5813.00
Precipitable water [mm] for entire sounding: 40.59

RESULTS AND DISCUSSION

Comparison between 00Z and 12Z sounding data of thunderstorm day on 17th April 2022 (Case 1) is shown in **Table 3.1** over Kolkata region

Table 3.1 Kolkata Observations at 00Z and 12Z sounding data of thunderstorm day on 17th April 2022 (Case 1) over Kolkata region

Index	00Z	12Z	Index	00Z	12Z
KI	36.50	25.50	RINO	61.57	137.10
TTI	52.50	49.20	SI	-2.61	-0.19
SLI	-7.26	-9.61	HI	46	65
CINE	-292.37	-87.25	DCI	43.66	43.41
SWEAT	275.40	149.81	BI	100	99.9
CAPE	2558.06	4175.20			

At 0000 UTC Sounding data of thunderstorm day, the CAPE is 2558.06 J/Kg which is very unstable. Then the TT index is 52.50 (thunderstorms are more likely, possibly severe) and KI index is 36.50(better potential for thunderstorms with heavy rain). The DCI is 43.66(potential for strong thunderstorms) and SLI is -7.26(very unstable). The RINO is 61.57(Relatively weak vertical wind shear and high CAPE. Suggest multicellular thunderstorm development is most likely) and SI is -2.61 which is moderately unstable. Suggesting high instability of the atmosphere suitable for thunderstorm formation .

But at 1200 UTC, the values of CAPE ,CINE and RINO values are increased and KI, TTI, SLI and SWEAT values are reduced because the thunderstorm might have started and getting stronger than previous atmosphere which may lead to thunderstorm .

2nd case on 21st April 2022 over Kolkata region, West Bengal, India of thunderstorm day

At 00Z Skew T - Log P diagram on 21st April is shown in **Figure 3.7** over Kolkata region of thunderstorm day.

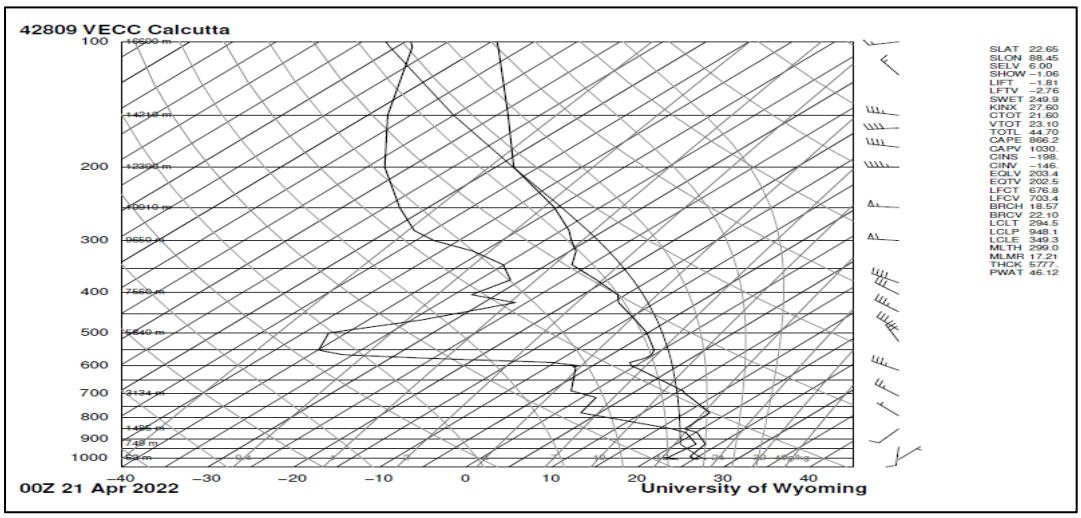

Figure 3.7 At 00Z Skew T - Log P diagram on 21st April 2022 over Kolkata region of thunderstorm day

Station identifier: VECC
Station number: 42809
Observation time: 220421/0000
Station latitude: 22.65
Station longitude: 88.45
Station elevation: 6.0
Showalter index: -1.06
Lifted index: -1.81
LIFT computed using virtual temperature: -2.76
SWEAT index: 249.98
K index: 27.60
Cross totals index: 21.60
Vertical totals index: 23.10
Totals totals index: 44.70
Convective Available Potential Energy: 866.24
CAPE using virtual temperature: 1030.54
Convective Inhibition: -198.92
CINS using virtual temperature: -146.86
Equilibrium Level: 203.49
Equilibrium Level using virtual temperature: 202.57
Level of Free Convection: 676.83
LFCT using virtual temperature: 703.45
Bulk Richardson Number: 18.57
Bulk Richardson Number using CAPV: 22.10
Temp [K] of the Lifted Condensation Level: 294.51
Pres [hPa] of the Lifted Condensation Level: 948.14
Equivalent potential temp [K] of the LCL: 349.34
Mean mixed layer potential temperature: 299.04
Mean mixed layer mixing ratio: 17.21
1000 hPa to 500 hPa thickness: 5777.00
Precipitable water [mm] for entire sounding: 46.12

At 12Z Skew T - Log P diagram on 21st April 2022 is shown in **Figure 3.8** over Kolkata region of thunderstorm day.

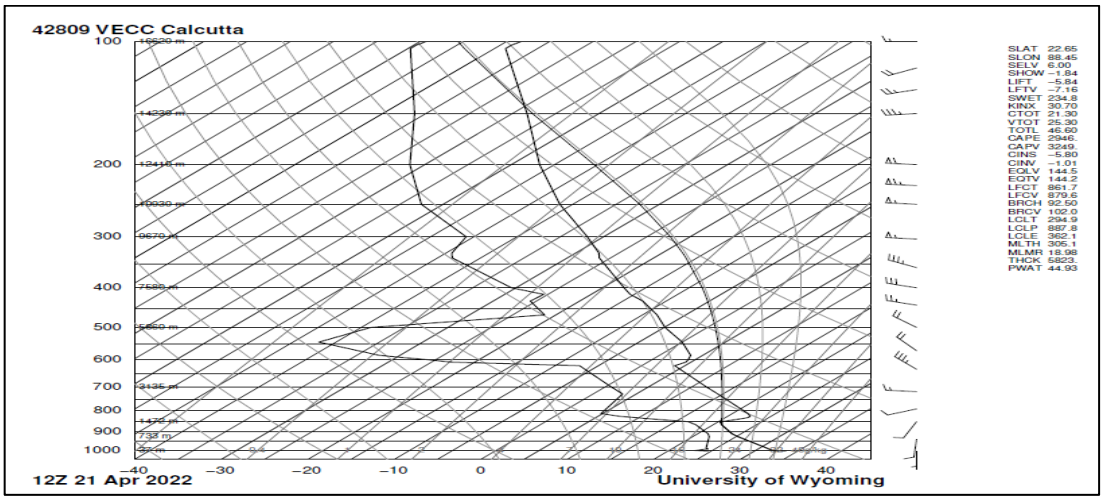

Figure 3.8 At 12 Z Skew T - Log P diagram on 21st April 2022 over Kolkata region of thunderstorm day

Station identifier: VECC
Station number: 42809
Observation time: 220421/1200
Station latitude: 22.65
Station longitude: 88.45
Station elevation: 6.0
Showalter index: -1.84
Lifted index: -5.84
LIFT computed using virtual temperature: -7.16
SWEAT index: 234.81
K index: 30.70
Cross totals index: 21.30
Vertical totals index: 25.30
Totals totals index: 46.60
Convective Available Potential Energy: 2946.18
CAPE using virtual temperature: 3249.63
Convective Inhibition: -5.80
CINS using virtual temperature: -1.01
Equilibrium Level: 144.54
Equilibrium Level using virtual temperature: 144.29
Level of Free Convection: 861.71
LFCT using virtual temperature: 879.60
Bulk Richardson Number: 92.50
Bulk Richardson Number using CAPV: 102.03
Temp [K] of the Lifted Condensation Level: 294.98
Pres [hPa] of the Lifted Condensation Level: 887.85
Equivalent potential temp [K] of the LCL: 362.18
Mean mixed layer potential temperature: 305.19
Mean mixed layer mixing ratio: 18.98
1000 hPa to 500 hPa thickness: 5823.00
Precipitable water [mm] for entire sounding: 44.93

RESULTS AND DISCUSSION

Comparison between 00Z and 12Z sounding data of thunderstorm day on 21st April 2022 (Case 2) is shown in **Table 3.2** over Kolkata region

Table 3.2 Kolkata Observations at 00Z and 12Z sounding data of thunderstorm day on 21st April 2022 (Case 2) over Kolkata region

Index	00Z	12Z	Index	00Z	12Z
KI	27.60	30.70	RINO	18.57	92.50
TTI	44.70	46.60	SI	-1.06	-1.84
SLI	-1.81	-5.84	HI	50.5	49
CINE	-146.86	-1.01	DCI	36.31	42.64
SWEAT	249.98	234.81	BI	95.9	98
CAPE	1030.54	3249.63			

At 0000 UTC Sounding data of thunderstorm day, the CAPE is 1030.54J/Kg which is high value. Then the TTI index is 44.70 (thunderstorm possible) and KI index is 27.60 (thunderstorms with heavy rain or severe weather are possible). The DCI is 36.31(potential for strong thunderstorms) and SLI is -1.81(marginally unstable). The RINO is 18.57(associated with super-cell development) and SI is -1.06 which is moderately unstable. Suggesting instability of the atmosphere suitable for thunderstorm formation .

But in at 1200 UTC , the values of CAPE ,CINE , SWEAT , KI , TTI , and RINO values are increased and SLI value is reduced because the thunderstorm might have started and getting stronger than previous atmosphere which may lead to thunderstorm .

3rd case on 22nd April 2022 over Kolkata region, West Bengal, Kolkata of thunderstorm day.

At 00Z Skew T - Log P diagram on 22nd April 2022 is shown in **Figure 3.9** over Kolkata region of thunderstorm day.

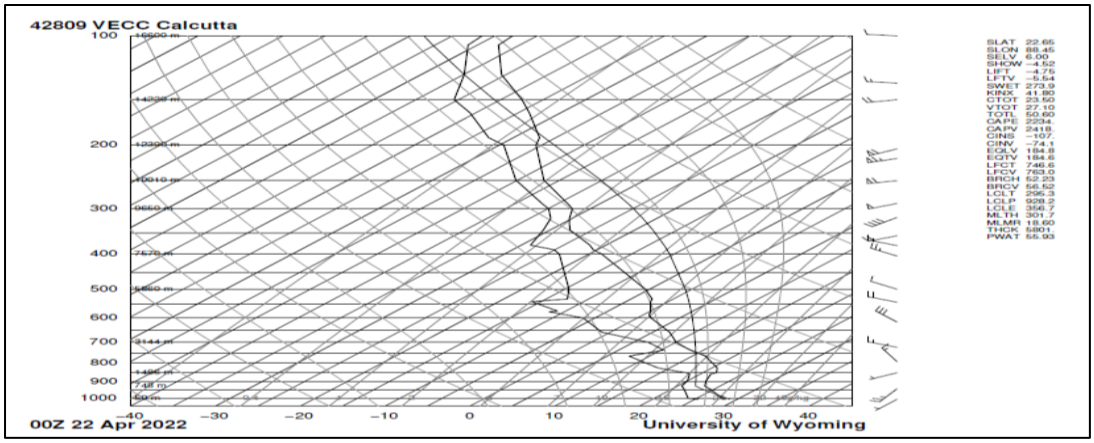

Figure 3.9 At 00 Z Skew T - Log P diagram on 22nd April 2022 over Kolkata region of thunderstorm day.

Station identifier: VECC
Station number: 42809
Observation time: 220422/0000
Station latitude: 22.65
Station longitude: 88.45
Station elevation: 6.0
Showalter index: -4.52
Lifted index: -4.75
LIFT computed using virtual temperature: -5.54
SWEAT index: 273.99
K index: 41.80
Cross totals index: 23.50
Vertical totals index: 27.10
Totals totals index: 50.60
Convective Available Potential Energy: 2234.98
CAPE using virtual temperature: 2418.84
Convective Inhibition: -107.75
CINS using virtual temperature: -74.17
Equilibrium Level: 184.87
Equilibrium Level using virtual temperature: 184.63
Level of Free Convection: 746.63
LFCT using virtual temperature: 763.04
Bulk Richardson Number: 52.23
Bulk Richardson Number using CAPV: 56.52
Temp [K] of the Lifted Condensation Level: 295.39
Pres [hPa] of the Lifted Condensation Level: 928.20
Equivalent potential temp [K] of the LCL: 356.78
Mean mixed layer potential temperature: 301.75
Mean mixed layer mixing ratio: 18.60
1000 hPa to 500 hPa thickness: 5801.00
Precipitable water [mm] for entire sounding: 55.93

At 12Z Skew T - Log P diagram on 22nd April 2022 is shown in **Figure 3.10** over Kolkata region of thunderstorm day.

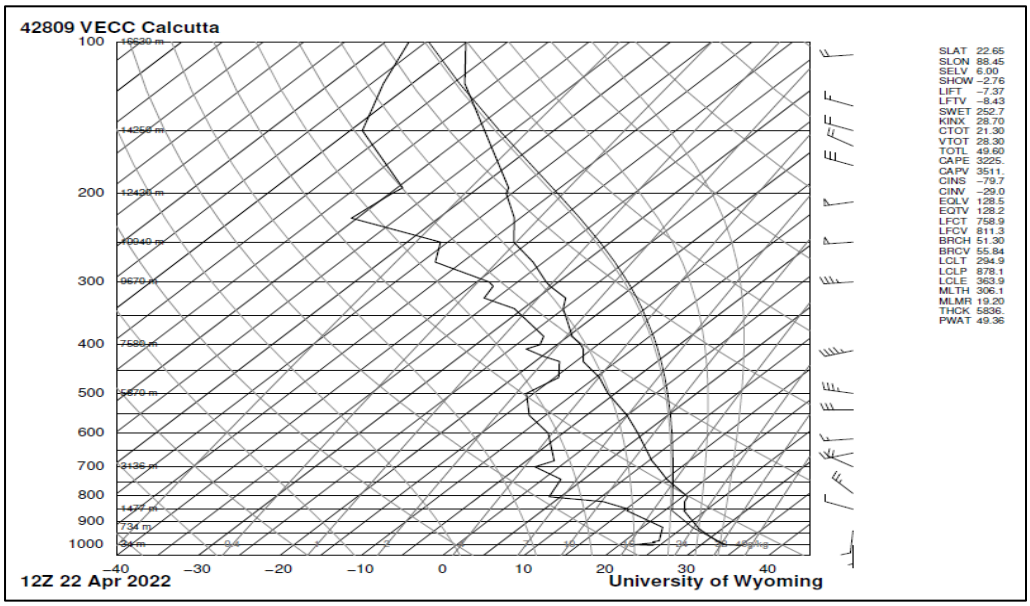

Figure 3.10 At 12 Z Skew T - Log P diagram on 22nd April 2022 over Kolkata region of thunderstorm day.

Station identifier: VECC
Station number: 42809
Observation time: 220422/1200
Station latitude: 22.65
Station longitude: 88.45
Station elevation: 6.0
Showalter index: -2.76
Lifted index: -7.37
LIFT computed using virtual temperature: -8.43
SWEAT index: 252.78
K index: 28.70
Cross totals index: 21.30
Vertical totals index: 28.30
Totals totals index: 49.60
Convective Available Potential Energy: 3225.61
CAPE using virtual temperature: 3511.15
Convective Inhibition: -79.73
CINS using virtual temperature: -29.01
Equilibrium Level: 128.51
Equilibrium Level using virtual temperature: 128.27
Level of Free Convection: 758.94
LFCT using virtual temperature: 811.30
Bulk Richardson Number: 51.30
Bulk Richardson Number using CAPV: 55.84
Temp [K] of the Lifted Condensation Level: 294.97
Pres [hPa] of the Lifted Condensation Level: 878.19
Equivalent potential temp [K] of the LCL: 363.95
Mean mixed layer potential temperature: 306.13
Mean mixed layer mixing ratio: 19.20
1000 hPa to 500 hPa thickness: 5836.00
Precipitable water [mm] for entire sounding: 49.36

RESULTS AND DISCUSSION

Comparison between 00Z and 12Z sounding data of thunderstorm day on 22nd April 2022 over Kolkata region.

Table 3.3 Kolkata Observations at 00Z and 12Z sounding data of thunderstorm day on 22nd April 2022 (Case 3) over Kolkata region.

Index	00Z	12Z	Index	00Z	12Z
K	41.80	28.70	RINO	52.23	51.30
TT	50.60	49.60	SI	-4.52	-2.76
SLI	-4.75	-7.37	HI	15.9	32
CINE	-74.17	-29.01	DCI	44.35	45.17
SWEAT	273.50	252.78	BI	98.5	98.2
CAPE	2418.84	3511.15			

At 0000 UTC Sounding data of thunderstorm day, the CAPE is 2418.84 J/Kg which is moderately unstable. Then the TTI index is 50.60 (thunderstorms are more likely, possible severe) and KI index is 41.80 (best potential for thunderstorms with heavy rain). The DCI is 44.35(potential for strong thunderstorms) and SLI is -4.75 (moderately unstable). The RINO is 52.23(Relatively weak vertical wind shear and high CAPE suggest multicellular thunderstorm development is most likely) and SI is -4.52 which is very unstable. Suggesting high instability of the atmosphere suitable for thunderstorm formation.

But in at 1200 UTC, the values of CAPE and CINE values are increased and K, TT, SLI, RINO and SWEAT values are reduced because the thunderstorm might have started and getting stronger than previous atmosphere which may lead to thunderstorm.

4th case on 29th April 2022 over Kolkata region, West Bengal, Kolkata of thunderstorm day

At 00Z Skew T - Log P diagram of thunderstorm day on 29th April 2022 is shown in **Figure 3.11** over Kolkata region.

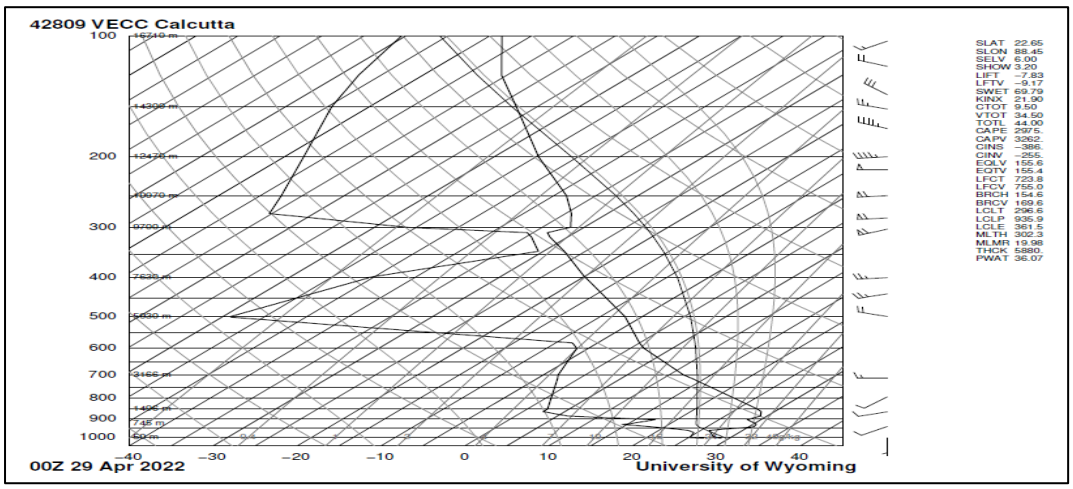

Figure 3.11 At 00 Z Skew T - Log P diagram of thunderstorm day on 29th April 2022 over Kolkata region

Station identifier: VECC
Station number: 42809
Observation time: 220429/0000
Station latitude: 22.65
Station longitude: 88.45
Station elevation: 6.0
Showalter index: 3.20
Lifted index: -7.83
LIFT computed using virtual temperature: -9.17
SWEAT index: 69.79
K index: 21.90
Cross totals index: 9.50
Vertical totals index: 34.50
Totals totals index: 44.00
Convective Available Potential Energy: 2975.15
CAPE using virtual temperature: 3262.42
Convective Inhibition: -386.39
CINS using virtual temperature: -255.80
Equilibrium Level: 155.61
Equilibrium Level using virtual temperature: 155.43
Level of Free Convection: 723.81
LFCT using virtual temperature: 755.06
Bulk Richardson Number: 154.67
Bulk Richardson Number using CAPV: 169.60
Temp [K] of the Lifted Condensation Level: 296.64
Pres [hPa] of the Lifted Condensation Level: 935.93
Equivalent potential temp [K] of the LCL: 361.54
Mean mixed layer potential temperature: 302.32
Mean mixed layer mixing ratio: 19.98
1000 hPa to 500 hPa thickness: 5880.00
Precipitable water [mm] for entire sounding: 36.07

At 12Z Skew T - Log P diagram of thunderstorm day on 29th April 2022 is shown in **Figure 3.12** over Kolkata region.

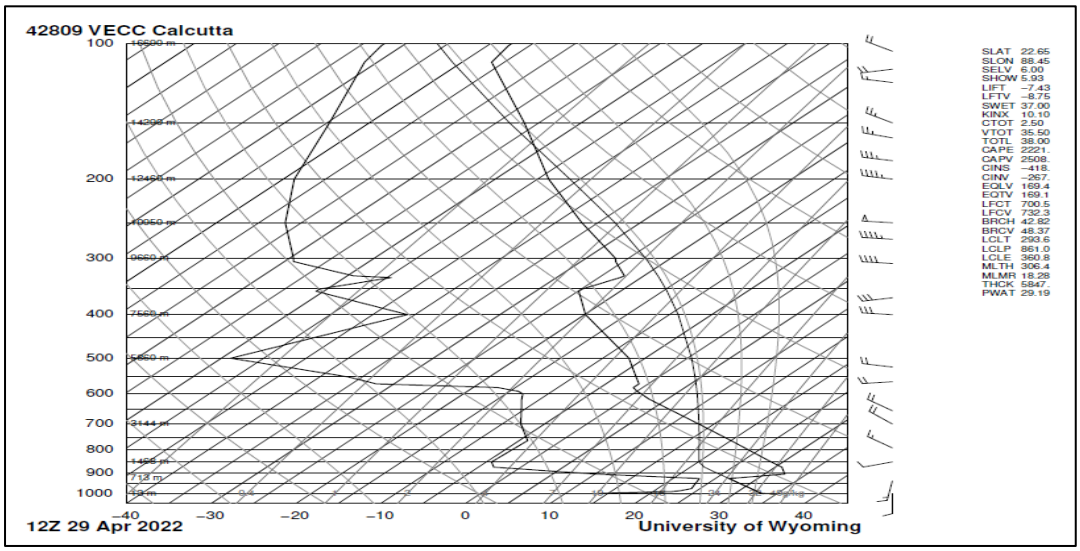

Figure 3.12 At 12 Z Skew T - Log P diagram of thunderstorm day on 29th April 2022 over Kolkata region.

Station identifier: VECC
Station number: 42809
Observation time: 220429/1200
Station latitude: 22.65
Station longitude: 88.45
Station elevation: 6.0
Showalter index: 5.93
Lifted index: -7.43
LIFT computed using virtual temperature: -8.75
SWEAT index: 37.00
K index: 10.10
Cross totals index: 2.50
Vertical totals index: 35.50
Totals totals index: 38.00
Convective Available Potential Energy: 2221.00
CAPE using virtual temperature: 2508.69
Convective Inhibition: -418.89
CINS using virtual temperature: -267.97
Equilibrium Level: 169.46
Equilibrium Level using virtual temperature: 169.17
Level of Free Convection: 700.53
LFCT using virtual temperature: 732.31
Bulk Richardson Number: 42.82
Bulk Richardson Number using CAPV: 48.37
Temp [K] of the Lifted Condensation Level: 293.65
Pres [hPa] of the Lifted Condensation Level: 861.06
Equivalent potential temp [K] of the LCL: 360.81
Mean mixed layer potential temperature: 306.48
Mean mixed layer mixing ratio: 18.28
1000 hPa to 500 hPa thickness: 5847.00
Precipitable water [mm] for entire sounding: 29.19

RESULTS AND DISCUSSION

Comparison between 00Z and 12Z sounding data of thunderstorm day on 29th April 2022 over Kolkata region.

Table 3.4 Kolkata Observations at 00Z and 12Z of sounding data of thunderstorm day on 29th April 2022 (Case 4) over Kolkata region.

Index	00Z	12Z	Index	00Z	12Z
K	21.90	10.10	RINO	154.67	42.82
TT	44	38	SI	3.20	5.93
SLI	-7.83	-7.43	HI	87	101
CINE	-255.80	-267	DCI	37.63	31.63
SWEAT	69.79	37	BI	99.8	99.9
CAPE	3262.42	2508.69			

At 0000 UTC Sounding data of thunderstorm day, the CAPE is 3262.42 J/Kg which is very unstable. Then the TTI index is 44 (thunderstorm possible) and KI index is 21.90 (thunderstorms with heavy rain or severe weather are possible). The DCI is 37.63 (potential for strong thunderstorms) and SLI is -7.83(very unstable). The RINO is 154.67 (Relatively weak vertical wind shear and high CAPE suggest multicellular thunderstorm development is most likely) and SI is 3.20 which is stable. Suggesting high instability of the atmosphere suitable for thunderstorm formation .

But at 1200 UTC , the values of CAPE, CINE, RINO, K, TT, SLI and SWEAT values are reduced because the thunderstorm might have started and the atmosphere has started releasing the energy .

5th case of thunderstorm day on 1st May 2022 over Kolkata region, Kolkata, West Bengal

At 00Z Skew T - Log P diagram of thunderstorm day on 1st May 2022 is shown in **Figure 3.13** over Kolkata region.

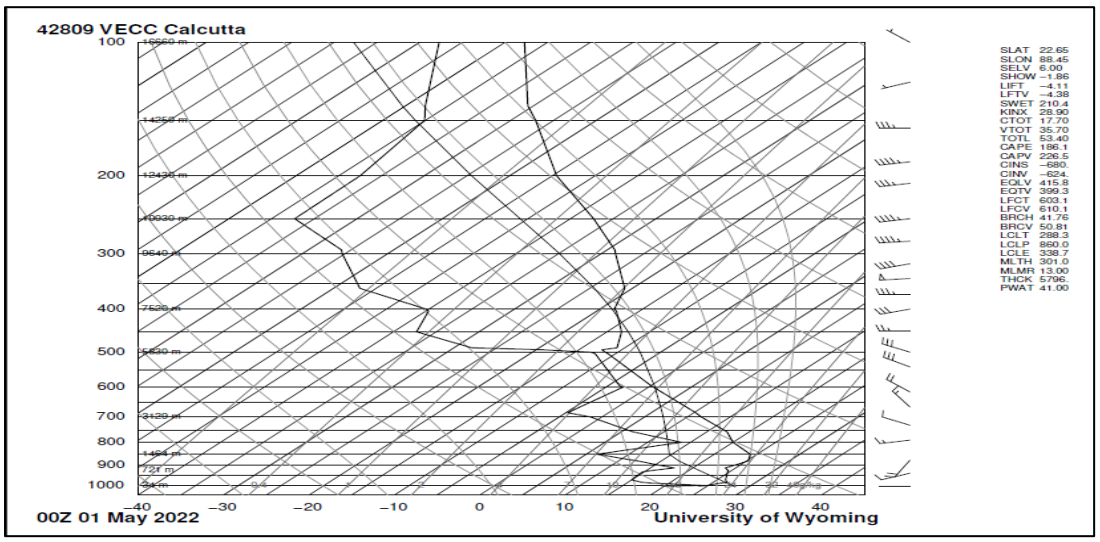

Figure 3.13 At 00 Z Skew T - Log P diagram of thunderstorm day on 1st May 2022 over Kolkata region.

Station identifier: VECC
Station number: 42809
Observation time: 220501/0000
Station latitude: 22.65
Station longitude: 88.45
Station elevation: 6.0
Showalter index: -1.86
Lifted index: -4.11
LIFT computed using virtual temperature: -4.38
SWEAT index: 210.40
K index: 28.90
Cross totals index: 17.70
Vertical totals index: 35.70
Totals totals index: 53.40
Convective Available Potential Energy: 186.18
CAPE using virtual temperature: 226.53
Convective Inhibition: -680.22
CINS using virtual temperature: -624.27
Equilibrium Level: 415.84
Equilibrium Level using virtual temperature: 399.30
Level of Free Convection: 603.13
LFCT using virtual temperature: 610.19
Bulk Richardson Number: 41.76
Bulk Richardson Number using CAPV: 50.81
Temp [K] of the Lifted Condensation Level: 288.32
Pres [hPa] of the Lifted Condensation Level: 860.03
Equivalent potential temp [K] of the LCL: 338.73
Mean mixed layer potential temperature: 301.02
Mean mixed layer mixing ratio: 13.00
1000 hPa to 500 hPa thickness: 5796.00
Precipitable water [mm] for entire sounding: 41.00

At 12Z Skew T - Log P diagram of thunderstorm day on 1st May 2022 is shown in **Figure 3.14** over Kolkata region.

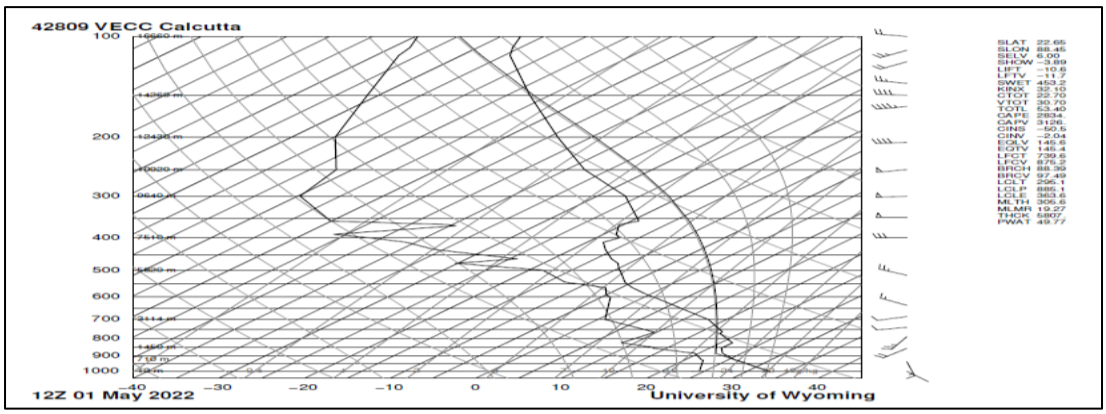

Figure 3.14 At 12 Z Skew T - Log P diagram of thunderstorm day on 1st May 2022 over Kolkata region.

Station identifier: VECC
Station number: 42809
Observation time: 220501/1200
Station latitude: 22.65
Station longitude: 88.45
Station elevation: 6.0
Showalter index: -3.89
Lifted index: -10.67
LIFT computed using virtual temperature: -11.79
SWEAT index: 453.27
K index: 32.10
Cross totals index: 22.70
Vertical totals index: 30.70
Totals totals index: 53.40
Convective Available Potential Energy: 2834.83
CAPE using virtual temperature: 3126.71
Convective Inhibition: -50.58
CINS using virtual temperature: -2.04
Equilibrium Level: 145.61
Equilibrium Level using virtual temperature: 145.48
Level of Free Convection: 739.66
LFCT using virtual temperature: 875.29
Bulk Richardson Number: 88.39
Bulk Richardson Number using CAPV: 97.49
Temp [K] of the Lifted Condensation Level: 295.18
Pres [hPa] of the Lifted Condensation Level: 885.18
Equivalent potential temp [K] of the LCL: 363.64
Mean mixed layer potential temperature: 305.65
Mean mixed layer mixing ratio: 19.27
1000 hPa to 500 hPa thickness: 5807.00
Precipitable water [mm] for entire sounding: 49.77

RESULTS AND DISCUSSION

Comparison between 00Z and 12Z sounding data of thunderstorm day on 1st May 2022 over Kolkata region.

Table 3.5 Kolkata Observations at 00Z and 12Z sounding data of thunderstorm day on 01st May 2022 (Case 5) over Kolkata region.

Index	00Z	12Z	Index	00Z	12Z
K	28.90	32.10	RINO	41.76	88.39
TT	53.40	53.40	SI	-1.86	-3.89
SLI	-4.11	-10.67	HI	32.7	29
CINE	-624.27	-2.04	DCI	34.51	45.47
SWEAT	210.40	453.27	BI	97.9	97.3
CAPE	226.53	3126.71			

At 0000 UTC Sounding data of thunderstorm day, the CAPE is 226.53 J/Kg which is marginally unstable. Then the TT index is 53.40 (thunderstorms are more likely, possibly severe) and K-index is 28.90 (thunderstorms with heavy rain or severe weather are possible). The DCI is 34.51 (potential for strong thunderstorms) and SLI is - 4.11(moderately unstable). The RINO is 41.76 (associated with super- cell development) and SI is -1.86 which is moderately unstable. Suggesting instability of the atmosphere suitable for thunderstorm formation.

But at 1200 UTC, the values of CAPE ,CINE , K, SWEAT , DCI and RINO values are increased and TT value as same and SLI, SI, HI and BI values are reduced because the thunderstorm might have started and getting stronger than previous atmosphere which may lead to thunderstorm.

6th case of thunderstorm day on 3rd May 2022 over Kolkata Region, West Bengal, India

At 00Z Skew T - Log P diagram of thunderstorm day on 3rd May 2022 is shown in **Figure 3.15** over Kolkata region.

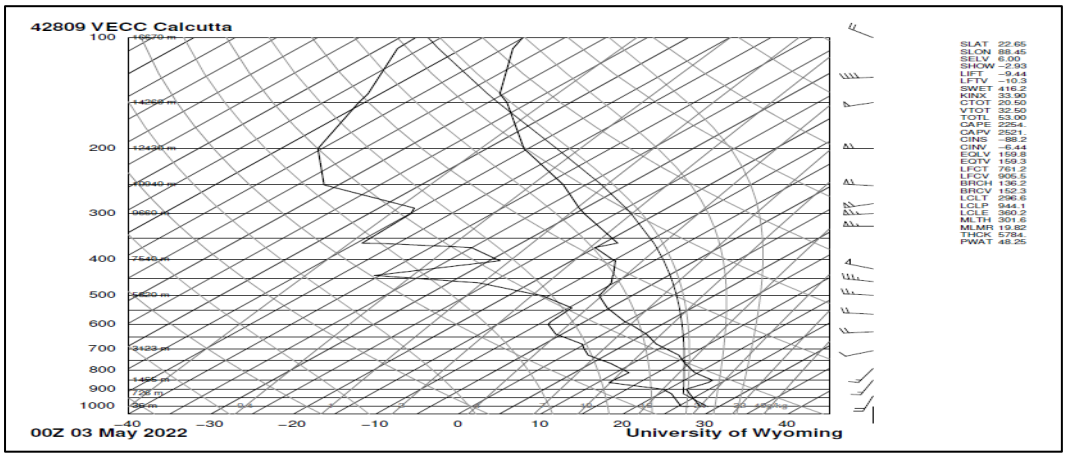

Figure 3.15 At 00Z Skew T - Log P diagram of thunderstorm day on 3rd May 2022 over Kolkata region.

Station identifier: VECC
Station number: 42809
Observation time: 220503/0000
Station latitude: 22.65
Station longitude: 88.45
Station elevation: 6.0
Showalter index: -2.93
Lifted index: -9.44
LIFT computed using virtual temperature: -10.39
SWEAT index: 416.25
K index: 33.90
Cross totals index: 20.50
Vertical totals index: 32.50
Totals totals index: 53.00
Convective Available Potential Energy: 2254.50
CAPE using virtual temperature: 2521.08
Convective Inhibition: -88.26
CINS using virtual temperature: -6.44
Equilibrium Level: 159.88
Equilibrium Level using virtual temperature: 159.37
Level of Free Convection: 761.20
LFCT using virtual temperature: 905.57
Bulk Richardson Number: 136.26
Bulk Richardson Number using CAPV: 152.38
Temp [K] of the Lifted Condensation Level: 296.68
Pres [hPa] of the Lifted Condensation Level: 944.17
Equivalent potential temp [K] of the LCL: 360.25
Mean mixed layer potential temperature: 301.61
Mean mixed layer mixing ratio: 19.82
1000 hPa to 500 hPa thickness: 5784.00
Precipitable water [mm] for entire sounding: 48.25

At 12Z Skew T - Log P diagram of thunderstorm day on 3rd May 2022 is shown in **Figure 3.16** over Kolkata region.

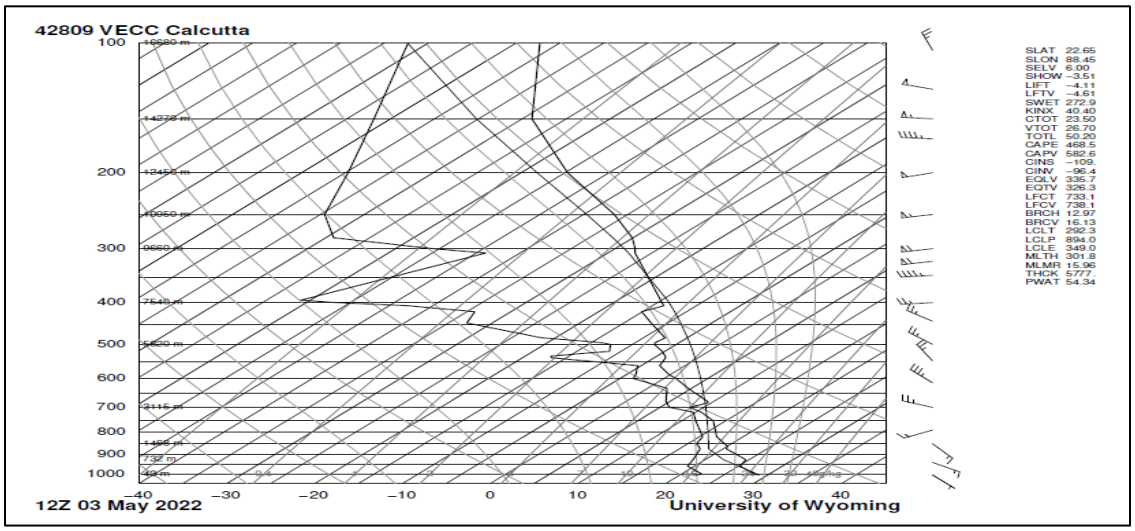

Figure 3.16 At 12 Z Skew T - Log P diagram of thunderstorm day on 3rd May 2022 over Kolkata region.

Station identifier: VECC
Station number: 42809
Observation time: 220503/1200
Station latitude: 22.65
Station longitude: 88.45
Station elevation: 6.0
Showalter index: -3.51
Lifted index: -4.11
LIFT computed using virtual temperature: -4.61
SWEAT index: 272.99
K index: 40.40
Cross totals index: 23.50
Vertical totals index: 26.70
Totals totals index: 50.20
Convective Available Potential Energy: 468.55
CAPE using virtual temperature: 582.64
Convective Inhibition: -109.05
CINS using virtual temperature: -96.43
Equilibrium Level: 335.76
Equilibrium Level using virtual temperature: 326.36
Level of Free Convection: 733.16
LFCT using virtual temperature: 738.11
Bulk Richardson Number: 12.97
Bulk Richardson Number using CAPV: 16.13
Temp [K] of the Lifted Condensation Level: 292.35
Pres [hPa] of the Lifted Condensation Level: 894.04
Equivalent potential temp [K] of the LCL: 349.02
Mean mixed layer potential temperature: 301.87
Mean mixed layer mixing ratio: 15.96
1000 hPa to 500 hPa thickness: 5777.00
Precipitable water [mm] for entire sounding: 54.34

RESULTS AND DISCUSSION

Comparison between 00Z and 12Z sounding data of thunderstorm day on 3rd May 2022 over Kolkata region

Table 3.6 Kolkata Observations at 00Z and 12Z sounding data of thunderstorm day on 3rd May 2022 (Case 6) over Kolkata region.

Index	00Z	12Z	Index	00Z	12Z
K	33.90	40.40	RINO	136.26	12.97
TT	53	50.20	SI	-2.93	-3.51
SLI	-9.44	-4.11	HI	29	10.5
CINE	-6.44	-96.43	DCI	44.24	39.31
SWEAT	416.25	272.99	BI	97.7	98.8
CAPE	2521.08	582.64			

At 0000 UTC Sounding data of thunderstorm day, the CAPE is 2521.08 J/Kg which is very unstable. Then the TT index is 53 (thunderstorms are more likely, possibly severe) and K-index is 33.90 (better potential for thunderstorms with heavy rain). The DCI is 44.24 (potential for strong thunderstorms) and SLI is -9.44 (extremely unstable). The RINO is 136.26 (Relatively weak vertical wind shear and high CAPE suggest multicellular thunderstorm development is most likely) and SI is -2.93 which is marginally unstable. Suggesting high instability of the atmosphere suitable for thunderstorm formation .

But at 1200 UTC , the values of CAPE, CINE, TT, SWEAT and RINO values are reduced and K and LI values are increased because the thunderstorm might have started and the atmosphere has started releasing the energy.

7th case of thunderstorm day on 13th May 2022 over Kolkata Region, West Bengal, India

At 00Z Skew T - Log P diagram of thunderstorm day on 13th May 2022 is shown in **Figure 3.17** over Kolkata region.

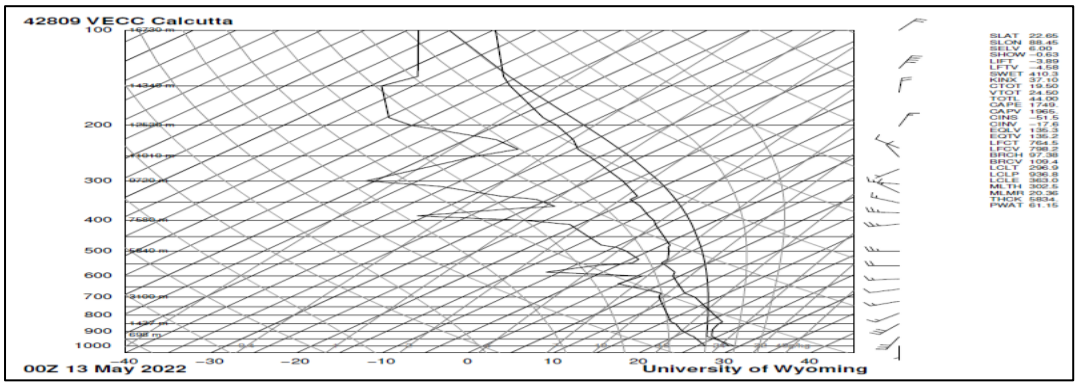

Figure 3.17 At 00 Z Skew T - Log P diagram of thunderstorm day on 13th May 2022 over Kolkata region.

Station identifier: VECC
Station number: 42809
Observation time: 220513/0000
Station latitude: 22.65
Station longitude: 88.45
Station elevation: 6.0
Showalter index: -0.63
Lifted index: -3.89
LIFT computed using virtual temperature: -4.58
SWEAT index: 410.35
K index: 37.10
Cross totals index: 19.50
Vertical totals index: 24.50
Totals totals index: 44.00
Convective Available Potential Energy: 1749.94
CAPE using virtual temperature: 1965.90
Convective Inhibition: -51.53
CINS using virtual temperature: -17.62
Equilibrium Level: 135.34
Equilibrium Level using virtual temperature: 135.28
Level of Free Convection: 764.56
LFCT using virtual temperature: 798.25
Bulk Richardson Number: 97.38
Bulk Richardson Number using CAPV: 109.40
Temp [K] of the Lifted Condensation Level: 296.98
Pres [hPa] of the Lifted Condensation Level: 936.88
Equivalent potential temp [K] of the LCL: 363.09
Mean mixed layer potential temperature: 302.58
Mean mixed layer mixing ratio: 20.36
1000 hPa to 500 hPa thickness: 5834.00
Precipitable water [mm] for entire sounding: 61.15

At 12Z Skew T - Log P diagram of thunderstorm day on 13th May 2022 is shown in **Figure 3.18** over Kolkata region.

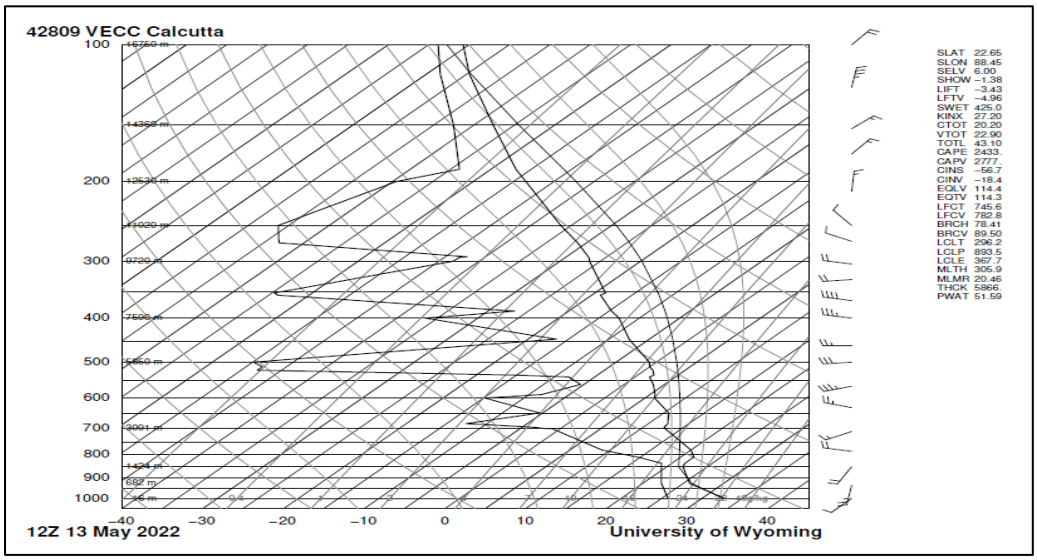

Figure 3.18 At 12 Z Skew T - Log P diagram of thunderstorm day on 13th May 2022 over Kolkata region.

Station identifier: VECC
Station number: 42809
Observation time: 220513/1200
Station latitude: 22.65
Station longitude: 88.45
Station elevation: 6.0
Showalter index: -1.38
Lifted index: -3.43
LIFT computed using virtual temperature: -4.96
SWEAT index: 425.00
K index: 27.20
Cross totals index: 20.20
Vertical totals index: 22.90
Totals totals index: 43.10
Convective Available Potential Energy: 2433.53
CAPE using virtual temperature: 2777.81
Convective Inhibition: -56.77
CINS using virtual temperature: -18.47
Equilibrium Level: 114.48
Equilibrium Level using virtual temperature: 114.38
Level of Free Convection: 745.68
LFCT using virtual temperature: 782.81
Bulk Richardson Number: 78.41
Bulk Richardson Number using CAPV: 89.50
Temp [K] of the Lifted Condensation Level: 296.29
Pres [hPa] of the Lifted Condensation Level: 893.56
Equivalent potential temp [K] of the LCL: 367.70
Mean mixed layer potential temperature: 305.98
Mean mixed layer mixing ratio: 20.46
1000 hPa to 500 hPa thickness: 5866.00
Precipitable water [mm] for entire sounding: 51.59

RESULTS AND DISCUSSION

Comparison between 00Z and 12Z sounding data of thunderstorm day on 13th May 2022 over Kolkata region

Table 3.7 Kolkata Observations at 00Z and 12Z sounding data of thunderstorm day on 13 May 2022 (Case 7) over Kolkata region.

Index	00Z	12Z	Index	00Z	12Z
K	37.10	27.20	RINO	97.38	78.41
TT	44	43.10	SI	-0.63	-1.38
SLI	-3.89	-3.43	HI	14.2	66.7
CINE	-17.62	-18.47	DCI	42.49	44.73
SWEAT	410.35	425	BI	97.2	9
CAPE	1965.90	2777.81			

At 0000 UTC Sounding data of thunderstorm day, the CAPE is 1965.90 J/Kg which is moderately unstable. Then the TT index is 44 (thunderstorm possible) and K-index is 37.10 (better potential for thunderstorms with heavy rain). The DCI is 42.49 (potential for strong thunderstorms) and SLI is -3.89 (moderately unstable). The RINO is 97.38 (Relatively weak vertical wind shear and high CAPE suggest multicellular thunderstorm development is most likely) and SI is -0.63 which is moderately unstable. Suggesting high instability of the atmosphere suitable for thunderstorm formation .

But at 1200 UTC , the values of CAPE, LI and SWEAT values are increased and K, TT, CINE and RINO values are reduced because the thunderstorm might have started and getting stronger than previous atmosphere which may lead to thunderstorm.

8th case of thunderstorm day on 17th May 2022 over Kolkata region, West Bengal, India

At 00Z Skew T - Log P diagram of thunderstorm day on 17th May 2022 is shown in **Figure 3.19** over Kolkata region.

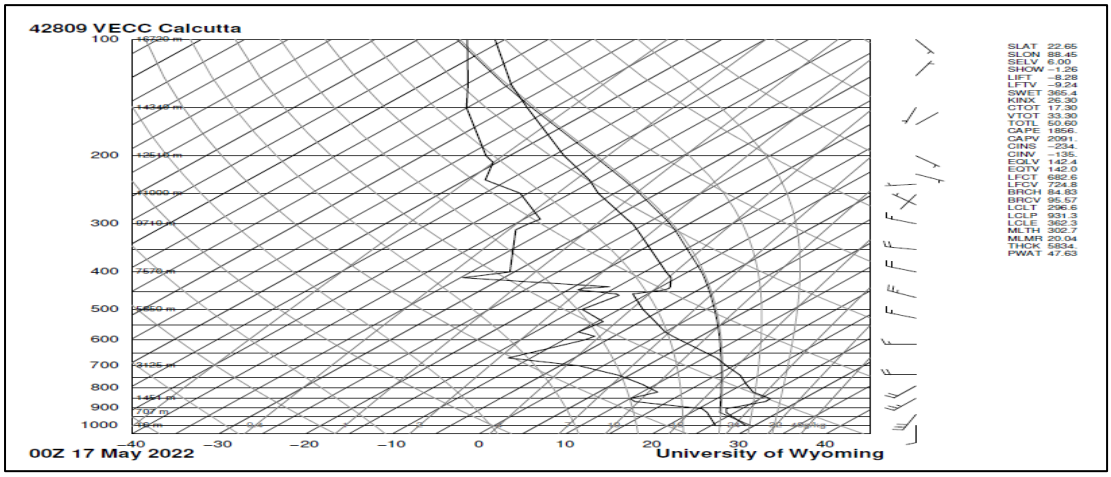

Figure 3.19 At 00 Z Skew T - Log P diagram of thunderstorm day on 17th May 2022 over Kolkata region.

Station identifier: VECC
Station number: 42809
Observation time: 220517/0000
Station latitude: 22.65
Station longitude: 88.45
Station elevation: 6.0
Showalter index: -1.26
Lifted index: -8.28
LIFT computed using virtual temperature: -9.24
SWEAT index: 365.44
K index: 26.30
Cross totals index: 17.30
Vertical totals index: 33.30
Totals totals index: 50.60
Convective Available Potential Energy: 1856.15
CAPE using virtual temperature: 2091.06
Convective Inhibition: -234.74
CINS using virtual temperature: -135.39
Equilibrium Level: 142.47
Equilibrium Level using virtual temperature: 142.03
Level of Free Convection: 682.67
LFCT using virtual temperature: 724.87
Bulk Richardson Number: 84.83
Bulk Richardson Number using CAPV: 95.57
Temp [K] of the Lifted Condensation Level: 296.64
Pres [hPa] of the Lifted Condensation Level: 931.36
Equivalent potential temp [K] of the LCL: 362.35
Mean mixed layer potential temperature: 302.74
Mean mixed layer mixing ratio: 20.04
1000 hPa to 500 hPa thickness: 5834.00
Precipitable water [mm] for entire sounding: 47.63

At 12Z Skew T - Log P diagram of thunderstorm day on 17th May 2022 is shown in **Figure 3.20** over Kolkata region

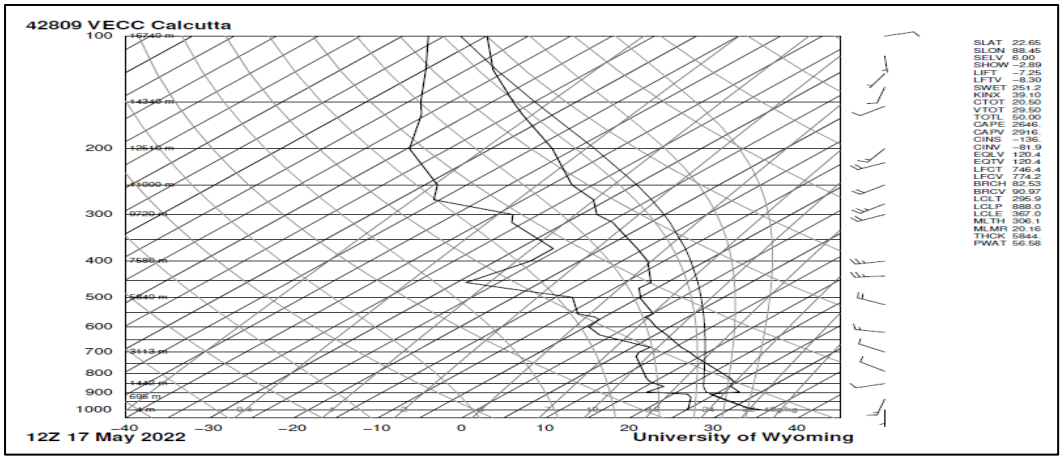

Figure 3.20 At 12 Z Skew T - Log P diagram of thunderstorm day on 17th May 2022 over Kolkata region.

Station identifier: VECC
Station number: 42809
Observation time: 220517/1200
Station latitude: 22.65
Station longitude: 88.45
Station elevation: 6.0
Showalter index: -2.89s
Lifted index: -7.25
LIFT computed using virtual temperature: -8.30
SWEAT index: 251.22
K index: 39.10
Cross totals index: 20.50
Vertical totals index: 29.50
Totals totals index: 50.00
Convective Available Potential Energy: 2646.29
CAPE using virtual temperature: 2916.78
Convective Inhibition: -136.86
CINS using virtual temperature: -81.91
Equilibrium Level: 120.49
Equilibrium Level using virtual temperature: 120.40
Level of Free Convection: 746.45
LFCT using virtual temperature: 774.29
Bulk Richardson Number: 82.53
Bulk Richardson Number using CAPV: 90.97
Temp [K] of the Lifted Condensation Level: 295.95
Pres [hPa] of the Lifted Condensation Level: 888.01
Equivalent potential temp [K] of the LCL: 367.03
Mean mixed layer potential temperature: 306.17
Mean mixed layer mixing ratio: 20.16
1000 hPa to 500 hPa thickness: 5844.00
Precipitable water [mm] for entire sounding: 56.58

RESULTS AND DISCUSSION

Comparison between 00Z and 12Z sounding data of thunderstorm day on 17th May 2022 over Kolkata region

Table 3.8 Kolkata Observations at 00Z and 12Z sounding data of thunderstorm day on 17 May 2022 (Case 8) over Kolkata region.

Index	00Z	12Z	Index	00Z	12Z
K	26.30	39.10	RINO	84.83	82.53
TT	50.60	50	SI	-1.26	-2.89
SLI	-8.28	-7.25	HI	40	23
CINE	-135.39	-81.91	DCI	44.28	47.45
SWEAT	365.44	251.22	BI	96.7	100.9
CAPE	2091.06	2916.78			

At 0000 UTC Sounding data of thunderstorm day, the CAPE is 2091.06 J/Kg which is moderately unstable. Then the TT index is 50.60 (thunderstorms are more likely, possibly severe) and K-index is 26.30 (thunderstorms with heavy rain or severe weather are possible). The DCI is 44.28 (potential for strong thunderstorms) and SLI is -8.28 (very unstable). The RINO is 84.83 (Relatively weak vertical wind shear and high CAPE suggest multicellular thunderstorm development is most likely) and SI is -1.26 which is moderately unstable. Suggesting high instability of the atmosphere suitable for thunderstorm formation .

But at 1200 UTC , the values of CAPE, CINE, SLI and K values are increased and TT, RINO and SWEAT values are reduced because the thunderstorm might have started and getting stronger than previous atmosphere which may lead to thunderstorm.

9th case of thunderstorm day on 19th May 2022 over Kolkata Region, West Bengal, India

At 00Z Skew T - Log P diagram of thunderstorm day on 19th May 2022 is shown in **Figure 3.21** over Kolkata region.

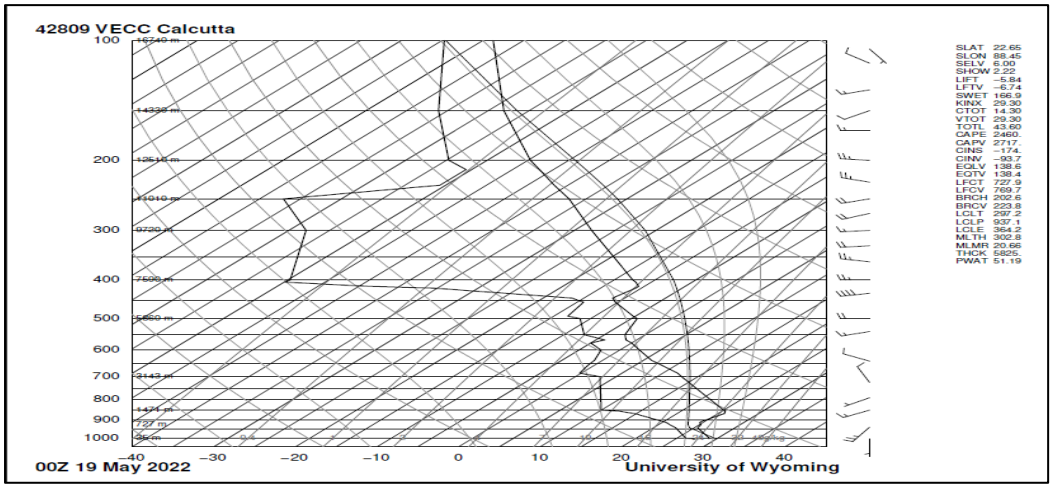

Figure 3.21 At 00 Z Skew T - Log P diagram of thunderstorm day on 19th May 2022 over Kolkata region

Station identifier: VECC
Station number: 42809
Observation time: 220519/0000
Station latitude: 22.65
Station longitude: 88.45
Station elevation: 6.0
Showalter index: 2.22
Lifted index: -5.84
LIFT computed using virtual temperature: -6.74
SWEAT index: 166.99
K index: 29.30
Cross totals index: 14.30
Vertical totals index: 29.30
Totals totals index: 43.60
Convective Available Potential Energy: 2460.29
CAPE using virtual temperature: 2717.73
Convective Inhibition: -174.62
CINS using virtual temperature: -93.79
Equilibrium Level: 138.63
Equilibrium Level using virtual temperature: 138.49
Level of Free Convection: 727.92
LFCT using virtual temperature: 769.74
Bulk Richardson Number: 202.65
Bulk Richardson Number using CAPV: 223.86
Temp [K] of the Lifted Condensation Level: 297.22
Pres [hPa] of the Lifted Condensation Level: 937.10
Equivalent potential temp [K] of the LCL: 364.26
Mean mixed layer potential temperature: 302.80
Mean mixed layer mixing ratio: 20.66
1000 hPa to 500 hPa thickness: 5825.00
Precipitable water [mm] for entire sounding: 51.19

At 12Z Skew T - Log P diagram of thunderstorm day on 19th May 2022 is shown in **Figure 3.22** over Kolkata region.

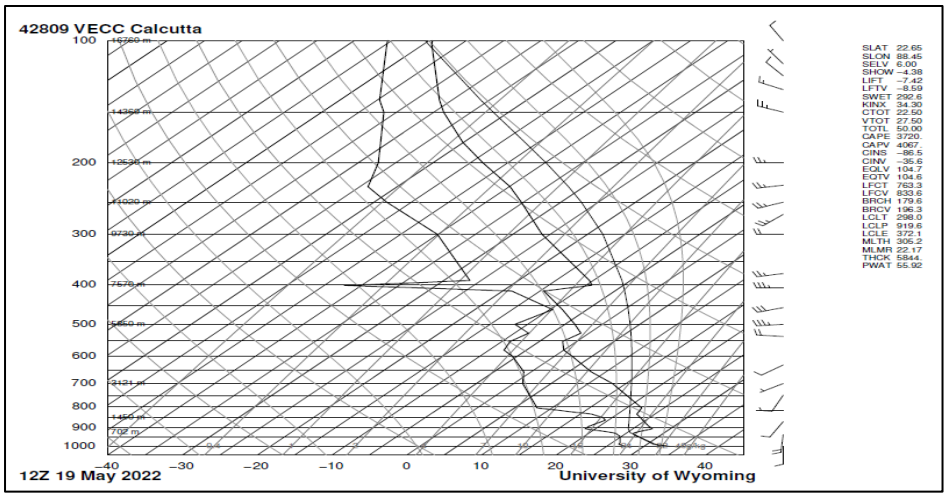

Figure 3.22 At 12 Z Skew T - Log P diagram of thunderstorm day on 19th May 2022 over Kolkata region.

Station identifier: VECC
Station number: 42809
Observation time: 220519/1200
Station latitude: 22.65
Station longitude: 88.45
Station elevation: 6.0
Showalter index: -4.38
Lifted index: -7.42
LIFT computed using virtual temperature: -8.59
SWEAT index: 292.61
K index: 34.30
Cross totals index: 22.50
Vertical totals index: 27.50
Totals totals index: 50.00
Convective Available Potential Energy: 3720.35
CAPE using virtual temperature: 4067.39
Convective Inhibition: -86.51
CINS using virtual temperature: -35.66
Equilibrium Level: 104.72
Equilibrium Level using virtual temperature: 104.66
Level of Free Convection: 763.36
LFCT using virtual temperature: 833.64
Bulk Richardson Number: 179.60
Bulk Richardson Number using CAPV: 196.35
Temp [K] of the Lifted Condensation Level: 298.06
Pres [hPa] of the Lifted Condensation Level: 919.68
Equivalent potential temp [K] of the LCL: 372.11
Mean mixed layer potential temperature: 305.28
Mean mixed layer mixing ratio: 22.17
1000 hPa to 500 hPa thickness: 5844.00
Precipitable water [mm] for entire sounding: 55.92

RESULTS AND DISCUSSION

Comparison between at 00Z and 12Z sounding data of thunderstorm day on 19th May 2022 over Kolkata region

Table 3.9 Kolkata Observations at 00Z and 12Z sounding data of thunderstorm day on 19th May 2022 (Case 9) over Kolkata region.

Index	00Z	12Z	Index	00Z	12Z
K	29.30	34.30	RINO	202.65	179.60
TT	43.60	50.00	SI	2.22	-4.38
SLI	-5.84	-7.42	HI	32	25
CINE	-93.79	-35.66	DCI	40.84	50.02
SWEAT	166.99	292.61	BI	97.8	98.3
CAPE	2717.73	4067.39			

At 0000 UTC Sounding data of thunderstorm day, the CAPE is 2717.73 J/Kg which is very unstable. Then the TT index is 43.60 (thunderstorms possible) and K-index is 29.30 (thunderstorms with heavy rain or severe weather are possible). The DCI is 40.84 (potential for strong thunderstorms) and SLI is -5.84 (moderately unstable). The RINO is 202.65 (Relatively weak vertical wind shear and high CAPE suggest multicellular thunderstorm development is most likely) and SI is 2.22 which is stable but weak convection is possible if strong lifting is present. Suggesting high instability of the atmosphere suitable for thunderstorm formation.

But at 1200 UTC , the values of CAPE, CINE, K, TT and SWEAT values are increased and, LI and RINO values are reduced because the thunderstorm might have started and getting stronger than previous atmosphere which may lead to thunderstorm .

10th case of thunderstorm day on 20th May 2022 over Kolkata Region, West Bengal, India

At 00Z Skew T - Log P diagram of thunderstorm day on 20th May 2022 is shown in **Figure 3.23** over Kolkata region.

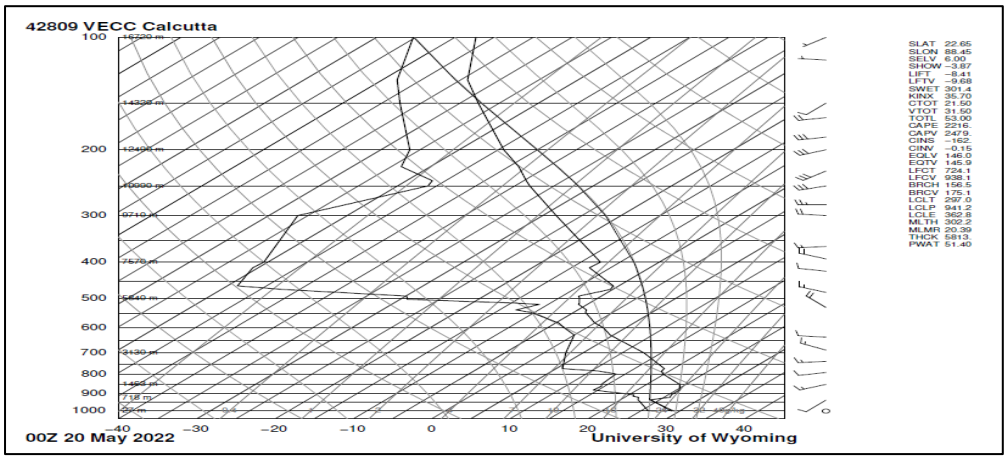

Figure 3.23 At 00 Z Skew T - Log P diagram of thunderstorm day on 20th May 2022 over Kolkata region.

Station identifier: VECC
Station number: 42809
Observation time: 220520/0000
Station latitude: 22.65
Station longitude: 88.45
Station elevation: 6.0
Showalter index: -3.87
Lifted index: -8.41
LIFT computed using virtual temperature: -9.68
SWEAT index: 301.41
K index: 35.70
Cross totals index: 21.50
Vertical totals index: 31.50
Totals totals index: 53.00
Convective Available Potential Energy: 2216.29
CAPE using virtual temperature: 2479.43
Convective Inhibition: -162.74
CINS using virtual temperature: -0.15
Equilibrium Level: 146.05
Equilibrium Level using virtual temperature: 145.95
Level of Free Convection: 724.16
LFCT using virtual temperature: 938.11
Bulk Richardson Number: 156.57
Bulk Richardson Number using CAPV: 175.16
Temp [K] of the Lifted Condensation Level: 297.09
Pres [hPa] of the Lifted Condensation Level: 941.28
Equivalent potential temp [K] of the LCL: 362.81
Mean mixed layer potential temperature: 302.28
Mean mixed layer mixing ratio: 20.39
1000 hPa to 500 hPa thickness: 5813.00
Precipitable water [mm] for entire sounding: 51.40

At 12Z Skew T - Log P diagram of thunderstorm day on 20th May 2022 is shown in **Figure 3.24** over Kolkata region.

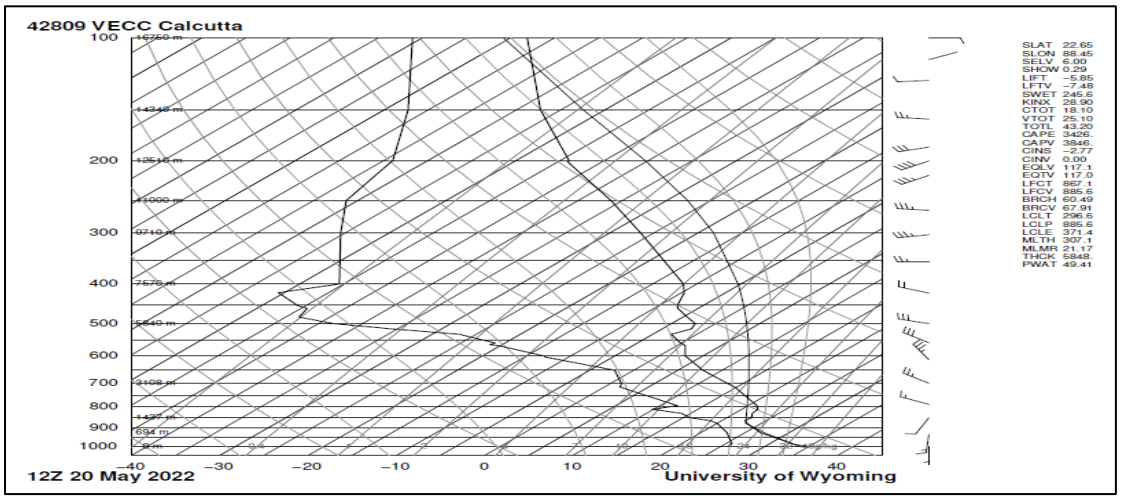

Figure 3.24 At 12 Z Skew T - Log P diagram of thunderstorm day of 20th May 2022 over Kolkata region.

Station identifier: VECC
Station number: 42809
Observation time: 220520/1200
Station latitude: 22.65
Station longitude: 88.45
Station elevation: 6.0
Showalter index: 0.29
Lifted index: -5.85
LIFT computed using virtual temperature: -7.48
SWEAT index: 245.60
K index: 28.90
Cross totals index: 18.10
Vertical totals index: 25.10
Totals totals index: 43.20
Convective Available Potential Energy: 3426.82
CAPE using virtual temperature: 3846.89
Convective Inhibition: -2.77
CINS using virtual temperature: 0.00
Equilibrium Level: 117.14
Equilibrium Level using virtual temperature: 117.07
Level of Free Convection: 867.13
LFCT using virtual temperature: 885.61
Bulk Richardson Number: 60.49
Bulk Richardson Number using CAPV: 67.91
Temp [K] of the Lifted Condensation Level: 296.69
Pres [hPa] of the Lifted Condensation Level: 885.61
Equivalent potential temp [K] of the LCL: 371.42
Mean mixed layer potential temperature: 307.17
Mean mixed layer mixing ratio: 21.17
1000 hPa to 500 hPa thickness: 5848.00
Precipitable water [mm] for entire sounding: 49.41

RESULTS AND DISCUSSION

Comparison at 00Z and 12Z sounding data of non-thunderstorm day on 20th May 2022 over Kolkata region

Table 3.10 Kolkata Observations at 00Z and 12Z sounding data of thunderstorm day on 20th May 2022 (Case 10) over Kolkata region.

Index	00Z	12Z	Index	00Z	12Z
K	35.70	28.90	RINO	156.57	60.49
TT	53	43.20	SI	-3.87	0.29
SLI	-8.41	-5.85	HI	42	60
CINE	-0.15	0.00	DCI	46.81	44.45
SWEAT	301.41	245.60	BI	97.5	98.4
CAPE	2479.43	3846.89			

At 0000 UTC Sounding data of thunderstorm day, the CAPE is 2479.43J/Kg which is moderately unstable. Then the TT index is 53 (thunderstorms are more likely, possibly severe) and K-index is 35.70 (better potential for thunderstorms with heavy rain). The DCI is 46.81 (potential for strong thunderstorms) and SLI is -8.41 (very unstable). The RINO is 156.57 (Relatively weak vertical wind shear and high CAPE suggest multicellular thunderstorm development is most likely) and SI is -3.87 which is very unstable. Suggesting high instability of the atmosphere suitable for thunderstorm formation .

But at 1200 UTC, the values of CAPE, CINE and SLI values are increased and K, TT, RINO and SWEAT values are reduced because the thunderstorm might have started and getting stronger than previous atmosphere which may lead to thunderstorm .

11th case of thunderstorm day on 21st May 2022 over Kolkata Region, West Bengal, India

At 00Z Skew T - Log P diagram of thunderstorm day on 21st May 2022 is shown in **Figure 3.25** over Kolkata region.

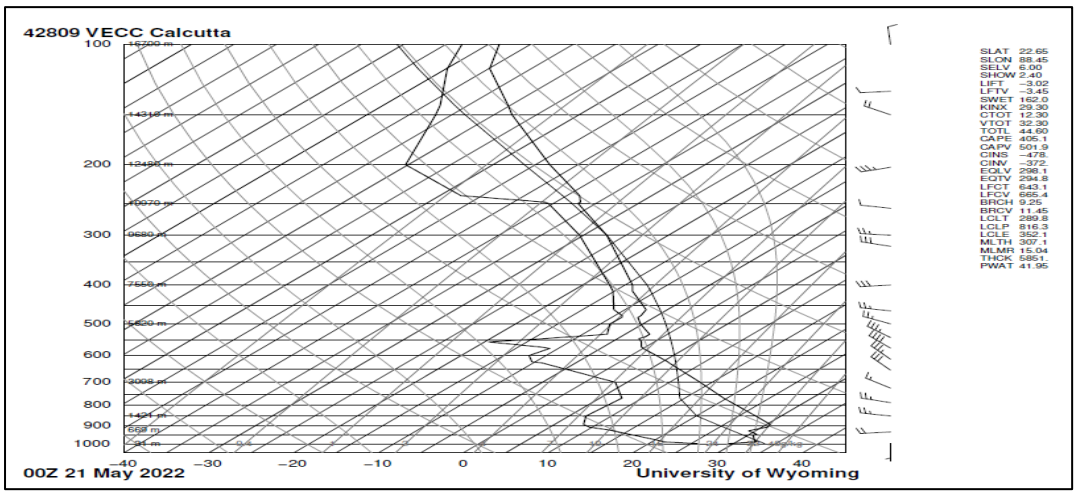

Figure 3.25 At 00 Z Skew T - Log P diagram of thunderstorm day on 21st May 2022 over Kolkata region.

Station identifier: VECC
Station number: 42809
Observation time: 220521/0000
Station latitude: 22.65
Station longitude: 88.45
Station elevation: 6.0
Showalter index: 2.40
Lifted index: -3.02
LIFT computed using virtual temperature: -3.45
SWEAT index: 162.01
K index: 29.30
Cross totals index: 12.30
Vertical totals index: 32.30
Totals totals index: 44.60
Convective Available Potential Energy: 405.16
CAPE using virtual temperature: 501.94
Convective Inhibition: -478.58
CINS using virtual temperature: -372.72
Equilibrium Level: 298.15
Equilibrium Level using virtual temperature: 294.87
Level of Free Convection: 643.10
LFCT using virtual temperature: 665.43
Bulk Richardson Number: 9.25
Bulk Richardson Number using CAPV: 11.45
Temp [K] of the Lifted Condensation Level: 289.83
Pres [hPa] of the Lifted Condensation Level: 816.36
Equivalent potential temp [K] of the LCL: 352.12
Mean mixed layer potential temperature: 307.14
Mean mixed layer mixing ratio: 15.04
1000 hPa to 500 hPa thickness: 5851.00
Precipitable water [mm] for entire sounding: 41.95

RESULTS AND DISCUSSION

Comparison at 00Z and 12Z sounding data of non-thunderstorm day on 21st May 2022 over Kolkata region.

Table 3.11 Kolkata Observations at 00Z and 12Z sounding data of thunderstorm day On 21st May 2022 (Case 11) over Kolkata region.

Index	00Z	Index	00Z
K	29.30	RINO	9,25
TT	44.60	SI	2.40
SLI	-3.02	HI	33.6
CINE	-372.72	DCI	37.02
SWEAT	162.01	BI	99.3
CAPE	501.94		

At 0000 UTC Sounding data of thunderstorm day, the CAPE is 501.94 J/Kg which is marginally unstable. Then the TT index is 44.60 (thunderstorms possible) and K-index is 29.30 (thunderstorms with heavy rain or severe weather are possible). The DCI is 37.02 (potential for strong thunderstorms) and SLI is -3.02 (moderately unstable). The RINO is 9.25 (strong vertical wind shear and weak CAPE. The shear may be too strong given the weak buoyancy to develop sustained convective updrafts. However, given sufficient forcing, thunderstorms may still develop; if so, rotating supercells could evolve given the high shear) and SI is 2.40 (stable but weak convection is possible if strong lifting is present). Suggesting instability of the atmosphere suitable for thunderstorm formation.

I have selected 11 cases of thunderstorms days such as (17th, 21st, 22nd, 29th) month of April and (1st, 3rd, 13th, 17th, 19th, 20th, 21st) month of May in the year 2022. From above mentioned Skew T-LogP curves shows that was high and CINE was less and other indices such as K-Index, TT, SLI, SWEAT, RINO also suggests high instability of the atmosphere which may lead to thunderstorm.

Observation based studies of Non - thunderstorm over Kolkata Region, West Bengal, India

1st case of Non-thunderstorm day on 16th April 2022 over Kolkata region

At 00Z Skew T - Log P diagram of non-thunderstorm day on 16th April 2022 is shown in **Figure 3.26** over Kolkata region.

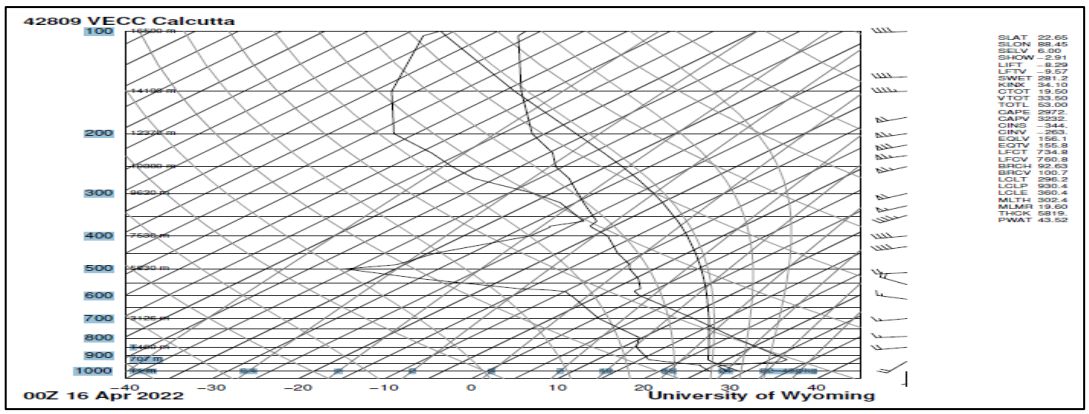

Figure 3.26 At 00Z Skew T - Log P diagram of non-thunderstorm day on 16th April 2022 over Kolkata region.

Station identifier: VECC
Station number: 42809
Observation time: 220416/0000
Station latitude: 22.65
Station longitude: 88.45
Station elevation: 6.0
Showalter index: -2.91
Lifted index: -8.29
LIFT computed using virtual temperature: -9.57
SWEAT index: 281.20
K index: 34.10
Cross totals index: 19.50
Vertical totals index: 33.50
Totals totals index: 53.00
Convective Available Potential Energy: 2972.61
CAPE using virtual temperature: 3232.04
Convective Inhibition: -344.51
CINS using virtual temperature: -263.17
Equilibrium Level: 156.10
Equilibrium Level using virtual temperature: 155.85
Level of Free Convection: 734.85
LFCT using virtual temperature: 760.87
Bulk Richardson Number: 92.63
Bulk Richardson Number using CAPV: 100.71
Temp [K] of the Lifted Condensation Level: 296.22
Pres [hPa] of the Lifted Condensation Level: 930.40
Equivalent potential temp [K] of the LCL: 360.42
Mean mixed layer potential temperature: 302.41
Mean mixed layer mixing ratio: 19.60
1000 hPa to 500 hPa thickness: 5819.00
Precipitable water [mm] for entire sounding: 43.52

At 12Z Skew T - Log P diagram of non-thunderstorm day on 16th April 2022 is shown in **Figure 3.27** over Kolkata region.

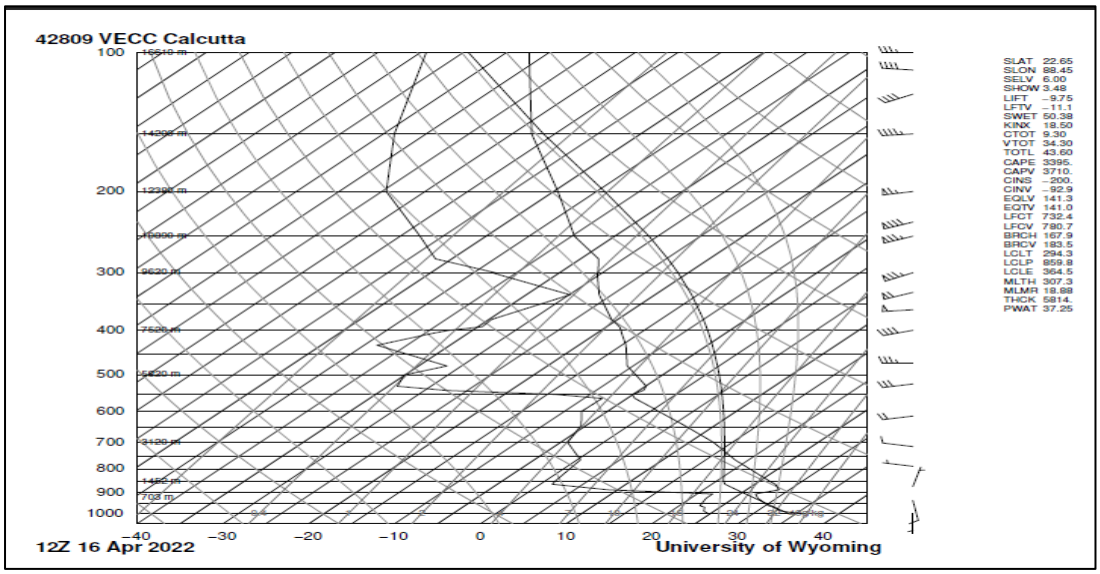

Figure 3.27 At 12Z Skew T - Log P diagram of non-thunderstorm day on 16th April 2022 over Kolkata region.

Station identifier: VECC
Station number: 42809
Observation time: 220416/1200
Station latitude: 22.65
Station longitude: 88.45
Station elevation: 6.0
Showalter index: 3.48
Lifted index: -9.75
LIFT computed using virtual temperature: -11.13
SWEAT index: 50.38
K index: 18.50
Cross totals index: 9.30
Vertical totals index: 34.30
Totals totals index: 43.60
Convective Available Potential Energy: 3395.07
CAPE using virtual temperature: 3710.68
Convective Inhibition: -200.08
CINS using virtual temperature: -92.95
Equilibrium Level: 141.32
Equilibrium Level using virtual temperature: 141.06
Level of Free Convection: 732.40
LFCT using virtual temperature: 780.77
Bulk Richardson Number: 167.93
Bulk Richardson Number using CAPV: 183.54
Temp [K] of the Lifted Condensation Level: 294.37
Pres [hPa] of the Lifted Condensation Level: 859.87
Equivalent potential temp [K] of the LCL: 364.55
Mean mixed layer potential temperature: 307.36
Mean mixed layer mixing ratio: 18.88
1000 hPa to 500 hPa thickness: 5814.00
Precipitable water [mm] for entire sounding: 37.25

RESULTS AND DISCUSSION

Comparison at 00Z and 12Z sounding data of non-thunderstorm day on 16th April 2022 over Kolkata region.

Table 3.12 Kolkata Observations at 00Z and 12Z sounding data of non-thunderstorm day on 16th April 2022 over Kolkata region

Index	00Z	12Z	Index	00Z	12Z
KI	34.10	18.50	RINO	92.63	167.93
TT	53	43.60	SI	-2.91	3.48
SLI	-8.29	-9.75	HI	58	69
CINE	-263.17	-92.95	DCI	45.49	37.15
SWEAT	281.20	50.38	BI	100.1	98.6
CAPE	3232.04	3710.68			

At 0000 UTC Sounding data, the CAPE is 3232.04 J/Kg which is very unstable. Then the TT index is 53 (thunderstorm are more likely, possibly severe) and K-index is 34.10 (better potential for thunderstorms with heavy rain). The DCI is 45.49 (potential for strong thunderstorms) and SLI is -8.29 (very unstable). The RINO is 92.63 (Relatively weak vertical wind shear and high CAPE suggest multicellular thunderstorm development is most likely) and SI is -2.91 which is moderately unstable. Suggesting high instability of the atmosphere suitable for thunderstorm formation.

But at 1200 UTC , the values of CAPE ,CINE, SI, HI and RINO values are increased and SLI, KI, TT, DCI, BI and SWEAT values are reduced because the thunderstorm might have started and getting stronger than previous atmosphere which may lead to thunderstorm. Next day on 17th April 2022 occurred thunderstorm with heavy rainfall over Kolkata region.

2nd case of Non-thunderstorm day on 18th April 2022 over Kolkata region

At 00Z Skew T - Log P diagram of non-thunderstorm day on 18th April 2022 is shown in **Figure 3.28** over Kolkata region.

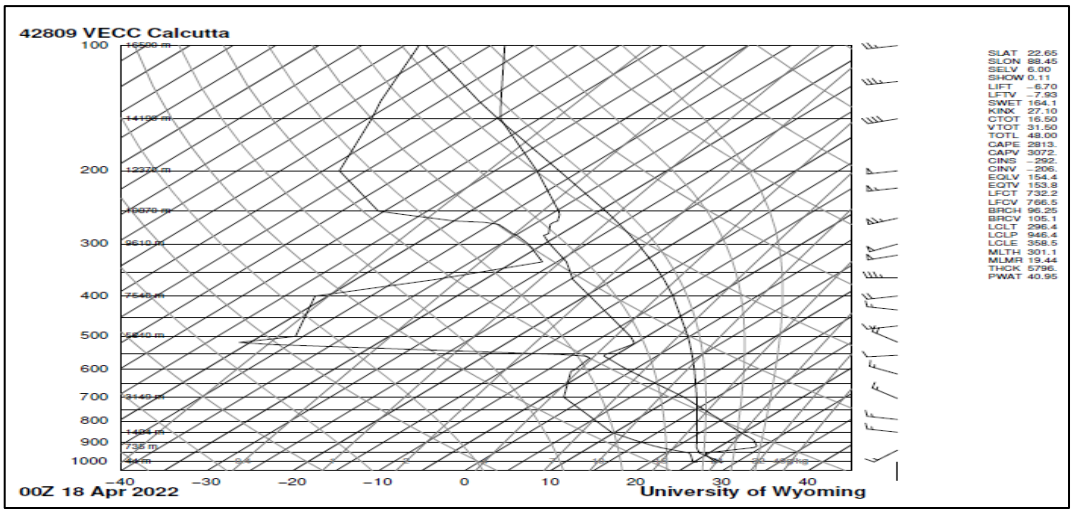

Figure 3.28 At 00 Z Skew T - Log P diagram of non-thunderstorm day on 18th April 2022 over Kolkata region.

Station identifier: VECC
Station number: 42809
Observation time: 220418/0000
Station latitude: 22.65
Station longitude: 88.45
Station elevation: 6.0
Showalter index: 0.11
Lifted index: -6.70
LIFT computed using virtual temperature: -7.93
SWEAT index: 164.19
K index: 27.10
Cross totals index: 16.50
Vertical totals index: 31.50
Totals totals index: 48.00
Convective Available Potential Energy: 2813.10
CAPE using virtual temperature: 3072.10
Convective Inhibition: -292.30
CINS using virtual temperature: -206.38
Equilibrium Level: 154.48
Equilibrium Level using virtual temperature: 153.89
Level of Free Convection: 732.22
LFCT using virtual temperature: 766.53
Bulk Richardson Number: 96.25
Bulk Richardson Number using CAPV: 105.11
Temp [K] of the Lifted Condensation Level: 296.42
Pres [hPa] of the Lifted Condensation Level: 946.42
Equivalent potential temp [K] of the LCL: 358.53
Mean mixed layer potential temperature: 301.13
Mean mixed layer mixing ratio: 19.44
1000 hPa to 500 hPa thickness: 5796.00
Precipitable water [mm] for entire sounding: 40.95

At 12Z Skew T - Log P diagram of non-thunderstorm day on 18th April 2022 is shown in **Figure 3.29** over Kolkata region.

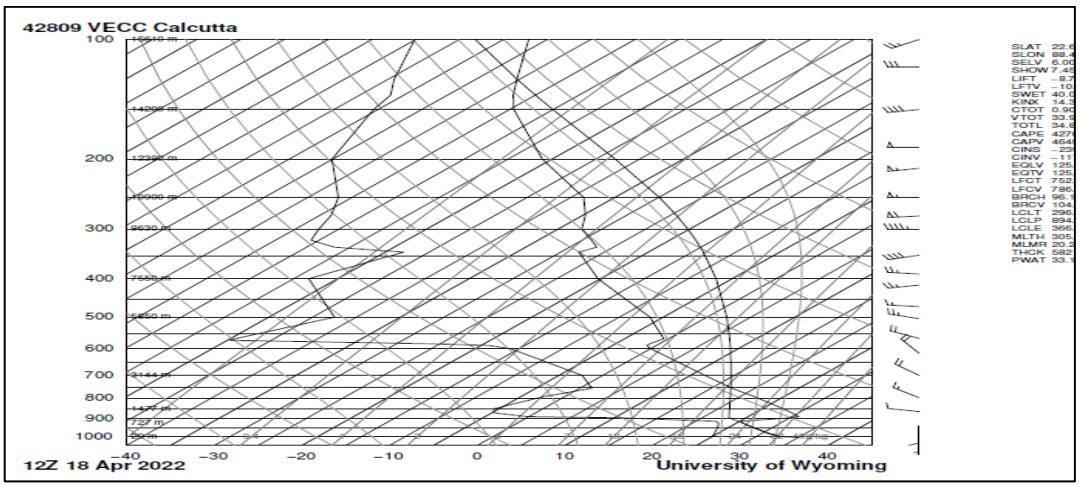

Figure 3.29 At 12Z Skew T - Log P diagram of non-thunderstorm day on 18th April 2022 over Kolkata region.

Station identifier: VECC
Station number: 42809
Observation time: 220418/1200
Station latitude: 22.65
Station longitude: 88.45
Station elevation: 6.0
Showalter index: 7.45
Lifted index: -8.78
LIFT computed using virtual temperature: -10.27
SWEAT index: 40.00
K index: 14.30
Cross totals index: 0.90
Vertical totals index: 33.90
Totals totals index: 34.80
Convective Available Potential Energy: 4270.86
CAPE using virtual temperature: 4645.42
Convective Inhibition: -239.08
CINS using virtual temperature: -117.75
Equilibrium Level: 125.82
Equilibrium Level using virtual temperature: 125.80
Level of Free Convection: 752.17
LFCT using virtual temperature: 786.51
Bulk Richardson Number: 96.19
Bulk Richardson Number using CAPV: 104.63
Temp [K] of the Lifted Condensation Level: 296.16
Pres [hPa] of the Lifted Condensation Level: 894.73
Equivalent potential temp [K] of the LCL: 366.81
Mean mixed layer potential temperature: 305.73
Mean mixed layer mixing ratio: 20.27
1000 hPa to 500 hPa thickness: 5821.00
Precipitable water [mm] for entire sounding: 33.11

RESULTS AND DISCUSSION

Comparison at 00Z and 12Z sounding data of non-thunderstorm on 18th April 2022 over Kolkata region

Table 3.13 42809 VECC Kolkata Observations at 00Z and 12Z sounding data of non-thunderstorm on 18th April 2022 Over Kolkata region

Index	00Z	12Z	Index	00Z	12Z
K	27.10	14.30	RINO	96.25	96.19
TT	48	34.80	SI	0.11	7.45
SLI	-6.70	-8.78	HI	68	83
CINE	-206.38	-117.75	DCI	40.9	30.58
SWEAT	164.19	40	BI	99.3	99.9
CAPE	3072.1	4645.42			

At 0000 UTC Sounding data, the CAPE is 3072.1 J/Kg which is very unstable. Then the TT index is 48 (thunderstorm possible) and K-index is 27.10 (thunderstorms with heavy rain or severe weather are possible). The DCI is 40.09 (potential for strong thunderstorms) and SLI is -6.70 (extremely unstable). The RINO is 96.25 (Relatively weak vertical wind shear and high CAPE suggest multicellular thunderstorm development is most likely) and SI is 0.11 which is stable but weak convection is possible if strong lifting is present. Suggesting high instability of the atmosphere suitable for thunderstorm formation.

But at 1200 UTC , the values of CAPE ,CINE, SI, HI and BI values are increased and SLI, KI , TT, DCI, RINO and SWEAT values are reduced because the thunderstorm getting stronger than previous atmosphere which may lead to formation of thunderstorm.

3rd case of Non-thunderstorm day on 19th April 2022 over Kolkata region

At 00Z Skew T - Log P diagram of non-thunderstorm day on 19th April 2022 is shown in **Figure 3.30** over Kolkata region.

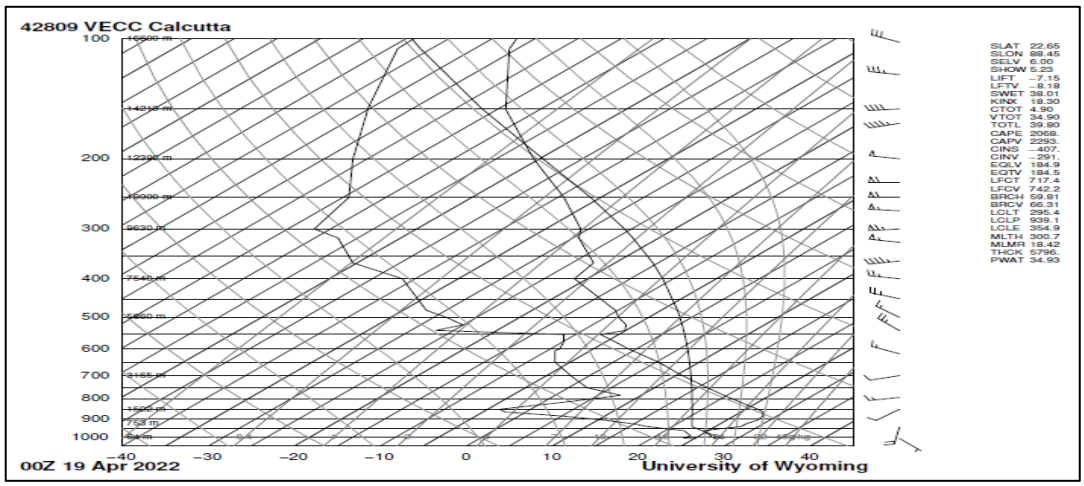

Figure 3.30 At 00Z Skew T - Log P diagram of non-thunderstorm day on 19th April 2022 over Kolkata region

Station identifier: VECC
Station number: 42809
Observation time: 220419/0000
Station latitude: 22.65
Station longitude: 88.45
Station elevation: 6.0
Showalter index: 5.23
Lifted index: -7.15
LIFT computed using virtual temperature: -8.18
SWEAT index: 38.01
K index: 18.30
Cross totals index: 4.90
Vertical totals index: 34.90
Totals totals index: 39.80
Convective Available Potential Energy: 2068.35
CAPE using virtual temperature: 2293.18
Convective Inhibition: -407.62
CINS using virtual temperature: -291.06
Equilibrium Level: 184.99
Equilibrium Level using virtual temperature: 184.51
Level of Free Convection: 717.49
LFCT using virtual temperature: 742.25
Bulk Richardson Number: 59.81
Bulk Richardson Number using CAPV: 66.31
Temp [K] of the Lifted Condensation Level: 295.41
Pres [hPa] of the Lifted Condensation Level: 939.13
Equivalent potential temp [K] of the LCL: 354.96
Mean mixed layer potential temperature: 300.77
Mean mixed layer mixing ratio: 18.42
1000 hPa to 500 hPa thickness: 5796.00
Precipitable water [mm] for entire sounding: 34.93

At 12Z Skew T - Log P diagram of non-thunderstorm day on 19th April 2022 is shown in **Figure 3.31** over Kolkata region.

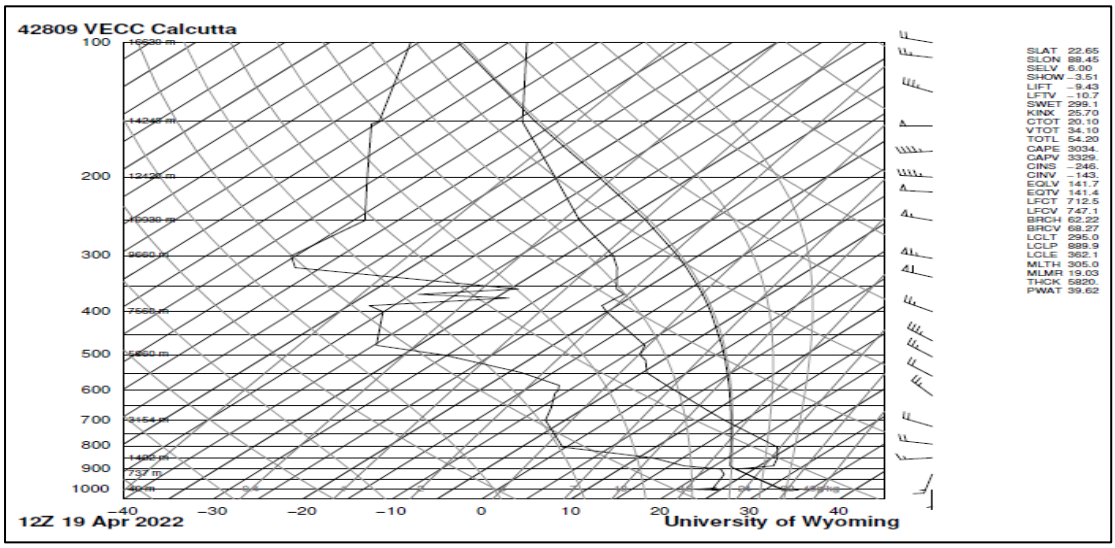

Figure 3.31 At 12Z Skew T - Log P diagram of non-thunderstorm day on 19th April 2022 over Kolkata region.

Station identifier: VECC
Station number: 42809
Observation time: 220419/1200
Station latitude: 22.65
Station longitude: 88.45
Station elevation: 6.0
Showalter index: -3.51
Lifted index: -9.43
LIFT computed using virtual temperature: -10.70
SWEAT index: 299.18
K index: 25.70
Cross totals index: 20.10
Vertical totals index: 34.10
Totals totals index: 54.20
Convective Available Potential Energy: 3034.01
CAPE using virtual temperature: 3329.02
Convective Inhibition: -246.40
CINS using virtual temperature: -143.80
Equilibrium Level: 141.70
Equilibrium Level using virtual temperature: 141.48
Level of Free Convection: 712.54
LFCT using virtual temperature: 747.15
Bulk Richardson Number: 62.22
Bulk Richardson Number using CAPV: 68.27
Temp [K] of the Lifted Condensation Level: 295.06
Pres [hPa] of the Lifted Condensation Level: 889.97
Equivalent potential temp [K] of the LCL: 362.16
Mean mixed layer potential temperature: 305.06
Mean mixed layer mixing ratio: 19.03
1000 hPa to 500 hPa thickness: 5820.00
Precipitable water [mm] for entire sounding: 39.62

RESULTS AND DISCUSSION

Comparison at 00Z and 12Z sounding data of non-Thunderstrom day On 19th April 2022 over Kolkata region

Table 3.14 42809 VECC Kolkata Observations at 00Z and 12Z sounding data on 19th April 2022 over Kolkata region

Index	00Z	12Z	Index	00Z	12Z
K	18.30	25.70	RINO	59.81	62.22
TT	39.80	299.18	SI	5.23	-3.51
SLI	-7.15	-9.43	HI	63	56
CINE	-291.06	-143.80	DCI	29.95	46.63
SWEAT	38.01	54.20	BI	99.3	98.6
CAPE	2293.18	3329.02			

At 0000 UTC Sounding data, the CAPE is 2293.18 J/Kg which is moderately unstable. Then the TT index is 39.80 (thunderstorm possible) and K-index is 18.30 (thunderstorms with heavy rain or severe weather are possible). The DCI is 29.95 (potential for strong thunderstorms) and SLI is -7.15 (very unstable). The RINO is 59.81 (Relatively weak vertical wind shear and high CAPE suggest multicellular thunderstorm development is most likely) and SI is 5.23 which is stable but weak convection is possible if strong lifting is present. Suggesting high instability of the atmosphere suitable for thunderstorm formation.

But at 1200 UTC , the values of CAPE ,CINE, SWEAT, KI, TT, DCI and RINO values are increased and SLI, SI, HI and BI values are reduced because the thunderstorm getting stronger than previous atmosphere which may lead to formation of thunderstorm.

4th case of Non-thunderstorm day on 20th April 2022 over Kolkata region

At 00Z Skew T - Log P diagram of non-thunderstorm day on 20th April 2022 is shown in **Figure 3.32** over Kolkata region.

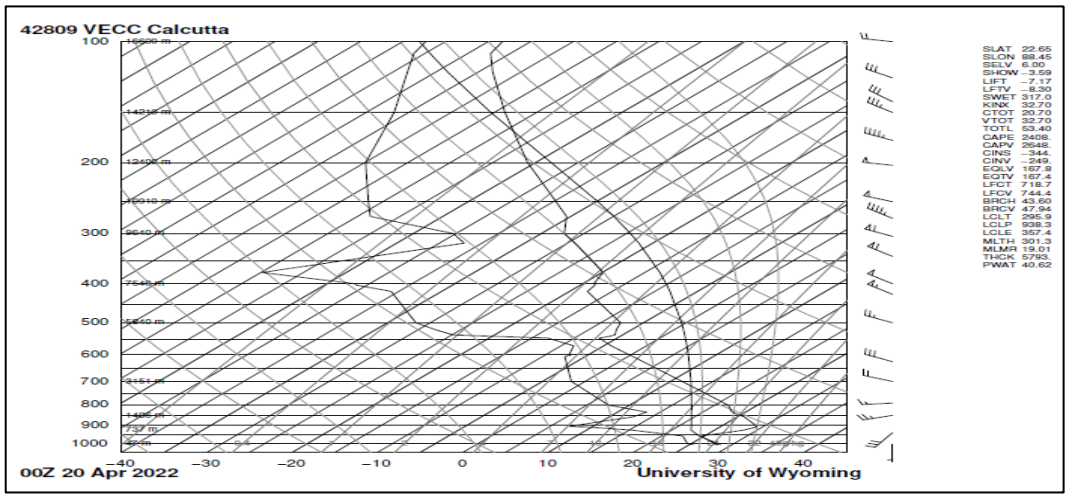

Figure 3.32 At 00Z Skew T - Log P diagram of non-thunderstorm day on 20th April 2022 over Kolkata region.

Station identifier: VECC
Station number: 42809
Observation time: 220420/0000
Station latitude: 22.65
Station longitude: 88.45
Station elevation: 6.0
Showalter index: -3.59
Lifted index: -7.17
LIFT computed using virtual temperature: -8.30
SWEAT index: 317.00
K index: 32.70
Cross totals index: 20.70
Vertical totals index: 32.70
Totals totals index: 53.40
Convective Available Potential Energy: 2408.23
CAPE using virtual temperature: 2648.19
Convective Inhibition: -344.25
CINS using virtual temperature: -249.61
Equilibrium Level: 167.85
Equilibrium Level using virtual temperature: 167.46
Level of Free Convection: 718.78
LFCT using virtual temperature: 744.45
Bulk Richardson Number: 43.60
Bulk Richardson Number using CAPV: 47.94
Temp [K] of the Lifted Condensation Level: 295.91
Pres [hPa] of the Lifted Condensation Level: 938.35
Equivalent potential temp [K] of the LCL: 357.48
Mean mixed layer potential temperature: 301.35
Mean mixed layer mixing ratio: 19.01
1000 hPa to 500 hPa thickness: 5793.00
Precipitable water [mm] for entire sounding: 40.62

At 12Z Skew T - Log P diagram of non-thunderstorm day on 20th April 2022 is shown in **Figure 3.33** over Kolkata region.

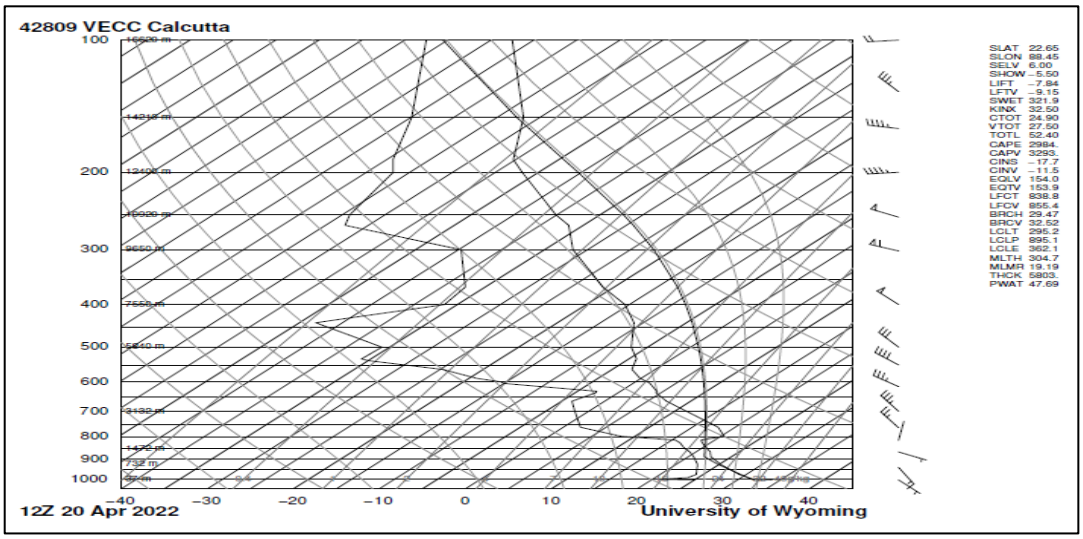

Figure 3.33 At 12Z Skew T - Log P diagram of non-thunderstorm day on 20th April 2022 over Kolkata region.

Station identifier: VECC
Station number: 42809
Observation time: 220420/1200
Station latitude: 22.65
Station longitude: 88.45
Station elevation: 6.0
Showalter index: -5.50
Lifted index: -7.84
LIFT computed using virtual temperature: -9.15
SWEAT index: 321.98
K index: 32.50
Cross totals index: 24.90
Vertical totals index: 27.50
Totals totals index: 52.40
Convective Available Potential Energy: 2984.61
CAPE using virtual temperature: 3293.21
Convective Inhibition: -17.79
CINS using virtual temperature: -11.57
Equilibrium Level: 154.00
Equilibrium Level using virtual temperature: 153.94
Level of Free Convection: 838.84
LFCT using virtual temperature: 855.44
Bulk Richardson Number: 29.47
Bulk Richardson Number using CAPV: 32.52
Temp [K] of the Lifted Condensation Level: 295.26
Pres [hPa] of the Lifted Condensation Level: 895.13
Equivalent potential temp [K] of the LCL: 362.19
Mean mixed layer potential temperature: 304.77
Mean mixed layer mixing ratio: 19.19
1000 hPa to 500 hPa thickness: 5803.00
Precipitable water [mm] for entire sounding: 47.69

RESULTS AND DISCUSSION

Comparison between at 00Z and 12Z sounding data on 20th April 2022 Over Kolkata region

Table 3.15 42809 VECC Kolkata Observations at 00Z and 12Z on 20th April 2022 over Kolkata region

Index	00Z	12Z	Index	00Z	12Z
K	32.70	32.50	RINO	43.60	29.47
TT	53.40	52.40	SI	-3.59	-5.50
SLI	-7.17	-7.84	HI	49	44.6
CINE	-249.61	-11.57	DCI	45.17	46.44
SWEAT	317	321.98	BI	99	98.1
CAPE	2648.19	3293.21			

At 0000 UTC Sounding data, the CAPE is 2648.19 J/Kg which is very high value and weather condition is very unstable. Then the TT index is 53.40 (thunderstorms are more likely, possibly severe) and K-index is 32.70 (better potential for thunderstorms with heavy rain). The DCI is 45.17 (potential for strong thunderstorms) and SLI is -7.17 (very unstable). The RINO is 43.60 (associated with supercell development) and SI is -3.59 which is moderately unstable. Suggesting high instability of the atmosphere suitable for thunderstorm formation .

But at 1200 UTC , the values of CAPE, CINE, SWEAT and DCI values are increased and KI, TT, SLI, RINO, SI, HI and BI values are reduced because the thunderstorm getting stronger than previous atmosphere which may lead to formation of thunderstorm.

5th case of Non-thunderstorm day on 20th April 2022 over Kolkata region.

At 00Z Skew T - Log P diagram of non-thunderstorm day on 23th April 2022 is shown in **Figure 3.34** over Kolkata region.

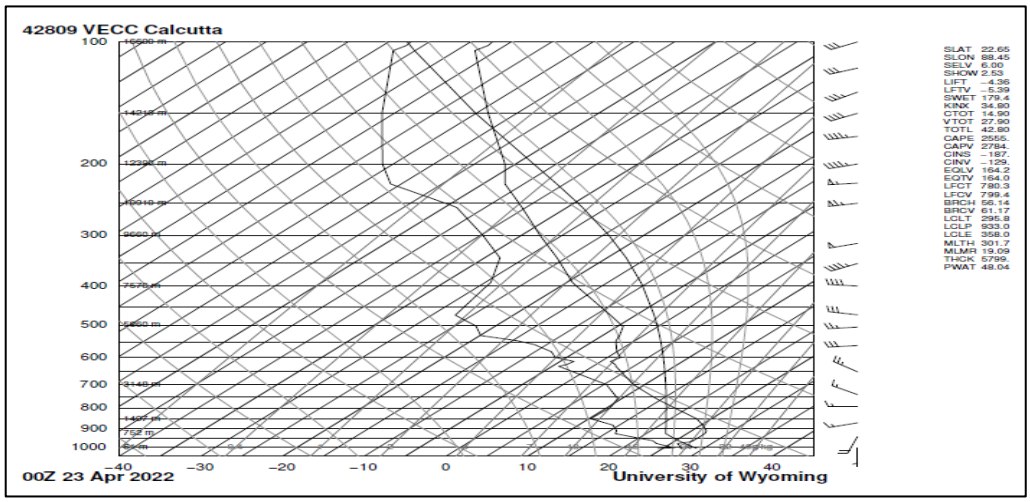

Figure 3.34 At 00Z Skew T - Log P diagram of non-thunderstorm day on 23rd April 2022 over Kolkata region.

Station identifier: VECC
Station number: 42809
Observation time: 220423/0000
Station latitude: 22.65
Station longitude: 88.45
Station elevation: 6.0
Showalter index: 2.53
Lifted index: -4.36
LIFT computed using virtual temperature: -5.39
SWEAT index: 179.41
K index: 34.80
Cross totals index: 14.90
Vertical totals index: 27.90
Totals totals index: 42.80
Convective Available Potential Energy: 2555.86
CAPE using virtual temperature: 2784.52
Convective Inhibition: -187.45
CINS using virtual temperature: -129.71
Equilibrium Level: 164.28
Equilibrium Level using virtual temperature: 164.01
Level of Free Convection: 780.39
LFCT using virtual temperature: 799.44
Bulk Richardson Number: 56.14
Bulk Richardson Number using CAPV: 61.17
Temp [K] of the Lifted Condensation Level: 295.83
Pres [hPa] of the Lifted Condensation Level: 933.00
Equivalent potential temp [K] of the LCL: 358.06
Mean mixed layer potential temperature: 301.77
Mean mixed layer mixing ratio: 19.09
1000 hPa to 500 hPa thickness: 5799.00
Precipitable water [mm] for entire sounding: 48.04

At 12Z Skew T - Log P diagram of non-thunderstorm day on 23th April 2022 is shown in **Figure 3.35** over Kolkata region.

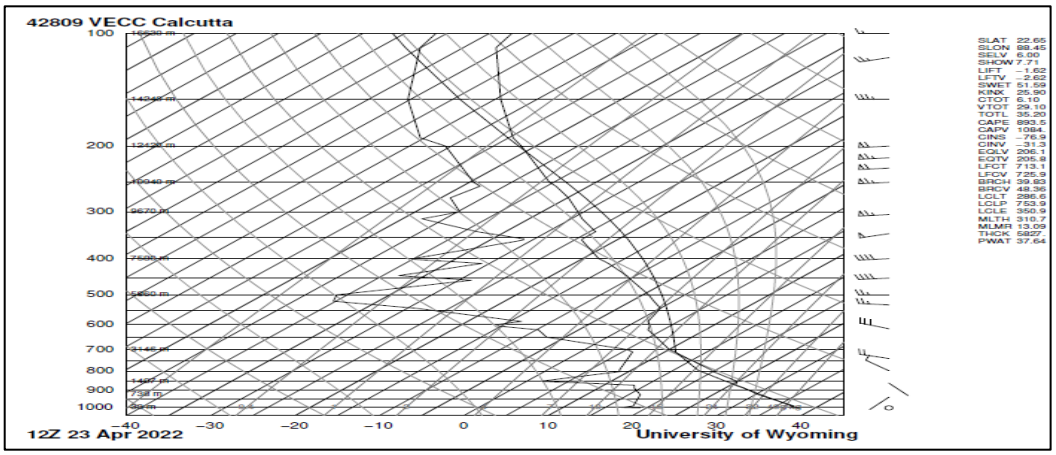

Figure 3.35 At 12Z Skew T - Log P diagram of non-thunderstorm day on 23rd April 2022 over Kolkata region.

Station identifier: VECC
Station number: 42809
Observation time: 220423/1200
Station latitude: 22.65
Station longitude: 88.45
Station elevation: 6.0
Showalter index: 7.71
Lifted index: -1.62
LIFT computed using virtual temperature: -2.62
SWEAT index: 51.59
K index: 25.90
Cross totals index: 6.10
Vertical totals index: 29.10
Totals totals index: 35.20
Convective Available Potential Energy: 893.51
CAPE using virtual temperature: 1084.85
Convective Inhibition: -76.97
CINS using virtual temperature: -31.34
Equilibrium Level: 206.17
Equilibrium Level using virtual temperature: 205.81
Level of Free Convection: 713.16
LFCT using virtual temperature: 725.98
Bulk Richardson Number: 39.83
Bulk Richardson Number using CAPV: 48.36
Temp [K] of the Lifted Condensation Level: 286.64
Pres [hPa] of the Lifted Condensation Level: 753.95
Equivalent potential temp [K] of the LCL: 350.92
Mean mixed layer potential temperature: 310.74
Mean mixed layer mixing ratio: 13.09
1000 hPa to 500 hPa thickness: 5827.00
Precipitable water [mm] for entire sounding: 37.64

RESULTS AND DISCUSSION

Comparison at 00Z and 12Z sounding data on 23th April 2022 over Kolkata region

Table 3.16 42809 VECC Kolkata Observations at 00Z and 12Z on 23th April 2022 sounding data over Kolkata region

Index	00Z	12Z	Index	00Z	12Z
K	34.80	25.90	RINO	56.14	39.83
TT	42.80	35.20	SI	2.53	7.71
SLI	-4.36	-1.62	HI	34.3	65
CINE	-129.71	-31.34	DCI	37.76	28.22
SWEAT	179.41	51.59	BI	101.1	101.3
CAPE	2784.52	1084.85			

At 0000 UTC Sounding data, the CAPE is 2784.52 J/Kg which is very high value and weather condition is very unstable. Then the TT index is 42.80 and K-index is 34.80 (better potential for thunderstorms with heavy rain). The DCI is 37.76 (potential for strong thunderstorms) and SLI is -4.36 (moderately unstable). The RINO is 56.14 (Relatively weak vertical wind shear and high CAPE suggest multicellular thunderstorm development is most likely) and SI is 2.53 which is stable but weak convection is possible if strong lifting is present. Suggesting high instability of the atmosphere suitable for thunderstorm formation .

But at 1200 UTC , the values of SLI, CINE, SI, HI and BI values are increased and KI, TT, SWEAT, RINO, CAPE and DCI values are reduced because the thunderstorm getting stronger than previous atmosphere which may lead to formation of thunderstorm.

6th case of Non-thunderstorm day on 28th April 2022 over Kolkata region.

At 00Z Skew T - Log P diagram of non-thunderstorm day on 28th April 2022 is shown in **Figure 3.36** over Kolkata region.

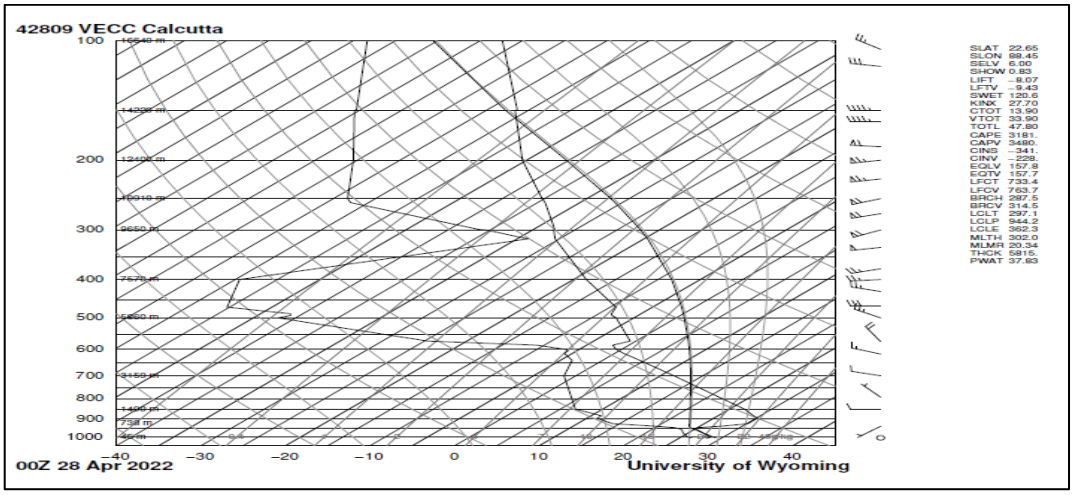

Figure 3.36 At 00Z Skew T - Log P diagram of non-thunderstorm day on 28th April 2022 over Kolkata region.

Station identifier: VECC
Station number: 42809
Observation time: 220428/0000
Station latitude: 22.65
Station longitude: 88.45
Station elevation: 6.0
Showalter index: 0.83
Lifted index: -8.07
LIFT computed using virtual temperature: -9.43
SWEAT index: 120.61
K index: 27.70
Cross totals index: 13.90
Vertical totals index: 33.90
Totals totals index: 47.80
Convective Available Potential Energy: 3181.72
CAPE using virtual temperature: 3480.92
Convective Inhibition: -341.07
CINS using virtual temperature: -228.85
Equilibrium Level: 157.84
Equilibrium Level using virtual temperature: 157.75
Level of Free Convection: 733.43
LFCT using virtual temperature: 763.72
Bulk Richardson Number: 287.50
Bulk Richardson Number using CAPV: 314.53
Temp [K] of the Lifted Condensation Level: 297.10
Pres [hPa] of the Lifted Condensation Level: 944.28
Equivalent potential temp [K] of the LCL: 362.35
Mean mixed layer potential temperature: 302.02
Mean mixed layer mixing ratio: 20.34
1000 hPa to 500 hPa thickness: 5815.00
Precipitable water [mm] for entire sounding: 37.83

At 12Z Skew T - Log P diagram of non-thunderstorm day on 28th April 2022 is shown in **Figure 3.37** over Kolkata region.

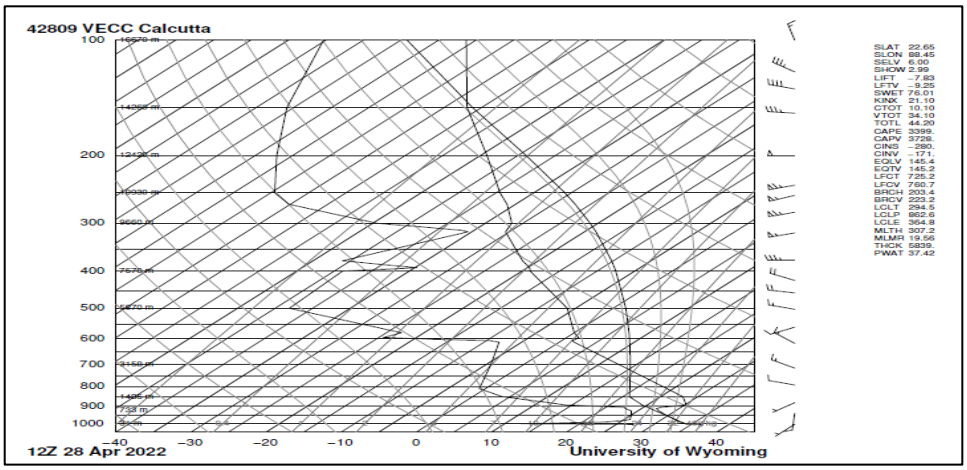

Figure 3.37 At 12Z Skew T - Log P diagram of non-thunderstorm day on 28th April 2022 over Kolkata region.

Station identifier: VECC
Station number: 42809
Observation time: 220428/1200
Station latitude: 22.65
Station longitude: 88.45
Station elevation: 6.0
Showalter index: 2.99
Lifted index: -7.83
LIFT computed using virtual temperature: -9.25
SWEAT index: 76.01
K index: 21.10
Cross totals index: 10.10
Vertical totals index: 34.10
Totals totals index: 44.20
Convective Available Potential Energy: 3399.13
CAPE using virtual temperature: 3728.91
Convective Inhibition: -280.91
CINS using virtual temperature: -171.40
Equilibrium Level: 145.40
Equilibrium Level using virtual temperature: 145.27
Level of Free Convection: 725.27
LFCT using virtual temperature: 760.71
Bulk Richardson Number: 203.49
Bulk Richardson Number using CAPV: 223.23
Temp [K] of the Lifted Condensation Level: 294.54
Pres [hPa] of the Lifted Condensation Level: 862.60
Equivalent potential temp [K] of the LCL: 364.84
Mean mixed layer potential temperature: 307.25
Mean mixed layer mixing ratio: 19.56
1000 hPa to 500 hPa thickness: 5839.00
Precipitable water [mm] for entire sounding: 37.42

RESULTS AND DISCUSSION

Comparison at 00Z and 12Z sounding data on 28th April 2022 over Kolkata region

Table 3.17 42809 VECC Kolkata Observations at 00Z and 12Z sounding data on 28th April 2022 over Kolkata region

Index	00Z	12Z	Index	00Z	12Z
K	27.70	21.10	RINO	287.50	203.49
TT	47.80	44.20	SI	0.83	2.99
SLI	-8.07	-7.83	HI	73	78
CINE	-228.85	-171.40	DCI	41.67	39.83
SWEAT	120.61	76.01	BI	99.8	100.1
CAPE	3480.92	3728.91			

At 0000 UTC Sounding data, the CAPE is 3480.92 J/Kg which is very high value and weather condition is extremely unstable. Then the TT index is 47.80 (thunderstorms possible) and K-index is 27.70 (thunderstorms with heavy rain or severe weather are possible). The DCI is 41.67 (potential for strong thunderstorms) and SLI is -8.07 (very unstable). The RINO is 287.50 (Relatively weak vertical wind shear and high CAPE suggest multicellular thunderstorm development is most likely) and SI is 0.83 which is stable but weak convection is possible if strong lifting is present. Suggesting high instability of the atmosphere suitable for thunderstorm formation .

But at 1200 UTC , the values of SLI, CINE, CAPE, SI, HI and BI values are increased and KI, TT, SWEAT, RINO and DCI values are reduced because the thunderstorm getting stronger than previous atmosphere which may lead to formation of thunderstorm.

7th case of Non-thunderstorm day on 30th April 2022 over Kolkata region

At 00Z Skew T - Log P diagram of non-thunderstorm day on 30th April 2022 is shown in **Figure 3.38** over Kolkata region

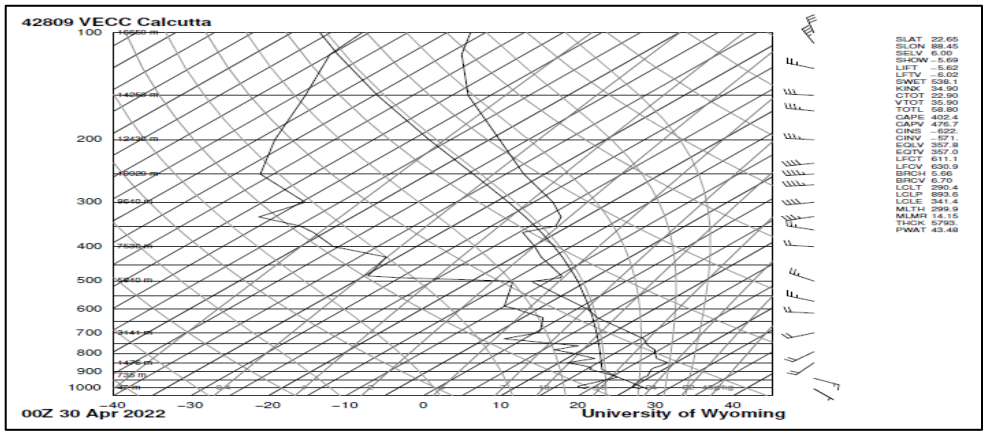

Figure 3.38 At 00Z Skew T - Log P diagram of non-thunderstorm day on 30th April 2022 over Kolkata region.

Station identifier: VECC
Station number: 42809
Observation time: 220430/0000
Station latitude: 22.65
Station longitude: 88.45
Station elevation: 6.0
Showalter index: -5.69
Lifted index: -5.62
LIFT computed using virtual temperature: -6.02
SWEAT index: 538.11
K index: 34.90
Cross totals index: 22.90
Vertical totals index: 35.90
Totals totals index: 58.80
Convective Available Potential Energy: 402.45
CAPE using virtual temperature: 476.78
Convective Inhibition: -622.95
CINS using virtual temperature: -571.48
Equilibrium Level: 357.81
Equilibrium Level using virtual temperature: 357.09
Level of Free Convection: 611.16
LFCT using virtual temperature: 630.92
Bulk Richardson Number: 5.66
Bulk Richardson Number using CAPV: 6.70
Temp [K] of the Lifted Condensation Level: 290.46
Pres [hPa] of the Lifted Condensation Level: 893.61
Equivalent potential temp [K] of the LCL: 341.43
Mean mixed layer potential temperature: 299.96
Mean mixed layer mixing ratio: 14.15
1000 hPa to 500 hPa thickness: 5793.00
Precipitable water [mm] for entire sounding: 43.48

At 12Z Skew T - Log P diagram of non-thunderstorm day on 30th April 2022 is shown in **Figure 3.39** over Kolkata region.

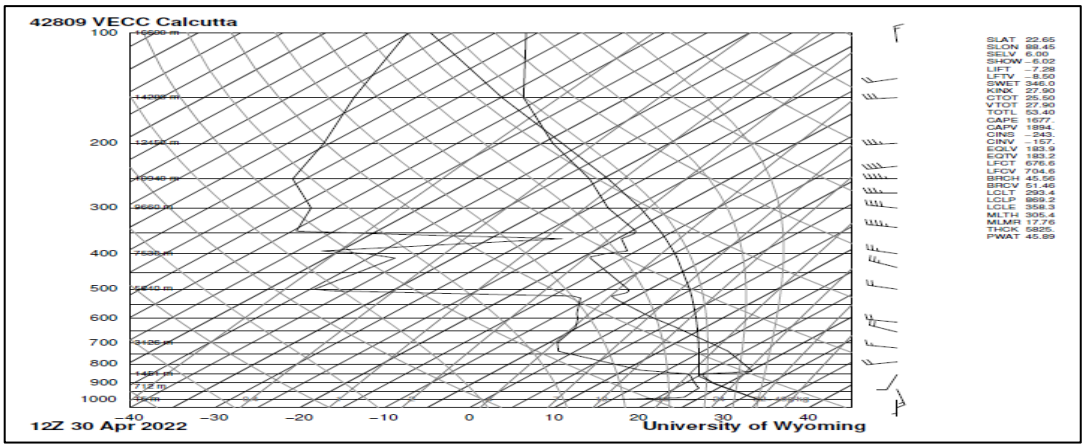

Figure 3.39 At 12Z Skew T - Log P diagram of non-thunderstorm day on 30th April 2022 over Kolkata region.

Station identifier: VECC
Station number: 42809
Observation time: 220430/1200
Station latitude: 22.65
Station longitude: 88.45
Station elevation: 6.0
Showalter index: -6.02
Lifted index: -7.28
LIFT computed using virtual temperature: -8.50
SWEAT index: 346.02
K index: 27.90
Cross totals index: 25.50
Vertical totals index: 27.90
Totals totals index: 53.40
Convective Available Potential Energy: 1677.50
CAPE using virtual temperature: 1894.94
Convective Inhibition: -243.39
CINS using virtual temperature: -157.79
Equilibrium Level: 183.96
Equilibrium Level using virtual temperature: 183.20
Level of Free Convection: 676.64
LFCT using virtual temperature: 704.67
Bulk Richardson Number: 45.56
Bulk Richardson Number using CAPV: 51.46
Temp [K] of the Lifted Condensation Level: 293.46
Pres [hPa] of the Lifted Condensation Level: 869.23
Equivalent potential temp [K] of the LCL: 358.39
Mean mixed layer potential temperature: 305.46
Mean mixed layer mixing ratio: 17.76
1000 hPa to 500 hPa thickness: 5825.00
Precipitable water [mm] for entire sounding: 45.89

RESULTS AND DISCUSSION

Comparison between at 00Z and 12Z sounding data on 30th April 2022 over Kolkata region

Table 3.18 42809 VECC Kolkata Observations at 00Z and 12Z sounding data on 30th April 2022 over Kolkata region

Index	00Z	12Z	Index	00Z	12Z
K	34.90	27.90	RINO	5.66	45.56
TT	58.80	53.40	SI	-5.69	-6.02
SLI	-5.62	-7.28	HI	28.4	57.4
CINE	-571.48	-157.79	DCI	40.62	45.68
SWEAT	538.11	346.02	BI	97	97.1
CAPE	476.78	1894.94			

At 0000 UTC Sounding data of non-thunderstorm, the CAPE is 476.78 J/Kg which is marginally unstable. Then the TT index is 58.80 (severe thunderstorms most likely) and K-index is 34.90 (better potential for thunderstorms with heavy rain). The DCI is 40.62 (potential for strong thunderstorms) and SLI is -5.62 (moderately unstable). The RINO is 45.56 (associated with supercell development) and SI is -5.69 which is very unstable. Suggesting high instability of the atmosphere suitable for thunderstorm formation.

But at 1200 UTC , the values of RINO, CINE, CAPE, DCI, HI and BI values are increased and KI, TT, SWEAT, SLI and SI values are reduced because the thunderstorm getting stronger than previous atmosphere which may lead to formation of thunderstorm.

8th case of Non-thunderstorm day on 2nd May 2022 over Kolkata region.

At 00Z Skew T - Log P diagram of non-thunderstorm day on 2nd May 2022 is shown in **Figure 3.40** over Kolkata region.

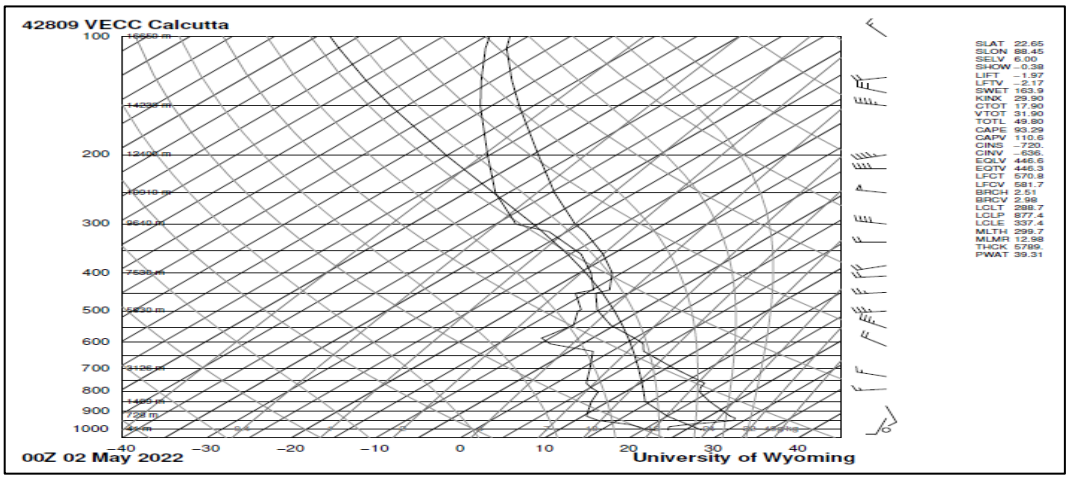

Figure 3.40 At 00Z Skew T - Log P diagram of non-thunderstorm day on 2nd May 2022 over Kolkata region

Station identifier: VECC
Station number: 42809
Observation time: 230502/0000
Station latitude: 22.65
Station longitude: 88.45
Station elevation: 6.0
Showalter index: -0.38
Lifted index: -2.15
LIFT computed using virtual temperature: -2.77
SWEAT index: 192.99
K index: 32.70
Cross totals index: 20.90
Vertical totals index: 25.70
Totals totals index: 46.60
Convective Available Potential Energy: 410.87
CAPE using virtual temperature: 530.63
Convective Inhibition: -97.39
CINS using virtual temperature: -74.03
Equilibrium Level: 358.19
Equilibrium Level using virtual temperature: 357.59
Level of Free Convection: 770.61
LFCT using virtual temperature: 782.91
Bulk Richardson Number: 13.56
Bulk Richardson Number using CAPV: 17.51
Temp [K] of the Lifted Condensation Level: 289.80
Pres [hPa] of the Lifted Condensation Level: 869.52
Equivalent potential temp [K] of the LCL: 342.76
Mean mixed layer potential temperature: 301.62
Mean mixed layer mixing ratio: 14.36
1000 hPa to 500 hPa thickness: 5744.00
Precipitable water [mm] for entire sounding: 42.75

At 12Z Skew T - Log P diagram of non-thunderstorm day on 2nd May 2022 is shown in **Figure 3.41** over Kolkata region.

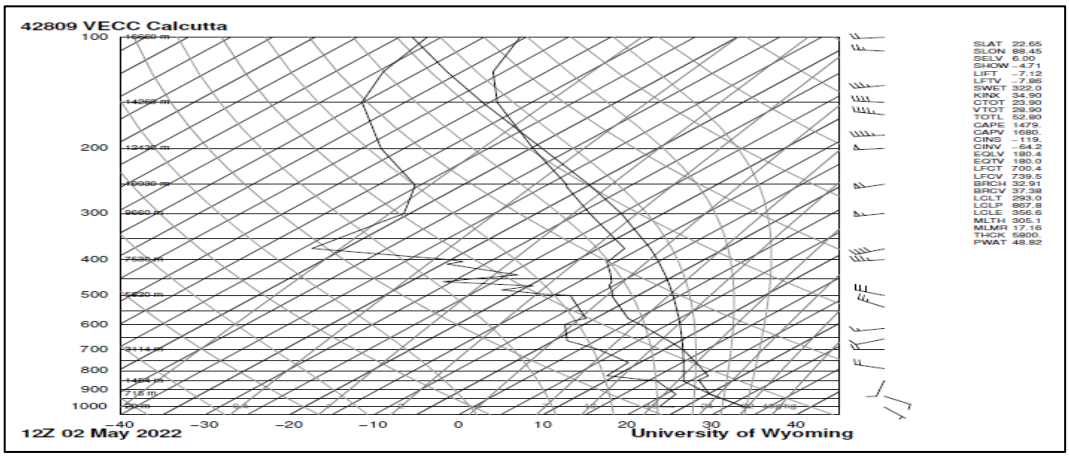

Figure 3.41 At 12Z Skew T - Log P diagram of non-thunderstorm day on 2nd May 2022 over Kolkata region

Station identifier: VECC
Station number: 42809
Observation time: 230502/1200
Station latitude: 22.65
Station longitude: 88.45
Station elevation: 6.0
Showalter index: 0.32
Lifted index: 0.37
LIFT computed using virtual temperature: 0.13
SWEAT index: 193.01
K index: 20.50
Cross totals index: 19.50
Vertical totals index: 26.50
Totals totals index: 46.00
Convective Available Potential Energy: 63.51
CAPE using virtual temperature: 74.01
Convective Inhibition: -178.98
CINS using virtual temperature: -56.01
Equilibrium Level: 437.29
Equilibrium Level using virtual temperature: 433.95
Level of Free Convection: 492.35
LFCT using virtual temperature: 651.17
Bulk Richardson Number: 4.20
Bulk Richardson Number using CAPV: 4.89
Temp [K] of the Lifted Condensation Level: 282.23
Pres [hPa] of the Lifted Condensation Level: 741.60
Equivalent potential temp [K] of the LCL: 337.51
Mean mixed layer potential temperature: 307.41
Mean mixed layer mixing ratio: 9.91
1000 hPa to 500 hPa thickness: 5780.00
Precipitable water [mm] for entire sounding: 34.02

RESULTS AND DISCUSSION

Comparison between at 00Z and 12Z sounding data of non-thunderstorm day on 2nd May 2022 over Kolkata region

Table 3.19 42809 VECC Kolkata Observations at 00Z and 12Z sounding data of non-thunderstorm day on 2nd May 2022 over Kolkata region

Index	00Z	12Z	Index	00Z	12Z
KI	32.70	20.50	RINO	13.56	4.20
TT	46.60	46	SI	-0.38	0.32
SLI	-2.15	0.37	HI	25.8	31
CINE	-74.03	-56.01	DCI	32.95	30.63
SWEAT	192.99	193.01	BI	98.9	99.4
CAPE	530.63	74.01			

At 0000 UTC Sounding data of non-thunderstorm, the CAPE is 530.63 J/Kg which is marginally unstable. Then the TT index is 46.60 (thunderstorm possible) and K-index is 32.70 (better potential for thunderstorms with heavy rain). The DCI is 32.95 (potential for strong thunderstorms) and SLI is -2.15 (marginally unstable). The RINO is 13.56 (associated with super-cell development) and SI is -0.38 which is moderately unstable. It is high instability of the atmosphere which is suggesting suitable for thunderstorm formation.

But at 1200 UTC , the values of SLI, CINE, SWEAT, SI, HI and BI values are increased and KI, TT, CAPE, RINO and DCI values are reduced because the thunderstorm getting stronger than previous atmosphere which may lead to formation of thunderstorm.

9th case of Non-thunderstorm day on 4nd May 2022 over Kolkata region.

At 00Z Skew T - Log P diagram of non-thunderstorm day on 4nd May 2022 is shown in **Figure 3.42** over Kolkata region.

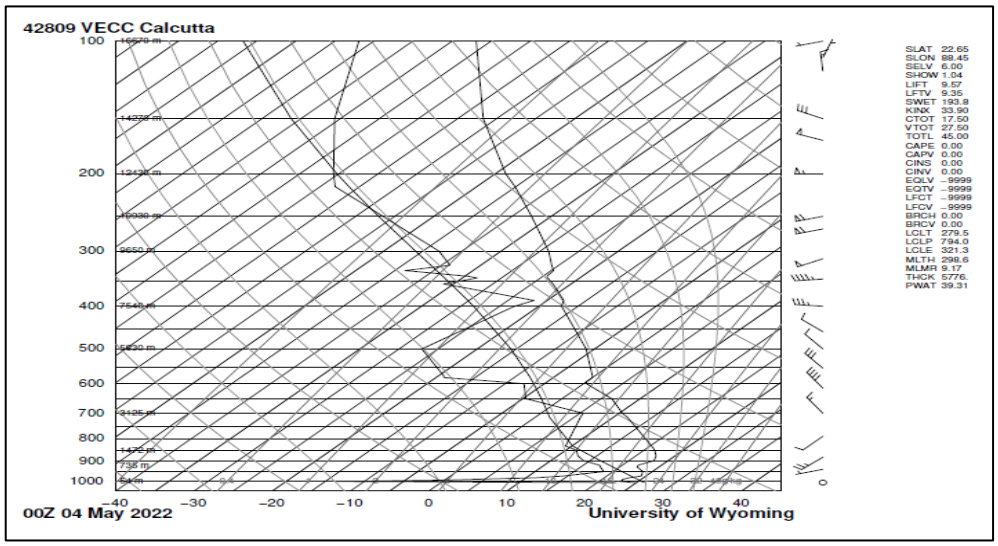

Figure 3.42 At 00Z Skew T - Log P diagram of non-thunderstorm day on 4nd May 2022 over Kolkata region

Station identifier: VECC
Station number: 42809
Observation time: 220504/0000
Station latitude: 22.65
Station longitude: 88.45
Station elevation: 6.0
Showalter index: 1.04
Lifted index: 9.57
LIFT computed using virtual temperature: 9.35
SWEAT index: 193.81
K index: 33.90
Cross totals index: 17.50
Vertical totals index: 27.50
Totals totals index: 45.00
Convective Available Potential Energy: 0.00
CAPE using virtual temperature: 0.00
Convective Inhibition: 0.00
CINS using virtual temperature: 0.00
Bulk Richardson Number: 0.00
Bulk Richardson Number using CAPV: 0.00
Temp [K] of the Lifted Condensation Level: 279.59
Pres [hPa] of the Lifted Condensation Level: 794.04
Equivalent potential temp [K] of the LCL: 321.38
Mean mixed layer potential temperature: 298.65
Mean mixed layer mixing ratio: 9.17
1000 hPa to 500 hPa thickness: 5776.00
Precipitable water [mm] for entire sounding: 39.31

At 12Z Skew T - Log P diagram of non-thunderstorm day on 4nd May 2022 is shown in **Figure 3.43** over Kolkata region.

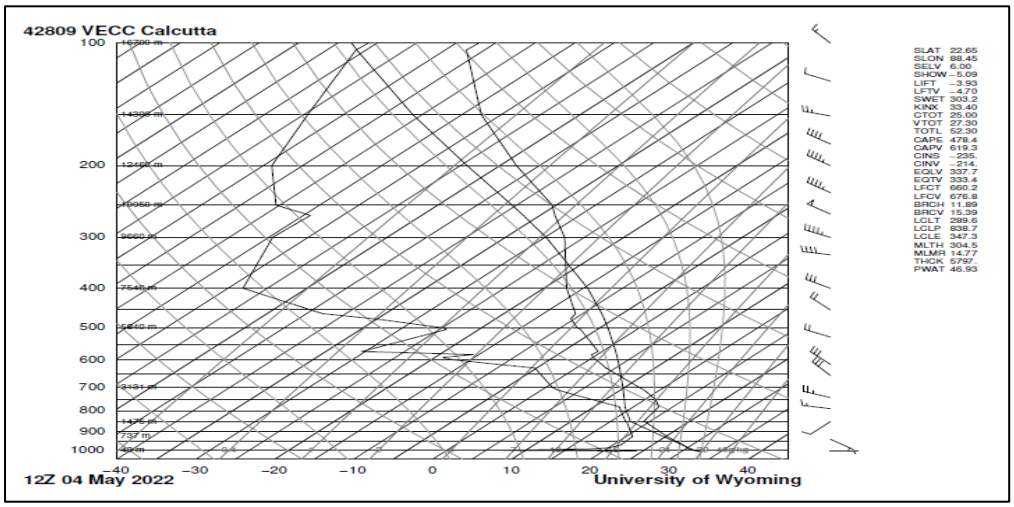

Figure 3.43 At 12Z Skew T - Log P diagram of non-thunderstorm day on 4nd May 2022 over Kolkata region

Station identifier: VECC
Station number: 42809
Observation time: 220504/1200
Station latitude: 22.65
Station longitude: 88.45
Station elevation: 6.0
Showalter index: -5.09
Lifted index: -3.93
LIFT computed using virtual temperature: -4.70
SWEAT index: 303.21
K index: 33.40
Cross totals index: 25.00
Vertical totals index: 27.30
Totals totals index: 52.30
Convective Available Potential Energy: 478.48
CAPE using virtual temperature: 619.32
Convective Inhibition: -235.96
CINS using virtual temperature: -214.91
Equilibrium Level: 337.78
Equilibrium Level using virtual temperature: 333.49
Level of Free Convection: 660.22
LFCT using virtual temperature: 676.80
Bulk Richardson Number: 11.89
Bulk Richardson Number using CAPV: 15.39
Temp [K] of the Lifted Condensation Level: 289.65
Pres [hPa] of the Lifted Condensation Level: 838.76
Equivalent potential temp [K] of the LCL: 347.39
Mean mixed layer potential temperature: 304.59
Mean mixed layer mixing ratio: 14.77
1000 hPa to 500 hPa thickness: 5797.00
Precipitable water [mm] for entire sounding: 46.93

RESULTS AND DISCUSSION

Comparison between 00Z and 12Z sounding data of non-thunderstorm on 4th May 2022 over Kolkata region

Table 3.20 42809 VECC Kolkata Observations at 00Z and 12Z sounding data of non-thunderstorm on 4th May 2022 over Kolkata region

Index	00Z	12Z	Index	00Z	12Z
KI	33.90	33.40	RINO	0	11.89
TT	45	52.30	SI	1.04	-5.09
SLI	9.57	-3.93	HI	36	30.3
CINE	0	-214.91	DCI	23.23	40.43
SWEAT	193.81	303.21	BI	96.7	97
CAPE	0	619.32			

At 0000 UTC Sounding data of non-thunderstorm, the CAPE is 0 J/Kg which is stable. Then the TT index is 45 (thunderstorm possible) and K-index is 33.90 (better potential for thunderstorms with heavy rain). Suggesting stability of the atmosphere and suitable for thunderstorm formation.

But at 1200 UTC , the values of TT, CAPE, SWEAT, RINO, DCI and BI values are increased and KI, SLI, CINE, SI and HI values are reduced because instability of the atmosphere suitable formation of thunderstorm.

10th case of Non-thunderstorm day 0n 12th May 2022 over Kolkata region.

At 00Z Skew T - Log P diagram of non-thunderstorm day on 12th May 2022 is shown in **Figure 3.44** over Kolkata region.

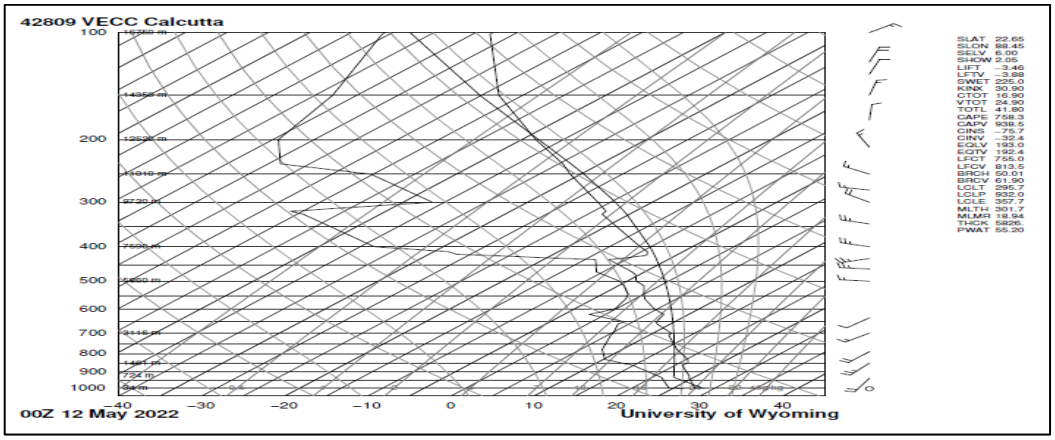

Figure 3.44 At 00Z Skew T - Log P diagram of non-thunderstorm day on 12th May 2022 over Kolkata region

Station identifier: VECC
Station number: 42809
Observation time: 220512/0000
Station latitude: 22.65
Station longitude: 88.45
Station elevation: 6.0
Showalter index: 2.05
Lifted index: -3.46
LIFT computed using virtual temperature: -3.88
SWEAT index: 225.00
K index: 30.90
Cross totals index: 16.90
Vertical totals index: 24.90
Totals totals index: 41.80
Convective Available Potential Energy: 758.36
CAPE using virtual temperature: 938.58
Convective Inhibition: -75.79
CINS using virtual temperature: -32.41
Equilibrium Level: 193.09
Equilibrium Level using virtual temperature: 192.47
Level of Free Convection: 755.02
LFCT using virtual temperature: 813.59
Bulk Richardson Number: 50.01
Bulk Richardson Number using CAPV: 61.90
Temp [K] of the Lifted Condensation Level: 295.73
Pres [hPa] of the Lifted Condensation Level: 932.01
Equivalent potential temp [K] of the LCL: 357.77
Mean mixed layer potential temperature: 301.76
Mean mixed layer mixing ratio: 18.94
1000 hPa to 500 hPa thickness: 5826.00
Precipitable water [mm] for entire sounding: 55.20

At 12Z Skew T - Log P diagram of non-thunderstorm day on 12th May 2022 is shown in **Figure 3.45** over Kolkata region.

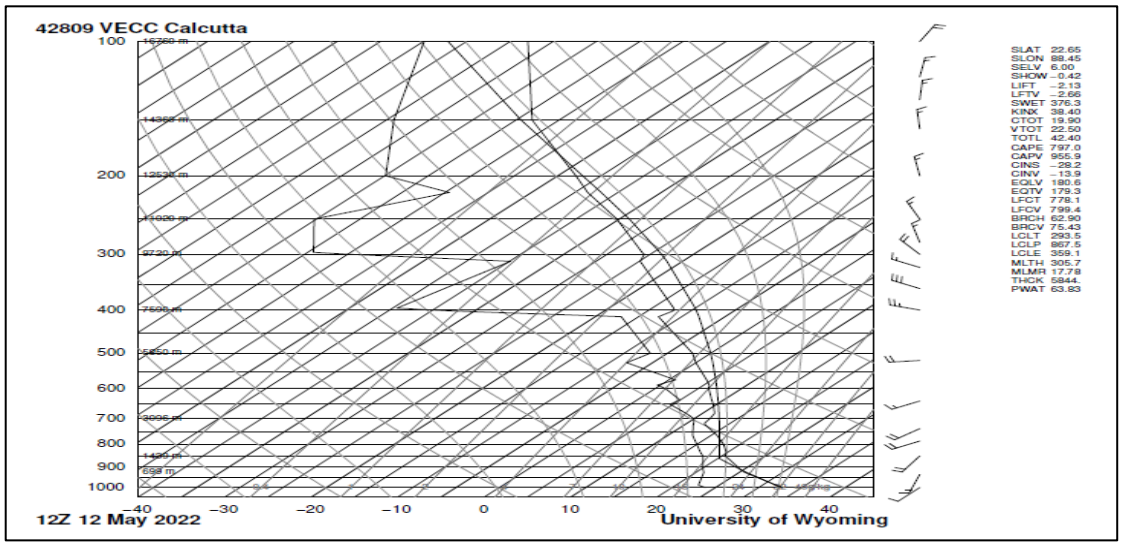

Figure 3.45 At 12Z Skew T - Log P diagram of non-thunderstorm day on 12th May 2022 over Kolkata region

Station identifier: VECC
Station number: 42809
Observation time: 220512/1200
Station latitude: 22.65
Station longitude: 88.45
Station elevation: 6.0
Showalter index: -0.42
Lifted index: -2.13
LIFT computed using virtual temperature: -2.66
SWEAT index: 376.30
K index: 38.40
Cross totals index: 19.90
Vertical totals index: 22.50
Totals totals index: 42.40
Convective Available Potential Energy: 797.08
CAPE using virtual temperature: 955.90
Convective Inhibition: -28.27
CINS using virtual temperature: -13.92
Equilibrium Level: 180.67
Equilibrium Level using virtual temperature: 179.31
Level of Free Convection: 778.19
LFCT using virtual temperature: 799.42
Bulk Richardson Number: 62.90
Bulk Richardson Number using CAPV: 75.43
Temp [K] of the Lifted Condensation Level: 293.57
Pres [hPa] of the Lifted Condensation Level: 867.52
Equivalent potential temp [K] of the LCL: 359.19
Mean mixed layer potential temperature: 305.74
Mean mixed layer mixing ratio: 17.78
1000 hPa to 500 hPa thickness: 5844.00
Precipitable water [mm] for entire sounding: 63.83

RESULTS AND DISCUSSION

Comparison between 00Z and 12Z sounding data of non-thunderstorm on 12th May 2022 over Kolkata region

Table 3.21 42809 VECC Kolkata Observations at 00Z and 12Z sounding data of non-thunderstorm day on 12th May 2022 over Kolkata region

Index	00Z	12Z	Index	00Z	12Z
KI	30.9	38.40	RINO	50.01	62.90
TT	41.80	42.40	SI	2.05	-0.42
SLI	-3.46	-2.13	HI	17	9.4
CINE	-32.41	-13.92	DCI	37.46	40.33
SWEAT	225	376.30	BI	96	97.2
CAPE	938.58	955.90			

At 0000 UTC Sounding data of non-thunderstorm, the CAPE is 938.58 J/Kg which is marginally unstable. Then the RINO index is 50.01 (relatively weak vertical wind shear and high CAPE, suggest multicellular thunderstorm development is most likely) and K-index is 30.9(better potential for thunderstorms with heavy rain). The DCI is 37.46 (potential for strong thunderstorms) and SLI is -3.46 (moderately unstable). Suggesting instability of the atmosphere and suitable for thunderstorm formation.

But at 1200 UTC, the values of KI, SLI, CINE, TT, CAPE, SWEAT, RINO, DCI and BI values are increased and SI and HI values are reduced because instability of the atmosphere suitable formation of thunderstorm.

11th case of Non-thunderstorm day on 16th May 2022 over Kolkata region.

At 00Z Skew T - Log P diagram of non-thunderstorm day on 16th May 2022 is shown in **Figure 3.46** over Kolkata region.

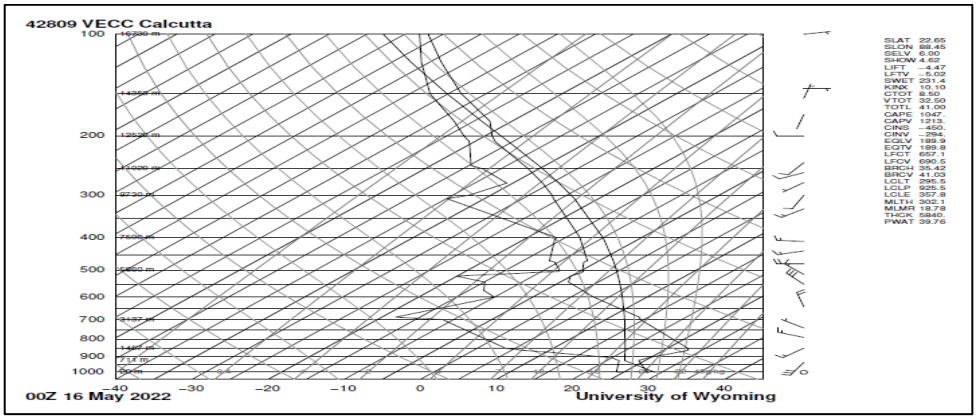

Figure 3.46 At 00Z Skew T - Log P diagram of non-thunderstorm day on 16th May 2022 over Kolkata region

Station identifier: VECC
Station number: 42809
Observation time: 220516/0000
Station latitude: 22.65
Station longitude: 88.45
Station elevation: 6.0
Showalter index: 4.62
Lifted index: -4.47
LIFT computed using virtual temperature: -5.02
SWEAT index: 231.45
K index: 10.10
Cross totals index: 8.50
Vertical totals index: 32.50
Totals totals index: 41.00
Convective Available Potential Energy: 1047.42
CAPE using virtual temperature: 1213.43
Convective Inhibition: -450.40
CINS using virtual temperature: -294.36
Equilibrium Level: 189.90
Equilibrium Level using virtual temperature: 189.80
Level of Free Convection: 657.19
LFCT using virtual temperature: 690.53
Bulk Richardson Number: 35.42
Bulk Richardson Number using CAPV: 41.03
Temp [K] of the Lifted Condensation Level: 295.50
Pres [hPa] of the Lifted Condensation Level: 925.56
Equivalent potential temp [K] of the LCL: 357.80
Mean mixed layer potential temperature: 302.12
Mean mixed layer mixing ratio: 18.78
1000 hPa to 500 hPa thickness: 5840.00
Precipitable water [mm] for entire sounding: 39.76

At 12Z Skew T - Log P diagram of non-thunderstorm day on 16th May 2022 is shown in **Figure 3.47** over Kolkata region.

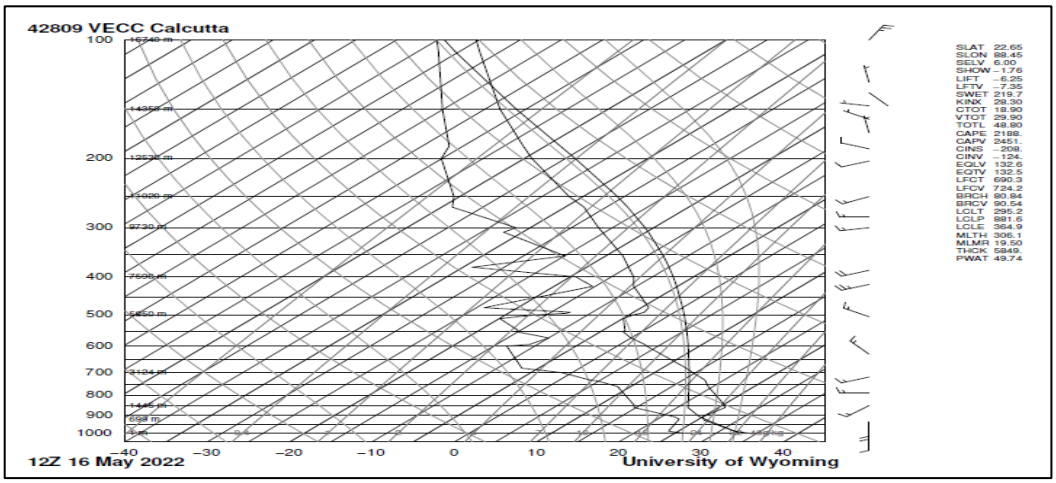

Figure 3.47 At 12Z Skew T - Log P diagram of non-thunderstorm day on 16th May 2022 over Kolkata region

Station identifier: VECC
Station number: 42809
Observation time: 220516/1200
Station latitude: 22.65
Station longitude: 88.45
Station elevation: 6.0
Showalter index: -1.76
Lifted index: -6.25
LIFT computed using virtual temperature: -7.35
SWEAT index: 219.79
K index: 28.30
Cross totals index: 18.90
Vertical totals index: 29.90
Totals totals index: 48.80
Convective Available Potential Energy: 2188.76
CAPE using virtual temperature: 2451.30
Convective Inhibition: -208.36
CINS using virtual temperature: -124.97
Equilibrium Level: 132.60
Equilibrium Level using virtual temperature: 132.53
Level of Free Convection: 690.38
LFCT using virtual temperature: 724.27
Bulk Richardson Number: 80.84
Bulk Richardson Number using CAPV: 90.54
Temp [K] of the Lifted Condensation Level: 295.29
Pres [hPa] of the Lifted Condensation Level: 881.67
Equivalent potential temp [K] of the LCL: 364.92
Mean mixed layer potential temperature: 306.12
Mean mixed layer mixing ratio: 19.50
1000 hPa to 500 hPa thickness: 5849.00
Precipitable water [mm] for entire sounding: 49.74

RESULTS AND DISCUSSION

Comparison between at 00Z and 12Z sounding data of non-thunderstorm on 16th May 2022 over Kolkata region

Table 3.21 42809 VECC Kolkata Observations at 00Z and 12Z sounding data of non-thunderstorm day on 16th May 2022 over Kolkata region

Index	00Z	12Z	Index	00Z	12Z
KI	10.10	28.30	RINO	35.42	80.84
TT	41	48.80	SI	4.62	-1.76
SLI	-4.47	-6.25	HI	53	39
CINE	-294.36	-124.97	DCI	35.67	46.05
SWEAT	231.45	219.79	BI	97.1	97.7
CAPE	1213.43	2451			

At 0000 UTC Sounding data of non-thunderstorm, the CAPE is 1213.43 J/Kg which is moderately unstable. Then the TT index is 41 (thunderstorm possible) and RINO index is 35.42 (associated with supercell development). The DCI is 35.67 (potential for strong thunderstorms) and SLI is -4.47 (moderately unstable). Suggesting instability of the atmosphere and suitable for thunderstorm formation.

But at 1200 UTC, the values of KI, TT, CAPE, CINE, RINO, DCI and BI values are increased and SLI, SWEAT, SI and HI values are reduced because instability of the atmosphere suitable formation of thunderstorm.

12th case of Non-thunderstorm day on 18th May 2022 over Kolkata region.

At 00Z Skew T - Log P diagram of non-thunderstorm day on 18th May 2022 is shown in **Figure 3.48** over Kolkata region.

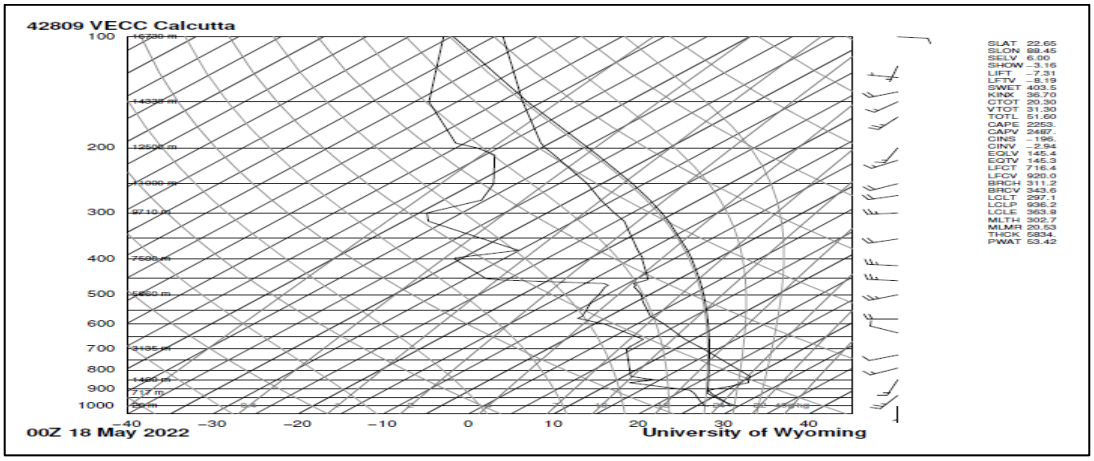

Figure 3.48 At 00Z Skew T - Log P diagram of non-thunderstorm day on 18th May 2022 over Kolkata region

Station identifier: VECC
Station number: 42809
Observation time: 220518/0000
Station latitude: 22.65
Station longitude: 88.45
Station elevation: 6.0
Showalter index: -3.16
Lifted index: -7.31
LIFT computed using virtual temperature: -8.19
SWEAT index: 403.56
K index: 36.70
Cross totals index: 20.30
Vertical totals index: 31.30
Totals totals index: 51.60
Convective Available Potential Energy: 2253.11
CAPE using virtual temperature: 2487.88
Convective Inhibition: -196.27
CINS using virtual temperature: -2.94
Equilibrium Level: 145.42
Equilibrium Level using virtual temperature: 145.34
Level of Free Convection: 716.49
LFCT using virtual temperature: 920.09
Bulk Richardson Number: 311.25
Bulk Richardson Number using CAPV: 343.68
Temp [K] of the Lifted Condensation Level: 297.10
Pres [hPa] of the Lifted Condensation Level: 936.20
Equivalent potential temp [K] of the LCL: 363.83
Mean mixed layer potential temperature: 302.77
Mean mixed layer mixing ratio: 20.53
1000 hPa to 500 hPa thickness: 5834.00
Precipitable water [mm] for entire sounding: 53.42

At 12Z Skew T - Log P diagram of non-thunderstorm day on 18th May 2022 is shown in **Figure 3.49** over Kolkata region.

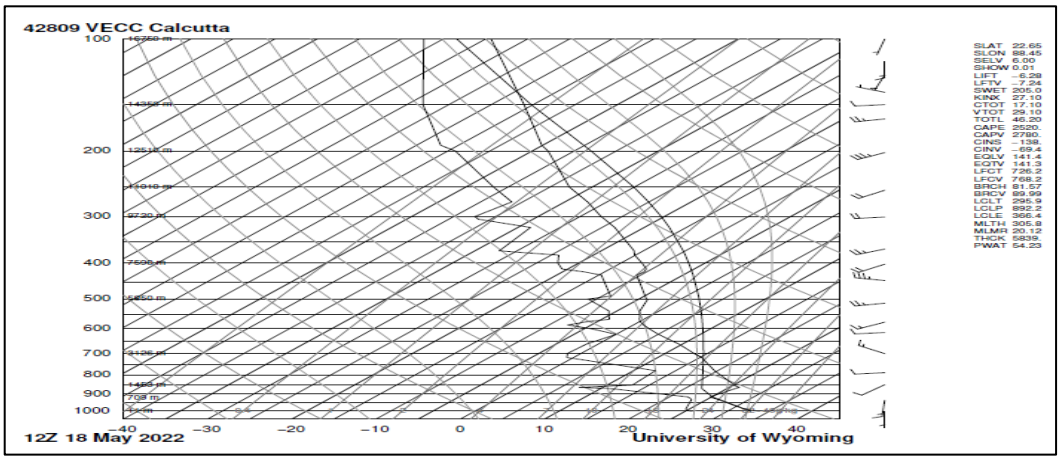

Figure 3.49 At 12Z Skew T - Log P diagram of non-thunderstorm day on 18th May 2022 over Kolkata region

Station identifier: VECC
Station number: 42809
Observation time: 220518/1200
Station latitude: 22.65
Station longitude: 88.45
Station elevation: 6.0
Showalter index: 0.01
Lifted index: -6.28
LIFT computed using virtual temperature: -7.24
SWEAT index: 205.01
K index: 27.10
Cross totals index: 17.10
Vertical totals index: 29.10
Totals totals index: 46.20
Convective Available Potential Energy: 2520.18
CAPE using virtual temperature: 2780.35
Convective Inhibition: -138.63
CINS using virtual temperature: -69.41
Equilibrium Level: 141.46
Equilibrium Level using virtual temperature: 141.37
Level of Free Convection: 726.20
LFCT using virtual temperature: 768.23
Bulk Richardson Number: 81.57
Bulk Richardson Number using CAPV: 89.99
Temp [K] of the Lifted Condensation Level: 295.99
Pres [hPa] of the Lifted Condensation Level: 892.27
Equivalent potential temp [K] of the LCL: 366.43
Mean mixed layer potential temperature: 305.80
Mean mixed layer mixing ratio: 20.12
1000 hPa to 500 hPa thickness: 5839.00
Precipitable water [mm] for entire sounding: 54.23

RESULTS AND DISCUSSION

Comparison between 00Z and 12Z sounding data of non-thunderstorm on 18th May 2022 over Kolkata region

Table 3.23 42809 VECC Kolkata Observations at 00Z and 12Z sounding data of non-thunderstorm day on 18th May 2022 over Kolkata region

Index	00Z	12Z	Index	00Z	12Z
KI	36.70	27.10	RINO	311.25	81.57
TT	51.60	46.20	SI	-3.16	0.01
SLI	-7.31	-6.28	HI	40.1	34
CINE	-2.94	-69.41	DCI	47.11	44.28
SWEAT	403.56	205.01	BI	97.7	98.1
CAPE	2487.88	2780.35			

At 0000 UTC Sounding data of non-thunderstorm, the CAPE is 2487.88 J/Kg which is very unstable. Then the TT index is 51.60 (thunderstorms are more likely, possibly severe) and KI index is 36.70 (better potential for thunderstorms with heavy rain). The DCI is 47.11 (potential for strong thunderstorms) and SLI is -7.31 (very unstable). Suggesting instability of the atmosphere and suitable for thunderstorm formation.

But at 1200 UTC, the values of SLI, CAPE, SI and BI values are increased and KI, TT, CINE, SWEAT, RINO, DCI and HI values are reduced because instability of the atmosphere suitable formation of thunderstorm.

13th case of Non-thunderstorm day on 22nd May 2022 over Kolkata region.

At 00Z Skew T - Log P diagram of non-thunderstorm day on 22nd May 2022 is shown in **Figure 3.50** over Kolkata region.

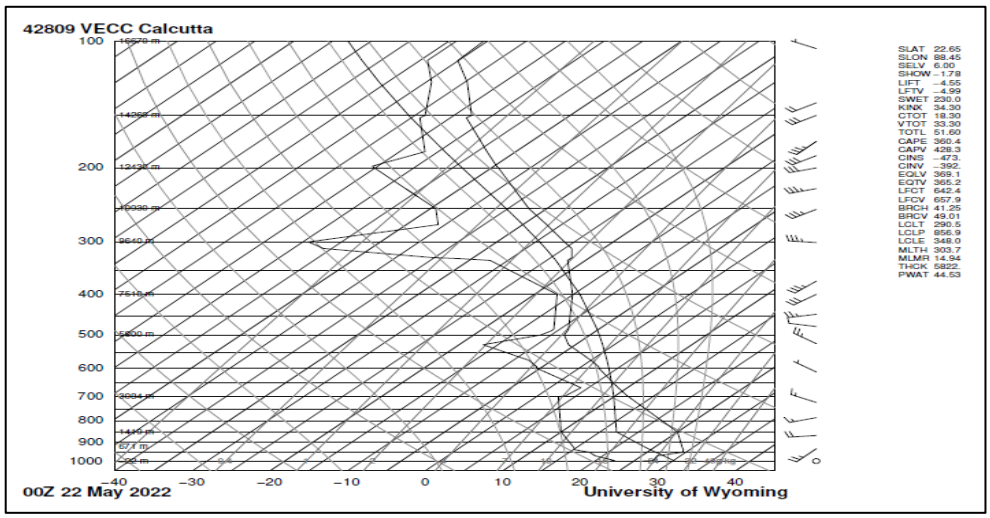

Figure 3.50 At 00Z Skew T - Log P diagram of non-thunderstorm day on 22nd May 2022 over Kolkata region

Station identifier: VECC
Station number: 42809
Observation time: 220522/0000
Station latitude: 22.65
Station longitude: 88.45
Station elevation: 6.0
Showalter index: -1.78
Lifted index: -4.55
LIFT computed using virtual temperature: -4.99
SWEAT index: 230.02
K index: 34.30
Cross totals index: 18.30
Vertical totals index: 33.30
Totals totals index: 51.60
Convective Available Potential Energy: 360.49
CAPE using virtual temperature: 428.34
Convective Inhibition: -473.21
CINS using virtual temperature: -392.82
Equilibrium Level: 369.12
Equilibrium Level using virtual temperature: 365.25
Level of Free Convection: 642.41
LFCT using virtual temperature: 657.97
Bulk Richardson Number: 41.25
Bulk Richardson Number using CAPV: 49.01
Temp [K] of the Lifted Condensation Level: 290.59
Pres [hPa] of the Lifted Condensation Level: 856.95
Equivalent potential temp [K] of the LCL: 348.02
Mean mixed layer potential temperature: 303.71
Mean mixed layer mixing ratio: 14.94
1000 hPa to 500 hPa thickness: 5822.00
Precipitable water [mm] for entire sounding: 44.53

At 12Z Skew T - Log P diagram of non-thunderstorm day on 22nd May 2022 is shown in **Figure 3.51** over Kolkata region

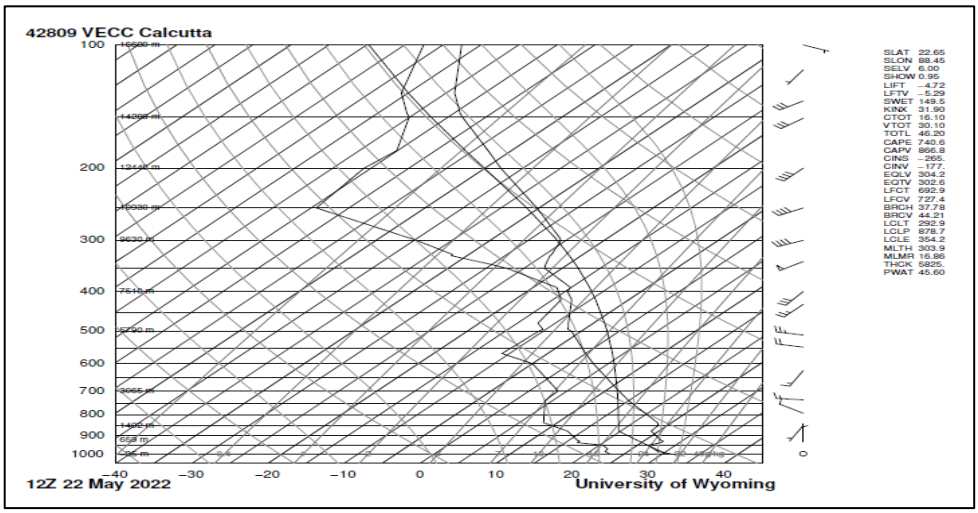

Figure 3.51 At 12Z Skew T - Log P diagram of non-thunderstorm day on 22nd May 2022 over Kolkata region

Station identifier: VECC
Station number: 42809
Observation time: 220522/1200
Station latitude: 22.65
Station longitude: 88.45
Station elevation: 6.0
Showalter index: 0.95
Lifted index: -4.72
LIFT computed using virtual temperature: -5.29
SWEAT index: 149.57
K index: 31.90
Cross totals index: 16.10
Vertical totals index: 30.10
Totals totals index: 46.20
Convective Available Potential Energy: 740.69
CAPE using virtual temperature: 866.88
Convective Inhibition: -265.87
CINS using virtual temperature: -177.93
Equilibrium Level: 304.25
Equilibrium Level using virtual temperature: 302.61
Level of Free Convection: 692.98
LFCT using virtual temperature: 727.40
Bulk Richardson Number: 37.78
Bulk Richardson Number using CAPV: 44.21
Temp [K] of the Lifted Condensation Level: 292.93
Pres [hPa] of the Lifted Condensation Level: 878.77
Equivalent potential temp [K] of the LCL: 354.22
Mean mixed layer potential temperature: 303.96
Mean mixed layer mixing ratio: 16.86
1000 hPa to 500 hPa thickness: 5825.00
Precipitable water [mm] for entire sounding: 45.60

RESULTS AND DISCUSSION

Comparison between 00Z and 12Z sounding data of non-thunderstorm on 22th May 2022 over Kolkata region

Table 3.24 42809 VECC Kolkata Observations at 00Z and 12Z sounding data of non-thunderstorm day on 22th May 2022 over Kolkata region

Index	00Z	12Z	Index	00Z	12Z
KI	34.30	31.90	RINO	41.25	37.78
TT	51.60	46.20	SI	-1.78	0.95
SLI	-4.55	-4.72	HI	27.1	26.3
CINE	-392.82	-177.93	DCI	39.55	38.32
SWEAT	230.02	149.57	BI	98.8	98.2
CAPE	428.34	866.88			

At 0000 UTC Sounding data of non-thunderstorm, the CAPE is 428.34 J/Kg which marginally unstable. Then the TT index is 51.60 (thunderstorms are more likely, possibly severe) and KI index is 34.30 (better potential for thunderstorms with heavy rain). The DCI is 39.55 (potential for strong thunderstorms) and SLI is -4.55 (moderately unstable). Suggesting instability of the atmosphere and suitable for thunderstorm formation.

But at 1200 UTC, the values of CAPE, CINE, SI and HI values are increased and KI, TT, SLI, SWEAT, RINO, DCI and BI values are reduced because instability of the atmosphere suitable formation of thunderstorm.

14th case of Non-thunderstorm day on 23rd May 2022 over Kolkata region

At 00Z Skew T - Log P diagram of non-thunderstorm day on 23rd May 2022 is shown in **Figure 3.52** over Kolkata region.

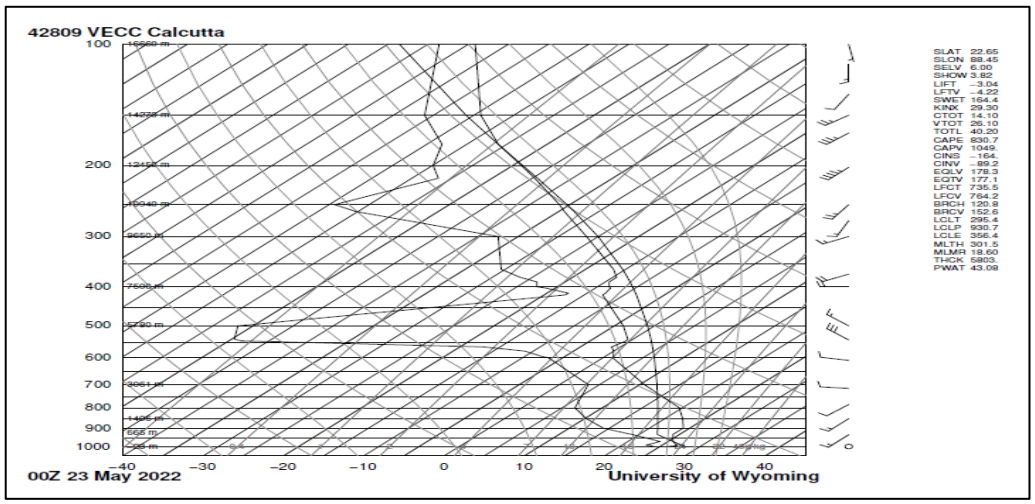

Figure 3.52 At 00Z Skew T - Log P diagram of non-thunderstorm day on 23rd May 2022 over Kolkata region

Station identifier: VECC
Station number: 42809
Observation time: 220523/0000
Station latitude: 22.65
Station longitude: 88.45
Station elevation: 6.0
Showalter index: 3.82
Lifted index: -3.04
LIFT computed using virtual temperature: -4.22
SWEAT index: 164.40
K index: 29.30
Cross totals index: 14.10
Vertical totals index: 26.10
Totals totals index: 40.20
Convective Available Potential Energy: 830.71
CAPE using virtual temperature: 1049.66
Convective Inhibition: -164.45
CINS using virtual temperature: -89.29
Equilibrium Level: 178.32
Equilibrium Level using virtual temperature: 177.13
Level of Free Convection: 735.58
LFCT using virtual temperature: 764.20
Bulk Richardson Number: 120.80
Bulk Richardson Number using CAPV: 152.64
Temp [K] of the Lifted Condensation Level: 295.41
Pres [hPa] of the Lifted Condensation Level: 930.70
Equivalent potential temp [K] of the LCL: 356.46
Mean mixed layer potential temperature: 301.55
Mean mixed layer mixing ratio: 18.60
1000 hPa to 500 hPa thickness: 5803.00
Precipitable water [mm] for entire sounding: 43.08

At 12Z Skew T - Log P diagram of non-thunderstorm day on 23rd May 2022 is shown in **Figure 3.53** over Kolkata region.

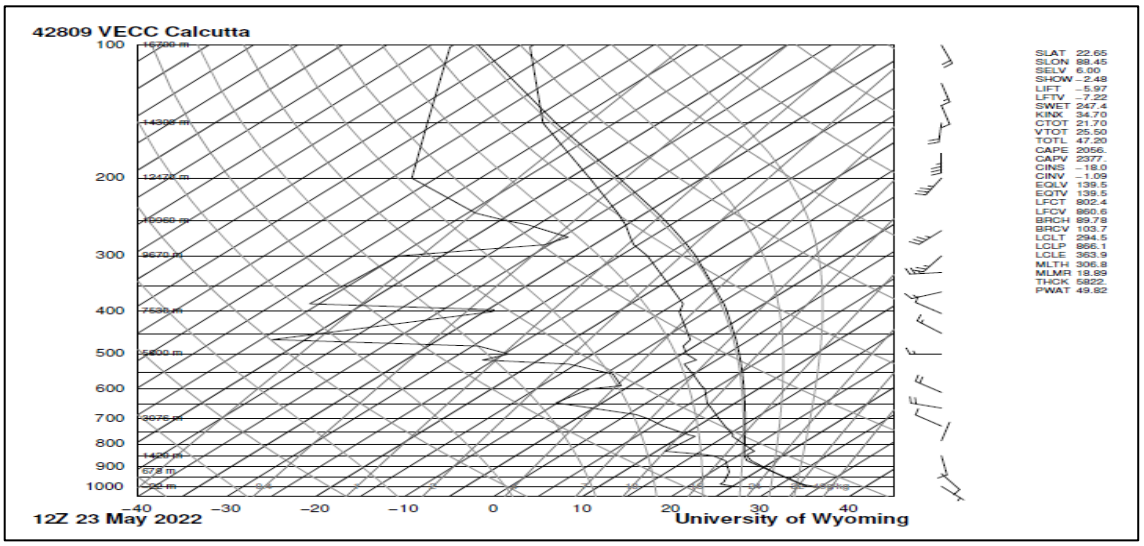

Figure 3.53 At 12Z Skew T - Log P diagram of non-thunderstorm day on 23rd May 2022 over Kolkata region

Station identifier: VECC
Station number: 42809
Observation time: 220523/1200
Station latitude: 22.65
Station longitude: 88.45
Station elevation: 6.0
Showalter index: -2.48
Lifted index: -5.97
LIFT computed using virtual temperature: -7.22
SWEAT index: 247.41
K index: 34.70
Cross totals index: 21.70
Vertical totals index: 25.50
Totals totals index: 47.20
Convective Available Potential Energy: 2056.98
CAPE using virtual temperature: 2377.95
Convective Inhibition: -18.00
CINS using virtual temperature: -1.09
Equilibrium Level: 139.59
Equilibrium Level using virtual temperature: 139.51
Level of Free Convection: 802.43
LFCT using virtual temperature: 860.63
Bulk Richardson Number: 89.78
Bulk Richardson Number using CAPV: 103.78
Temp [K] of the Lifted Condensation Level: 294.50
Pres [hPa] of the Lifted Condensation Level: 866.14
Equivalent potential temp [K] of the LCL: 363.96
Mean mixed layer potential temperature: 306.85
Mean mixed layer mixing ratio: 18.89
1000 hPa to 500 hPa thickness: 5822.00
Precipitable water [mm] for entire sounding: 49.82

RESULTS AND DISCUSSION

Comparison between 00Z and 12Z sounding data of non-thunderstorm on 23rd May 2022 over Kolkata region

Table 3.25 42809 VECC Kolkata Observations at 00Z and 12Z sounding data of non-thunderstorm day on 23rd May 2022 over Kolkata region

Index	00Z	12Z	Index	00Z	12Z
KI	29.30	34.70	RINO	120.80	89.78
TT	40.20	47.20	SI	3.82	-2.48
SLI	-3.04	-5.97	HI	67	31.8
CINE	-89.29	-1.09	DCI	35.44	44.17
SWEAT	164.40	247.41	BI	97.8	98.8
CAPE	1049.66	2377.95			

At 0000 UTC Sounding data of non-thunderstorm, the CAPE is 1049.66 J/Kg which is moderately unstable. Then the RINO index is 120.80 (relatively weak vertical wind shear and high CAPE suggest multicellular thunderstorm development is most likely) and KI index is 29.30 (thunderstorms with heavy rain or severe weather are possible). The DCI is 35.44 (potential for strong thunderstorms) and SLI is -3.04 (moderately unstable). Suggesting instability of the atmosphere and suitable for thunderstorm formation.

But at 1200 UTC , the values of KI, TT, CAPE, SWEAT, CINE, DCI and BI values are increased and SLI, RINO, SI and HI values are reduced because instability of the atmosphere suitable formation of thunderstorm.

Chapter - 4

Use Of NCMRWF Model Based Imaginaries Studies on Thunderstorms Over Kolkata Region, West Bengal

NCMRWF Unified Model and Data Assimilation System

NCMRWF Unified model (NCUM) is being used for generating10-day numerical weather forecasts routinely since 2012. The NCUM system is based on the Unified Model (UM) developed under the UM Partnership by Met Office, UK, BoM/CSIRO, Australia, KMA, South Korea, NIWA, New Zealand and MoES/NCMRWF, India. The NCUM system is upgraded periodically to adapt new Scientific and Technological developments for improving the global and regional numerical weather predictions (NWP).

Uniqueness of the Unified Model is its seamless modelling approach. The same dynamical core and, where possible, the same parameterization schemes are used across a broad range of spatial and temporal scales. The UM's dynamical core solves compressible non-hydrostatic equations of motion with semi-Lagrangian Advection and semi-implicit time stepping. Sub-grid scale processes such as convection, boundary layer turbulence, radiation, cloud, microphysics and orographic drag are represented by parameterization schemes, which are being improved over the years. The model uses "END Game" dynamics. Important aspect of End Game is that it is designed around an iterative approach to solving the semi-implicit aspects of the scheme. This permits more accurate coupling of the scheme to the physics parameterizations. This was major step forward in atmospheric modelling which helps the seamless modelling approach.

Prediction of future state of the atmosphere by the NWP model is largely depends upon the initial condition (analysis) used by the model. The process of preparation of the "analysis" is known as Data Assimilation (DA). Quality controlled (and thinned, if required) observations are used in the DA system for the preparation of analysis. Data assimilation techniques provide the best estimate of the state of a physical system by combining the information from model and observations. Advanced data assimilation methods have the ability to extract more useful information on the state of the atmosphere from the observations assimilated. Four-dimensional variational data assimilation (4DVar) is one of the advanced data assimilation methods used by many global NWP centers.

NCMRWF adapted the 4D-Var data assimilation system of UK Met Office and is being used for preparation of analysis for NCUM operationally since April 2012. In October, 2016 the 4D-Var systems was upgraded to Hybrid 4D-Var data assimilation system. One of the major weakness of traditional 4D-Var approach is the difficulty of representing 'Errors of the Day' –

the variations in error due to the locations of recent instabilities and observations. To address this issue, hybrid 4D-Var method was developed, where the term "hybrid" refers to the combination of climatological covariance model with co-variances calculated from an ensemble of forecasts, designed to sample the current forecast uncertainty.The Hybrid 4D-Var system combines the advantages of traditional 4DVar and the ensemble data assimilation. NCUM hybrid 4D-Var system uses the forecasts from the NCMRWF Ensemble Prediction System (NEPS).

In the new 2.8 PF HPC (Mihir) at NCMRWF, the NCUM has been upgraded to the latest operational high resolution analysis-forecast system of UM. Major improvement of this system in comparison with the earlier version of NCUM system is the use of higher resolution global model and improvements in data assimilation system. A detailed description of the new NCUM system is presented in following sections.

New NCUM System

In the new upgradation of NCUM, horizontal resolution of the model is increased from ~17 km (N768L70) to ~12 km (N1024L70). Hybrid 4D-Var method is used for data assimilation. Major improvements of the new NCUM data assimilation system in comparisons with previous system used at NCMRWF is the use of improved version of the radioactive transfer model and the improved ability of the new system to assimilate more satellite observations. The global ensemble prediction system is also upgraded with high resolution model (12 km). A brief description of various components of the data assimilation system (Observation pre- processing system, Observation Processing System, Variational Assimilation), model and ensemble prediction system are given below:

Observation Pre-processing system

NCMRWF receives global meteorological observations through Global Telecommunication System (GTS) via Regional Telecommunication Hub (RTH) at IMD, New Delhi and large volume of satellite observations through internet data services directly from various satellite data producers (NOAA/NESDIS, EUMETSAT, ISRO etc.). Continuous efforts are on to acquire and utilize maximum number of observations from various platforms, with special emphasis on Indian satellite observations.

The NCUM observation pre-processor system packs observations in the "obstore" format which can be read by the Observation Processing System. The new observation preprocessing system developed at NCMRWF now has the ability to processes and pack more types of observations (Newly added observations includeFY3C, Himawari-8, Meteosat-11, AMSR-2 radiances, Wind-Sat ocean surface winds, Meteosat-11 Atmospheric Motion Vectors). List of observations assimilated in the new NCUM DA system is given in **Table 4.1.**

Table 4.1 Observations Assimilated in NCUM Global Data Assimilation System

Observation Type	**Observation Description**	**Assimilated Variables**
AHIClear	Advanced Himawari Imager radiances from Himawari-8	*Brightness Temperature (*Tb)
Aircraft	Upper-air wind and temperature from aircraft	u, v, T
AIRS	Atmospheric Infrared Sounder of MODIS	Tb
AMSR	Radiances from AMSR-2 onboard GCOM satellite	Tb
ATOVS	AMSU-A, AMSU-B/MHS, HIRS from NOAA-18 &19, MetOp A&B	Tb
ATMS	Advanced Technology Microwave Sounder in NPP satellite	Tb
CrIS	Cross-track Infrared Sensor observations in NPP satellite	Tb
FY3C	MWHS radiances from FY3C	Tb
GOESClear	Cloud clear Imager radiances from GOES	Tb
GPSRO	Global Positioning System Radio Occultation observations from various satellites (including MT ROSA)	Bending Angle
GroundGPS	Ground based GPS observations from various locations	Zenith Total Delay
IASI	Infrared Atmospheric Sounding Interferometer from MetOp A&B	Tb
IN3DSndr	INSAT-3D Sounder Radiances	Tb
MTSAPHIR	SAPHIR microwave radiances from Megha-Tropiques	Tb
Satwind	Atmospheric Motion Vectors from various geostationary and polar orbiting satellites (including INSAT-3D)	u, v
Scatwind	Advanced Scatterometer in MetOp-A & B, ScatSat-1, WindSat	u, v
SEVIRIClear	Cloud clear observations from SEVIRI of METEOSAT 8 &11	Tb

Sonde	Radiosonde observations, upper-air wind profile from pilot balloons,wind profiles, VAD wind observation from Indian DWR	u, v, T, q
Surface	Surface observations over Land and Ocean	u, v, T, q, Ps
SSMIS	SSMIS Radiances	Tb

Observation Processing System (OPS)

The OPS (OPS component of extract and process) prepares quality controlled observations for Hybrid 4D-Var in the desired format. OPS reads the decoded observations packed by the OPPS in the "obstore" format. OPS perform quality control on the observations and reformat the observations for its use in the Hybrid 4D-Var. OPS extract and process has two components, the extract component retrieves the observations and calculates background values at the observation locations and the process component performs the quality control and reformats them ready for its use in the Hybrid 4D-Var. The OPS system processes and packs observations within the six hourly assimilation window (plus or minus 3 hour in the DA cycle of 00, 06, 12 and 18 UTC).

Hybrid 4D-Var Data Assimilation (VAR)

The Hybrid 4D-Var system blends the "climatological" background error with day-to-day varying flow dependent background errors from the new high resolution NCMRWF ensemble prediction system (NEPS). The hybrid approach is scientifically attractive because it elegantly combines the benefits of ensemble data assimilation with the known benefits of 4D-Var within a single data assimilation system. Global atmospheric analysis is produced at 00, 06, 12 and 18 UTC. Various components of the data assimilation system and their dependences are depicted in **Figure 4.1**. Salient features of the data assimilation system are given in **Table 4.2.**

Surface Analysis Preparation System (SURF)

The surface analysis system ("SURF") implemented at NCMRWF prepares the surface initial fields of Snow (amount and depth), Sea Surface Temperature (SST), Sea Ice extent & depth and Soil Moisture for NCUM model forecast. SST and Sea Ice conditions are obtained from the OSTIA analysis. The SURF system interpolates these analyses to the model resolution for its use in the model (surface boundary conditions). The Snow analysis (snow depth and amount) is produced by the SURF system using the using snow cover data from NESDIS ("IMS Snow") and the model forecast. In the new SURF implementation also, Extended Kalman Filter (EKF) based system prepares soil moisture analysis. EKF system implemented at NCMRWF uses JULES (the Joint UK Land Environment Simulator) land surface model. Soil moisture observations from ASCAT as well as the surface analysis increments of moisture and temperatures (prepared by 3D-Var screen analysis system) are used in the EKF system. Some of the important aspects of new SURF system are given in **Table 4.2**.

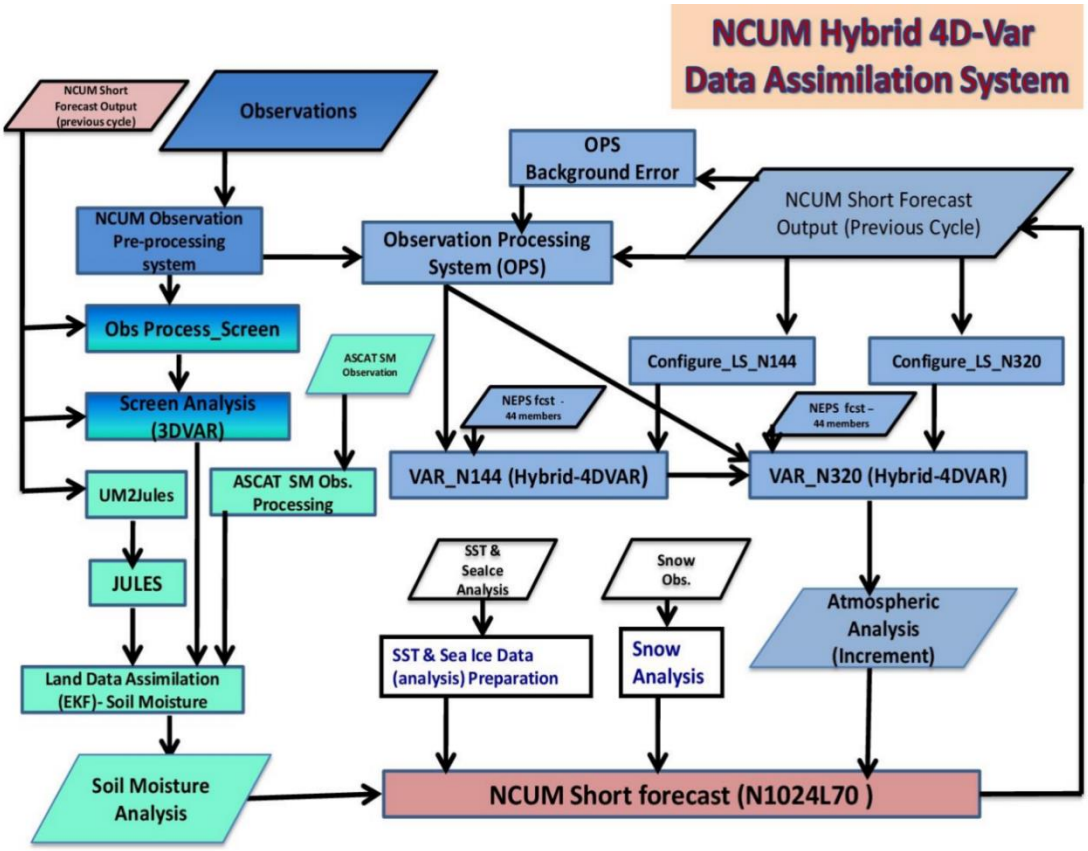

Figure 4.1 ***F***low chart of NCUM Data Assimilation System

NCMRWF Unified Model (NCUM)

Unified Model version 10.8 (UM10.8), which is the part of latest "Operational Global Suite" (PS40) of UK Met Office, is adapted as the new NCUM. There is not much difference in dynamics or representation of physical processes in the new model version in comparison with previous version (UM10.2) used at NCMRWF. However, the horizontal resolution of the model is increased to ~12 km in this up-gradation. Details are given in **Table 4.2.**

Table 4.2 Details of the new NCUM system

Model	**Atmospheric Data Assimilation**	**Surface analysis**
Model: Unified Model; Version 10.8 **Domain:** Global and regional **Resolution:** 12 km, Levels 70 **Grid:** 2048x1536 **Time Step:** 5 minutes	**Resolution:** N320L70 (~40 km) with N144L70 Hessian based pre-conditioning **Method:** Hybrid incremental 4D-Var. Information on "errors of the day" is provided by NEPS	**Soil Moisture analysis:** *Method:* Extended Kalman Filter *Analysis time:* 00, 06, 12 and 18 UTC ***Observations assimilated:***

Physical Parameterizations: based on GA6.1 (Walters et al, Geo sci. Model Dev., 10: 1487-1520, 2017) **Dynamical Core:** END Game **Forecast length:** 10 days (based on 00 UTC and 12 UTC initial conditions)	forecast at every data assimilation cycle **Data Assimilation Cycles:** 4 analyses per day at 00, 06, 12 and 18 UTC. Observations within +/- 3 hrs from the cycle time is assimilated in the respective DA cycle **Observations:** Observation Processing System does the quality control of observations. Variational bias correction is applied to satellite radiance observations. List of observations assimilated are given in Table-1	ASCAT soil wetness observations, Screen Temperature and Humidity (pseudo observations from 3D-Var screen analysis) **SST**: Updated at 12 UTC DA cycle with OSTIA based SST and sea-ice analysis **Snow Analysis:** Satellite derived snow analysis. Updated at 12 UTC DA cycle

NCMRWF Ensemble Prediction System (NEPS)

The new global ensemble prediction system (NEPS) prepares 10 day forecasts at 12 km horizontal resolution. Details of the new NEPS system is given in **Table 4.3.**

Table 3 Details of the new NEPS system

Model Details	**Initial Condition and Perturbations**	**Forecast length and Ensemble size**
Model: Unified Model; Version 10.8 **Resolution:** 12 km, Levels 70 **Domain:** Global **Grid:** 2048x1536 **Time Step:** 5 minutes **Physical Parametrizations**: based on GA6.1 **Dynamical Core:** ENDGame	**nitial condition:** Analysis from global deterministic Hybrid 4D Var data assimilation system. **Initial Condition Perturbations:**Perturbations are generated by Ensemble Transform Kalman Filter (ETKF). **Surface Perturbations:** SST perturbations, Deep soil temperature and soil moisture perturbations **Model Perturbations:** Stochastic Kinetic Energy Backscatter (SKEB) scheme and Random Parameters	**Forecast length:** 10 days **Number of Ensemble members:** 22

Rose/Cylc Software Environment for development & managing suites

NCUM system uses the Python based Rose/cylc environment for managing and running operational jobs. Rose is a framework for managing and running suites (suite is a collection of scientific application software for a common purpose).Rose contains all the features required for configuration management of suites and their components. Cylc is the suite engine or work flow engine (tools formanaging the workflows required by the Rose) that drives task submission and monitoring. Cylc has all the key features required for both operational and research job scheduling including run, rerun, kill, poll, hold individual task or a family of tasks. NCMRWF uses Rosie database for suite management. Both Rose and Cylc are Open Source software managed under GitHub.

NCUM-Writeup.pdf (Source - https://www.ncmrwf.gov.in)

1st CASE LOCAL SEVERE THUNDERSTORM ON 17th APRIL 2022 FORECAST OVER KOLKATA REGION

Wind discontinuity is likely to develop from northern parts of Sub Himalayan West Bengal to Telangana in the lower levels. Thunderstorm activity is east India (West Bengal). On account of prevailing southwesterly wind flow in the lower levels, the thunderstorm activity is likely to be accompanied by strong gusty winds (40-50 kmph) over Sub Himalayan West Bengal.

Mesoscale model forecasts (lightning forecast from NCUM 4km model initialized at 00 UTC of today, lightning forecast from WRF model using DLP scheme initialized at 00 UTC of today) and Global models (ECMWF model thunderstorm forecast product) also indicate that there is strong likelihood of enhanced thunderstorm activity accompanied by cloud-to-ground lightning over the Bengal today. NCMRWF regional 4-km model forecast on 17th April 2022 are shown in **Figure 4.2.**

NCMRWF: NCUM Regional (4km) (forecast based on 00 UTC the day)

1. Convergence at 850 hPa:

Day/Index: Subdivisions with Lower -Level Convergence > 15 x 10-5/s

Day1: Gangetic_WB

2. Low level Vorticity: -Positive Vorticity:

Day/Index: Subdivisions with Lower- Level Vorticity > 15 x 10-5 /s

Day0, Day1 and Day2: Gangetic_WB

3. Spatial distribution of Showalter Index:

Day/Index: Subdivisions with Showalter Index < -4

Day1: Gangetic_WB

Day2: Gangetic_WB

4. Spatial distribution of TTI:

Day/Index: Subdivision with Total Totals Index > 52

Day0 and Day1: Gangetic_WB

5. K-Index :> 35[Very Unstable thunderstorm likely]:

Day/Index: Subdivisions with K Index > 40

Day1 and Day2: Gangetic_WB

6. Rainfall and thunder storm activity:

Day/Index: Subdivisions with Precipitation > 2 cm

Day0, Day1 and Day2: Gangetic_WB

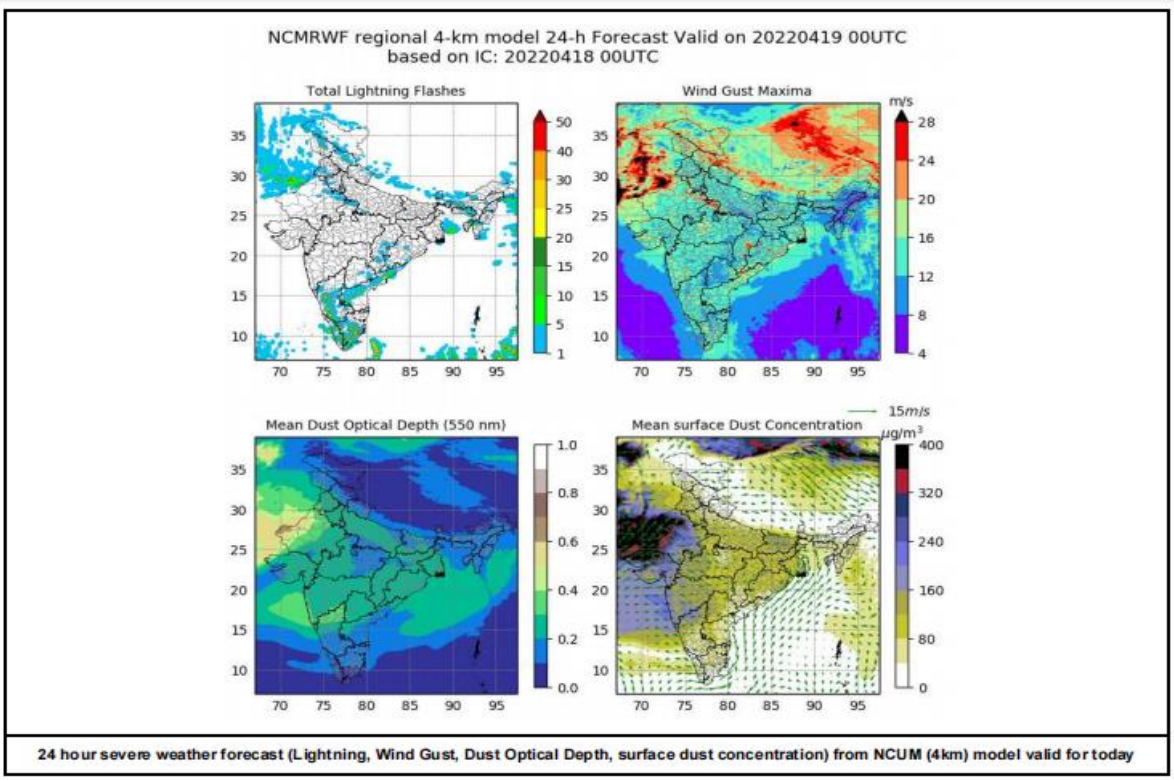

Figure 4.2. NCMRWF regional 4-km model forecast on 17th April 2022(Source - IITM Pune)

2ND CASE LOCAL SEVERE THUNDERSTORM ON 21ST APRIL 2022 FORECAST OVER KOLKATA REGION

On account of the high surface temperature and the strength of the wind discontinuity between the dry north westerlies and moist southeasterlies from the Bay of Bengal, the thunderstorms are likely to be moderate to severe over much of the east Indian region today. They are likely to be accompanied by strong gusty winds (30-50 kmph) over West Bengal.

Mesoscale model forecasts (lightning forecast from NCUM 4km model initialized at 00 UTC of today also indicate that there is strong likelihood of enhanced thunderstorm activity accompanied by cloud-to-ground lightning over Bengal today. NCMRWF regional 4-km model forecast on 21th April 2022 are shown in **Figure 4.3.**

NCMRWF: NCUM Regional (4km) (forecast based on 00 UTC the day):

1. Convergence at 850 hPa:

Day/Index: Subdivisions with Lower-Level Convergence > 15 x 10-5/s

Day0, Day1 and Day2: Gangetic_WB

2. Low level Vorticity: -Positive Vorticity:

Day/Index: Subdivisions with Lower-Level Vorticity > 15 x 10-5 /s

Day0, Day1 and Day2: Gangetic_WB

3. Spatial distribution of Showalter Index:

Day/Index: Subdivisions with Showalter Index < -4 Nil

4. Spatial distribution of TTI:

Day/Index: Subdivision with Total Totals Index > 52 Nil

5. K-Index :> 35[Very Unstable thunderstorm likely]:

Day/Index: Subdivisions with K Index > 40 Nil

6. Rainfall and thunder storm activity:

Day/Index: Subdivisions with Precipitation > 2 cm

Day0: Gangetic_WB

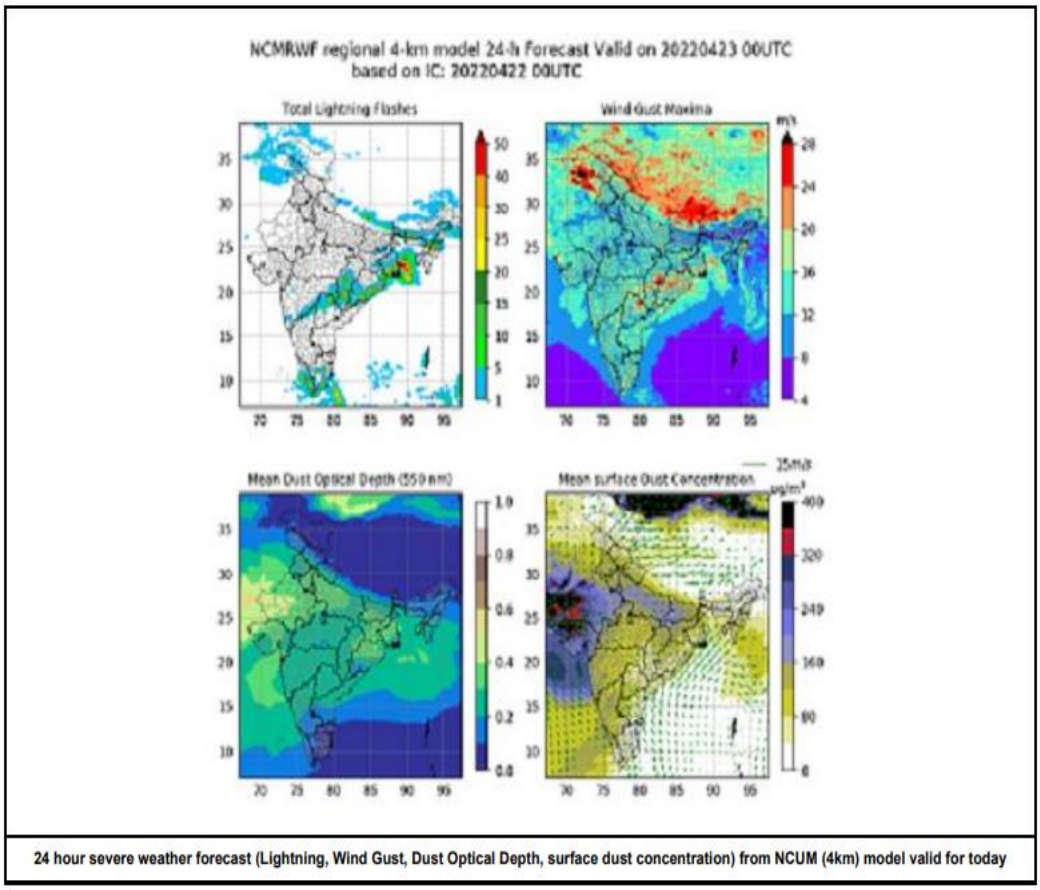

Figure 4.3. NCMRWF regional 4-km model forecast on 21st April 2022 (Source -IITM Pune)

3RD CASE LOCAL SEVERE THUNDERSTORM ON 22ND APRIL 2022 FORECAST OVER KOLKATA REGION

On account of the high surface temperature and the strength of the wind discontinuity between the dry north westerlies and moist southeasterlies from the Bay of Bengal, the thunderstorms are likely to be moderate to severe over much of the central and east Indian region today. They are likely to be accompanied by strong gusty winds (30-50 kmph) over West Bengal. NCMRWF regional 4-km model forecast on 22nd April 2022 are shown in **Figure 4.4.**

NCMRWF: NCUM Regional (4km) (forecast based on 00 UTC the day)

1. Convergence at 850 hPa:

Day/Index: Subdivisions with Lower-Level Convergence > 15 x 10-5/s

Day0 and Day1: Gangetic_WB

2. Low level Vorticity: -Positive Vorticity:

Day/Index: Subdivisions with Lower-Level Vorticity > 15 x 10-5 /s

Day0, Day1 and Day2: Gangetic_WB

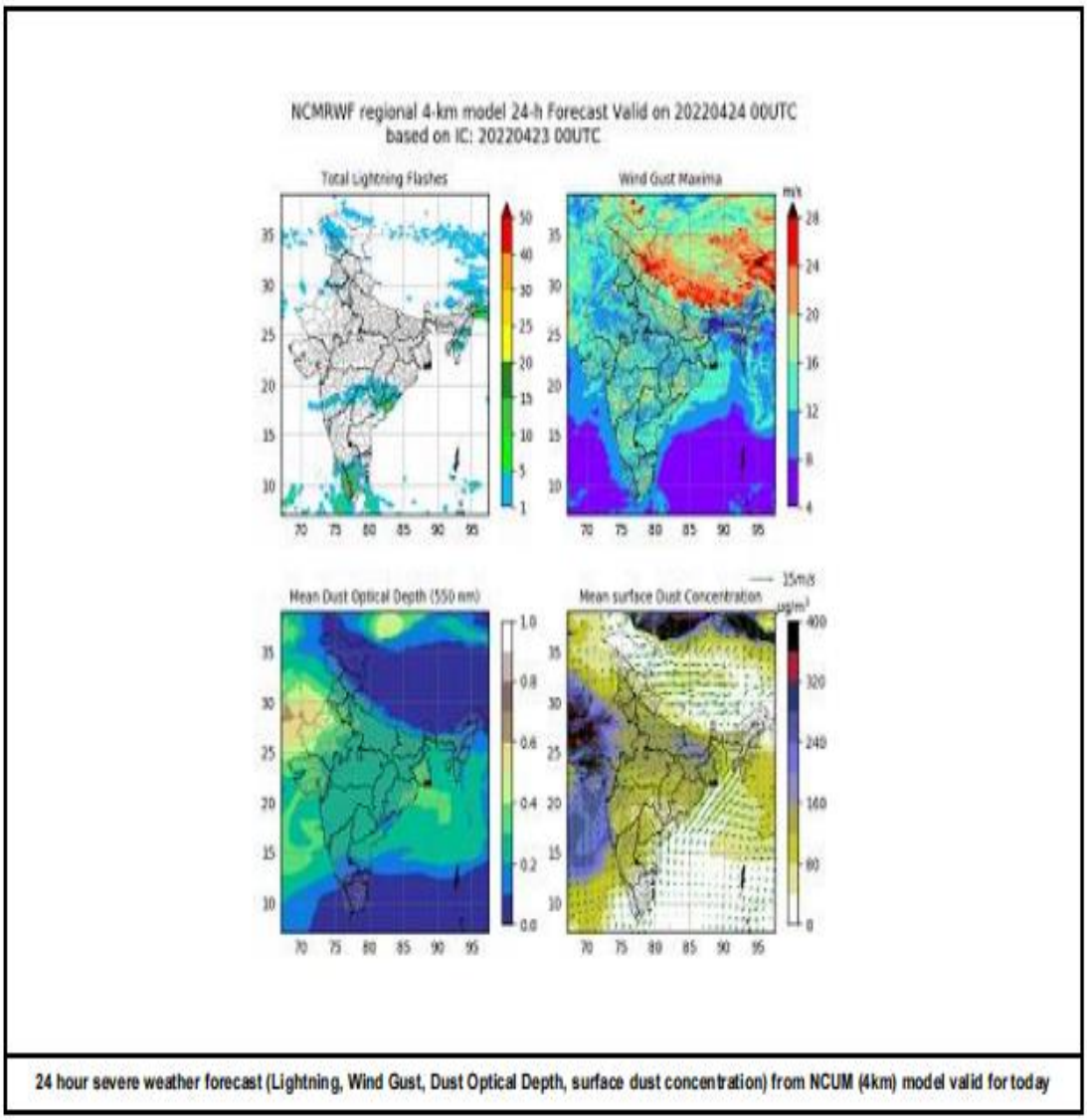

Figure 4.4. NCMRWF regional 4-km model forecast on 22th April 2022
(Source - IITM Pune)

4TH CASE LOCAL SEVERE THUNDERSTORM ON 29TH APRIL 2022 FORECAST OVER KOLKATA REGION

The east-west oriented trough runs from West Uttar Pradesh to Gangetic West Bengal across south Bihar & north Jharkhand in the lower levels. Global model forecasts (ECMWF and IMD GFS) indicate that in the absence of a strong anticyclone over central Bay of Bengal, the trough across central and peninsular India is likely to shift eastwards and link with the north-south trough over north India. This is likely to create a northeast-southwest oriented wind discontinuity across the Indian subcontinent extending from Gangetic West Bengal to Kerala. This zone along the trough /wind discontinuity, and to the east of it, is likely to see thunderstorm activity, over east India (west Bengal) and northeast India today and tomorrow.

Mesoscale model forecasts (lightning forecast from NCUM 4km model initialized at 00 UTC of today) and Global model forecasts (ECMWF Thunderstorm forecast product) also indicate that there is strong likelihood of enhanced thunderstorm activity accompanied by cloud-to-ground lightning along the line of discontinuity over the states of east, and the east Indian peninsula today. NCMRWF regional 4-km model forecast on 29th April 2022 are shown in **Figure 4.5.**

NCMRWF: NCUM Regional (4km) (forecast based on 00 UTC the day):

1. Convergence at 850 hPa:

Day/Index: Subdivisions with Lower-Level Convergence > 15 x 10-5/s

Day0, Day1 and Day2: Gangetic_WB

2. Low level Vorticity: -Positive Vorticity:

Day/Index: Subdivisions with Lower-Level Vorticity > 15 x 10-5 /s

Day0, Day1 and Day2: Gangetic_WB

3. Spatial distribution of Showalter Index:

Day/Index: Subdivisions with Showalter Index < -4

Day0, Day1 and Day2: Gangetic_WB

4. Spatial distribution of TTI:

Day/Index: Subdivision with Total Totals Index > 52

Day0, Day1 and Day2: Gangetic_WB

5. K-Index :> 35[Very Unstable thunderstorm likely]:

Day/Index: Subdivisions with K Index > 40

Day0, Day1 and Day2: Gangetic_WB

6. Rainfall and thunder storm activity:

Day/Index: Subdivisions with Precipitation > 2 cm

Day0, Day1 and Day2: Gangetic_WB

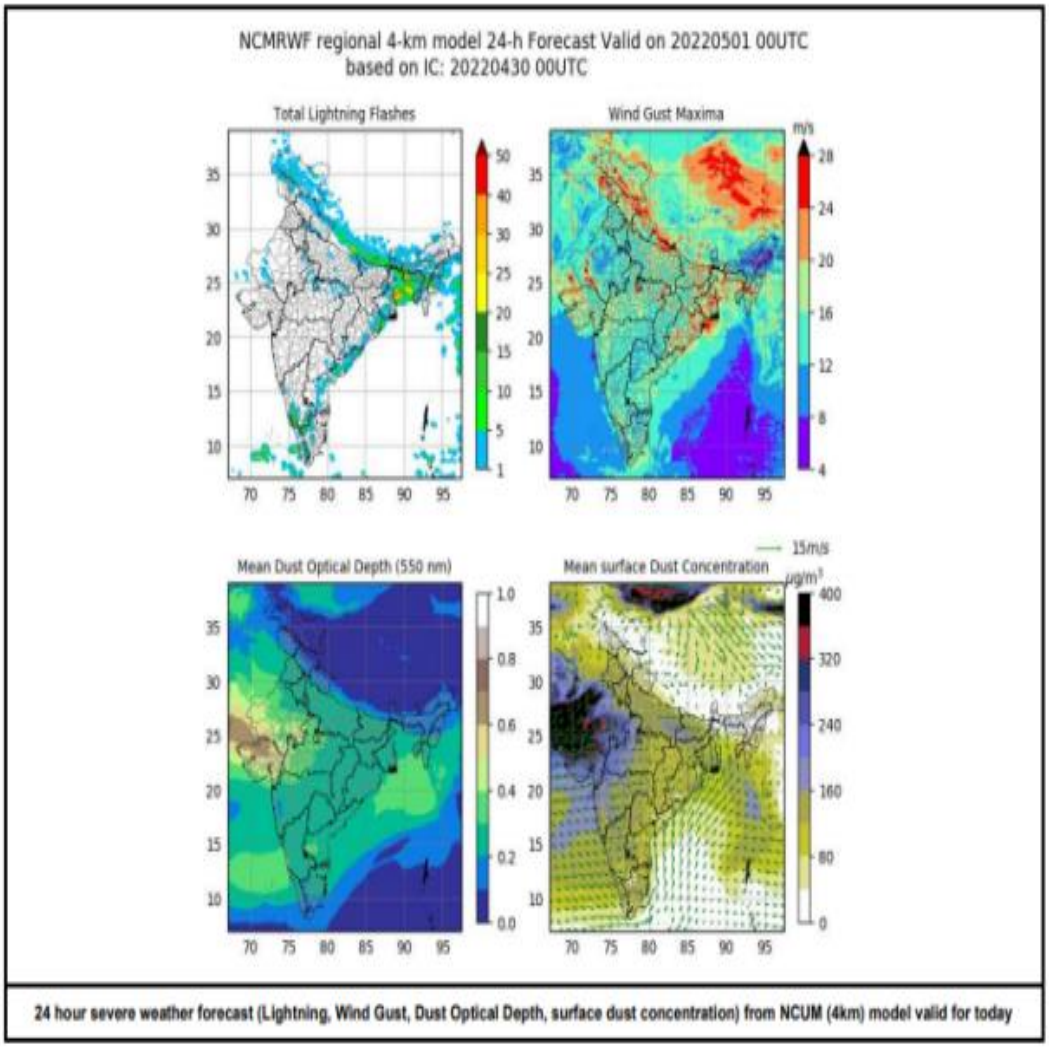

Figure 4.5. NCMRWF regional 4-km model forecast on 29th April 2022
(Source - IITM Pune)

5TH CASE LOCAL SEVERE THUNDERSTORM ON 1ST MAY 2022 FORECAST OVER KOLKATA REGION

The north-south oriented trough across central and peninsular India today runs from southeast Madhya Pradesh to interior Tamil Nadu across Vidarbha, Telangana and Rayalaseema. Global model forecasts (ECMWF and IMD GFS) indicate that in the afternoon, the cyclonic circulation is likely to move eastwards to over Jharkhand and adjoining Gangetic West Bengal and deepen.

There is likelihood of squally winds over this region (50-60 kmph) today over Gangetic West Bengal and 40-50 kmph winds over the remaining region. On account of the diurnal weakening of the east-west trough during the afternoon hours of today, and re-strengthening thereafter, isolated thunderstorm activity is likely over northwest India today, intensifying tomorrow as the Westerly trough further approaches the Indian region. Thunderstorm activity accompanied by frequent cloud to ground lightning is likely along the east peninsula today and tomorrow. NCMRWF regional 4-km model forecast on 17th April 2022 are shown in **Figure 4.6.**

NCMRWF: NCUM Regional (4km) (forecast based on 00 UTC the day):

1. Convergence at 850 hPa:

Day/Index: Subdivisions with Lower-Level Convergence > 15 x 10-5 /s

Day0, Day1 and Day2: Gangetic_WB

2. Low level Vorticity: -Positive Vorticity:

Day /Index: Subdivisions with Lower- Level Vorticity > 15 x 10-5 /s

Day0, Day1 and Day2: Gangetic_WB

3. Spatial distribution of Showalter Index:

Day/Index: Subdivisions with Showalter Index < -4

Day0, Day1 and Day2: Gangetic_WB

4. Spatial distribution of TTI:

Day/Index: Subdivision with Total Totals Index > 52

Day0 and Day1: Gangetic_WB

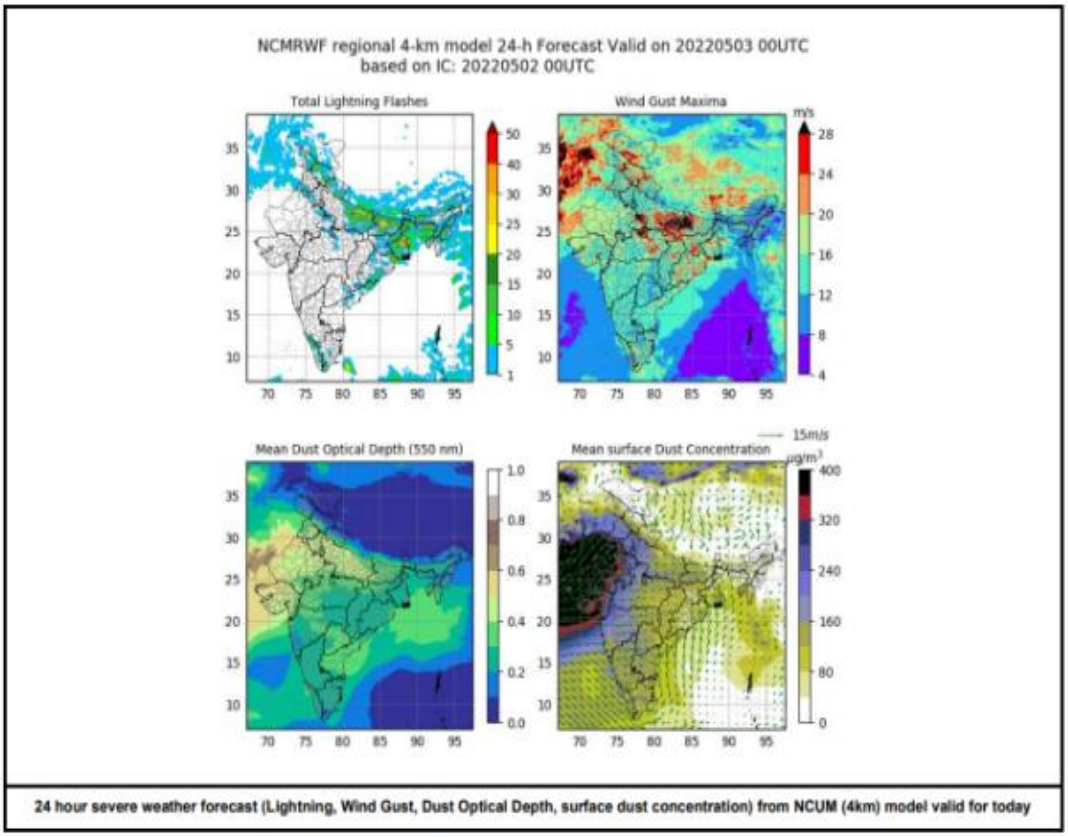

Figure 4.6 NCMRWF regional 4-km model forecast on 1st May 2022(Source - IITM Pune)

6TH CASE LOCAL SEVERE THUNDERSTORM ON 3RD MAY 2022 FORECAST OVER KOLKATA REGION

NCMRWF: NCUM Regional (4km) (forecast based on 00 UTC the day):

1. Convergence at 850 hPa: Day/Index: Subdivisions with Lower-Level Convergence > 15 x 10-5 /s

Day0, Day1 and Day2: Gangetic_WB

2. Low level Vorticity: -Positive Vorticity: Day/Index: Subdivisions with Lower- Level Vorticity > 15 x 10-5 /s

Day0, Day1 and Day2: Gangetic_WB

3.Spatial distribution of Showalter Index: Day/Index: Subdivisions with Showalter Index < -4

Day0 and Day1: Gangetic_WB

4. Spatial distribution of TTI: Day/Index:

Subdivision with Total Totals Index > 52

Day0 and Day1: Gangetic_WB

5. K-Index :> 35[Very Unstable thunderstorm likely]:

Day/Index: Subdivisions with K Index > 40

Day1 and Day2: Gangetic_WB

6. Rainfall and thunder storm activity: Day/Index:

Subdivisions with Precipitation > 2 cm

Day0, Day1 and Day2: Gangetic_WB

NCMRWF regional 4-km model forecast on 3rd May 2022 are shown in **Figure 4.7.**

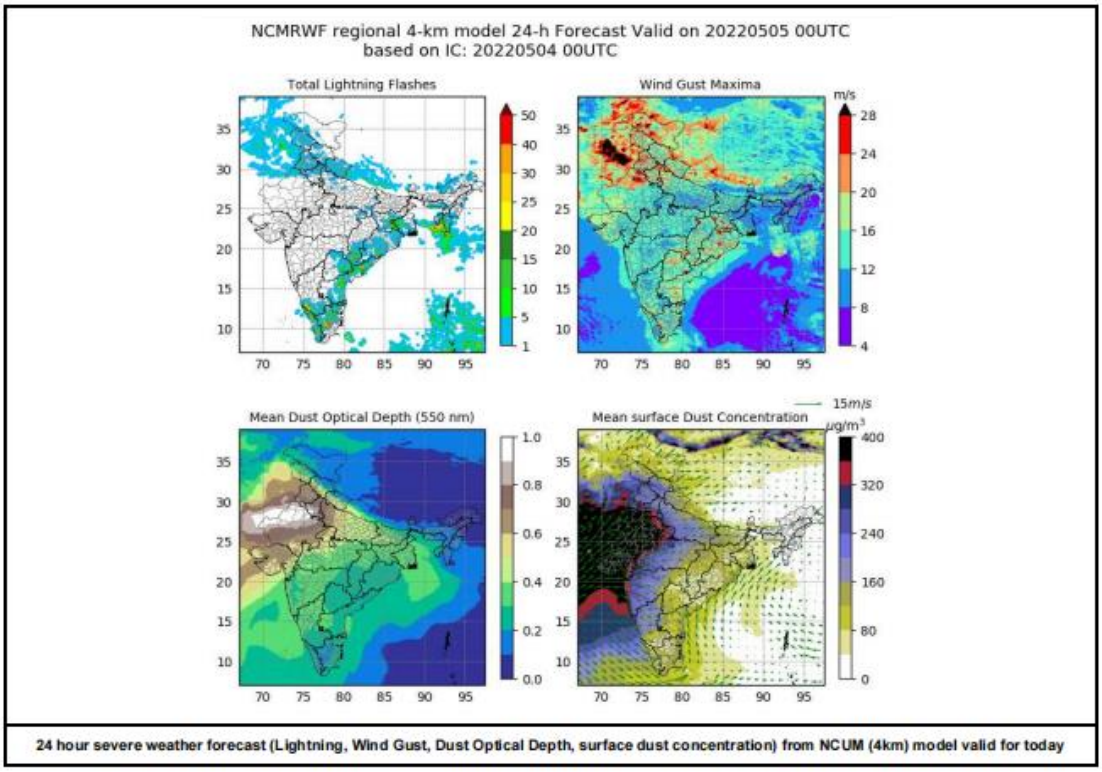

Figure 4.7. NCMRWF regional 4-km model forecast on 3rd May 2022(Source - IITM Pune)

7TH CASE LOCAL SEVERE THUNDERSTORM ON 19TH MAY 2022 FORECAST OVER KOLKATA REGION

NCMRWF: NCUM Regional (4km) (forecast based on 00 UTC the day)

1. Convergence at 850 hPa:

Day/Index: Subdivisions with Lower -Level Convergence > 15 x 10-5:

Day0, Day1 and Day2: Gangetic_WB.

2. Low level Vorticity: -Positive Vorticity:

Day/Index: Subdivisions with Lower- Level Vorticity > 15 x 10-5 /s

Day0, Day1 and Day2: Gangetic_WB.

3. Spatial distribution of Showalter Index:

Day/Index: Subdivisions with Showalter Index < -4

Day0, Day1 and Day2: Gangetic_WB.

4.Spatial distribution of TTI:

Day/Index: Subdivision with Total Totals Index > 52.

Day0, Day1 and Day2: Gangetic_WB.

5.K-Index :> 35[Very Unstable thunderstorm likely]: Day d/Index:

Subdivisions with K Index > 40

Day1 and Day2: Gangetic_WB.

6. Rainfall and thunder storm activity:

Day/Index: Subdivisions with Precipitation > 2 cm.

Day1 and Day2: Gangetic_WB.

NCMRWF regional 4-km model forecast on 19th May 2022 are shown in **Figure 4.8.**

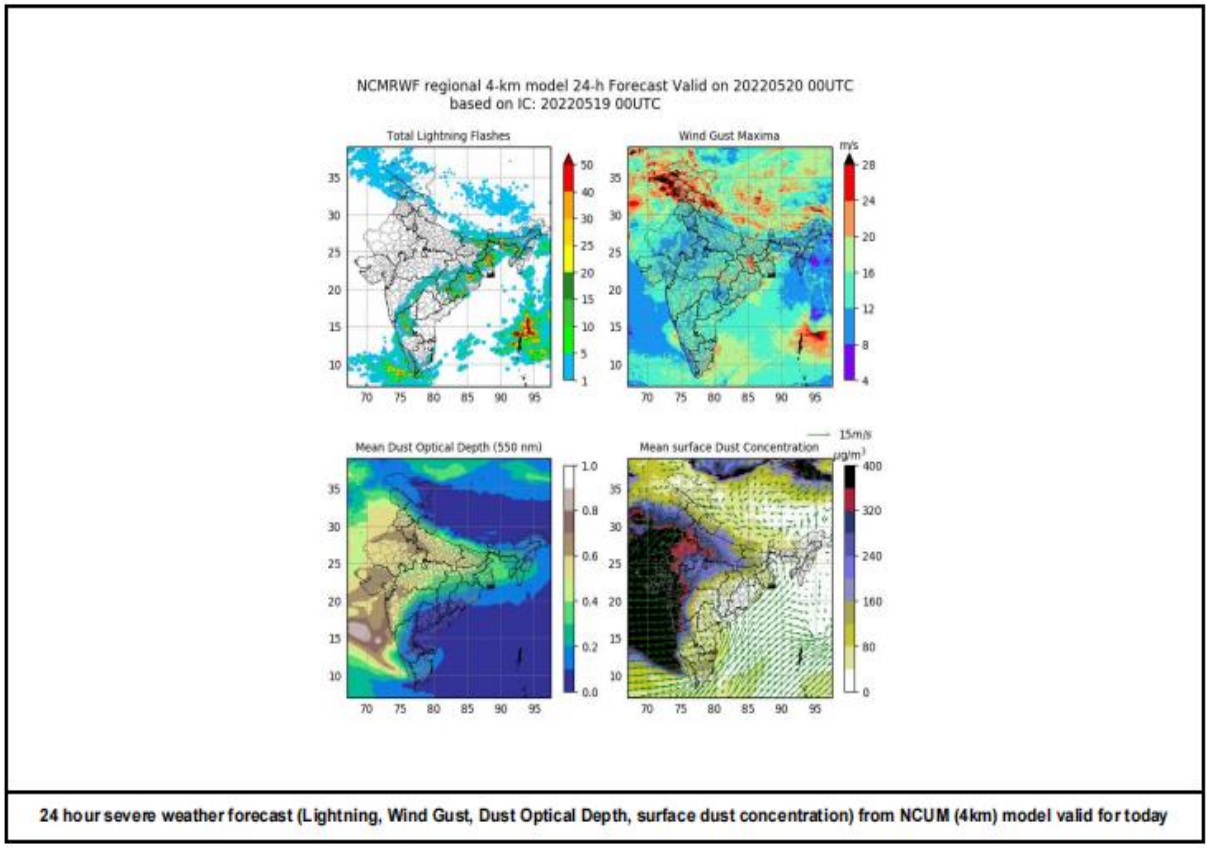

24 hour severe weather forecast (Lightning, Wind Gust, Dust Optical Depth, surface dust concentration) from NCUM (4km) model valid for today

Figure 4.8. NCMRWF regional 4-km model forecast on 19th May 2022(Source - IITM Pune)

8TH CASE LOCAL SEVERE THUNDERSTORM ON 20TH MAY 2022 FORECAST OVER KOLKATA REGION

Low Level Convergence (850-925hPa) based on 0500 UTC:

Positive Low-Level Convergence up to +5 to +10 (x10^-5/s) observed over Gangetic west Bengal. NCMRWF regional 4-km model forecast on 20th May 2022 are shown in **Figure 4.9.**

NCMRWF: NCUM Regional (4km) (forecast based on 00 UTC the day):

1. Convergence at 850 hPa:

Day/Index: Subdivisions with Lower Level Convergence > 15 x 10-5 :

Day0, Day1 and Day2 : Gangetic_WB .

2. Low level Vorticity:-Positive Vorticity:

Day/Index: Subdivisions with Lower Level Vorticity > 15 x 10-5 /s

Day0, Day1 and Day2 : Gangetic_WB .

3. Spatial distribution of Showalter Index:

Day/Index: Subdivisions with Showalter Index < -4

Day0, Day1 and Day2 : Gangetic_WB .

4.Spatial distribution of TTI:

Day/Index**:** Subdivision with Total Totals Index > 52 .

Day0, Day1 and Day2 : Gangetic_WB .

5.K-Index :> 35[Very Unstable thunderstorm likely]:Day d/Index:

Subdivisions with K Index > 40

Day1 and Day2 : Gangetic_WB .

6. Rainfall and thunder storm activity:

Day/Index: Subdivisions with Precipitation > 2 cm .

Day1 and Day2 : Gangetic_WB .

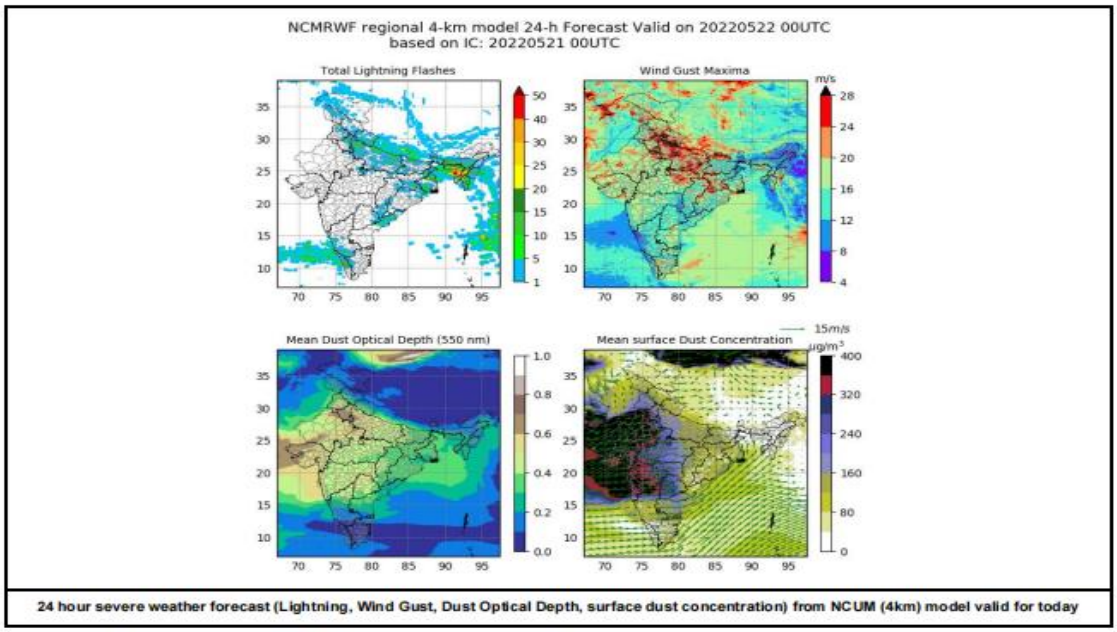

Figure 4.9. NCMRWF regional 4-km model forecast on 20st May 2022 (Source - IITM Pune)

9TH CASE LOCAL SEVERE THUNDERSTORM ON 21ST MAY 2022 FORECAST OVER KOLKATA REGION

NCMRWF: NCUM Regional (4km) (forecast based on 00 UTC the day):

1. Convergence at 850 hPa:

Day/Index: Subdivisions with Lower- Level Convergence > 15 x 10-5/s

Day0, Day1 and Day2: Gangetic_WB.

2. Low level Vorticity: -Positive Vorticity:

Day/Index: Subdivisions with Lower -Level Vorticity > 15 x 10-5/s

Day0 and Day2: Gangetic_WB.

3. Spatial distribution of Showalter Index:

Day/Index: Subdivisions with Showalter Index < -4

Day0 and Day2: Gangetic_WB.

4. Spatial distribution of TTI:

Day/Index: Subdivision with Total Totals Index > 52

Day0 and Day2: Gangetic_WB.

5. K-Index :> 35[Very Unstable thunderstorm likely]:

Day/Index: Subdivisions with K Index > 40

Day0, Day1 and Day2: Gangetic_WB.

6. Rainfall and thunder storm activity:

Day/Index: Subdivisions with Precipitation > 2 cm

Day0, Day1 and Day2: Gangetic_WB.

NCMRWF regional 4-km model forecast on 21th April 2022 are shown in **Figure 4.10.**

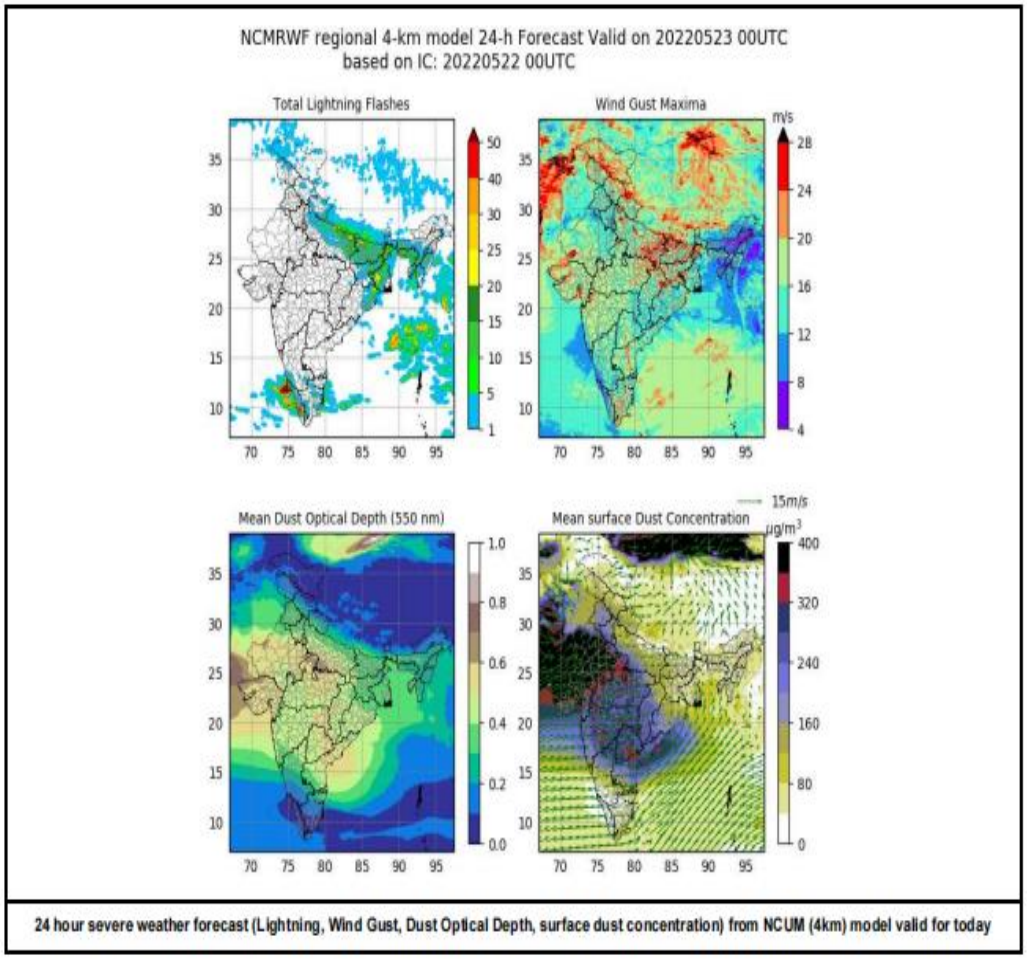

Figure 4.10. NCMRWF regional 4-km model forecast on 22nd May 2022 (Source - IITM Pune)

Chapter - 5

A study on thunderstorm prediction prior to the monsoon over Kolkata region, West Bengal (India)

ABSTRACT

In the present work, we use thermodynamic indices to analyze thunderstorm episodes over the Kolkata region by using sounding data for the pre-monsoon period of April to May, 2022. We examine how well indices distinguish between days with and without thunder. The predicted values of these indices show how thunderstorm activity varies in kind.

Different types of indices used are, the Surface Lifted Index (SLI), K Index (KI), Convective Available Potential Energy (CAPE), Convective Inhibition (CIN), Severe Weather Threat Index (SWEAT), Total Totals Index (TTI), Bulk Richardson Number (BRN), Deep Convection Index (DCI), Humidity Index (HI), Boyden Index (BI), Showalter Index (SI), Dew point temperature at 500 hpa, 700 hpa and 850 hpa (DEW) and height, 700 hpa and 1000 hpa (H). Probability distribution curves are represented to identify the ability of the indices to differentiate between thunder and without thunder days. We have estimated the mean, standard deviations, and Z scores. Z scores of 75% or more are considered significant for further analysis, and the rest are rejected. It is not possible to forecast the occurrence of thunderstorm activity depending on only one index. This study suggests that the indexes with excellent skills for thunder forecasting are, BI, SLI and DCI, while the forecasting ability is deficient for other observed values. Observed values of these indices also reveal that different types of thunder were possible over Kolkata during the studied pre-monsoon months of April and May, 2022. The study's conclusion offers important new information about enhancing index forecasting abilities for more accurate prediction.

Keywords: Kolkata, Thunderstorm prediction, Indices, Nor'wester, Climate change.

INTRODUCTION

The Nor'wester is a concern of general interest for many reasons. It not only gives comfort in the afternoon heat through rain which is needed for pre-monsoonal cultivation but the associated gusty wind, lightning, etc. cause significant damage to public life and properties. During the warm climate season i.e., from March to May, Kolkata faces a sudden change in climate with a special type of strong thunderstorm known as Nor'wester. In Bengal, it is known as 'KalBaisakhi' (15 April to 15 May). Apart from its calamitous outcomes like an unexpected increase in wind speed, lightning, thunder, hail and the rainfall associated with the storm, although small in amount, is especially helpful for the pre-Kharif crops like jute, paddy, and a large number of vegetables and fruits. These storms are more frequent in the late afternoon although they are known to occur at other times of the day as well.

Nor'westers are thunderstorms that originate mostly in the northwest (NW) direction (Desai, 1950; Kessler, 1982). These Nor'westers are not local typical heat storms. The warm, moist, southerly low-level flow from the Bay of Bengal and a cool, dry, westerly, or northwesterly upper-level flow existing over the region, have a mesoscale rise to a synoptic situation for the formation of Nor'westers. These have a mesoscale structure with a very rapid development often associated with moderate to severe squalls, achieving a speed in the range of 130 to 150 mph, which may even reach tornadic violence, causing considerable damage to property and loss of life (Ghosh et al., 2008). Tyagi et al. (2011) assessed the skill of various indices and parameters and proposed suitable threshold values for forecasting the occurrences of thunderstorm activity in Kolkata. Meteorologists use stability indices and skill scores to assess the occurrence of thunderstorms quickly. Stability indices are usually calculated following Peppier (1988). Ravi et al. (1999) presented two objective methods based on stability indices to forecast the occurrence of thunderstorms in Delhi. Mukhopadhyay et al. (2003) worked on the objective forecast of thundery to non-thundery days using conventional indices over three NE Indian stations. Haklander and Delden (2003) reported the thunderstorm predictors and their forecast skills for the Netherlands. Kunz (2007) investigated the skill of convective parameters and indices to predict isolated and severe thunderstorms over southwest (SW) Germany. Similarly, Dhawan et al. (2008) have suggested statistical techniques for forecasting pre-monsoon thunderstorms for NW India. Litta and Mohanty (2008) have also used a few thermodynamic indices values given in the literature to identify the occurrence of thunderstorm activity in their modeling study of a thunderstorm events. In a similar manner, Sa´nchez et al. (2008) studied the pre-convective conditions leading to thunderstorm activity over SW Argentina and developed a short-term forecast model.

Nevertheless, such efforts are lacking for the Kolkata region, which is prone to thunderstorms, although, Tyagi et al. 2011 did make an attempt. In the present study, we evaluate the efficiency of several stability indices and thermodynamic parameters in forecasting the occurrence of thunderstorms over the Kolkata region located in the Gangetic West Bengal Region during the pre-monsoon period for the April–May, 2022. We have tried to assess the skill of various thermodynamic indices and propose suitable

threshold values for indices to predict the future occurrences of thunderstorm activity during the pre-monsoon months.

DATA

The Department of Atmospheric Science at the University of Wyoming, provided the information (http://weather.uwyo.edu/upperair/sounding.html) that is being used in the present study. The information on the frequency of thunderstorms and FDP reports are utilized. The 16th to 23rd April, 28th to 30th April, 1st to 4th May, 12th to 13th May and 16th to 23th May in the year 2022, are the days of pre-monsoon months which are used in the current study. For the year 2022, the total number of 11 days with thunder and 14 days without thunder is taken into account. The thunderstorm and non-thunderstorm cases chosen for the present study over the Kolkata region, West Bengal (India) are shown in **Table 5.1.**

COMMON SYNOPTIC FEATURES DURING THE PRE-MONSOON SEASON OVER THE KOLKATA REGION

The study area Kolkata, situated in the eastern part of India is associated with the tropical monsoon climate . During the pre-monsoon season, there is the conversion from winter monsoon to summer monsoon circulations, and the region receives very severe insolation, which results in the development of heat flow.

Over the West Bengal region, two distinct air masses coexist, west-to-northwest winds from the land and moist winds from the Bay (Pramanik, 1939). There exists a low-pressure system over the Chota Nagpur Plateau, West Bengal, Assam, Bangladesh and the bordering regions, and a seasonal high-pressure system over the Bay of Bengal around this time (Weston, 1972; Lohar and Pal, 1995). The high surface temperature and heavy convective activities are prominent characteristics of the season. A shallow layer of moist southerlies / southwestern from the Bay of Bengal, is present in the upper air flow over the Gangetic West Bengal and the surrounding areas, while dry westerlies are present in the upper atmosphere. A weak surface pressure field associated with weak surface and lower atmospheric winds, coupled with the strong daytime heating, makes the atmosphere potentially unstable in the pre-monsoon months of April and May. However, thunderstorms may not occur every day, even though a favorable environment exists virtually daily during these months for their occurrence. Synoptic systems or features that supply the trigger could be the cause. Earlier Srinivasan et al. (1973) have discovered that there may be 30-40 thunderstorm days with less rainfall during this season. Pre-monsoon thunderstorms over West Bengal's Gangetic Plain,

which fall under the category of severe local storms, primarily occur around 11 UTC, however, nocturnal thunderstorms also occur (Patra et al., 1998).

Table 5.1 Thunderstorm and non-thunderstorm cases over the Kolkata region, West Bengal (India) used in the present study

S.No.	Thunderstorm dates	Thunderstorm Time	Non-thunderstorm dates	Non-thunderstorm Time
1	17.04.2022	0000UTC 1200UTC	16.04.2022	0000UTC 1200UTC
2	21.04.2022	0000UTC 1200UTC	18.04.2022	0000UTC 1200UTC
3	22.04.2022	0000UTC 1200UTC	19.04.2022	0000UTC 1200UTC
4	29.04.2022	0000UTC 1200UTC	20.04.2022	0000UTC 1200UTC
5	01.05.2022	0000UTC 1200UTC	23.04.2022	0000UTC 1200UTC
6	03.05.2022	0000UTC 1200UTC	28.04.2022	0000UTC 1200UTC
7	13.05.2022	0000UTC 1200UTC	30.04.2022	0000UTC 1200UTC
8	17.05.2022	0000UTC 1200UTC	02.05.2022	0000UTC 1200UTC
9	19.05.2022	0000UTC 1200UTC	04.05.2022	0000UTC 1200UTC
10	20.05.2022	0000UTC 1200UTC	12.05.2022	0000UTC 1200UTC
11	21.05.2022	0000UTC	16.05.2022	0000UTC 1200UTC
12	—	—	18.05.2022	0000UTC 1200UTC
13	—	—	22.05.2022	0000UTC 1200UTC
14	—	—	23.05.2022	0000UTC 1200UTC

METHODOLOGY

Several indexes such as, Surface Lifted Index (SLI), Humidity Index (HI), K Index (K), Boyden Index (BI), Severe Weather Threat Index (SWEAT), Total Totals Index (TT), Deep Convective Index (DCI), Convective Available Potential Energy (CAPE), Showalter Index (SI), Bulk Richardson Number (BRN), Relative Humidity (RH) at 700 hpa, and Dew point temperature (DEW) at 850 hpa, are all considered in this study. SLI, SWEAT, TT, CAPE, BRN, K, RH, CINE, and DEWS are thermodynamic indices and parameters extracted from the description of indices (Mukhopadhyay et al., 2003), whereas HI, BI, and DCI are estimated using sounding observations. The procedures for computing all the indexes are given in **Table 5.2**.

Showalter Index (SI)

The SI is based on the 850 and 500 mb levels' characteristics. The SI is computed by elevating a parcel dry adiabatically from 850 mb to its LCL, then

moistening it adiabatically to 500 mb, and comparing the parcel, in comparison to environmental 500 mb temperatures equivalent to the LI. SI can be represented as,

SI = T (500 mb envir) – T (500 mb parcel) in degrees C (weather.gov/lmk/indices)

Given a shallow low-level cool air mass north of a frontal boundary, the SI may be more accurate than the LI in detecting instability aloft. However, if the low-level moisture does not reach up to the 850 mb level, the SI is an unrepresentative index and inferior to the LI in indicating instability.

Convective Inhibition (CIN)

The quantity of negative buoyant energy available to hinder or suppress upward vertical acceleration, or the amount of effort the environment must make on the parcel to raise it to its LFC, is represented by CIN. It is inverse of CAPE and reflects the negative energy area (B-) on the sounding where the parcel temperature is lower than the ambient temperature. The smaller (bigger) the CIN, the less synoptic and especially mesoscale forceful lift must be required to bring the package to its LFC. Despite possibly high CAPE levels, high CIN values in the presence of little or no lift can cap or limit convective development. Remember that CAPE stands for available potential energy, that must be expended (weather.gov/lmk/indices). Details of stability indexes are given in **Table 5.2.**

TABLE 5. 2 Details of stability indexes

Index	Expression	References
Boyden-Index (BI)	$BI = H_{700} - H_{1000} - T_{700} - 200$	Boyden (1963)
Surface-Lifted (SLI)	$SLI = T_{500} - T_{sfc8500}$	Means (1952)
K Index (K)	$K = (T + T_d)_{850} - T_{500} - (T_{700} - T_{d700})$	George (1960)
Total-Total Index (TT)	$TT = 2(T_{850} - T_{500}) - (T_{850} - T_{d850})$	Miller (1967)
Deep Convective Index (DCI)	$DCI = (T + T_d)_{850} + SLI$	Barlow (1993)
Humidity-Index (HI)	$HI = (T-T_d)_{850} + (T-T_d)_{700} + (T-T_d)_{500}$	Litynska et al. (1976)
Severe weather Threat(SWEAT)	$SWEAT = 12T_{d850} + 20(TT-49) + 4V_{850} + 2V_{500} + 125SHEAR_{8506500}$	Bidner (1970)
Convective Available Potential Energy(CAPE)	$CAPE = g\int_{Z_{LFC}}^{Z_{LNB}} \frac{T_{ve} - T_{vp}}{T_{ve}} dz$	Moncrieff and Miiller (1976)
Bulk Richardson No(BRN)	$BRN = CAPE / (0.5)\,[SHEAR]^2$	Weissman and Klemp (1982)

H: decameter height of the specified pressure level, T: dew point and ambient temperature (0°C), T_d : dry bulb temperatures, V : wind speed, SHEAR: wind shear, T_{ve} : virtual temperature of the environment, T_{vp} re: virtual temperature of the parcel, Z_{LNB}: heights at neutral buoyancy, Z_{LFC}: heights at free convection, g: gravity's acceleration, sfc: surface.

Environmental parameters and indices for the convective season

The range of different indices considered for the study are

TT Index	
TT = 45 to 50	Thunderstorms possible
TT = 50 to 55	Thunderstorms are more likely, possibly severe.
TT = 55 to 60	Severe thunderstorms most likely.
K Index	
K below 30	Thunderstorms with heavy rain or severe weather are possible
K over 30	Better potential for thunderstorms with heavy rain.
K = 40	Best potential for thunderstorms with very heavy rain.
SWEAT Index	
SWEAT over 300	Potential for severe thunderstorms.
SWEAT over 400	Potential for tornadoes.
CAPE Index	
CAPE below 0	Stable.
CAPE = 0 to 1000	Marginally unstable.
CAPE = 1000 to 2500	Moderately unstable.
CAPE = 2500 to 3500	Very unstable.
CAPE = above 3500 – 4000	Extremely unstable.
BRN Index	
Below 10	Strong vertical wind shear and weak CAPE. The shear may be too strong given the weak buoyancy to develop sustained convective updrafts. However, given sufficient forcing, thunderstorms may still develop; if so, rotating supercells could evolve given the high shear.
10 to 45	Associated with supercell development.
over 50	Relatively weak vertical wind shear and high CAPE suggest multicellular thunderstorm development is most likely.
SLI Index	(Continued)

over 0	Stable but weak convection is possible for LI = 1-3 if strong lifting is present
0 to -3	Marginally unstable.
-3 to -6	Moderately unstable.
-6 to -9	Very unstable.
below -9	Extremely unstable.
SI Index	
SI over 0	Stable but weak convection is possible for SI = 1-2, if strong lifting is present
SI = 0 to -3	Moderately unstable.
SI = -4 to -6	Very unstable.
SI below -6	Extremely unstable.
DCI	30 or higher indicate the potential for strong thunderstorms.

Generally, SI values will not be quite as unstable as LI values (except for the case of shallow low-level cool air as discussed above). The mean, standard deviation, and ability distribution (Grosh and Morgan, 1975) of each index are calculated. Additionally, statistical methods are well-used to quantify the usefulness of the selected indices.

Statistical inferences

To determine statistically which index best distinguishes thundery (X) and nonthundery (Y) atmospheres, McClave and Dietrich (1988) proposed measuring test statistics (Z_{xy})

$$Z_{xy} = (M_x - M_y) / [s^2_x /n_x + s^2_y /n_y]$$

Where, M_x and M_y are the mean stability values of any index for categories X and Y, respectively, while n_x and n_y are the numbers of occurrences in each category. The related standard deviations are s_x and s_y. Greater absolute values of Z_{xy} indicate the index's utility in distinguishing between thunderous and non-thunderous days. However, this method does not quantify forecast accuracy. As a result, numerous skill scores are produced to grade each index's forecasting abilities.

Skill ratings

It consists of four events A, B, C, and D for each index, where, A: The number of correctly forecasted events, B: Events not correctly forecasted, C: Events forecasted but not observed, False Alarms, and D: Events not forecasted and also not observed. Different skill levels can be written as (Brier and Allen, 1952; Hansen and Kuipers, 1965; Donaldson et al., 1975):

Probability Of Detection (POD) $= \frac{\text{The number of correctly forecasted events}}{\text{Total number of observed event}} = \frac{A}{A+B}$

False Alarm Ratio (FAR) $= \frac{\text{Events forecasted but not observed}}{\text{Total number of observed event}} = \frac{C}{A+C}$

Critical Success Index (CSI) $= \frac{\text{The number of correctly forecasted events}}{\text{The sum of the total number of events and false alarm}}$

$= \frac{A}{A+B+C}$

True Skill Statistics (TSS) = The probability of detection of an event – The probability of detection of a false event $= \frac{A}{A+B} - \frac{C}{C+D} = \frac{(AD-BC)}{(A+B)(C+D)}$

Hiedke Skill Score (HSS) =

$$\frac{\text{Total number of correct forecast} - \text{Expected number of correct forecast by chance}}{\text{Total number of events} - \text{Expected number of correct forecast by chance}}$$

$$HSS = \frac{CF-E}{N-E} = \frac{2(AD-BC)}{(A+B)(B+D)+(A+C)(C+D)}$$

Where, CF = Total number of correct forecasts = A + D

N = Total number of events = A + B + C + D

A + C = Total number of forecasts for the event

A + B = Total number of observed events

C + D = Total number of observed nonevents

B + D = Total number of forecasts for the nonevent

A + B + C = The sum of the total number of events and false alarm

E = Expected number of correct forecasts by chance

E = (A + C) (A + B) + (C + D) (B + D) / N

POD is proportional to A and inversely proportional to (A + B). FAR is proportional to C and inversely proportional to (A + C). CSI is proportional to A and inversely proportional to (A + B + C). There is no explanation in CSI for non-thundery days forecasts (D). As a result, Scheafer (1990) stated that CSI is a biased score that depends on the frequency of the projected occurrence. The best and lowest possible TSS scores are 1 and -1, respectively. HSS is calculated in such a way that a perfect collection of forecasts (all categorized hits) has a score of 1, a set of random forecasts has a score of 0, and having less hits associated to the forecast by chance has a negative score. Although TSS and HSS take into account the number of valid nonevent forecasts, CSI does not. The restriction of CSI is that if A and D are swapped and B and C are swapped, the score changes but the TSS and HSS scores remain same. According to Doswell et al. (1990), no single measure of forecasting

success can provide a complete picture, and it is desirable to include, in addition to HSS, the CSI, POD, and FAR in any summary of forecasting success.

The forecast will be valid for 12 hours following prediction and will conclude at 1200 UTC based on 0000 UTC sounding data by indices. Similarly, the next forecast will be valid for the next 12 hours after prediction based on 1200 UTC sounding data by indices and will terminate at 0000 UTC. The forecast is only good for 12 hours.

RESULTS

Prediction at 0000 UTC

The mean and standard deviation of all the indices for two months in 2022 for the Kolkata station are shown in **Table 5.3** The probability distribution curves of these are shown in **Figure 5.1 a, b and c**. The probability distribution curves of TT and SWEAT are such that they do not describe distinct difference between thundery and nonthundery days.

Table 5.3 Mean and standard deviation of indices based on 0000 UTC data from Kolkata stations

Index	Thundery day (mean)	Thundery day standard deviation	Non-thundery day (mean)	Non-thundery day standard deviation
K	31.66	5.8	29.82	7.36
TT	48.55	4.29	47.24	5.83
SLI	-5.88	2.52	-4.48	4.49
DCI	41.1	4.08	38.07	6.46
HI	38.45	19.64	45.69	18.25
BI	98.02	1.28	98.47	1.46
SWEAT	263.82	108.22	234.27	123.32
CAPE	1979.41	971.14	1759.7	1209.2
CIN	-183.6	190.6	-201.87	161.63
BRN	92.34	62.97	86.71	96.49
SI	-0.99	2.6	0.19	3.31

For this reason, these indices are less effective for explanation of thunderstorm existence and nonexistence. Among the remaining of the indices K, SLI, DCI, BI, HI, CAPE, CIN, BRN and SI show skewed distribution of thundery days frequency with respect to non-thundery days frequency curve. The six stability indices (HI, SWEAT, CAPE,

CIN, DCI and BRN) have greater differences in mean values between the two categories, thundery and non-thundery days.

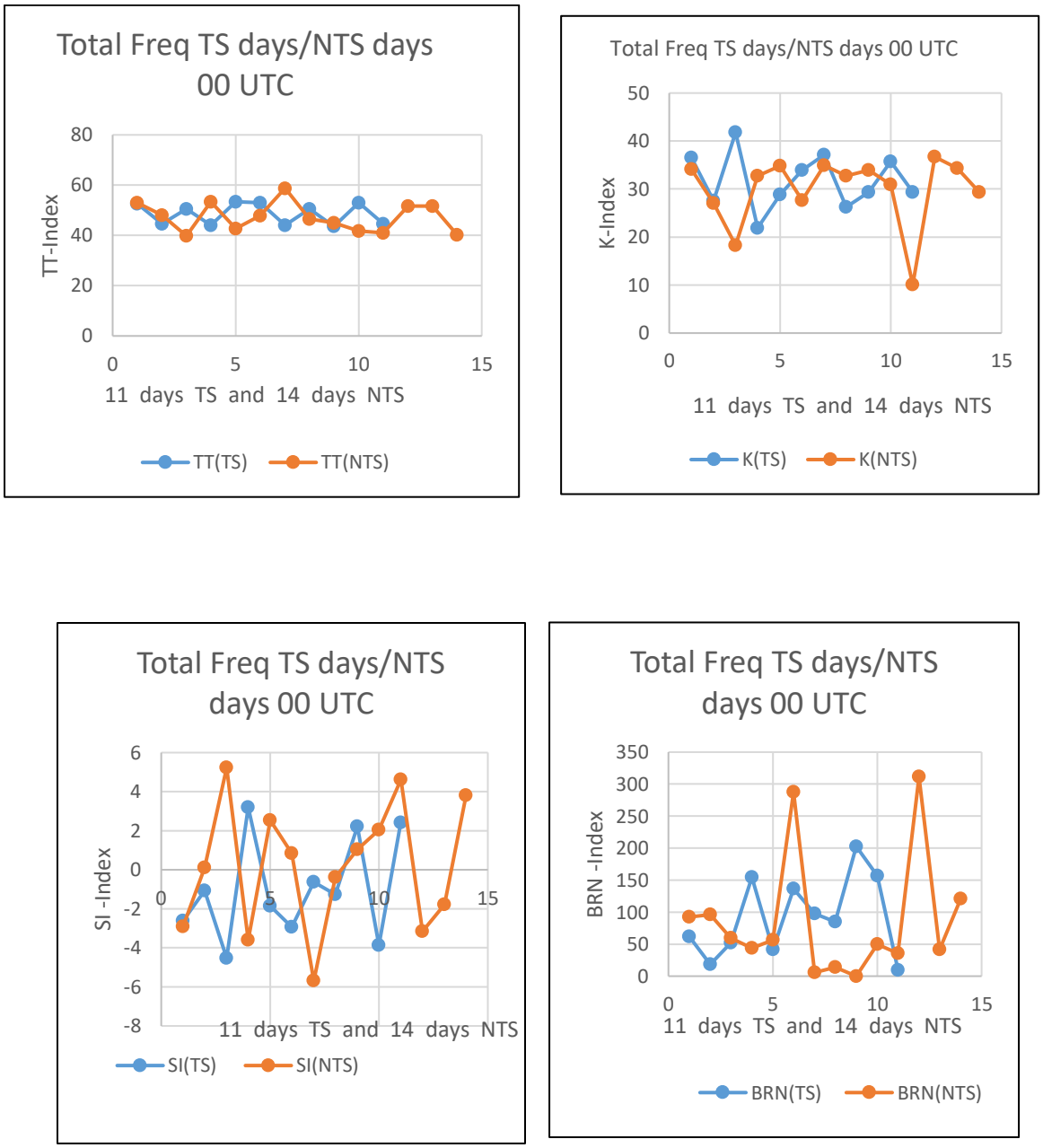

Figure 5.1(a) Frequency of thunderous (TS) and no thunderous (NTS) days at 0000 UTC, plotted against different indexes for the Kolkata station.

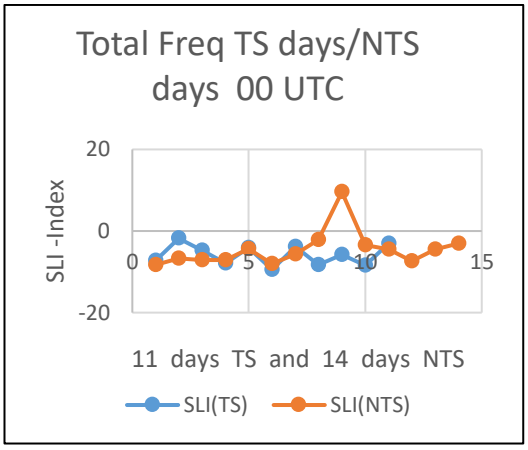

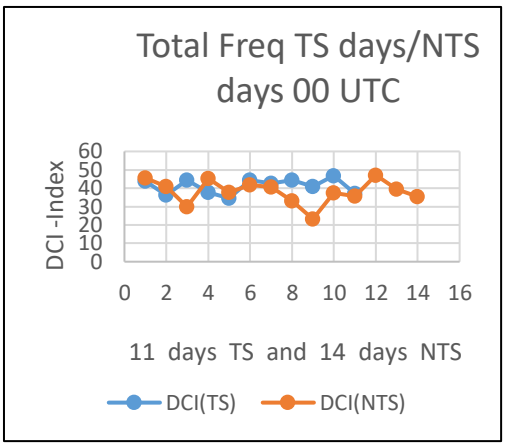

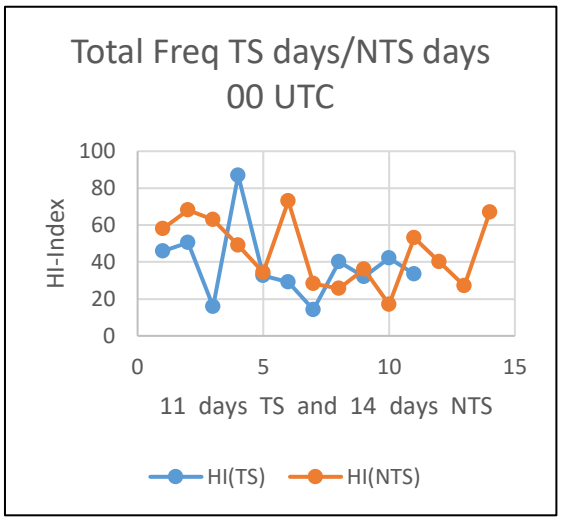

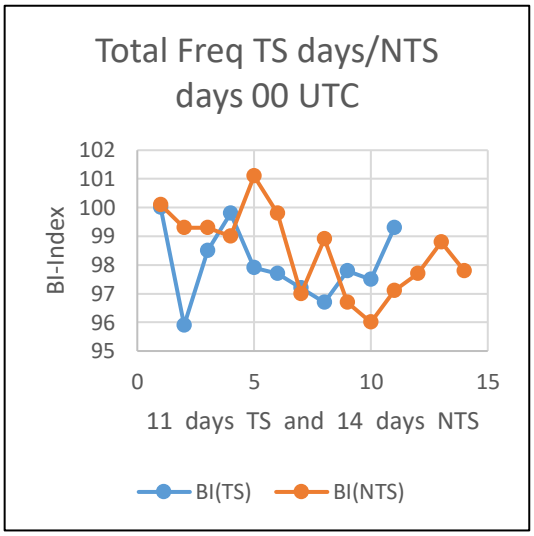

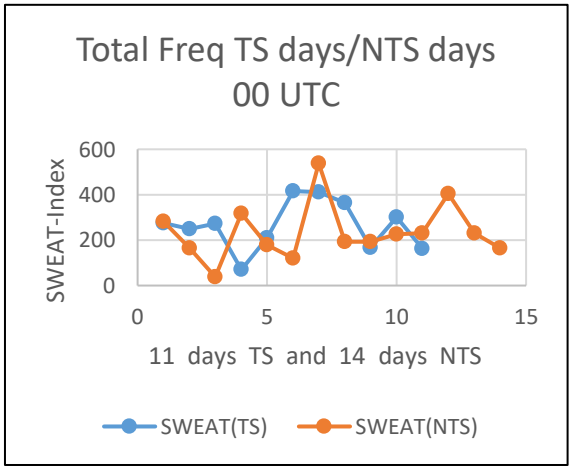

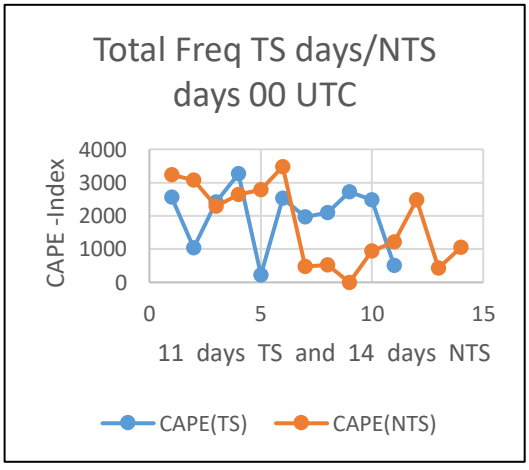

Figure 5.1(b) Frequency of thunderous (TS) and no thunderous (NTS) days at 0000 UTC, plotted against different indexes for the Kolkata station.

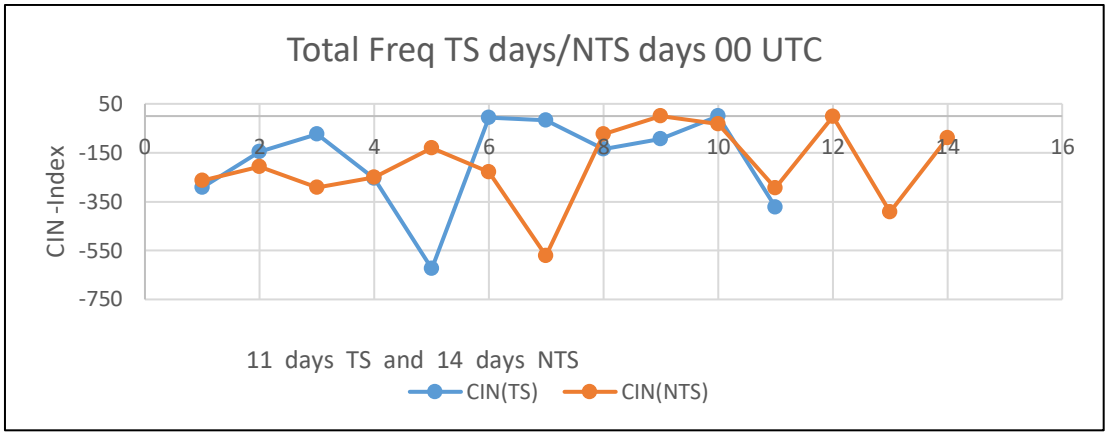

Figure 5.1 (c) Frequency of thunderous (TS) and no thunderous (NTS) days at 0000 UTC, plotted against different indexes for the Kolkata station.

To select those indices that will pass the significance test, Z statistics (Z_{xy}) is calculated for all the eleven indices as shown in **Table 5.4** So far as to statistical significance is concerned, DCI, SLI, BI, and SI appeared to have the highest Z_{xy} value and thus signifies that these four indices are having the best potential to differentiate the thundery and non-thundery days. The rest of the seven indices do not have the desired level of significance to be designed as predictors of thundery and non-thundery days and hence denied. In order to quantify the accuracy of forecasts, different skill scores are calculated for the four indices namely DCI, SLI, BI, and SI, which have shown at least a 75% significant level or more

Table 5. 4 Test statistics (Z_{xy}) for eleven indices at the Kolkata station at 0000 UTC

Index	Z_{xy} Values	Index	Z_{xy} Values
K	0.27	SWEAT	0.01
TT	0.32	CAPE	0.00
SLI	-0.69	CIN	0.00
DCI	0.67	BRN	0.00
HI	-0.12	SI	-0.84
BI	-1.49		

SLI value has 75% significant level. DCI, 75% significant level. While BI value, 93%. SI value has 80% significant level. For best possible forecast, we have considered above mention indices. We have considered best threshold value for calculating skill score of thundery and non-thundery days with the help of iteration process for perfect result.

Table 5.5 gives the recommended threshold and corresponding skill scores for these identified indices. The best skill is obtained from DCI and BI with threshold values 38.0^0C and 98 respectively. This means that thundery (non-thundery) days can be forecasted when DCI is greater (less) than 38.0^0C and for BI the forecast will be thundery (non-thundery) when its value will be greater (less) than 98. From the skill score point of view, POD score of 0.636 for DCI is highest. The best CSI, TSS and HSS scores are found for DCI and the values are 0.388, 0.136 and 0.132 respectively. Earlier, it has already been discussed that TSS and HSS are used for correct forecasting to show the true skill of categorically. The POD score (0.545) for SLI with threshold (-5) less or equal to. The POD score (0.364) for BI with threshold 98 greater or equal to. The POD score (0.364) for SI with threshold (-2) less or equal to. So far as FAR score is (0.5) for DCI and SI indices. In other category CSI, TSS and HSS, DCI has shown highest skill with prescribed threshold. These values of skill scores are to be consistent with the results reported earlier on Kolkata location (Tyagi et al., 2011).

Table 5.5 Skill ratings and specified threshold values of chosen metrics for the Kolkata station at 0000 UTC

Indices	POD	FAR	CSI	TSS	HSS
DCI ≥ 38	0.636	0.5	0.388	0.136	0.132
SLI ≤ -5	0.545	0.538	0.333	0.054	0.045
BI ≥ 98	0.364	0.667	0.211	-0.208	-0.206
SI ≤ -2	0.364	0.5	0.267	0.078	0.080

Verification of prediction at 0000 UTC

The contingency table and different skill scores for DCI, BI, SLI, and SI are shown in **Table 5.6** DCI has predicted the highest percentage of correct thundery days (38%) out of 42% realized and this is reflected in POD score (0.9). Both DCI and BI have predicted highest percentage of false alarm (42%) in the thundery days forecast and their FAR score are 0.526 and 0.556 respectively. They have produced only 16% correct nonthundery days forecast. Thus, other skill scores for DCI and BI have very low POD of BI of 0.8. Due to large false alarm, TSS and HSS have very low value for DCI and BI. DCI in five categories, as 0.9 (POD), 0.526 (FAR), 0.45 (CSI), 0.186 (TSS) and 0.165 (HSS). BI in five categories is 0.8 (POD), 0.556

(FAR), 0.4 (CSI), 0.086 (TSS) and 0.077 (HSS). SLI has predicted 34% thundery days correctly, 37% is the false alarm and 21% is the correct non-thundery days forecast and the skill scores of SLI in five categories are, 0.8 (POD), 0.529 (FAR), 0.421 (CSI), 0.157 (TSS) and 0.143 (HSS).

Table 5.6 Contingency table and skill scores for April and May, 2022, based on 0000 UTC data and validated with the following 1200 UTC observations of the Kolkata station given numbers are the best indices scores. Total number of thundery days (TD) observed - 42%. Total number of non-thunderstorm days observed - 58%.

Index	Observation	Prediction TD (%)	Prediction NTD (%)
DCI ≥ 38 (POD=0.9, FAR=0.526, CSI=0.45, TSS=0.186, HSS = 0.165)	TD (%) NTD (%)	38 42	4 16
BI ≥ 98 (POD=0.8, FAR = 0.556, CSI = 0.4, TSS = 0.086, HSS = 0.077)	TD (%) NTD (%)	34 42	8 16
SLI ≤ -5 (POD = 0.8, FAR = 0.529, CSI = 0.421, TSS = 0.157, HSS = 0.143)	TD (%) NTD (%)	34 37	8 21
SI ≤ -2 (POD = 0.6, FAR = 0.455, CSI = 0.4, TSS = 0.243, HSS = 0.239)	TD (%) NTD (%)	25 21	17 37

SI has predicted 25% thundery days correctly, 21% is the false alarm and 37% is the correct non-thundery days forecast and the skill scores of SI in five categories are 0.6 (POD), 0.455 (FAR), 0.4 (CSI), 0.243 (TSS) and 0.239 (HSS). The skill score of SI is not good because low percentage of correct thundery days forecast and large false alarms. SLI has predicted 34% of thundery days correctly, 37% is the false alarm and 21% is the correct non-thundery days forecast. BI has predicted 34% of thundery days correctly, 42% is the false alarm and 16% is the correct non-thundery days forecast. Due to low false alarm, TSS and HSS have the highest value for SI. POD score is same of SLI and BI, but FAR score is different. Thus, from all the aspects of forecast, DCI shows to perform better than other indices at 0000 UTC over the Kolkata station.

Prediction at 1200 UTC

The mean and standard deviation of all the indices for the two months of 2022 for the Kolkata station are shown in the **Table 5.7**. The probability distribution curves of these are shown in **Figure 5.2 a, b and c**. The probability distribution curves of TT, BRN and CIN are such that they do not describe distinct difference between thundery and non-thundery days. For this reason, these indices are less effective for explanation of thunderstorm existence and nonexistence. Among the remaining of the indices, K, SLI, DCI, BI, HI, CAPE, SWEAT and SI show skewed distribution of thundery days frequency with respect to non-thundery days frequency curve. BI, DCI and SLI have

Table 5.7 Indices mean and standard deviation based on 1200 UTC data from Kolkata stations

Index	Thundery day (mean)	Standard deviation		Non-thundery day (mean)	Standard deviation
K	29.7	8.44		27.16	6.79
TT	47.33	4.6		63.71	68
SLI	-6.9	2.22		-5.82	3.07
DCI	43.43	5.01		39.91	6.3
HI	46.12	27.35		46.77	21.7
BI	98.74	1.14		98.58	1.24
SWEAT	261.51	119.55		188.18	120.22
CAPE	3076.29	1036.04		2272.32	1389.74
CIN	-61.98	81.29		-98.92	69.73
BRN	82.61	47.64		72.4	55.93
SI	-1.46	3.01		-0.13	4.39

shown a skewed distribution at 0000 UTC between thundery and non-thundery days. Thus, qualitatively BI, DCI and SLI have shown better ability to differentiate the two categories of the atmosphere at 1200 UTC. The mean values of K and HI (**Table 5.7**) for thundery and non-thundery are very much identical which indicates the inefficiency of these indices to distinctly differentiate the two types of (thundery and non-thundery) atmosphere. The seven stability indices (DCI, TT, SWEAT, CAPE, CIN, BRN and K) are observed to have greater difference in mean values between the two categories (thundery and non-thundery days).

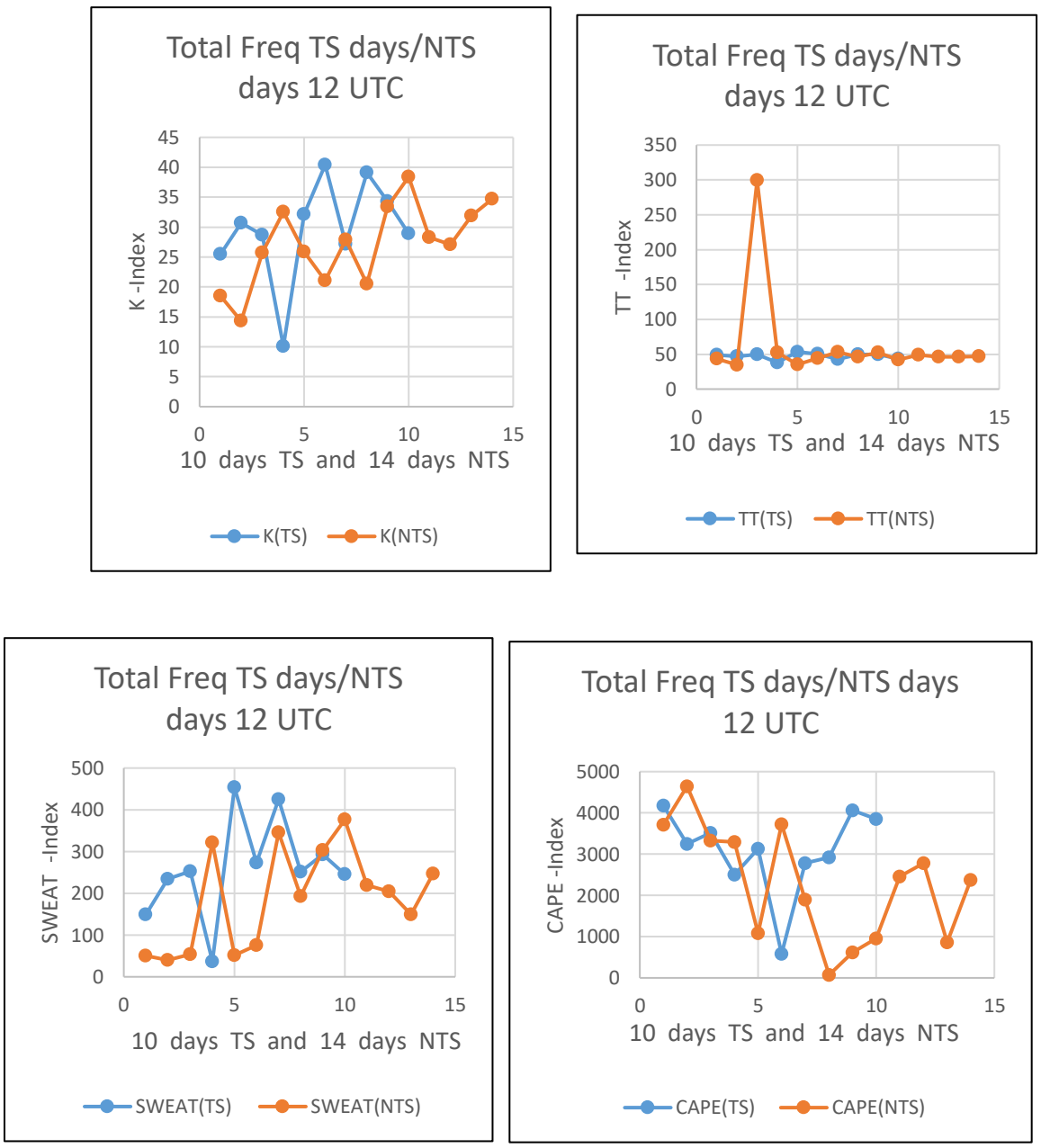

Figure 5.2(a) The frequency of thunderous (TS) and no thunderous (NTS) days at 1200 UTC plotted against different indexes for the Kolkata station.

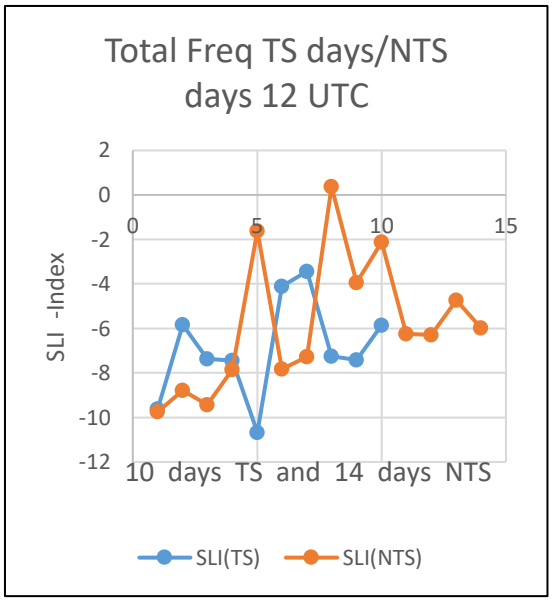

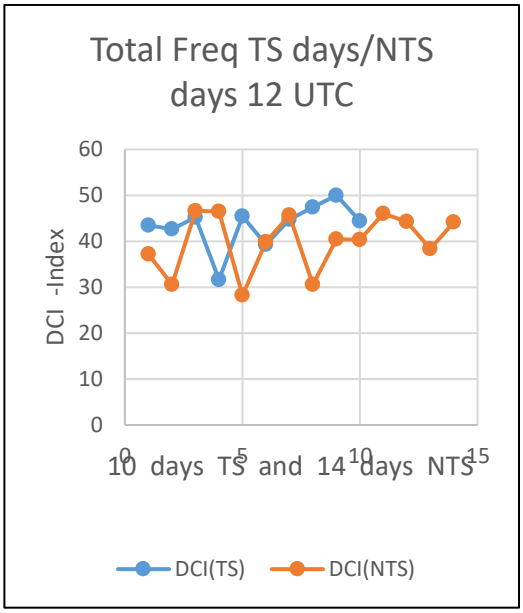

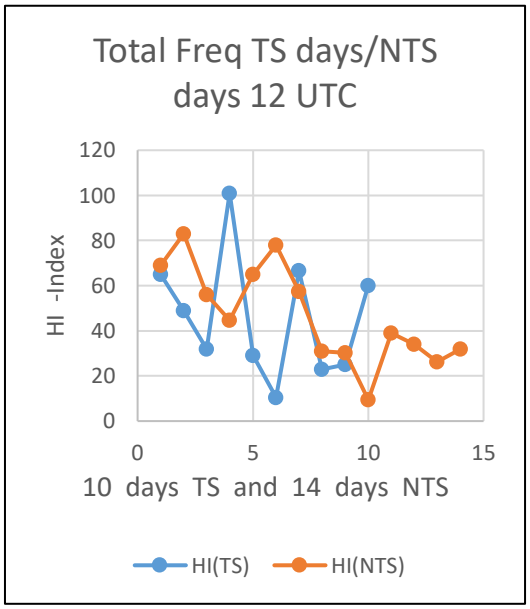

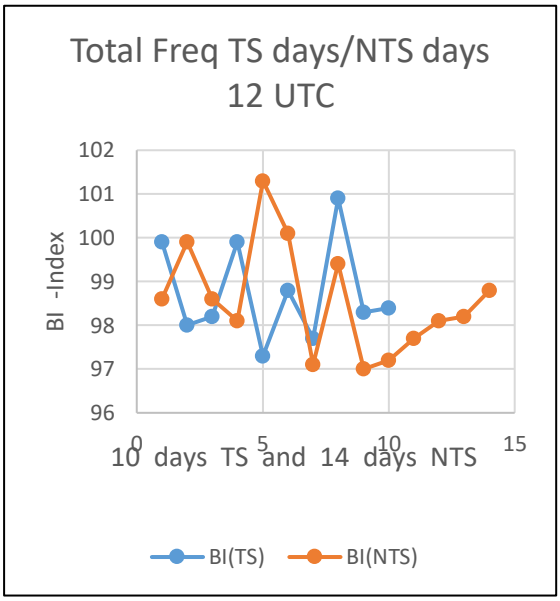

Figure 5.2(b) The frequency of thunderous (TS) and no thunderous (NTS) days at 1200 UTC plotted against different indexes for the Kolkata station.

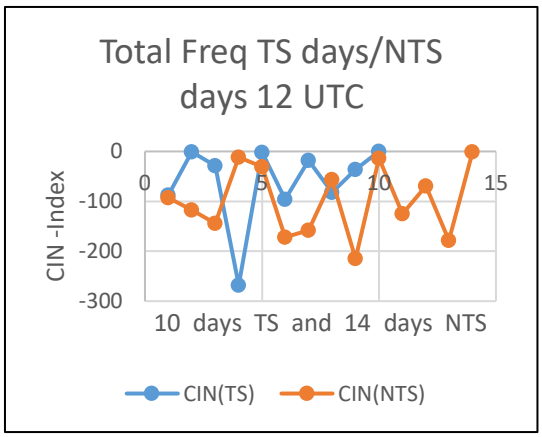

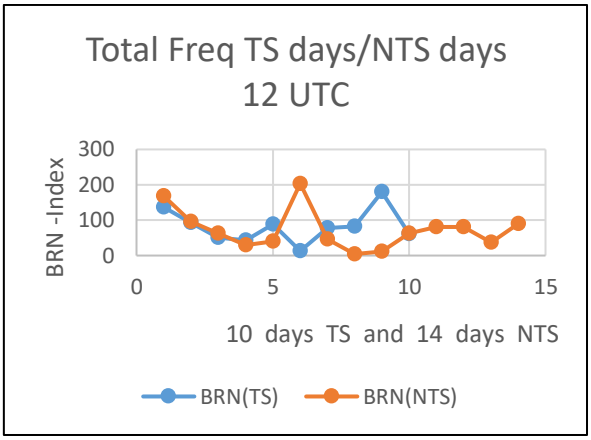

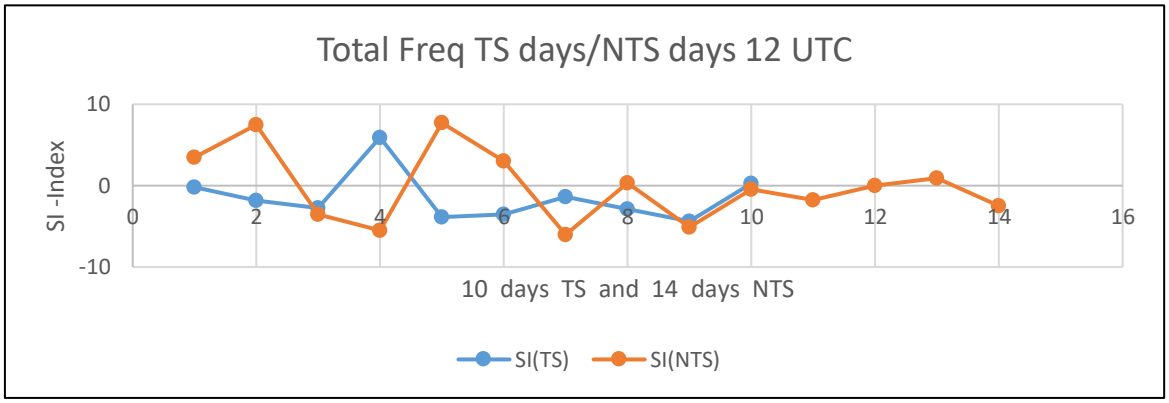

Figure 5.2(c) The frequency of thunderous (TS) and no thunderous (NTS) days at 1200 UTC plotted against different indexes for the Kolkata station.

To select those indices that will pass the significance test, Z statistics (Z_{xy}) is calculated for all the eleven indices as shown in **Table 5.8**. So far as statistical significance (**Table 5.8)**, DCI, SLI, and BI appear to have the highest Z_{xy} value and thus signifies that these four have the best potential to differentiate the thundery and non-thundery days. The rest of the eight indices do not appear to have the desired level of significance to be designed as predictors of thundery and non- thundery days and hence denied. To quantify the accuracy of forecasts, different skill scores are calculated for the three indices namely DCI, SLI, and BI, which have shown at least 75% significant level or more. SLI value has 82% significant level, DCI 75% significant level and BI 75% significant level. For best possible forecast, we have considered above mention indices. We have considered best threshold value for calculating skill score of thundery and non-thundery days with the help of iteration process for perfect result.

Table 5.8 Test statistics (Z_{xy}) for Different indices at the Kolkata station at 1200 UTC

Index	Z_{xy} Values	Index	Z_{xy} Values
K	0.24	SWEAT	0.03
TT	-0.05	CAPE	0
SLI	-0.93	CIN	0.04
DCI	0.66	BRN	0.02
HI	- 0.01	SI	-0.58
BI	0.67		

Table 5. 9 gives the recommended threshold and corresponding skill scores for these identified indices. The best skill is obtained from DCI and BI with threshold values of 42.0^0 C and 98.2 respectively. This means that thundery (non-thundery) days can be forecasted when DCI is greater (less) than 42.0^0 C and for BI the forecast will be thundery (non-thundery) when its value will be greater (less) than 98.2. From the skill score point of view, a POD score of 0.8 for DCI is the highest. The best CSI, TSS, and HSS scores are found for DCI and the values are 0.5, 0.371, and 0.351 respectively. Previous section already has discussed that TSS and HSS are used for correct forecasting to show the true skill of categorically. The POD score (0.6) for SLI with a threshold (-6) less or equal to. The POD score (0.7) for BI with threshold 98.2 is greater or equal to. So far FAR scores for DCI, BI, and SLI indices are (0.429), (0.533), and (0.571) respectively. In other category CSI, TSS and HSS, DCI has shown highest skill with the prescribed threshold. These values of skill scores are to be consistent with the results reported earlier on Kolkata location (Tyagi et al., 2011).

Table 5.9 Skill ratings and defined threshold values of selected metrics for the Kolkata station at 1200 UTC

Indices	POD	FAR	CSI	TSS	HSS
DCI ≥ 42	0.8	0.429	0.5	0.371	0.351
SLI ≤ -6	0.6	0.571	0.333	0.029	0.027
BI ≥ 98.2	0.7	0.533	0.389	0.129	0.12

Verification of prediction at 1200 UTC

The contingency table and different skill scores for DCI, BI, and SLI are shown in **Table 5.10**. DCI has predicted the highest percentage of correct thundery days (24%) out of 44% realized and this is reflected in the POD score (0.545). BI has predicted highest percentage of false alarm (32%) in the thundery days forecast and their FAR score 0.667. It produces only 24% correct non-thundery days forecast. Thus, other skill scores for BI are very low. POD of BI is 0.363. Due to large false alarm, TSS and HSS have very low value for BI. DCI in five categories is 0.545 (POD), 0.333 (FAR), 0.429 (CSI), 0.331 (TSS) and 0.338 (HSS). BI in five categories are 0.363 (POD), 0.667 (FAR), 0.211 (CSI), -0.208 (TSS) and -0.206 (HSS). SLI has predicted 20% thundery days correctly, 24% is the false alarm and 32% is the correct non-thundery days forecast and the skill scores of SLI in five categories are 0.455 (POD), 0.545 (FAR), 0.294 (CSI), 0.026 (TSS) and 0.026 (HSS). BI has predicted 16% of thundery days correctly, 32% is the false alarm and 24% is the correct non-thundery days forecast. Due to low false alarm, TSS and HSS have the highest value for DCI. Thus, from all the aspects of forecast, DCI shows to perform better than other indices at 1200 UTC over the Kolkata station.

Table 5.10 Contingency table and skill scores for April and May, 2022 based on 1200 UTC data and validated with following 0000 UTC observations from the Kolkata station given numbers are the best indices scores. Total number of thundery days (TD) observed - 44%. Total number of non-thunderstorm days (NTD) observed - 56%

Index	Observation	Prediction TD (%)	Prediction NTD (%)
DCI ≥ 42 (POD = 0.545, FAR = 0.333,CSI = 0.429, TSS = 0.331, HSS = 0.338)	TD (%) NTD (%)	24 12	20 44
BI ≥ 98.2 (POD = 0.363, FAR = 0.667, CSI = 0.211, TSS = -0.208, HSS = -0.206)	TD (%) NTD (%)	16 32	28 24
SLI ≤ -6 (POD = 0.455, FAR = 0.545, CSI = 0.294, TSS = 0.026, HSS = 0.026)	TD (%) NTD (%)	20 24	24 32

DISCUSSION

In this study, we have considered the pre-monsoon months (April and May) for the year 2022 over the Kolkata station. Eleven indices namely K, TT, SLI, DCI, HI, BI, SWEAT, CAPE, CIN, BRN, and SI, are calculated for April and May months of 2022. The probability distribution of all the indices is plotted to make a qualitative measurement of the potential of each index to differentiate the thundery and non-thundery days. The mean and standard deviation are calculated for each index for 0000 and 1200 UTC and are used to calculate the test statistics (Z_{xy}) in order to check if the difference of mean values of the indices for thundery and non-thundery days are significant. The index that is found significant with at least 75% level is accepted. The selected indices for 0000 UTC for Kolkata station are DCI, BI, SLI, and SI, and that for 1200 UTC are DCI, BI and SLI. The threshold values of the statistically significant indices are evaluated through an iterative process. After fixation of threshold, the indices are computed to predict thundery and non-thundery days. The efficiency of the forecast is correlated with five different skill scores. DCI is found to be a significant best predictor for 0000 and 1200 UTC. After that, SLI is the 2nd position for prediction for 0000 and 1200 UTC. TT is commonly used for operational thunderstorm forecasting over Indian region. In our study, TT shows that it is an inefficient predictor for 0000 and 1200 UTC. To find out the TT value, the lapse rate can be take between 850 and 500 hpa and measure of saturation, 850 hpa. It does not take into account the measure of saturation at any other level 700 hpa and 500 hpa. For thunderstorm formation, the measure of saturation at 700 hpa and 500 hpa are important. For this reason, TT is an unsuccessful predictor for 0000 and 1200 UTC. BI has been found to be a predictor as 3rd position for 0000 and 1200 UTC. SI has been found to be a predictor as 4th position for 0000 and 1200 UTC. In this study, BI shows significant difference (more than 75%) between the mean values for thundery and non-thundery days at 0000 UTC. It does not show good forecast skills. Similarly, SI at 0000 UTC and SLI at 1200 UTC, are not able to show good forecast skills.

The availability of moisture at lower and middle level of troposphere shows that the atmospheric instability leads to the development of thunderstorm over Kolkata station. Among the eleven indices, DCI is found to be the best indices in predicting thunderstorm at 0000 and 1200 UTC, for the Kolkata station. In contingency **Tables 5. 6** and **5.10**, some thundery days are missed in the forecast of the indices. For some of these missed thundery days, the value of the selected index is found close to the threshold. For these days, weather observed is severe and index value, closer to threshold.

CONCLUTIONS

In this paper, we made an attempt to study pre-monsoon thunderstorm events over Kolkata located in the Gangetic region of West Bengal using the data of thunderstorm and non-thunderstorm days. We have shown the usefulness of thermodynamic stability indices to predict the thundery and non-thundery days corresponding to Nor'wester events around Kolkata. The skill indices provide a very good opportunity to study probable occurrence of thunderstorm. More specific observational data for a wide range of pre-monsoon months are needed to be analyzed in order to get a new insight into enhanced efficiency of indices for more specific and localize prediction.

Chapter - 6

Predictability of local thunderstorms and associated moisture and Precipitable water content prior to the monsoon over Kolkata region, West Bengal (India)

ABSTRACT

The current study focuses on the local thunderstorms in Kolkata.9 thunderstorm days are considered in this study. The mixing ratio ranges at 00 and 12 UTC varies between 16.23g/kg to 23.67g/kg at 1000 hPa. This indicates a significant presence of moisture near the surface. In the occurrence of local severe storms in Kolkata, the relative humidity at 00 and 12 UTC ranges from 52% to 100%, indicating a substantial amount of moisture near the surface. The mean mixed layer mixing ratio in Kolkata the occurrence of thunderstorms varies from 13 g/kg to 22.17 g/kg, showing a significant amount of moisture in the mixed layer of the troposphere. The amount of Precipitable water in Kolkata during local storms at 00 and 12 UTC varies from 36.70 mm to 56.58 mm. It is worth noting that the Precipitable water in Kolkata was significantly higher during local storms at 00 UTC compared to days when no storms occurred. DRCT varies from 45 deg to 290 deg and SKNT varies from 1 to 8 knot at 00 and 12 UTC.

Keywords: Kolkata, Thunderstorm, Precipitable water, Mixing ratio, Relative humidity.

INTRODUCTION

Water precipitation and atmospheric moisture play a crucial role in the hydrological cycle, exerting a significant influence on weather patterns and climate dynamics. In the specific case of Kolkata, a metropolitan region located in eastern India, these factors are influenced by a combination of natural phenomena and human activities. Extensive research has demonstrated that Kolkata is particularly susceptible to heightened precipitation as a result of climate change, with intense rainfall, river overflow, and storm surges being the primary contributors to flooding incidents (Sarraf and Dasgupta, 2011). Empirical evidence indicates that the expansion of urban land cover in Kolkata has played a role in the notable rise of pre-monsoonal rainfall (PMR). This demonstrates the connection between urbanization and changes in precipitation patterns (Mitra and Jordon, 2011). It is noteworthy that urbanization and climate change have an impact on precipitation in Kolkata. In addition to these factors, soil moisture and atmospheric water vapor content also contribute to the dynamics of rainfall. The correlation between soil moisture and afternoon rainfall is influenced by atmospheric moisture convergence, where wetter soils and higher relative humidity tend to promote rainfall in situations of low convergence (Santanello and Welty, 2020). Furthermore, the climate of the area, characterized as a prolonged weather pattern, has undergone modifications due to climatic

shifts, resulting in disrupted precipitation cycles and recurrent instances of urban flooding (Majumder and Das, 2021). Kolkata's precipitation and atmospheric moisture levels are influenced by a combination of climate change, urbanization, and land-atmosphere interactions. The rise in PMR and alterations in rainfall distribution reflect these factors, highlighting important consequences for urban development, public well-being, and environmental stability within the area (Sarraf and Dasgupta, 2011; Mitra and Jordon, 2011; Santanello and Welty, 2020; Majumder and Das, 2021).

The occurrence of local thunderstorms can be accurately forecasted by analyzing the moisture and Precipitable water content in the troposphere. Research indicates that a rise in Precipitable water results in higher levels of water vapor in the lower atmosphere, causing atmospheric instability and the formation of thunderstorms (Wakimizu and Jinno K, 2002). Moreover, accurate prediction of severe thunderstorms heavily relies on the thermodynamic characteristics of the planetary boundary layer (PBL), including temperature and water vapor content (Vivekanandan and Sahoo, 2011). The influence of atmospheric circulation on the development of moisture levels has been verified, showcasing notable variations in the connection between circulation patterns and moisture content across different regions (Różycki and Wypych, 2018). The presence of water vapor below the freezing level has been recognized as a contributing factor to the electrical phenomena occurring in thunderstorms. The response to higher concentrations of cloud condensation nuclei (CCN) varies depending on the amount of water vapor present (Zhou and Liu, 2016). Local thunderstorm predictability is improved through precise measurements of moisture and Precipitable water content in the troposphere. These techniques have demonstrated positive outcomes in enhancing weather forecasting models and comprehending the mechanisms behind thunderstorm development (Wakimizu and Jinno K, 2002; Vivekanandan and Sahoo, 2011; Różycki and Wypych, 2018; Zhou and Liu, 2016).

Local severe storms are intense thunderstorms that take place in Kolkata during the pre-monsoon season, which falls between March and May. These extreme weather occurrences result in significant damage to properties and loss of lives across Kolkata. The economic impact of these storms is also substantial. The transition periods between the southwest and northeast monsoons in the India-Bangladesh-Pakistan subcontinent are marked by the occurrence of local severe storms. In Kolkata, these transition periods are referred to as the pre-monsoon season (March-May) and post-monsoon season (October-November). Among these, it is during the pre-monsoon season that most of the local severe storms hit various parts of Kolkata frequently. These storms are commonly known as Nor'westers or Kalbaishakhi in West Bengal, Bangladesh, and Assam in India, and Andhis (dust storms) in North India.

The purpose of this study is to acquire understanding regarding the potential changes in the occurrence of severe storms in terms of time and location. Additionally, it aims to examine the moisture and Precipitable water content, as well as their distribution, in relation to recent severe storms that took place in Kolkata, West Bengal during the pre-monsoon season.

DATA

The University of Wyoming's Department of Atmospheric Science has provided the data (http://weather.uwyo.edu/upperair/sounding.html) utilized in this study. 9 days thunderstorm cases are chosen for this study over the Kolkata region, West Bengal (India). 9 days thunderstorm cases are explained in **Table 6.1** and data details are given in **Table 6.2, 6.3, 6.4** and **6.5** in this study.

Table 1. Local thunderstorms cases over the Kolkata region, West Bengal (India) used in this study

No.	DATE	THUNDERSTORM at GWB
1	17.04.2022	1. RMC Kolkata Thunderstorm occur: Two persons died along with several others severely injured due to uprooting of trees and electric pole in Cooch Behar on 17th April, 2022 2. Total Death Toll: 02 persons Source: Uttrabanga Sambaed epaper dated 18.04.2022 3. Two persons died along with several others severely injured due to uprooting of trees and electric pole in Cooch Beha on 17th April, 2022 Total Death Toll: 02 persons Source: Uttrabanga Sambaed epaper dated 18.04.2022 due to Nor'westers
2	21.04.2022	RMC Kolkata Thunderstorm and gusty wind with rain has been reported in Jamshedpur leading to felling of trees and electric poles and damage of house sheds. Casualty: 00 persons Source: Prabhat Khabar Jamshedpur epaper dt. 22.04.2022
3	22.04.2022	RMC Kolkata Murshidabad district lighting strike
4	29.04.2022	1. RMC Kolkata Hailstorm occurred over Durgapur region of West Burdwan districts 2. RMC Kolkata Two persons died due to felling of tree branches in Krishnanagar and Katwa region due to thunderstorm
5	01.05.2022	Alipore Gaya: squall
6	03.05.2022	Digha squall
7	19.05.2022	1. RMC Kolkata Severe damage caused in Shamuktala block of Alipurduar district due to Thunderstorm and squally wind. Source: Uttarbanga Sambaed dated 20.05.2022 2. RMC Kolkata Immense damage caused to houses, trees and crops due to ravaging thunderstorm and squally wind in Dhupguri block of Jalpaiguri district. Source: Kolkata TV Website 3. Malda, Patna, Ranchi: Squall
8	20.05.2022	RMC Kolkata: Nor'westers occurred in Malda district on 19th May leading to severe damage to houses and felling of trees resulting in the death of 1 elderly woman and injuring others. Casualty: 01person Source: Uttarbanga Sambaed Pg. 1 dated 21.05.2022
9	21.05.2022	RMC Kolkata: 1. Two teenage rowers drowned in Rabindra Sarovar Lake in the middle of Nor'westers that clocked 90kmph on Saturday evening. Casualty: 02 persons Source: Telegraph epaper dated 22/05/2022 2. Nor'westers at 90 kilometer per hour grounds flights in Kolkata, kills one. Casualty: 01person Source: India today Website dated 22/05/2022 3.One elderly woman died after a branch of a tree fell on her in Howrah district. Casualty: 01person Source: Ananda bazar Epaper dated 22/05/2022. 4.Two persons died in Burdwan districts died after being struck by lightning. Casualty: 02 persons Source: Aajkal epaper dated 22/05/2022 .

Thunderstorm Data

Table 6.2 42809 VECC Kolkata Observations at 00Z thunderstorm data

Dates	PRES hPa	HGHT m	RELH %	MIXR g/kg	DRCT Deg	SKNT Knot
17.04.2022	1000.0	22	80	18.98	175	4
21.04.2022	1000.0	63	83	16.23	45	5
22.04.2022	1000.0	59	79	19.21	205	7
29.04.2022	1000.0	50	84	20.69	170	4
01.05.2022	1000.0	34	100	20.19	290	3
03.05.2022	1000.0	36	87	20.82	175	3
19.5.2022	1000.0	35	84	21.87	180	4
20.5.2022	1000.0	27	84	21.60	200	1
21.05.2022	996	6	81	21.43	180	6

Table 6.3 42809 VECC Kolkata Observations at 12Z thunderstorm data

Dates	PRES hPa	HGHT m	RELH %	MIXR g/kg	DRCT Deg	SKNT Knot
17.04.2022	1000.0	17	59	18.98	180	6
21.04.2022	1000.0	37	59	18.05	190	6
22.04.2022	1000.0	34	52	16.75	170	6
29.04.2022	1000.0	13	53	18.74	180	8
01.05.2022	1000.0	13	63	19.69	135	2
03.05.2022	1000.0	43	70	17.39	140	3
19.5.2022	1000.0	6	71	23.67	180	8
20.5.2022	999	6	60	21.49	180	4

Non-Thunderstorm Data

Table 6.4 42809 VECC Kolkata Observations at 00Z non-thunderstorm data

Dates	PRES	HGHT	RELH	MIXR	DRCT	SKNT
	hPa	m	%	g/kg	Deg	Knot
16.04.2022	1000.0	11	89	21.47	180	6
18.04.2022	1000.0	44	86	20.19	170	3
20.04.2022	1000.0	47	83	19.94	190	7
23.04.2022	1000.0	61	94	21.73	175	6
28.04.2022	1000.0	45	85	21.47	205	1
30.04.2022	1000.0	47	65	13.67	115	7
02.05.2022	1000.0	41	85	15.05	65	1
18.05.2022	1000.0	26	84	21.73	185	6
22.05.2022	997	6	78	17.01	0	0

Table 6.5 42809 VECC Kolkata Observations at 12Z non-thunderstorm data

Dates	PRES	HGHT	RELH	MIXR	DRCT	SKNT
	hPa	m	%	g/kg	Deg	Knot
16.04.2022	1000.0	6	53	20.19	180	4
18.04.2022	1000.0	29	63	20.44	170	5
20.04.2022	1000.0	37	52	15.73	140	6
23.04.2022	1000.0	33	31	12.34	220	1
28.04.2022	1000.0	31	26	9.0	220	6
30.04.2022	1000.0	15	56	18.28	180	6
02.05.2022	1000.0	20	56	16.96	130	4
18.05.2022	1000.0	11	63	20.95	180	6
22.05.2022	996	6	62	18.13	0	0

METHODOLOGY

Theoretical background Mixing ratio and humidity Mixing ratio

Mixing ratio is expressed as a ratio as the mass of water vapor, m_v, per kilogram of dry air, m_d, at a given pressure. That is, mixing ratio is defined as the mass of water vapor to the mass of dry air. The mixing ratio can be defined as:

$$r = \frac{m_v}{m_d}$$

Where m_v = mass of water vapor and m_d = mass of dry air.
The colloquial term moisture content is also used instead of mixing ratio.

Relative humidity

Humidity is the amount of water vapor in the air. Relative humidity is defined as the ratio of partial pressure of water vapor in a parcel of air to the saturated vapor pressure of water vapor at a prescribed temperature and is expressed as percentage.

$$R.H. = \frac{e}{e_s} \times 100$$

Mean mixed layer mixing ratio

The atmospheric mixed layer is a zone having nearly constant potential temperature and specific humidity with height. The depth of the atmospheric mixed layer is known as the mixing height. Turbulence typically plays a role in the formation of fluid mixed layers.

The convective air motions during the middle of the day lead to the formation of the atmospheric mixed layer. This occurs when the surface air is heated and rises, causing it to mix due to Rayleigh-Taylor instability. To determine the depth of the mixed layer, the standard procedure involves analysing the potential temperature profile. Potential temperature refers to the temperature that the air would have if it were brought to the pressure at the surface. Since increasing pressure involves compressing the air, the potential temperature is higher than the in-situ temperature, and this difference increases with altitude. The atmospheric mixed layer is defined as a layer with approximately constant potential temperature or a layer where the temperature decreases at a rate of around 10 °C/km. While this layer may have variations in humidity, it is generally devoid of clouds. Similar to the ocean mixed layer, velocities within the atmospheric mixed layer are not constant throughout. The mean mixing ratio of the mixed layer has been determined and extensively studied.

Precipitable water

The Precipitable water in the atmospheric layer, bounded by p_1 and p_2 pressure surfaces, can be expressed by (Ananthakrishnan et al., 1965; Karmakar et al., 1981)

$$W = \frac{1}{g}\int_{p_1}^{p_2} q\,dp$$

Where g is the acceleration due to gravity and q is the specific humidity at pressure level p.

Generally, the water vapor is mainly concentrated in the lower atmosphere up to about 500 hPa above which it has negligible contribution. For this reason, the vertically integrated magnitude of the Precipitable water vapor is approximated by

$$W = -\frac{1}{g}\int_{1000}^{500} q\,dp$$

To obtain W, one can utilize the trapezoidal rule (Haydu and Krishnamurthy, 1981; Karmakar et al., 1981) which can be performed in the following manner

$$W = \frac{1}{g}\left[q_{1000}\int_{925}^{1000} dp + q_{850}\int_{775}^{925} dp + q_{700}\int_{600}^{775} dp + q_{500}\int_{500}^{600} dp\right]$$

$$W = \frac{75}{g}q_{1000} + \frac{150}{g}q_{850} + \frac{175}{g}q_{700} + \frac{100}{g}q_{500}$$

The units used here are $gmkg^{-1}$, $cm\ sec^{-2}$, and $gm\ cm^{-2}$ for q, g and W, respectively. The value of W can be converted into mm by using 1 kg m^{-2} = 1 mm.(Mclntosh and Thom, 1973; Karmakar et al., 1981)

RESULT AND DISCUSSION

Verification of prediction at 0000 UTC and 0012 UTC

Spatial distribution of mean mixed layer mixing ratio

9 Mean mixed layer mixing ratios at Kolkata on the dates of occurrence of local storms at 00 UTC and 12 UTC are given in **Table 6.6.** The table shows that the mean mixed layer mixing ratio at Kolkata ranges from 13 g/kg to 22.17 g/kg during thunderstorm and 12.98 g/kg to 20.53 g/kg during non-thunderstorm, indicating considerable moisture content in the mixed layer of the troposphere. This amount of moisture is favorable for the formation of clouds after condensation. The mean mixing ratio are shown in **Figure 6.1 a, b**.

Table 6.6 Mean mixed layer mixing ratio at Kolkata on the dates of occurrence and non-occurrence of local severe storms at 00 UTC and 12 UTC Dates of non-occurrence of local severe storms.

Dates of occurrence of local severe storms	Mean mixed layer mixing ratio (g/kg) on the dates of occurrence 00 UTC	Mean mixed layer mixing ratio (g/kg) on the dates of occurrence 12 UTC	Dates of non-occurrence of local severe storms	Mean mixed layer mixing ratio (g/kg) on the dates of non-occurrence 00 UTC	Mean mixed layer mixing ratio (g/kg) on the dates of non-occurrence 12 UTC
17.04.2022	18.63	20.07	16.04.2022	19.60	18.88
21.04.2022	17.21	18.98	18.04.2022	19.44	20.27
22.04.2022	18.60	19.20	20.04.2022	19.01	19.19
29.04.2022	19.98	18.28	23.04.2022	19.09	13.09
01.05.2022	13	10.27	28.04.2022	20.34	19.56
03.05.2022	19.82	15.96	30.04.2022	14.15	17.76
19.5.2022	20.66	22.17	02.05.2022	12.98	17.16
20.5.2022	20.39	21.17	18.05.2022	20.53	20.12
21.05.2022	15.04	-	22.05.2022	14.94	16.86

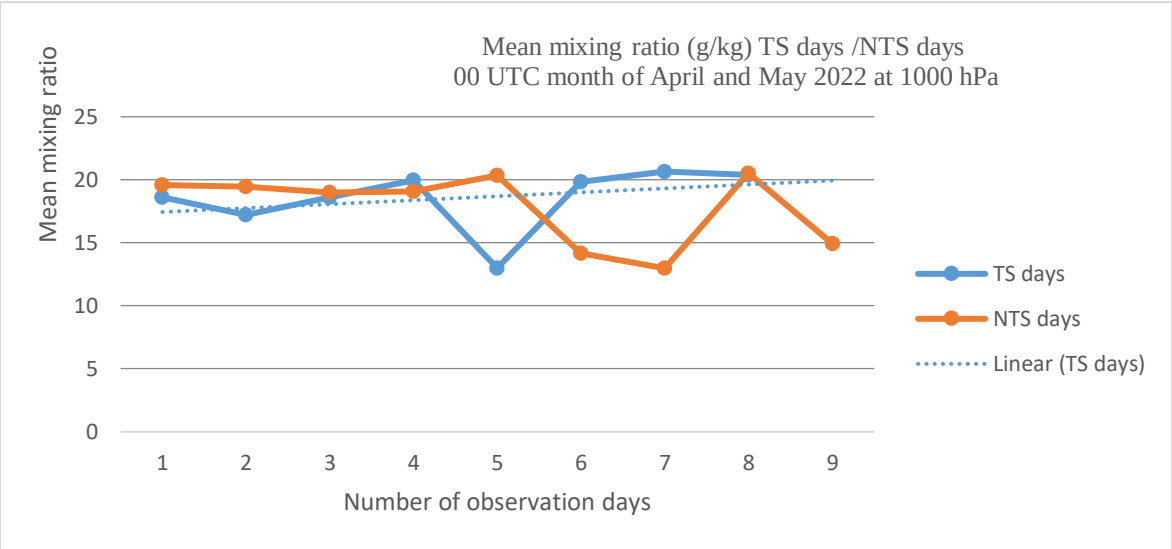

Figure 6.1 a The mean mixing ratio of thunderous (TS) and no thunderous (NTS) days at 00 UTC plotted for Kolkata Station.

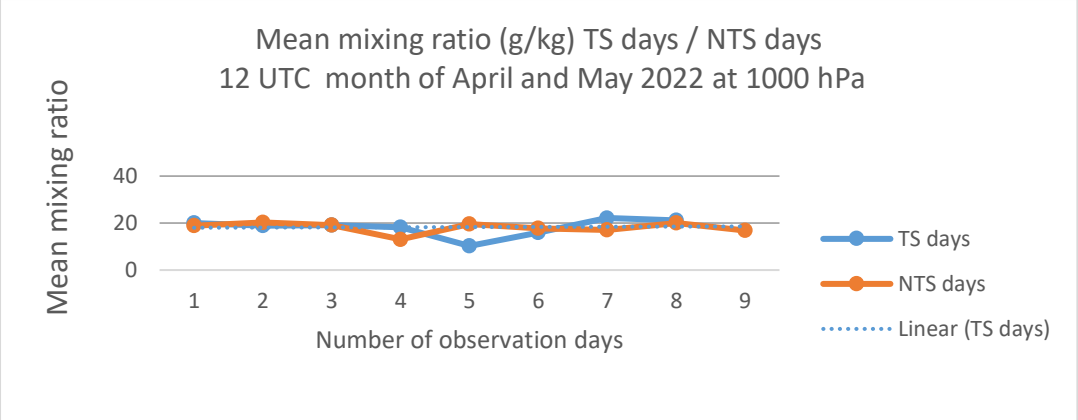

Figure 6.1 b The mean mixing ratio of thunderous (TS) and no thunderous (NTS) days at 12 UTC plotted for Kolkata Station.

Mixing ratio

Vertical distribution of mixing ratio over Kolkata at 00 UTC and 12 UTC on the dates of occurrence of 9 local severe storms has been studied. The analysis has shown that the mixing ratio is maximum near the surface and decreases significantly with height, becoming zero at the upper troposphere at or above 400 hPa. Mixing ratio at 1000 hPa level at Kolkata on the dates of occurrence and non-occurrence of local severe storms are given in **Table 6.2 to 6.5**. It is seen that the mixing ratio at 00 UTC and 12UTC on the dates of occurrence of local severe storms ranges from 9 g/kg to 23.67 g/kg at Kolkata, showing a considerable amount of moisture near the surface. On 28th April 2022, mixing ratio is the lowest value and 9th May 2022, mixing ratio is the highest value. The date of non-occurrence i.e., dryness is found at 1000 hPa on 28th April 2022 and this sometimes happen in the morning on the occurrence date as found earlier by (Chowdhuary et al., 1986; Karmakar et al., 1981). **Table 6.2 to 6.5** mixing ratio at 1000 hPa at Kolkata on the dates of occurrence and non-occurrence of local severe storms at 00 UTC and 12 UTC. The mixing ratio are shown in **Figure 6.2 a, b**.

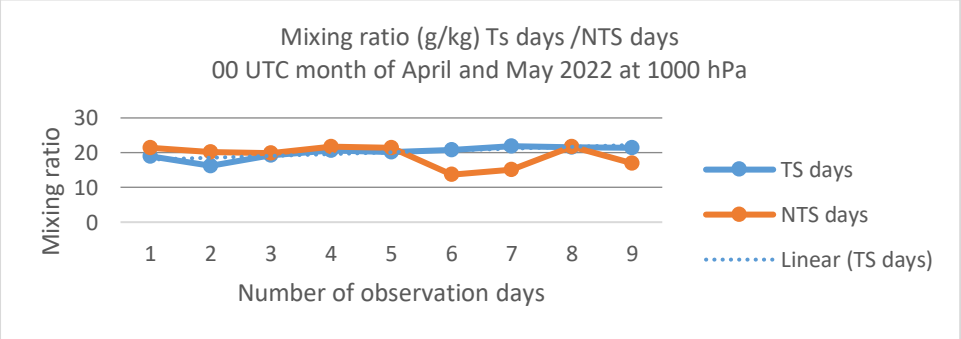

Figure 2 a. The mixing ratio of thunderous (TS) and no thunderous (NTS) days at 00 UTC plotted for Kolkata Station.

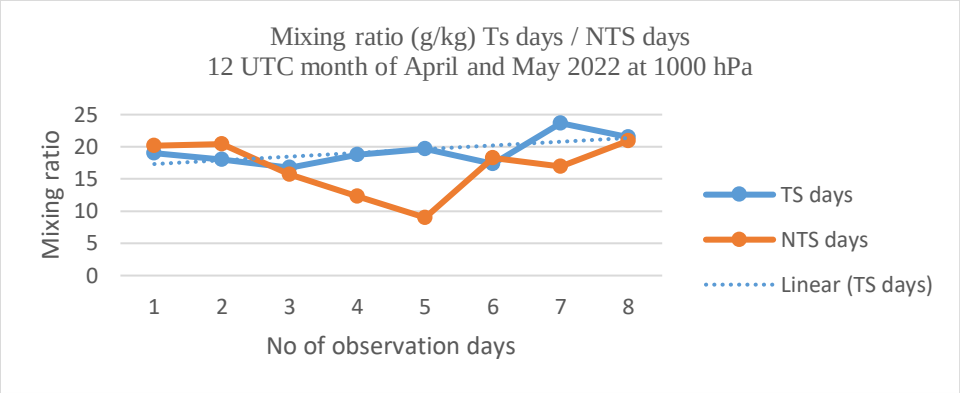

Figure 6.2 b. The mixing ratio of thunderous (TS) and no thunderous (NTS) days at 12 UTC plotted for Kolkata Station.

The above **Figure 6.2 a, b.** shows the slightly increasing trend line of mixing ratio.

Relative humidity

Vertical distribution of mixing ratio over Kolkata at 00 UTC and 12UTC on the dates of occurrence of 9 local severe storms has been studied. The analysis has shown that the relative humidity is maximum near the surface, sometimes 100% and decreases significantly with height. This may be attributed to the vertical transfer of moisture due to strong vertical current in the troposphere on this day of occurrence of local severe storm. Relative humidity at 1000 hPa level at Kolkata on the dates of occurrence of local severe storms are given in **Table 6.2 to 6.5** above. It is seen that the relative humidity at 00 UTC on the dates of occurrence of local severe storms ranges from 79% to 100% at Kolkata, showing a significant amount of moisture near the surface. When convection starts, the moisture indicated by mixing ratio and relative humidity, is transported upwards in the troposphere and is condensed to form cumulonimbus clouds which subsequently cause local storms. **Table 6.2 to 5** relative humidity at 1000 hPa at Kolkata on the dates of occurrence and nonoccurrence of local severe storms at 00 UTC and 12 UTC. The relative humidity is shown in **Figure 6.3 a, b**.

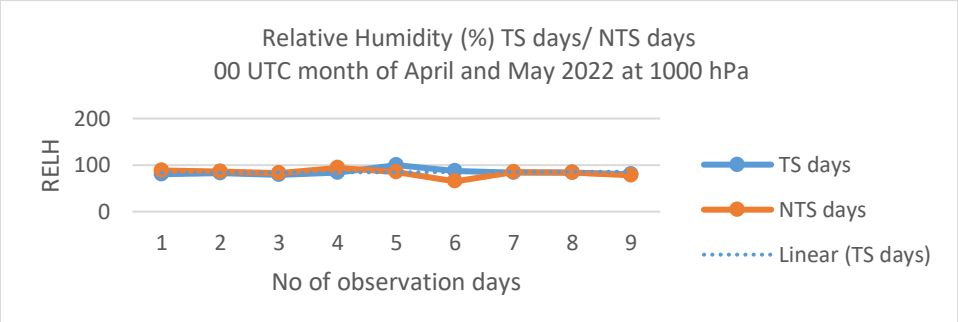

Figure 3 a. The mean relative humidity of thunderous (TS) and no thunderous (NTS) days at 00 UTC plotted for Kolkata Station.

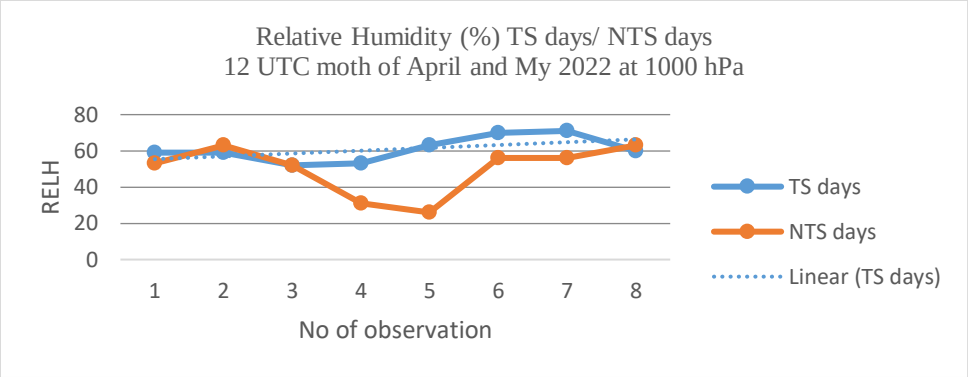

Figure 6.3 b. The mean relative humidity of thunderous (TS) and no thunderous (NTS) days at 12 UTC plotted for Kolkata Station.
The above **Figure 6.3 a, b.** shows the slightly increasing trend line of RELH.

Spatial distribution of local severe storm/thunderstorm frequency in Kolkata. Distribution of mixing ratio and relative humidity over Kolkata Humidity and mixing ratio are the measurements of moisture present in the troposphere and are responsible for the making of weather including local severe storms.

Spatial distribution of Precipitable water content of the troposphere

Precipitable water at Kolkata on the dates of non-occurrence and occurrence of 9 local severe storms at 00 UTC and 12 UTC is given in **Table 6.7.**

Table 6.7 Precipitable water at Kolkata on the dates of occurrence and non-occurrence of local severe storms at 00 UTC and 12 UTC

Date of occurrence of local severe storms	Precipitable water (mm) occurrence of local severe storms 00 UTC	Precipitable water (mm) occurrence of local severe storms 12 UTC	Date of non-occurrence of local severe storms	Precipitable water (mm) non-occurrence of local severe storms 00 UTC	Precipitable water (mm) non-occurrence of local severe storms 12 UTC
17.04.2022	44.18	40.59	16.04.2022	43.52	37.25
21.04.2022	46.12	44.93	18.04.2022	40.95	33.11
22.04.2022	55.93	49.36	20.04.2022	40.62	47.69
29.04.2022	36.07	29.19	23.04.2022	48.04	37.64
01.05.2022	41.00	49.77	28.04.2022	37.83	37.42
03.05.2022	48.25	54.34	30.04.2022	43.48	45.89
19.5.2022	51.19	55.92	02.05.2022	39.31	48.82
20.5.2022	51.40	49.41	18.05.2022	53.42	54.23
21.05.2022	41.95	-	22.05.2022	44.53	45.60

It is seen from the table that Precipitable water at Kolkata on the dates of occurrence of local storms at 00 UTC ranges from 36.07 to 55.93 mm with the lowest one on 29 April 2022, which falls in the pre-monsoon season when less moisture is available in the troposphere. The maximum Precipitable water is 55.93 mm on 22nd April 2022 when very severe local

storms at Kolkata occurred over West Bengal. However, the Precipitable water at Kolkata is significantly higher on the dates of occurrence of local storms at 00 UTC. On the dates of occurrence of local severe storms, especially one day of occurrence (except 9th cases when 12 UTC data are not available on 21 May 2022 is considered in this case). The Precipitable water are shown in **Figure 6.4.** The DRCT are shown in **Figure 6.5 a, b.** The SKNT are shown in **Figure 6.6.** DRCT at 1000 hPa level at Kolkata on the dates of occurrence and non-occurrence of local severe storms are given in **Table 6.2 to 6.5**. It is seen that the DRCT at 00 UTC and 12UTC on the dates of occurrence of local severe storms ranges from 45 deg to 290 deg at Kolkata. SKNT at 1000 hPa level at Kolkata on the dates of occurrence and non-occurrence of local severe storms are given in **Table 6.2 to 6.5**. It is seen that the SKNT at 00 UTC and 12UTC on the dates of occurrence of local severe storms ranges from 1 knot to 8 knot at Kolkata.

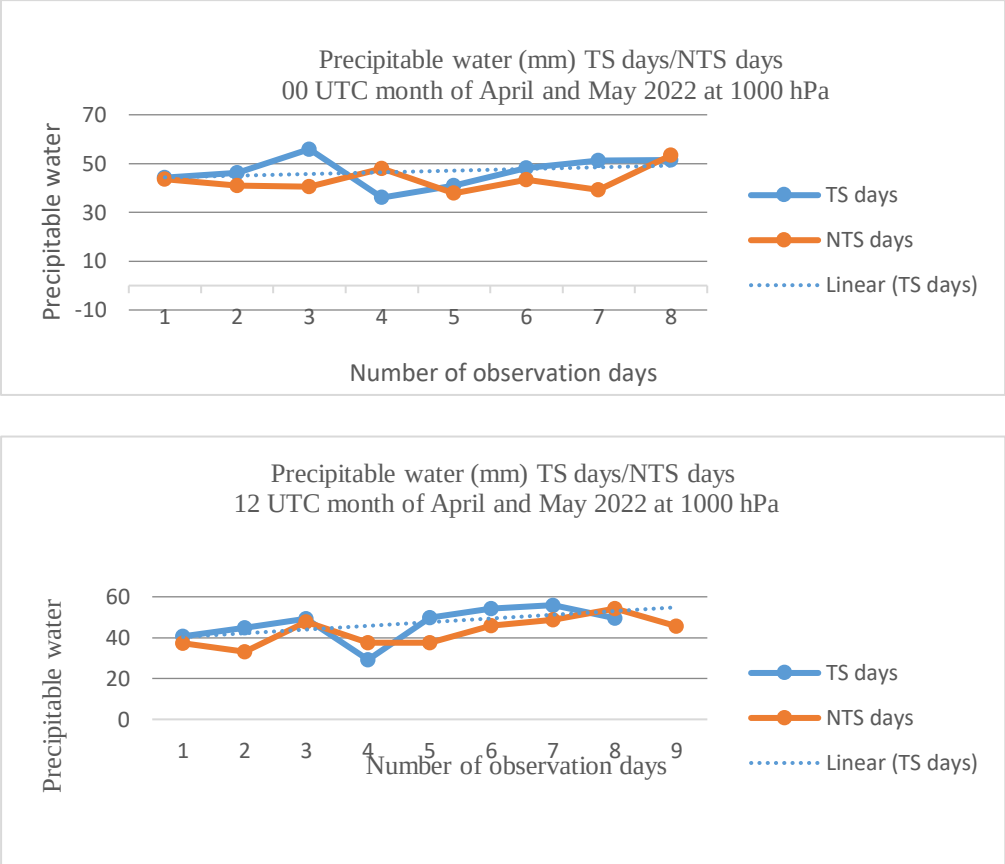

Figure 6.4 The Precipitable water of thunderous (TS) and no thunderous (NTS) days at 00 UTC and 12 UTC plotted for Kolkata Station.

The above **Figure 6.4** shows the slightly increasing trend line of Precipitable water.

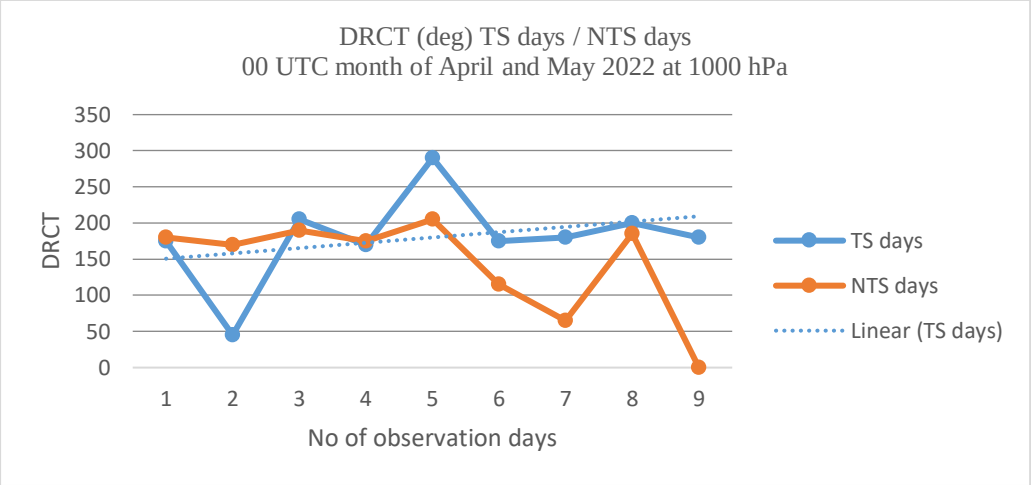

Figure 6.5 a The DRCT of thunderous (TS) and no thunderous (NTS) days at 00 UTC plotted for Kolkata Station.

The above **Figure 6.5 a** shows the slightly increasing trend line of DRCT.

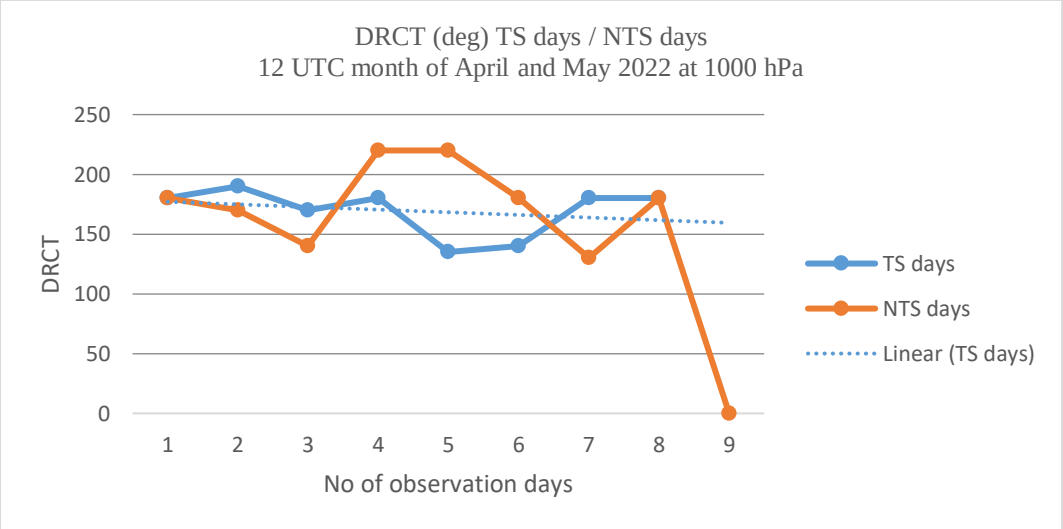

Figure 6.5 b The DRCT of thunderous (TS) and no thunderous (NTS) days at 12 UTC plotted for Kolkata Station

The above **Figure 6.5 b** shows the slightly decreasing trend line of DRCT.

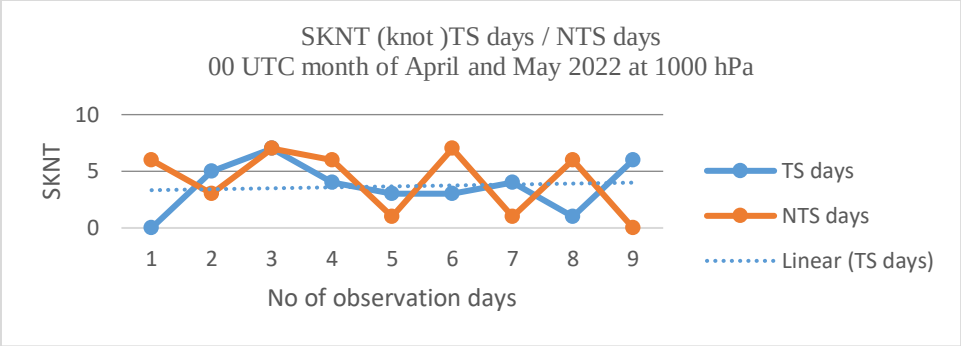

The above **Figure 6.6 a** shows the slightly increasing trend line of SKNT at 00 UTC

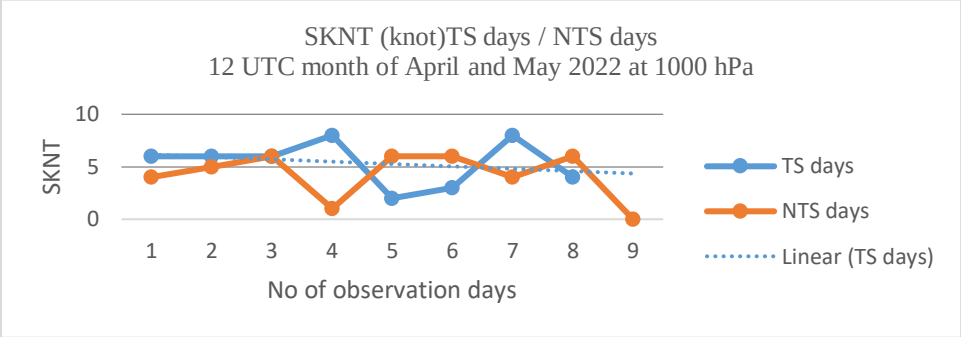

The above **Figure 6.6 b** shows the slightly decreasing trend line of SKNT at 12 UTC

The RELH on the dates of occurrence and non-occurrence of 1 case of local severe storms have been compared and the pattern of the vertical profiles of RELH over Kolkata at 00 UTC and 12 UTC are shown in **Figure 7, 8**respectively as examples.

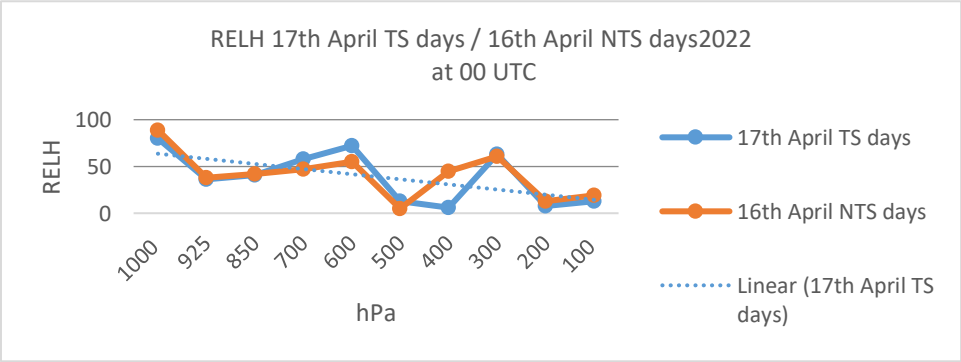

Figure 6.7 Comparison Vertical distribution of RELH over Kolkata on the dates of occurrence (17th April 2022) and non-occurrence (16th April 2022) at 00 UTC over Kolkata

The above **Figure 6.7** shows the decreasing trend line of RELH.

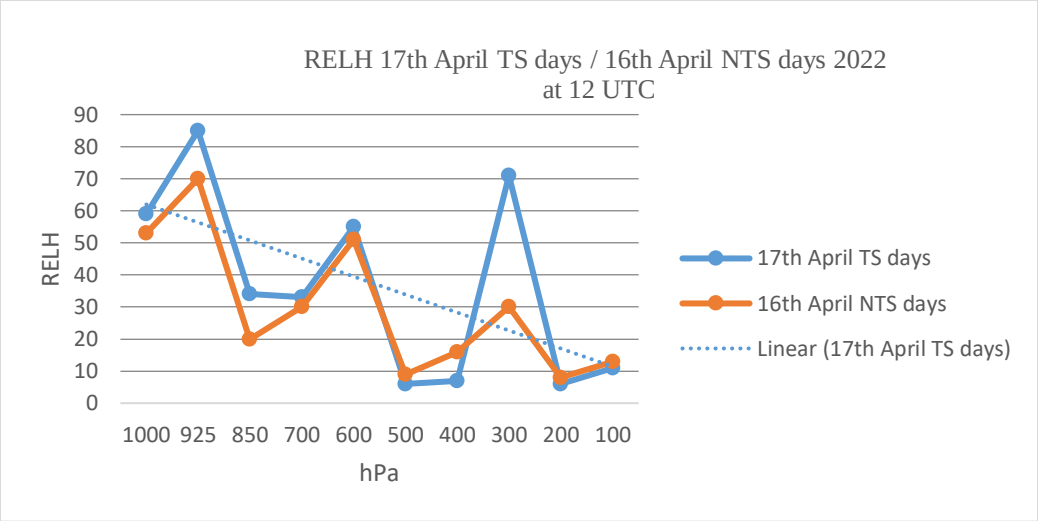

Figure 6.8 Comparison Vertical distribution of RELH over Kolkata on the dates of occurrence (17th April 2022) and non-occurrence (16th April 2022) at 12 UTC over Kolkata

The above **Figure 6.8** shows that decreasing trend line of RELH.

The mixing ratio on the dates of occurrence and non-occurrence of 1 case of local severe storms have been compared and the pattern of the vertical profiles of mixing ratio over Kolkata at 00 UTC and 12 UTC are shown in **Figure 6.9, 6.10** respectively as examples.

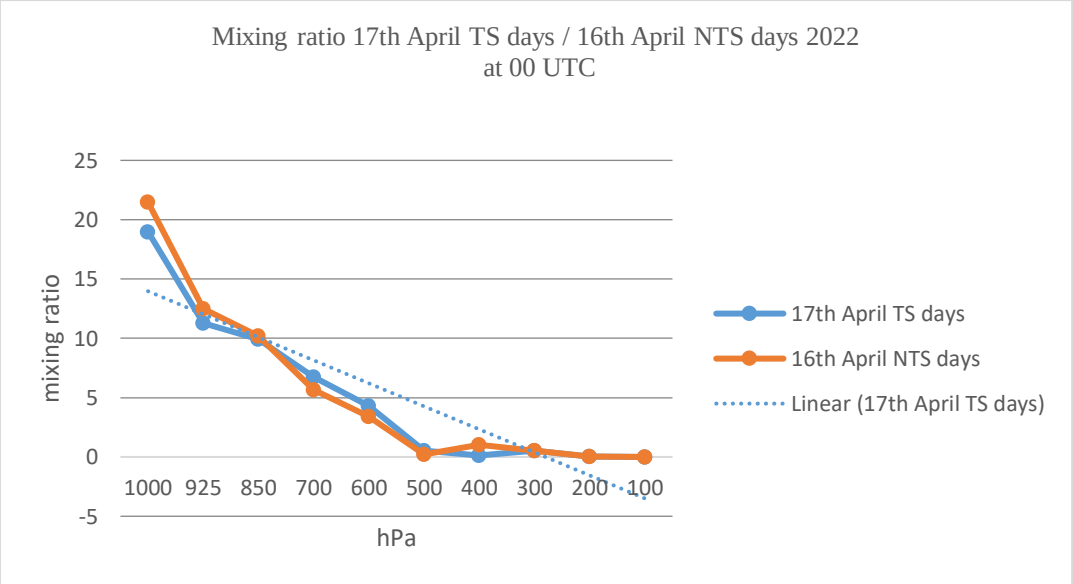

Figure 6.9 Comparison Vertical distribution of mixing ratio over Kolkata on the dates of occurrence (17th April 2022) and non-occurrence (16th April 2022) at 00 UTC over Kolkata

The above **Figure 6.9** shows that decreasing trend line of mixing ratio.

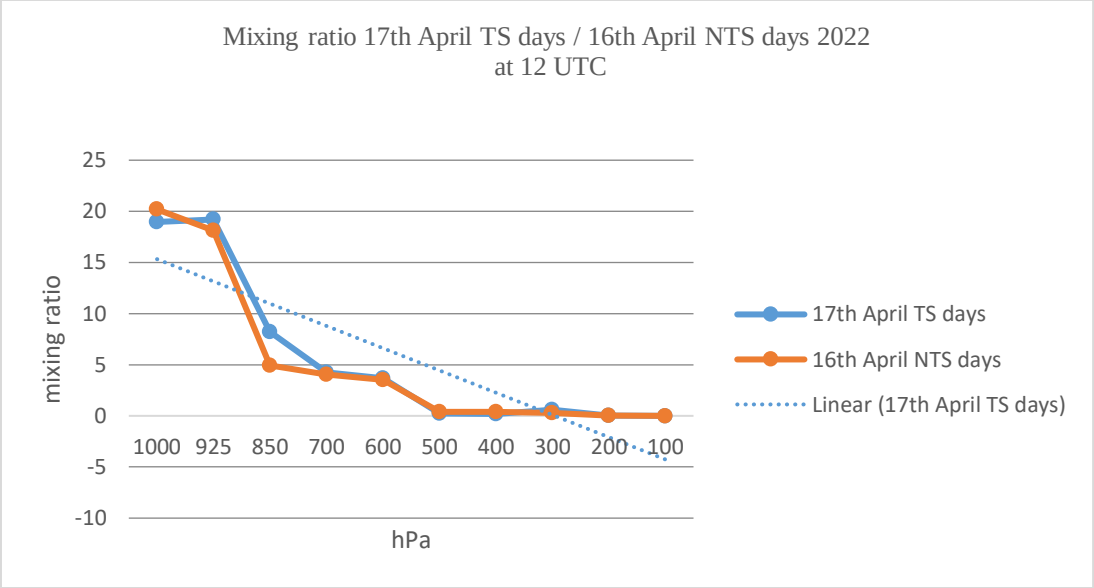

Figure 6.10 Comparison Vertical distribution of mixing ratio over Kolkata on the dates of occurrence (17th April 2022) and non-occurrence (16th April 2022) at 12 UTC over Kolkata

The above **Figure 6.10** shows that decreasing trend line of mixing ratio.

The DRCT on the dates of occurrence and non-occurrence of 1 case of local severe storms have been compared and the pattern of the vertical profiles of DRCT over Kolkata at 00 UTC and 12 UTC are shown in **Figure 6.11, 6.12** respectively as examples.

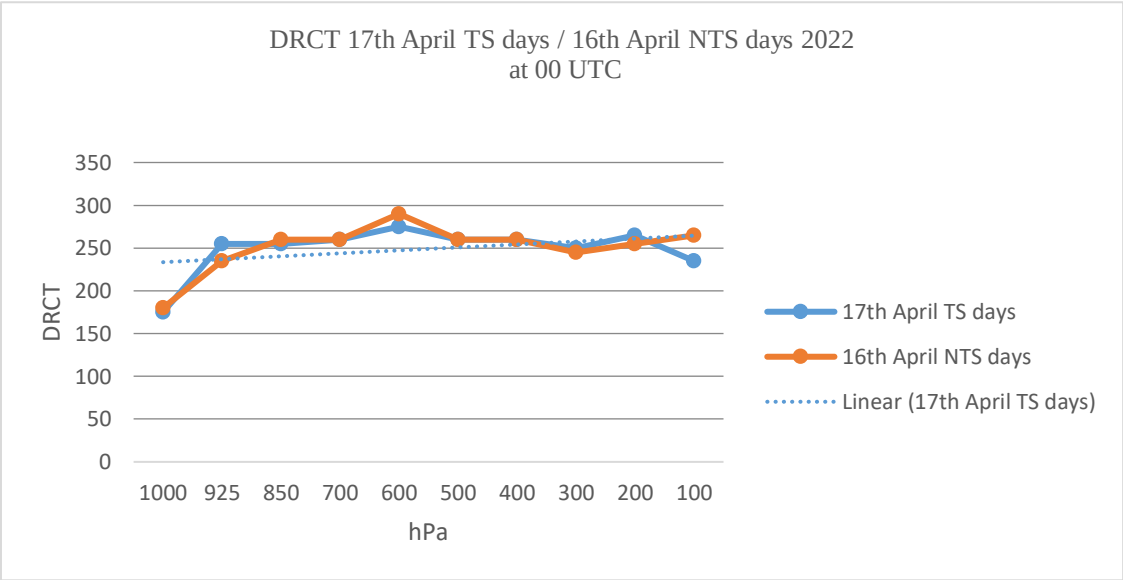

Figure 6.11 Comparison Vertical distribution of DRCT over Kolkata on the dates of occurrence (17th April 2022) and non-occurrence (16th April 2022) at 00 UTC over Kolkata

The above **Figure 6.11** shows that slightly increasing trend line of DRCT.

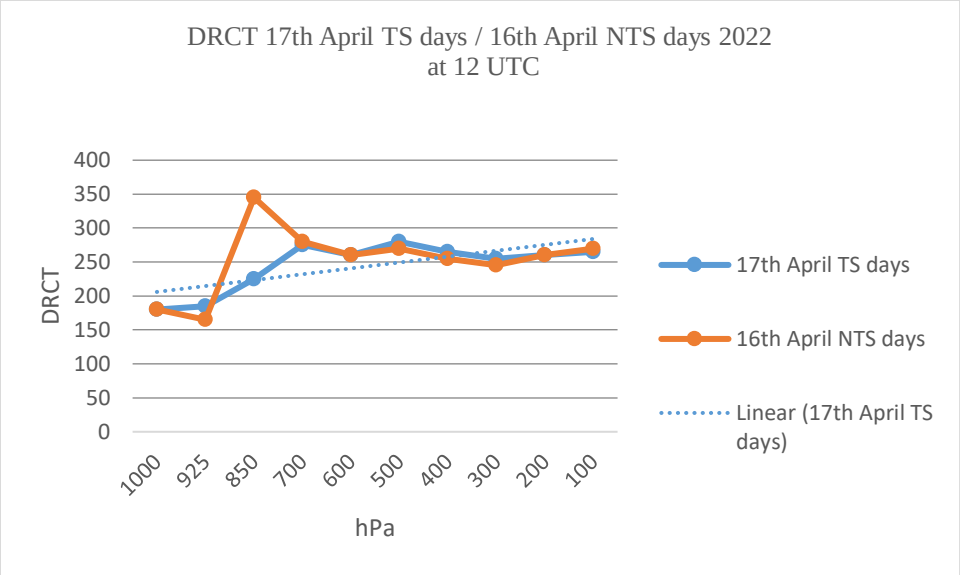

Figure 6.12 Comparison Vertical distribution of DRCT over Kolkata on the dates of occurrence (17th April 2022) and non-occurrence (16th April 2022) at 12 UTC over Kolkata.

The above **Figure 6.12** shows that DRCT value lies 175 to 275 deg. The above **Figure 6.12** shows that slightly increasing trend line of DRCT.

The SKNT on the dates of occurrence and non-occurrence of 1 case of local severe storms have been compared and the pattern of the vertical profiles of SKNT over Kolkata at 00 UTC and 12 UTC are shown in **Figure 6.13, 6.14** respectively as examples.

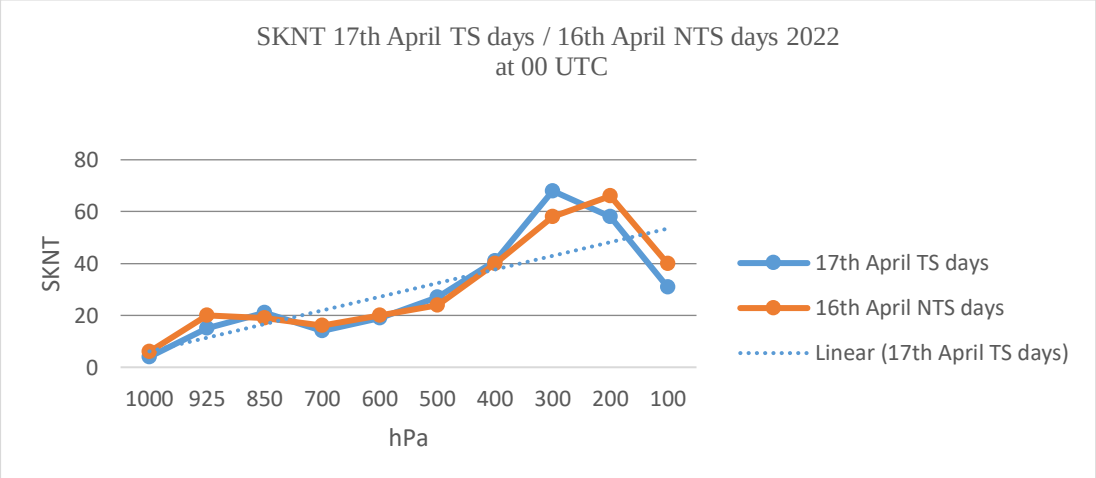

Figure 6.13 Comparison Vertical distribution of SKNT over Kolkata on the dates of occurrence (17th April 2022) and non-occurrence (16th April 2022) at 00 UTC over Kolkata.

The above **Figure 6.13** shows that increasing trend line of SKNT.

The above figure shows that at 1000 hPa to 300 hPa SKNT value increasing, after that value decreases.

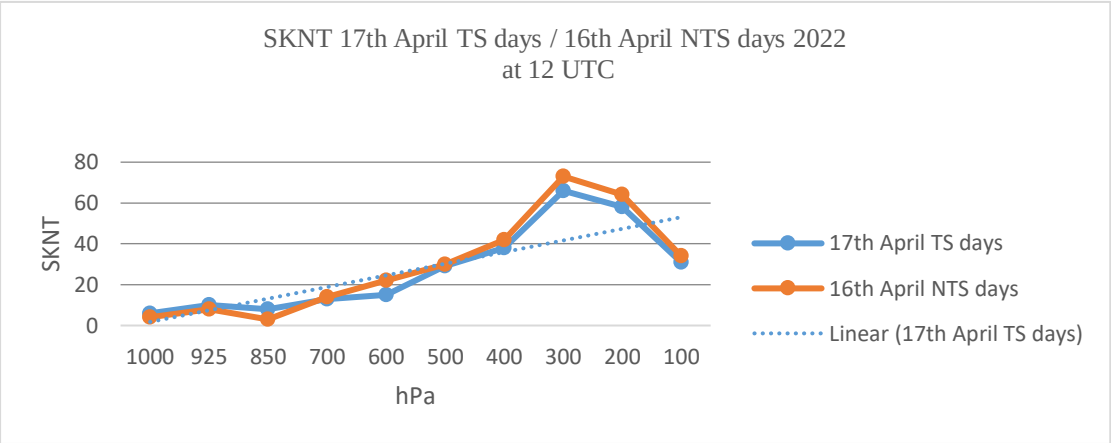

Figure 6.14 Comparison Vertical distribution of SKNT over Kolkata on the dates of occurrence (17th April 2022) and non-occurrence (16th April 2022) at 12 UTC over Kolkata

The above **Figure 6.14** shows that increasing trend line of SKNT. The above figure shows that at 1000 hPa to 300 hPa SKNT value increasing, after that value decreases.

CONCLUSIONS

On the basis of this study, following conclusions can be drawn.

The mean mixing ratio at 00 UTC and 12 UTC at Kolkata on the dates of occurrence of 9 local severe storms ranges from 13 g/kg to 22.17 g/kg during thunderstorm and 12.98 g/kg to 20.53 g/kg during non-thunderstorm days at Kolkata. The mixing ratio has a tendency to increase at 1000 hPa. More moisture becomes available in the lower troposphere and/or upwards in the morning on the dates of occurrence of local severe storms as compared to that on the dates of non-occurrence. The mixing ratio is the lowest at 28th April 2022 (9 g/kg) and greatest at 9th May 2022 (23.67 g/kg). **Figure 6.9, 6.10** shows that the decreasing trend line of the mixing ratio at 00 UTC and 12 UTC.

The relative humidity is maximum near the surface, sometimes 100% and decreases significantly with height, becoming zero at the upper troposphere. The relative humidity at 00 UTC on the dates of occurrence of local severe storms ranges from 79% to 100% at Kolkata, a significant amount of moisture near the surface. Relative humidity increases in the lower troposphere, sometimes extending up to upper troposphere in most cases on the dates of occurrence of local severe storms. **Figure 6.7** is the comparison of vertical distribution of relative humidity (RELH) over Kolkata on the dates of occurrence (17th April 2022) and non-occurrence (16th April 2022) at 00 UTC. It shows that the decreasing trend line.**Figure 6.8** shows that the decreasing trend line of the RELH.

The Precipitable water at Kolkata on the dates of occurrence of local storms at 00 UTC ranges from 36.07 mm to 55.93 mm with the lowest one on 29th April 2022. The maximum Precipitable water is 55.93 mm on 22 April 2022. The Precipitable water at Kolkata was significantly higher on the dates of occurrence of local storms at 00 UTC as compared to that on the dates of non-occurrence. The Precipitable water content is maximum over Kolkata and/or over the places where local severe storms occur, especially over Bangladesh, Tripura, West Bengal and north Orissa.

The wind direction (DRCT) at 00 UTC and 12 UTC at Kolkata on the dates of occurrence of 9 local severe storms ranges from 1 knot to 8 knot. **Figure 6.5 a** shows that the slightly increasing trend line of DRCT at 00 UTC and Figure **6.5 b** shows that the slightly decreasing trend line of SKNT at 12 UTC. **Figure 6.11, 6.12** shows that the slightly increasing trend line of comparison of vertical distribution of DRCT over Kolkata on the dates of occurrence (17th April 2022) and non-occurrence (16th April 2022) at 00 UTC and 12 UTC over Kolkata.

The wind speed (SKNT) at 00 UTC and 12 UTC at Kolkata on the dates of occurrence of 9 local severe storms ranges from 45 deg to 290 deg. **Figure 6.6 a** shows that the slightly increasing trend line of SKNT at 00 UTC and **Figure 6 b** slightly decreasing trend line of SKNT at 12 UTC. **Figure 6.13, 6.14** shows that the increasing trend line of the comparison of the vertical distribution of SKNT over Kolkata on the dates of occurrence (17th April 2022) and non-occurrence (16th April 2022) at 00 UTC and 12 UTC over Kolkata. **Figure 6.13, 6.14** shows that the SKNT value increasing at 1000 hPa to 300 hPa, after that value decreases.

Chapter – 7

Investigation Of Potential Temperatures Of The Troposphere on Thunderstorms And Non-Thunderstorms Days Prior To The Monsoon Over Kolkata Region, West Bengal

Introduction

A local severe storm is nothing more or less than a severe thunderstorm occurring locally. Local severe storms are characterized by high cumulus clouds, strong surface winds, heavy rainfall events and hail. Local severe thunderstorms are often accompanied by lightning and thunder. A thunderstorm develops when warm moist air rises high above the surface of the Earth. The three primary ingredients for the formation of a storm are warm moist air and unstable atmospheric conditions. A thunderstorm also develops when there is a mechanism that will cause surface air to rise rapidly through the atmosphere. These mechanisms include strong surface warming, uplift over mountain ranges, convergence of surface wind, and uplift on weather fronts. Although storms can develop at any time of year and at any time of day, the most common time of year for a thunderstorm is in the late afternoon or early evening. A large part of storm forecasting is based on the interpretation of instability parameters as well as the sources for the lift needed to induce deep convection. The basic thermodynamic diagrams illustrate the paths that followed by lifted parcels.

This sounding diagram is called a "skew T" diagram as the temperature lines are "skewed" to the potential temperature lines so that the instability parameters are easily visualized in **Figure 7.1**, **7.2** The basic curves are temperature, potential temperature, equivalent potential temperature , moist Adiabats.

At 00Z Skew T - Log P diagram of thunderstorm day on 17th April is shown in **Figure 7.1** over Kolkata region.

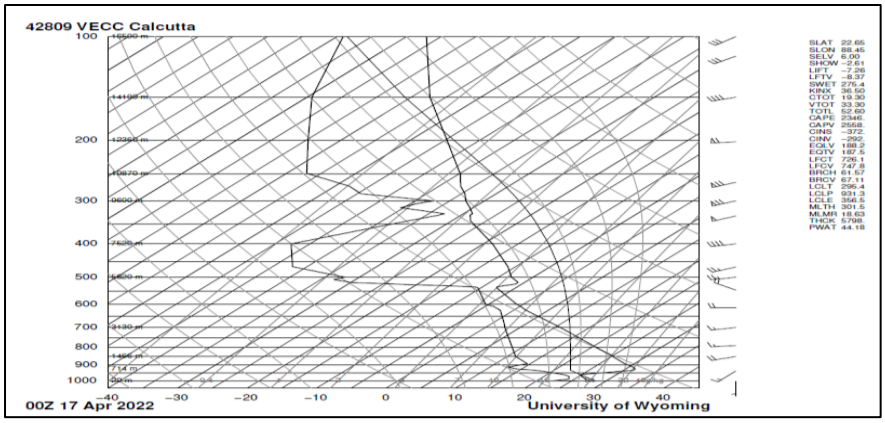

Figure 7.1 At 00Z Skew T - Log P diagram of thunderstorm day on 17th April 2022 over Kolkata region

At 12Z 17th April Skew T - Log P diagram of thunderstorm day of is shown in **Figure 7.2** Over Kolkata region

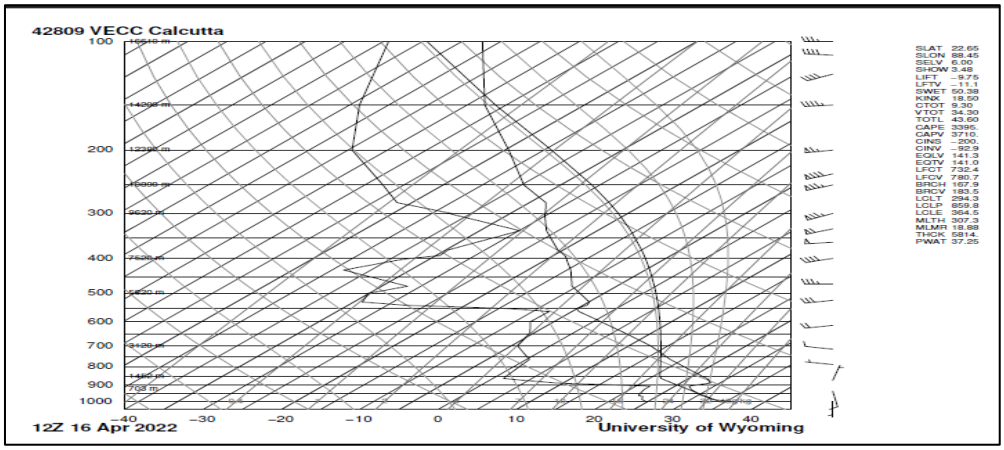

Figure 7.2 At 12 Z Skew T - Log P diagram of thunderstorm day on 17th April 2022 over Kolkata region

Lifted air parcels are limited by the curves shown on the diagram unsaturated parcels follow dry adiabats upward until they become saturated and then follow "moist" adiabats saturated parcels, if moving downward, follow a moist adiabats until they are no longer saturated and then they follow a dry adiabats. In estimating various parameters using "parcel theory" and this diagram, the following assumptions are made. The condensed water is not carried with the parcel and all fall out. "The pressure of the parcel immediately adapts to the environment". "There are no external sources or sinks" of heat and moisture outside of the parcel and ice processes are ignored. The parcel warms at faster rate while sinking and unsaturated.

Weather balloons are launched twice a day, at 0Z and 12Z (Z is Greenwich Mean Time), from various locations around the world. Each balloon carries with it an instrument package known as a radiosonde. The radiosonde measures temperatures, pressures, humidity, and wind speeds

and directions at various levels of the atmosphere. As the weather balloons rise through the atmosphere, they send this data back to computers on the ground. These computers plot the data on special diagrams known as skew-t log-p diagrams (or just skew-t for short). From these few variables, we can learn a great deal about the condition of the atmosphere, including stability, wind speeds, cloud base heights, cloud top heights, etc. This data can be used to predict whether local severe storms are likely to occur in the afternoon or evening (Karmakar and Quadir, 2014).

Kolkata experiences local severe storms each year during the months of March-May and the months of October-November. Local severe storms are the most common cause of loss of life and damage to property in the Kolkata area and surrounding areas. Local severe storms, also known as Nor'westers or Kalbaishakhi, are the deadliest in the country during this time. Local severe storms also affect several Indian states surrounding Bangladesh. Various studies have been conducted on various parameters in the troposphere that are associated with local severe storm formation in Kolkata and Bangladesh to identify the conditions that create local severe storms. These studies are follows as Mukherjee and Bhattacharya (1972), and Mukherjee et al. (1977), Mowla, (1986), Chowdhury and Karmakar (1986), Chowdhury et al. (1991), Das et al. (1994), Akram and Karmakar (1998), Karmakar (2005), Karmakar and Quadir (2014), and Karmakar and Alam (2005, 2006, 2007, 2011). No work has yet been done on the potential, equivalent potential and virtual potential temperatures of the tropospheric environment in Kolkata in the context of local severe storms. The present study has been undertaken to investigate the changes in different potential temperatures of the troposphere associated with local severe storms over Kolkata during the pre-monsoon season.

DATA

The University of Wyoming's Department of Atmospheric Science has provided the data (http://weather.uwyo.edu/upperair/sounding.html) utilized in this study. Five days thunderstorm and Non-Thunderstorm cases are chosen for this study over the Kolkata region, West Bengal (India). Five cases of local severe storms have been investigated. The thunderstorm and Non-Thunderstorm cases chosen for the present study over the Kolkata region, West Bengal (India) are shown in **Table 7.1**. **Table 7.2, 7.3, 7.4** and **7.5** are given data details in the present study.

Table 7.1 Local thunderstorms cases over the Kolkata region, West Bengal (India) used in the present study

Number of Observation	Date of observation of Thunderstorm cases	Dates of observation of Non-Thunderstorm cases
1st	17th April 2022	16.04.2022
2nd	21st April 2022	18.04.2022
3rd	29th April 2022	23.04.2022
4th	03rd May 2022	30.04.2022
5th	20th May 2022	18.05.2022

Thunderstorm Data

Table 7.2 42809 VECC Kolkata Observations at 00Z thunderstorm data

Dates	PRES hPa	THTA k	THTE k	THTV K
17.04.2022	1000.0	300.8	356.8	304.1
21.04.2022	1000.0	297.6	344.8	300.4
29.04.2022	1000.0	301.4	362.7	305.1
03.05.2022	1000.0	300.8	362.3	304.5
20.5.2022	1000.0	301.9	366.2	305.8

Table 7.3 42809 VECC Kolkata Observations at 00Z thunderstorm data

Dates	PRES hPa	THTA k	THTE k	THTV K
17.04.2022	500	323.1	325.1	323.2
21.04.2022	500	326.8	327.5	326.8
29.04.2022	500	324.3	324.5	324.3
03.05.2022	500	321.9	329.5	322.3
20.5.2022	500	324.1	326.6	324.2

Non-Thunderstorm Data

Table 7.4 42809 VECC Kolkata Observations at 00Z Non-thunderstorm data

Dates	PRES hPa	THTA k	THTE k	THTV K
16.04.2022	1000.0	300.9	364.5	304.8
18.04.2022	1000.0	300.6	360.1	304.2
23.04.2022	1000.0	300.1	364.3	304
30.04.2022	1000.0	298.8	338.8	301.2
18.05.2022	1000.0	302.1	366.9	306.1

Table 7.5 42809 VECC Kolkata Observations at 00Z Non-thunderstorm data

Dates	PRES hPa	THTA k	THTE k	THTV K
16.04.2022	500	323.3	324.2	323.4
18.04.2022	500	324.6	325.1	324.6
23.04.2022	500	327.2	331.8	327.5
30.04.2022	500	318.5	326.4	318.9
18.05.2022	500	325.8	337.3	326.4

METHODOLOGY

Theoretical background

Potential temperature

The potential temperature of a parcel of fluid at a pressure level is the temperature that the parcel would acquire if adiabatically brought to a standard reference pressure, usually 1000 hPa. The potential temperature is denoted for air is often given by (Wikipedia, the free encyclopedia)

$$\theta = T \left(\frac{P_0}{P}\right)^{\frac{R_d}{Cp}},$$

where, T is the current absolute temperature (in K) of the parcel, R_d is the gas constant of air, and C_p is the specific heat capacity at a constant pressure. This equation is often known as Poisson's equation.

Potential temperature is a more dynamically important quantity than the actual temperature. This is because it is not affected by the physical lifting or sinking associated with flow over obstacles or large-scale atmospheric turbulence. A parcel of air moving over a small mountain will expand and cool as it ascends the slope, then compress and warm as it descends on the other side but the potential temperature will not change in the absence of heating, cooling, evaporation, or condensation (processes that exclude these effects are referred to as dry adiabatic). Since parcels with the same potential temperature can be exchanged without work or heating being required, lines of constant potential temperature are natural flow pathways. Under almost all circumstances, potential temperature increases upwards in the atmosphere, unlike actual temperature which may increase or decrease. potential temperature is conserved for all dry adiabatic processes, and as such is an important quantity in the planetary boundary layer (which is often very close to being dry adiabatic).

Potential temperature is a useful measure of the static stability of the unsaturated atmosphere. Under normal, stably stratified conditions, the potential temperature increases with height, and vertical motions are suppressed. If the potential temperature decreases with height, the atmosphere is unstable to vertical motions, and convection is likely. Since convection acts to quickly mix the atmosphere and return to a stably stratified state, observations of decreasing potential temperature with height are uncommon, except while vigorous convection is underway or during periods of strong insolation. Situations in which the equivalent potential temperature decreases with height, indicating instability in saturated air, are much more common. Since potential temperature is conserved under adiabatic or isentropic air motions, in steady, adiabatic flow lines or surfaces of constant potential temperature act as streamlines or flow surfaces, respectively. This fact is used in isentropic analysis, a form of synoptic analysis

which allows visualization of air motions and in particular analysis of large-scale vertical motion. (http://www.theweatherprediction.com/habyhints/162/)

Derivation of potential temperature

The enthalpy form of the first law of thermodynamics can be written as:

$$dh = Tds + vdp$$

where dh denotes the enthalpy change, T the temperature, dS the change in entropy, v the specific volume, and p the pressure.

For adiabatic processes, the change in entropy is 0 and the 1st law simplifies to:

$$dh = vdp.$$

For approximately ideal gases, such as the dry air in the Earth's atmosphere, the equation of state can be substituted into the 1st law yielding, after some rearrangement:

$$\frac{dp}{p} = \frac{C_P}{R_d}\frac{dT}{T}$$

Where the $dh = C_p\, dT$ is used and both terms are divided by the product.

Integrating yields :

$$\ln\left(\frac{P}{P_0}\right) = \frac{C_p}{R_d} \ln\frac{T}{T_0}$$

and solving for T_0 , the temperature a parcel would acquire if moved adiabatically to the pressure level P_0, we get:

$$T_0 = T\left(\frac{P_0}{P}\right)^{R_d/C_P}$$

$$\rightarrow \theta = T\left(\frac{1000}{P}\right)^{R_d/C_P}$$

Where $T_0 = \theta$, $P_0 = 1000$ hPa and $\frac{R_d}{C_p} = 0.286$

Potential temperature decreasing with height is an indication of atmospheric instability.

Equivalent potential temperature

Equivalent potential temperature, commonly referred to as theta-e, (θ_e) is a quantity related to the stability of a column of air in the atmosphere. θ_e is the temperature a parcel of air would reach if all the water vapor in the parcel were to condense, releasing its latent heat, and the parcel was brought adiabatically to a standard reference pressure, usually 1000 hPa (1000 mbar) which is roughly equal to atmospheric pressure at sea level. In stable conditions, increases with altitude and decreases with height, convection can be occur. The comparison of the equivalent potential temperature of parcels of air at different pressures thus provides a measure of the instability of the column of air. (www.theweatherprediction.com)

The formula for θ_e is the following:

$$\Theta_e = T_e \left(\frac{P_0}{P}\right)^{R_d/C_P} \approx \left(T + \frac{L_v}{C_P} r\right) X \left(\frac{P_0}{P}\right)^{R_d/C_P}$$

Where:

T_e = equivalent temperature

T = Temperature of air at pressure

p = pressure at the point (in same units as)

P_0 = standard reference pressure (1000 mbar or 100 kPa)

R_d = specific gas constant for air (287 J/(kg·K))

C_p = specific heat of dry air at constant pressure (1004 J/(kg·K))

L_v = latent heat of evaporation (2400 kJ/kg {at 25 °C} to 2600 kJ/kg {at −40 °C})

r = mixing ratio of water vapor mass per mass of dry air (g/Kg or in Kg/Kg.

Equivalent potential temperature can also be calculated with the empirical formula:

$$\Theta_e = T \left(\frac{100}{p}\right)^{0.286} + 3r$$

T = Temperature in Kelvins

P = Pressure in hPa or millibars

r = Mixing ratio in grams per kilogram

Theta-E is a function of moisture (via r) and temperature (via potential temperature). Theta-E increases by either increasing moisture content of the air or increasing the temperature. Areas

with higher Theta-E have a greater potential for positive buoyancy

Virtual temperature *(*http://en.wikipedia.org/wiki/Virtual_temperature)

In atmospheric thermodynamics, the virtual temperature T_v of a moist air parcel is the temperature at which a theoretical dry air parcel would have a total pressure and density equal to the moist parcel of air.

Let us consider an air parcel containing masses m_d and m_v of water vapor in a given

volume V. The density is given by :

$$\rho = \frac{m_d + m_v}{V} = \rho_d + \rho_v$$

where ρ_d and ρ_v are the densities of dry air and water vapor. Rearranging the standard ideal gas equation with these variables gives:

$$e = \rho_v R_v T \quad \text{and} \quad p_d = \rho_d R_d T$$

Where e is the vapour pressure. Solving for the densities in each equation and combining with the law of partial pressures yields:

$$\rho = \frac{p - e}{R_d T} + \frac{e}{R_v T}$$

Then, solving for P and using $\epsilon = \frac{R_d}{R_v} = \frac{M_v}{M_d}$ is approximately 0.622 in Earth's atmosphere:

$$P = \rho R_d T_v$$

Where the virtual temperature T_v is

$$T_v = \frac{T}{1 - (1 - \epsilon)\frac{e}{p}}$$

We now have a non-linear scalar for temperature dependent purely on the unit less value $\frac{e}{p}$.

Allowing for varying amounts of water vapor in an air parcel, the virtual temperature T_v in units of Kelvin can be used seamlessly in any thermodynamic equation in it. Often more easily accessible atmospheric parameter is the mixing ratio r. Through expansion upon the definition of vapor pressure in the law of partial pressures as presented above and the definition of mixing ratio:

$$\frac{e}{p} = \frac{r}{r+\epsilon}$$

Which allows:

$$T_v = \mathrm{T}\ \frac{r+\epsilon}{\epsilon(1+r)}$$

Algebraic expansion of that equation, ignoring higher orders of r due to its typical order in Earth's atmosphere of 10^{-3}, and substituting with its constant value yields the linear approximation:

$$T_v \approx \mathrm{T}\ (1 + 0.61\mathrm{r})$$

The virtual potential temperature is the temperature a parcel at a specific pressure level and virtual temperature would have if it were lowered or raised to 1000 hPa. This is defined by Poisson's equation:

$$\Theta_\mathrm{v} = T_v\ \left(\frac{1000}{P}\right)^{R_d/C_P}$$

Results and discussion

Sounding data at standard isobaric levels from 1000 hPa to 100 hPa over Kolkata on the dates of occurrence and non-occurrence of local severe storms have been utilized to compute potential temperature, equivalent potential temperature and virtual potential temperature. Their vertical profiles of the occurrence of 5 local severe storms have been studied. The results are discussed in the following sub-sections.

Vertical profiles of potential temperature, equivalent potential temperature and virtual potential temperature over Kolkata

Vertical profiles of potential temperature over Kolkata

Vertical profiles of potential temperature over Kolkata at 00 UTC on the dates of occurrence of 5 local severe storms are shown in **Figure 7. 3 a, b, c, d, e.** The F**igures 7. 3 a, b, c, d, e s**how that the potential temperature increases with height, becoming maximum at the top of the troposphere. This indicates that instability exists in the troposphere, which is favorable for the occurrence of local severe storms. The difference in potential temperature between 1000 hPa and 500 hPa on the dates of occurrence of local storms is more than 29 K ranging from 21.1 to 29.2 K as can be seen from **Table 7.6**. On the dates of occurrence, the difference in potential temperature between 1000 and 500 hPa levels at 00 UTC is higher in one case out of 5 cases and lower in 4 cases and the values range from 21.1 K to 29.2 K (**Table 7.6).**

Table 7.6 The difference in potential temperature (THAT) between 1000 hPa and 500 hPa over Kolkata on the dates of occurrence and non-occurrence of local severe storms at 00 UTC

Dates of occurrence of local severe storms	Difference in potential temperature (K) between 1000 and 500 hPa ($\theta_{500} - \theta_{1000}$) levels on the occurrence of local severe storms	Dates of non-occurrence of local severe storms	Difference in potential temperature (K) between 1000 and 500 hPa ($\theta_{500} - \theta_{1000}$) levels on the non-occurrence of local severe storms
17.04.2022	22.3	16.04.2022	22.4
21.04.2022	29.2	18.04.2022	24
29.04.2022	22.9	23.04.2022	27.1
03.05.2022	21.1	30.04.2022	19.7
20.5.2022	22.2	18.05.2022	23.7

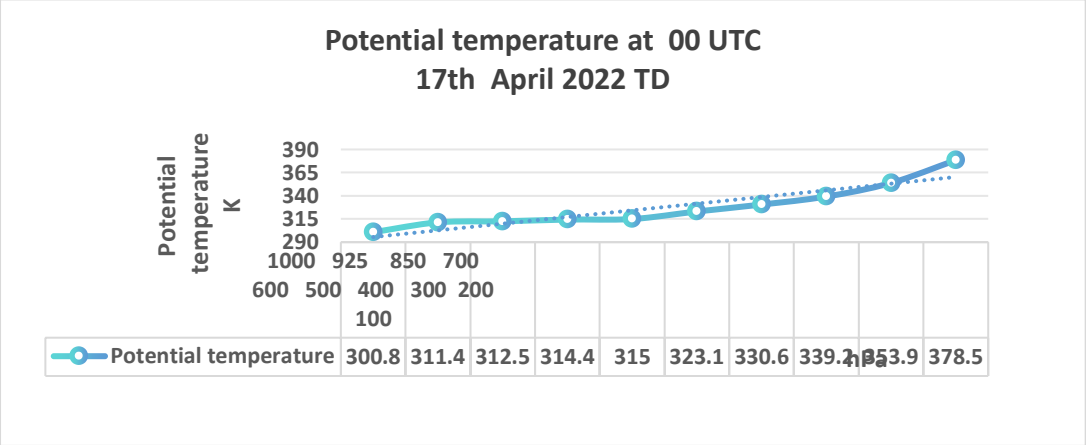

Figure 7.3 a Vertical distribution of potential temperature (K) over Kolkata at 00 UTC on 17 th April 2022

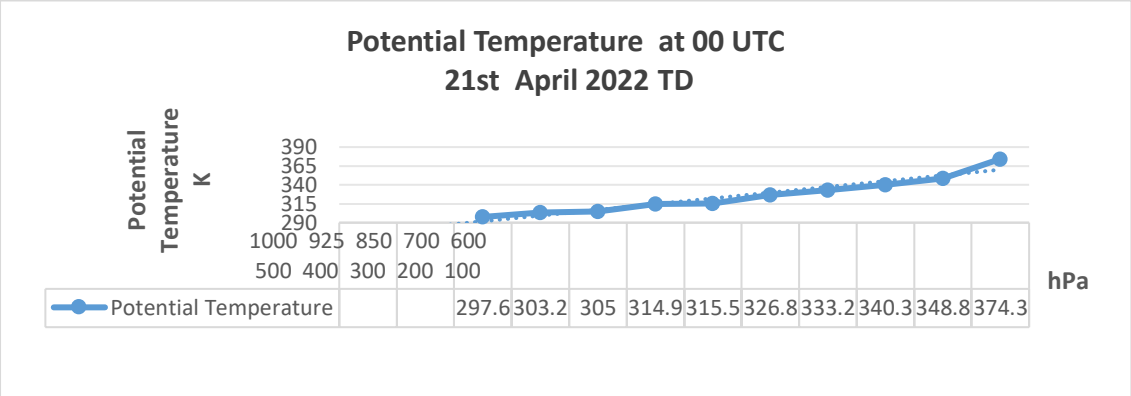

Figure 7.3 b Vertical distribution of potential temperature (K) over Kolkata at 00 UTC on 21st April 2022

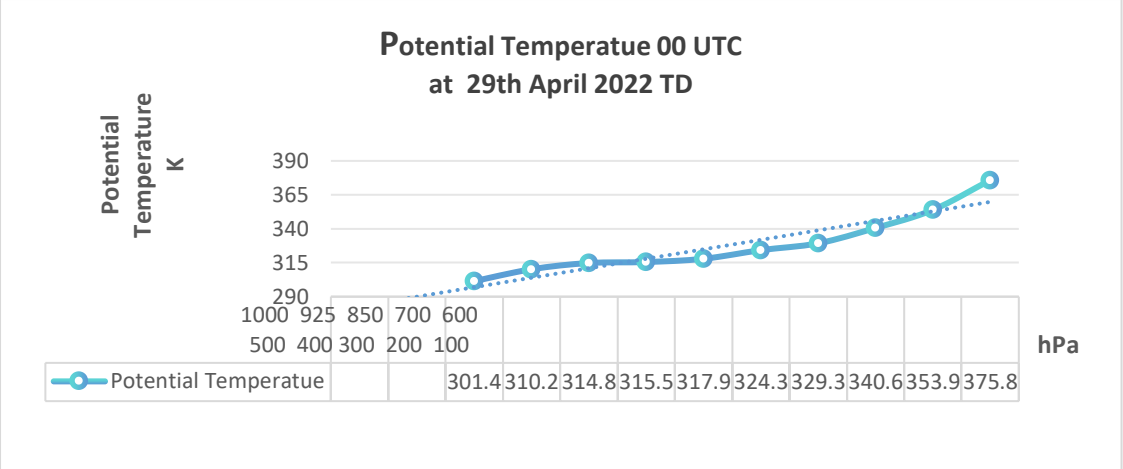

Figure 7.3 c Vertical distribution of potential temperature (K) over Kolkata at 00 UTC on 29 th April 2022

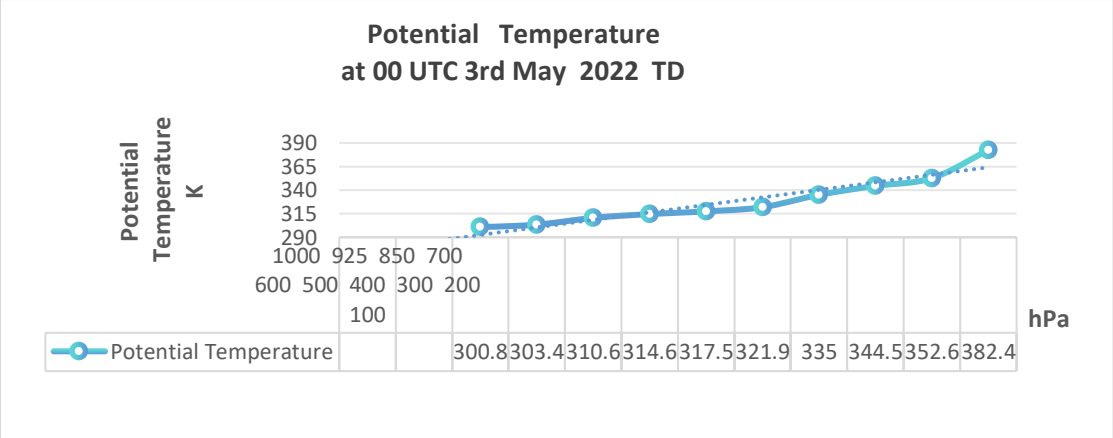

Figure 7.3 d Vertical distribution of potential temperature (K) over Kolkata at 00 UTC on 3rd May 2022

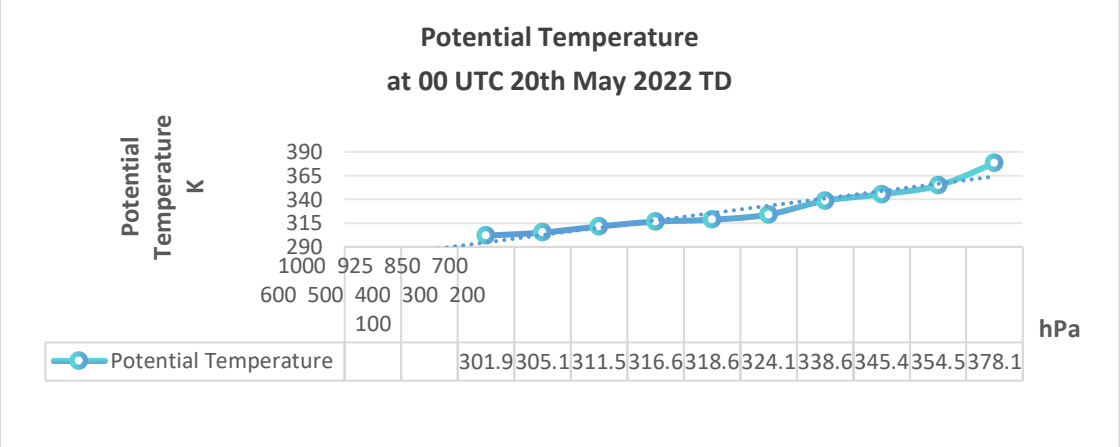

Figure 7.3 e Vertical distribution of potential temperature (K) over Kolkata at 00 UTC on 20th May 2022

The vertical profiles of the difference in potential temperature over Kolkata at 00 UTC are shown in **Figure 7. 3 f, g, h, i, j.** On 17th April 2022, the potential temperature is seen to increase from 700 hPa to 200 hPa (**Figure 7.3 a**). On 21st April 2022, the potential temperature is seen to increase significantly from 500 hPa to 100 hPa and from 850 hPa to 700 hPa and found to decrease from 700 hPa to 600 hPa significantly (**Figure 7.3 b**). On 29th April, 3rd May and 20th May, the potential temperature is seen to increase significantly from 1000 hPa to 100 hPa in **Figure 7.3 c, d, e.**

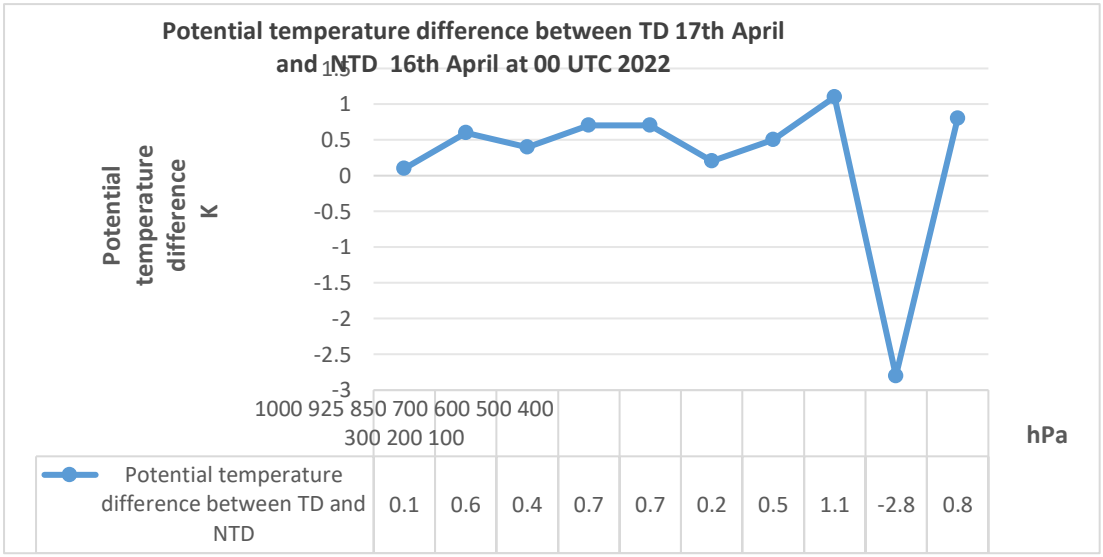

Figure 7.3 f Vertical profile of difference in potential temperature (K) between the dates of occurrence (17th April 2022) and non-occurrence (16th April 2022) at 00 UTC

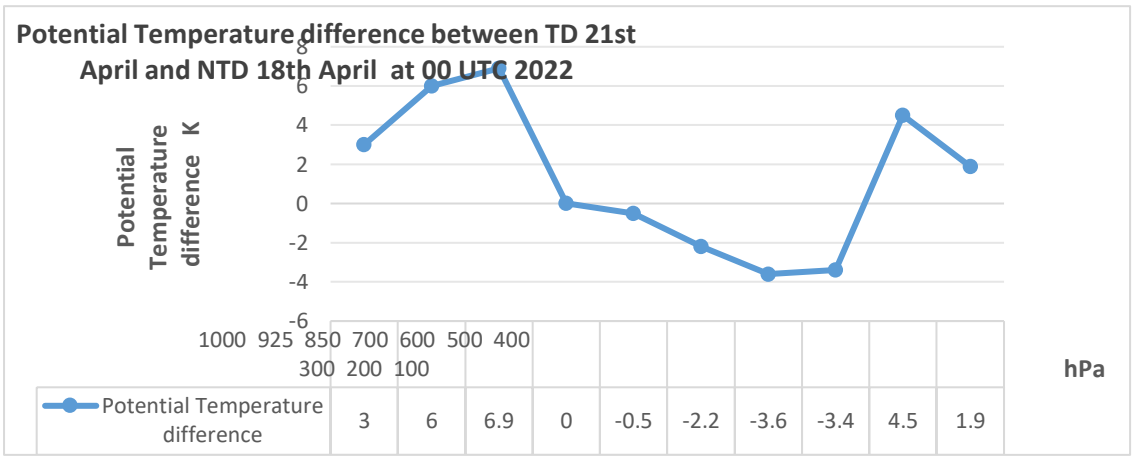

Figure 7.3 g Vertical profile of difference in potential temperature (K) between the dates of occurrence (21st April 2022) and non-occurrence (18th April 2022) at 00 UTC

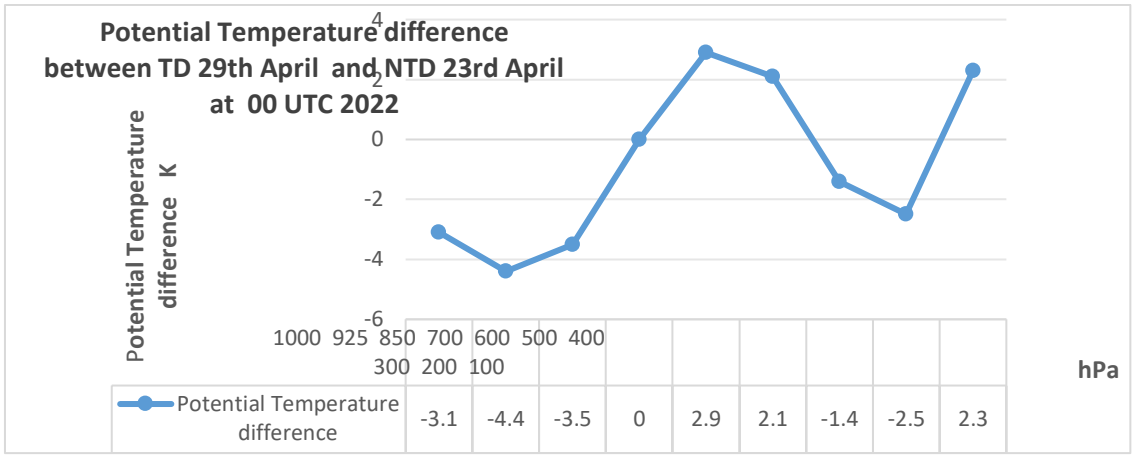

Figure 7.3 h Vertical profile of difference in potential temperature (K) between the dates of occurrence (29th April 2022) and non-occurrence (23rd April 2022) at 00 UTC

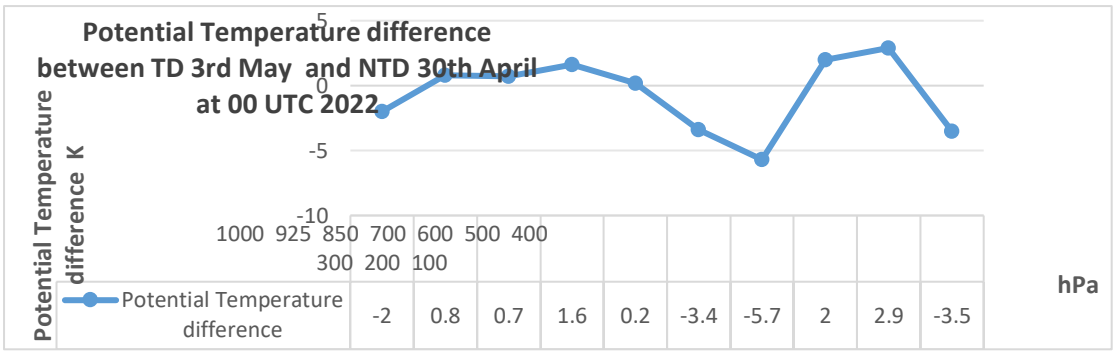

Figure 7.3 i Vertical profile of difference in potential temperature (K) between the dates of occurrence (3rd May 2022) and non-occurrence (30th April 2022) at 00 UTC

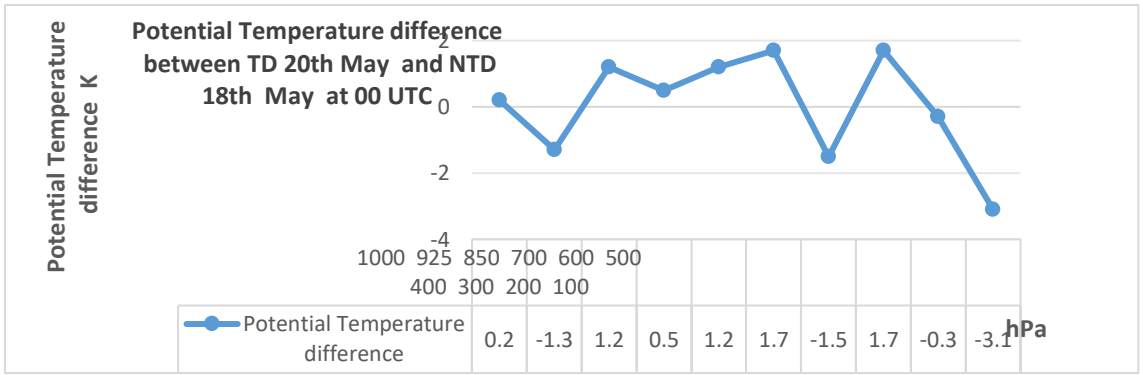

Figure 7.3 j Vertical profile of difference in potential temperature (K) between the dates of occurrence (20th May 2022) and non-occurrence (18th May 2022) at 00 UTC

On 17th April and 16th April 2022, the difference in potential temperature has no definite pattern and has alternate increase and decrease in potential temperature (**Figure 7.3 f)**. On 29th April and 23rd April 2022, there is a definite and significant increase the difference in potential temperature from 200 hPa to about 100 hPa and from 925 hPa to 600 hPa (**Figure 7.3 h**). The

vertical profile of difference in potential temperature (K) between the dates of occurrence and non-occurrence at 00 UTC are shown fluctuating in **Figure 7. 3 f, g, h, i, j.** Therefore, it apparent from the above discussion that the potential temperature has a tendency to increase especially from 925 hPa to mid-troposphere on the dates of occurrence of local severe storms in most of the cases as compared to that on the dates of non-occurrence. The gradient of potential temperature between 1000 hPa and 500 hPa is relatively higher on the dates of occurrence in most cases.

Vertical profiles of equivalent potential temperature over Kolkata

Vertical profiles of equivalent potential temperature over Kolkata at 00 UTC on the dates of occurrence of 5 local severe storms are shown in **Figures 7.4 a, b, c, d, e**. The figures show that the equivalent potential temperature decreases with height, becoming minimum at the mid troposphere (500 hPa), except on 21 April 2022 when equivalent potential temperature increases from 1000 hPa to about 925 hPa and then decreases up to 500 hPa. This indicates that conditional instability exists in the troposphere, which is favourable for the occurrence of local severe storms. The equivalent temperature then increases significantly beyond 500 hPa.

The difference in equivalent potential temperature between 1000 hPa and 500 hPa on the dates of occurrence of local storms is less than -17.3 K ranging from -17.3 to -39.6 K as can be seen from **Table 7.7.** This difference in potential temperature i.e. gradient of equivalent temperature between 1000 hPa and 500 hPa ranges from -17.3K to -39.6K and is less on the dates of occurrence of local storms in three cases as compared to those on the dates of non-occurrence. This gradient indicates sufficient instability favourable for the development of local severe storms.

Table 7.7 The difference in equivalent potential temperature between 1000 hPa and 500 hPa over Kolkata on the dates of occurrence and non-occurrence of local severe storms at 00 UTC

Dates of occurrence of local severe storms	Difference in equivalent potential temperature (K) between 1000 and 500 hPa (θ_{500} - θ_{1000}) levels on the occurrence of local severe storms	Dates of non-occurrence of local severe storms	Difference in equivalent potential temperature (K) between 1000 and 500 hPa (θ_{500} - θ_{1000}) levels on the non-occurrence of local severe storms
17.04.2022	-31.77	16.04.2022	-40.3
21.04.2022	-17.3	18.04.2022	-35
29.04.2022	-38.2	23.04.2022	-32.5
03.05.2022	-32.8	30.04.2022	-12.4
20.5.2022	-39.6	18.05.2022	-29.6

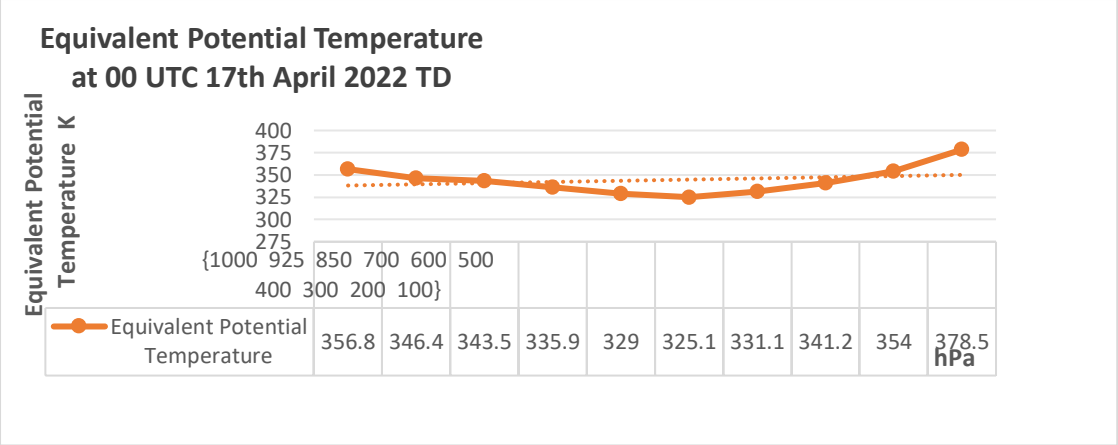

Figure 7.4 a Vertical distribution of equivalent potential temperature (K) over Kolkata at 00 UTC on 17th April 20222

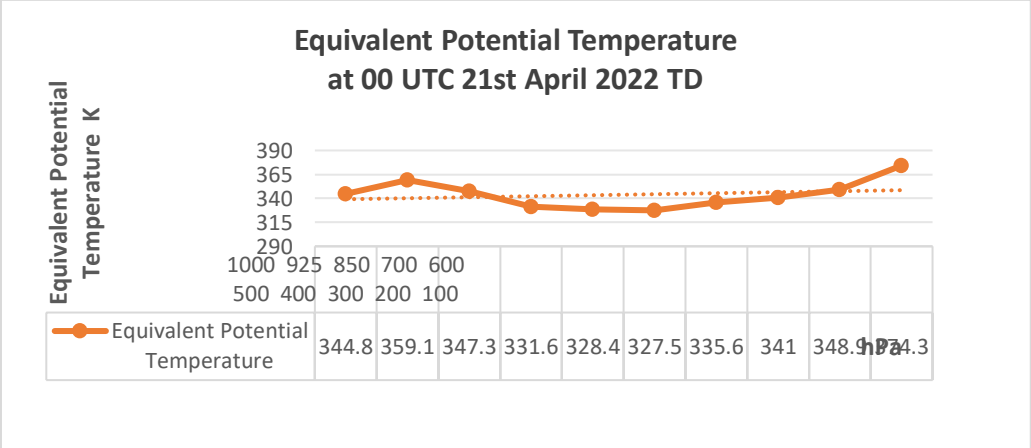

Figure 7.4 b Vertical distribution of equivalent potential temperature (K) over Kolkata at 00 UTC on 21st April 20222

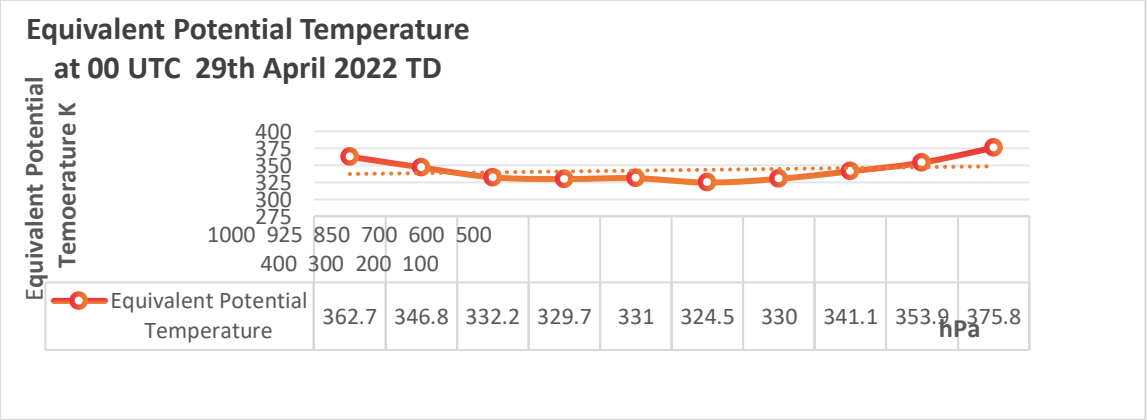

Figure 7.4 c Vertical distribution of equivalent potential temperature (K) over Kolkata at 00 UTC on 29th April 20222

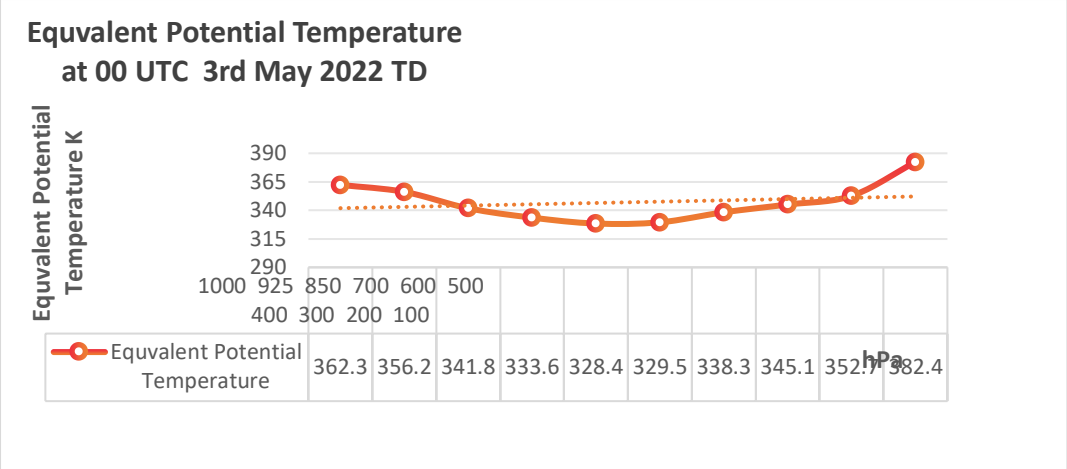

Figure 7.4 d Vertical distribution of equivalent potential temperature (K) over Kolkata at 00 UTC on 3rd May 20222

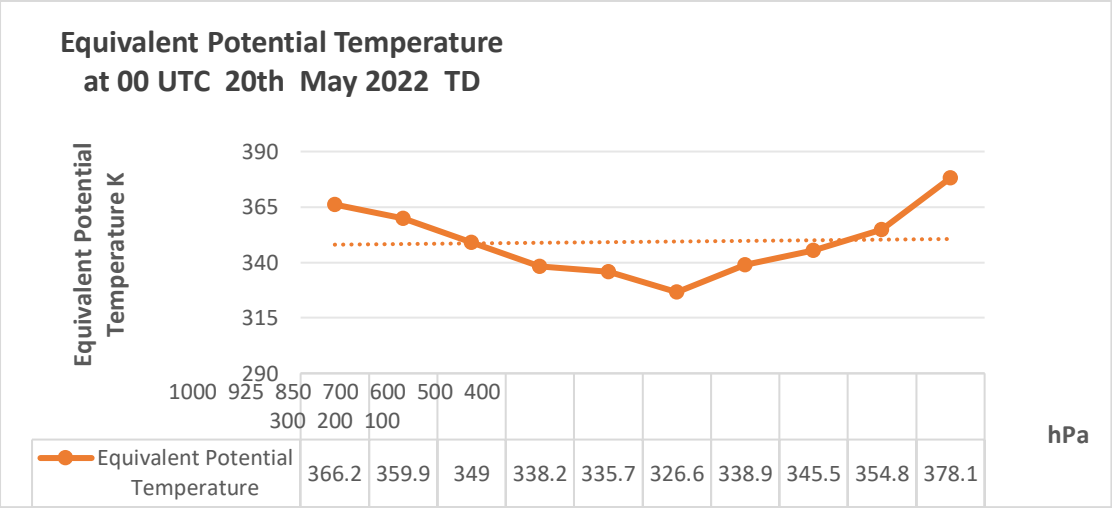

Figure 7.4 e Vertical distribution of equivalent potential temperature (K) over Kolkata at 00 UTC on 20th May 20222

The vertical profiles of the difference in equivalent potential temperature over Kolkata at 00 UTC are shown in **Figure 7.4 f, g, h, i, j**. On 21st April 2022, the equivalent potential temperature over Kolkata at 00 UTC is found to increase from about 1000 hPa level to 925 hPa and 500 hPa to 100 hPa, and then it decreases significantly up to about 925 hPa to 500 hPa level (**Figure 7.4 b**). On 17th April, 29th April, 3rd May and 20th May 2022, the equivalent potential temperature increases from 500 hPa to about 100 hPa and it decreases from 1000 hPa to 500 hPa (**Figure 7.4 a, c, d, e**).

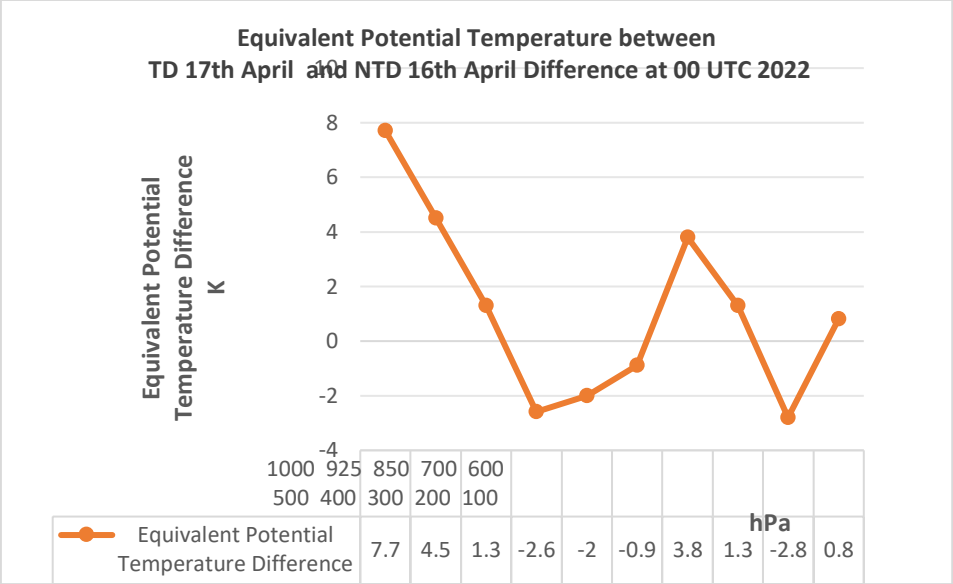

Figure 7. 4 f Difference in equivalent potential temperature (K) between the dates of occurrence (17th April 2022) and non-occurrence (16th April 2022) at 00 UTC over Kolkata

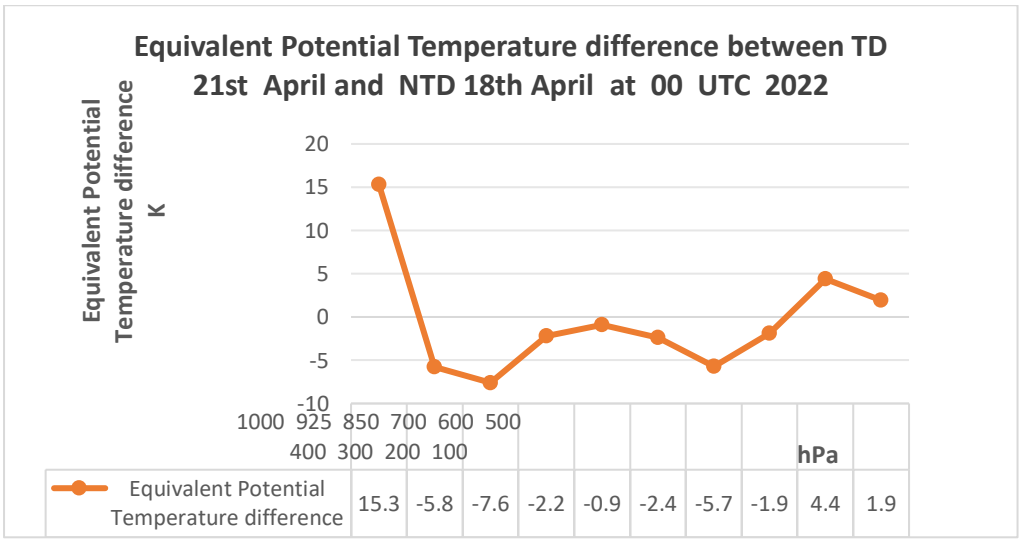

Figure 7. 4 g Difference in equivalent potential temperature (K) between the dates of occurrence (21st April 2022) and non-occurrence (18th April 2022) at 00 UTC over Kolkata

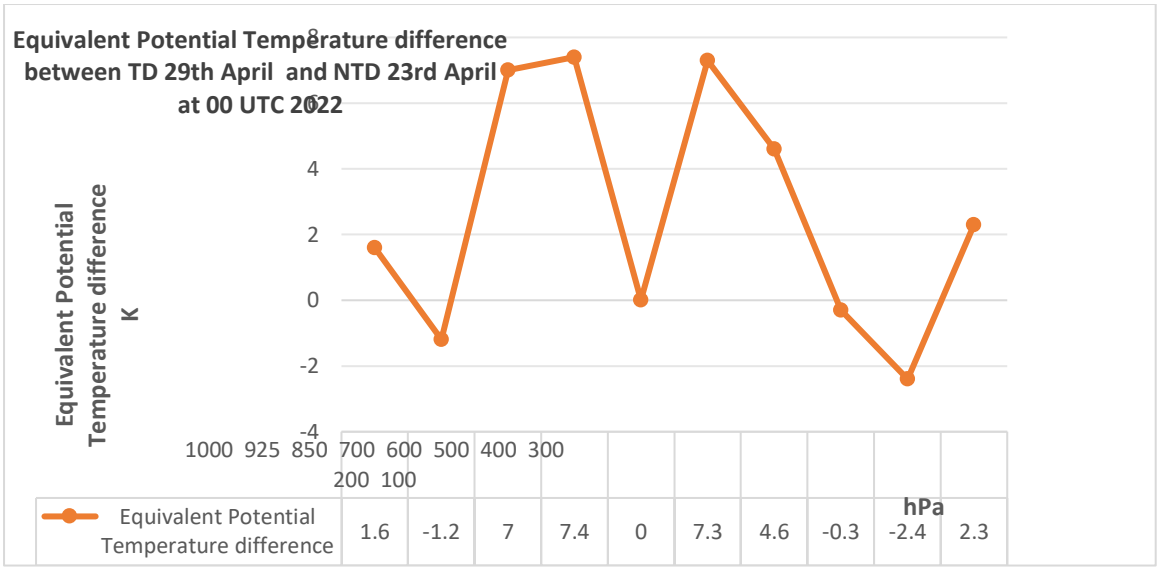

Figure 7.4 h Difference in equivalent potential temperature (K) between the dates of occurrence (29th April 2022) and non-occurrence (23rd April 2022) at 00 UTC over Kolkata

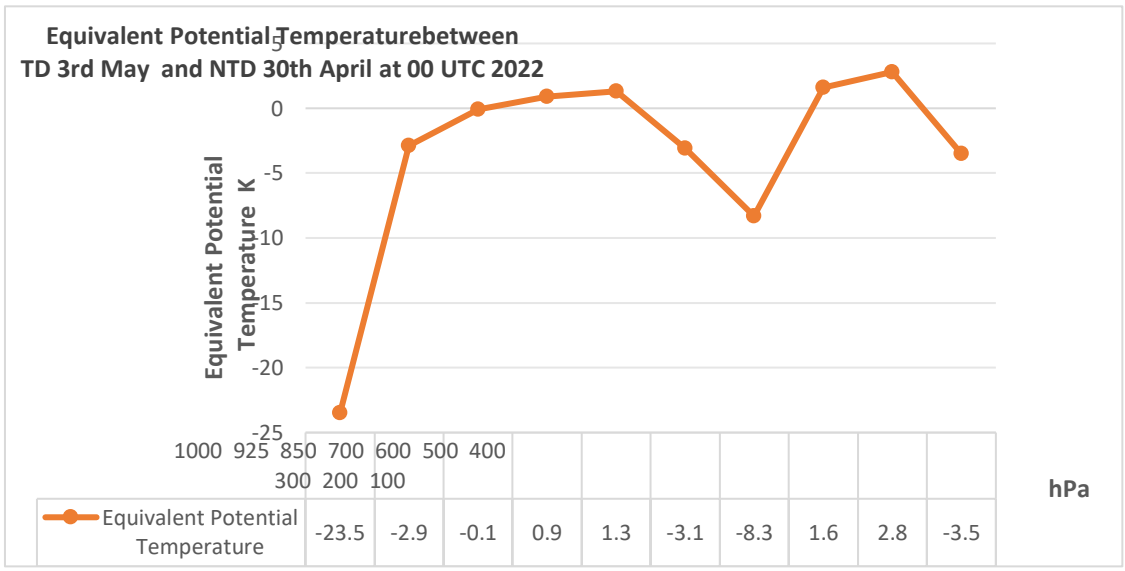

Figure 7.4 i Difference in equivalent potential temperature (K) between the dates of occurrence (3rd May 2022) and non-occurrence (23rd April 2022) at 00 UTC over Kolkata

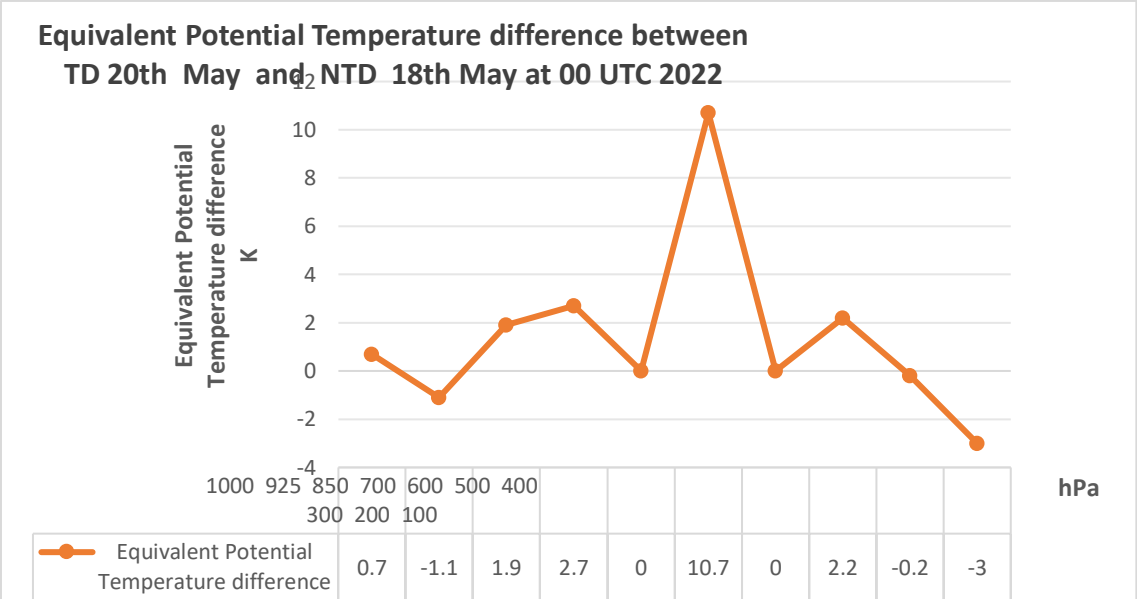

Figure 7. 4 j Difference in equivalent potential temperature (K) between the dates of occurrence (20th May 2022) and non-occurrence (18th May 2022) at 00 UTC over Kolkata

The vertical profile of difference in equivalent potential temperature (K) between the dates of occurrence and non-occurrence at 00 UTC are shown fluctuating in **Figure 7. 4 f, g, h, i, j.** The increase in equivalent potential temperature on the dates of occurrence of local severe storms may be attributed to the latent heat of condensation in the lower troposphere. So, from the above discussion it may be concluded that the equivalent potential temperature has the tendency to increase in the lower troposphere on the dates of occurrence with some exceptions.

Vertical profiles of virtual potential temperature over Kolkata

Vertical profiles of virtual potential temperature over Kolkata at 00 UTC on the dates of occurrence of 5 local severe storms are shown in **Figure 7.5 a, b, c, d, e**. The figures show that the virtual potential temperature increases with height, becoming maximum at the top of the troposphere. This indicates that instability exists in the troposphere, which is favourable for the Occurrence of local severe storms. The difference in virtual potential temperature between 1000 hPa and 500 hPa on the dates of occurrence of local storms is more than 17.8 K ranging from 17.8 to 26.4 K as can be seen from **Table 7.8.** The **Table 7.8** also shows that the difference in Virtual potential temperature between 1000 hPa and 500 hPa i.e. gradient in virtual temperature on the dates of occurrence of local storms (17th April 2022, 21st April 2022 and 3rd May 2022) is higher in three cases and lower in two cases as compared to that on the dates of nonoccurrence of local storms (29th April and 20th May 2022).

Table 7.8 The difference in virtual potential temperature between 1000 hPa and 500 hPa over Kolkata on the dates of occurrence and non-occurrence of local severe storms at 00 UTC

Dates of occurrence of local severe storms	Difference in virtual potential temperature (K) between 1000 and 500 hPa (θ_{500} - θ_{1000}) levels on the occurrence of local severe storms	Dates of non-occurrence of local severe storms	Difference in virtual potential temperature (K) between 1000 and 500 hPa (θ_{500} - θ_{1000}) levels on the non-occurrence of local severe storms
17.04.2022	19.1	16.04.2022	18.6
21.04.2022	26.4	18.04.2022	20.4
29.04.2022	19.2	23.04.2022	23.5
03.05.2022	17.8	30.04.2022	17.7
20.5.2022	18.4	18.05.2022	20.3

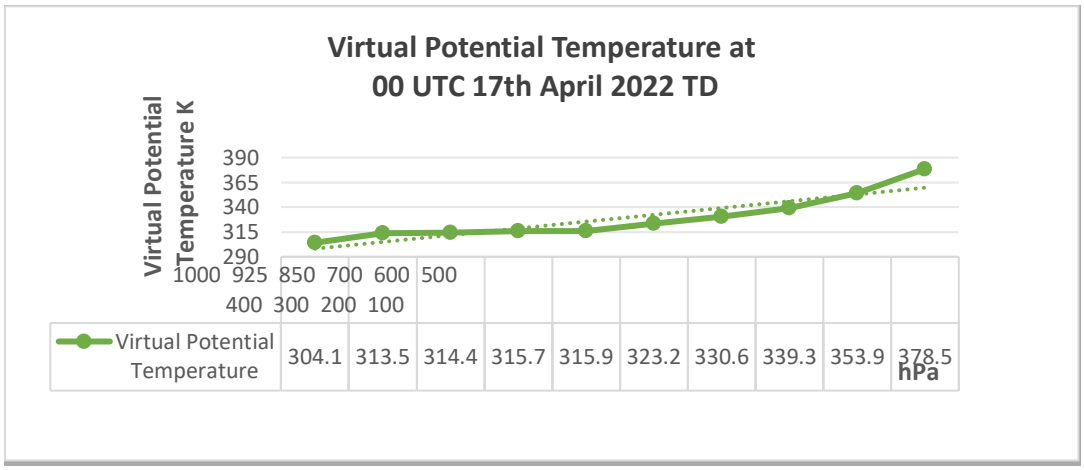

Figure 7.5 a Vertical distribution of virtual potential temperature (K) over Kolkata at 00 UTC on 17th April 2022

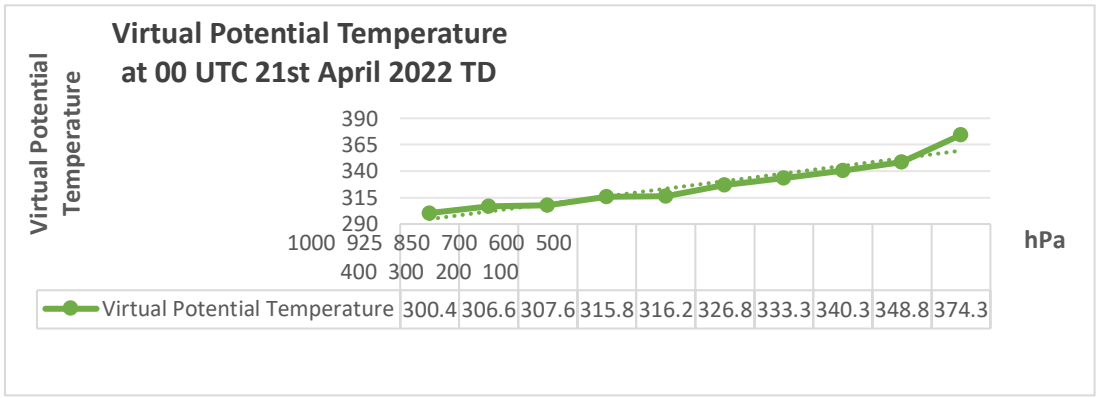

Figure 7.5 b Vertical distribution of virtual potential temperature (K) over Kolkata at 00 UTC on 21st April 2022

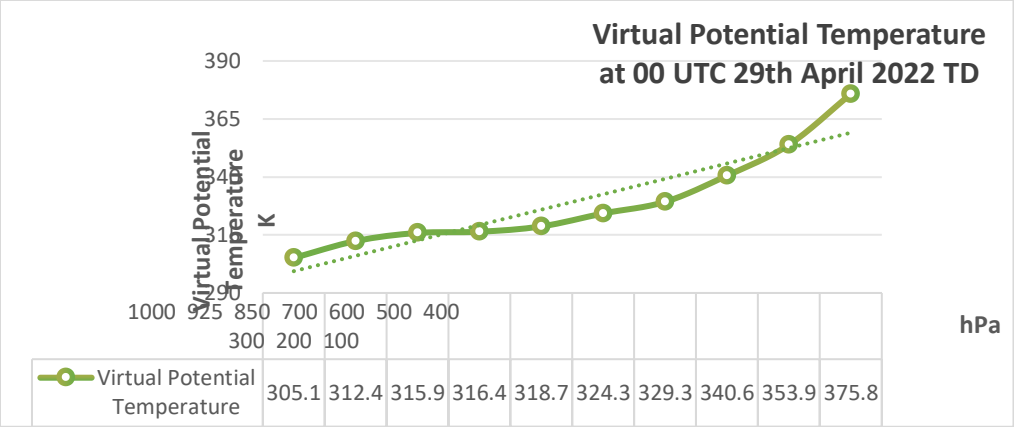

Figure 7.5 c Vertical distribution of virtual potential temperature (K) over Kolkata at 00 UTC on 29th April 2022

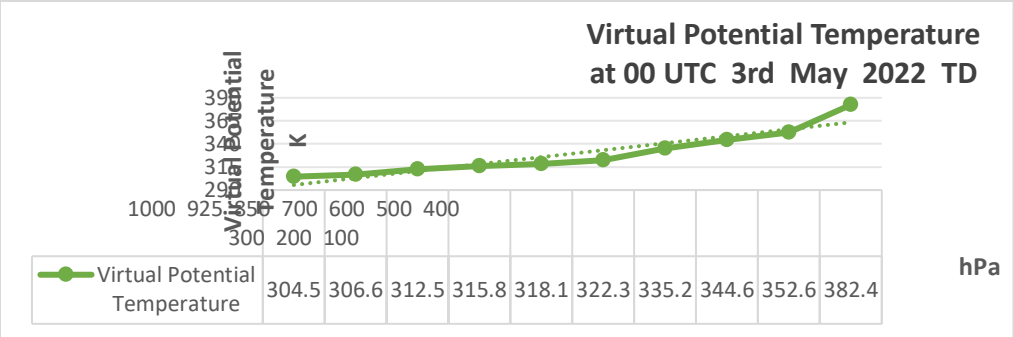

Figure 7.5 d Vertical distribution of virtual potential temperature (K) over Kolkata at 00 UTC on 3rd May 2022

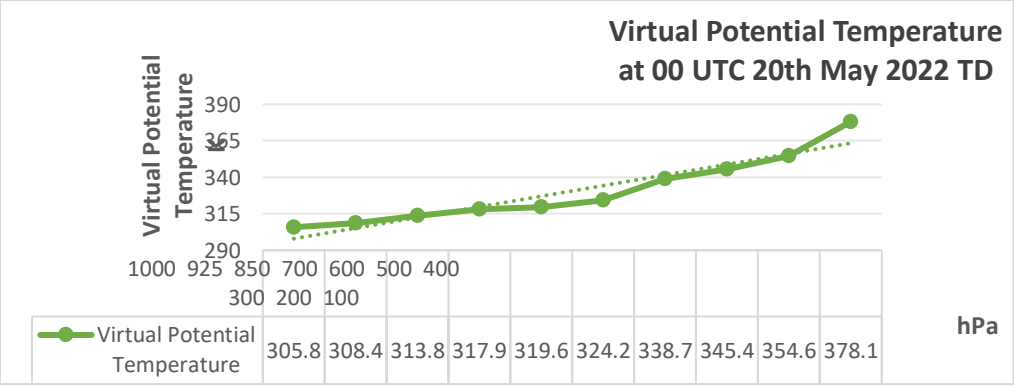

Figure 7.5 e Vertical distribution of virtual potential temperature (K) over Kolkata at 00 UTC on 20th May 2022

The vertical profiles of the difference in virtual potential temperature over Kolkata at 00 UTC are shown in **Figure 7.5 f, g, h, i, j** for the 5 cases of local severe storms. On 16th April 2022 (date of non-occurrence, **Figure 7.5 f**), the virtual potential temperature is seen to increase from 500 hPa to 300 hPa significantly as compared to that on 17th April 2022 (date of occurrence). But on 18th April 2022 (**Figure 7.5 g**) , the virtual potential temperature is found to increase from 1000 hPa to about 850 hPa with a significant decrease from 850 hPa to about 300 hPa as compared to that on 21st April 2022 (date of occurrence).

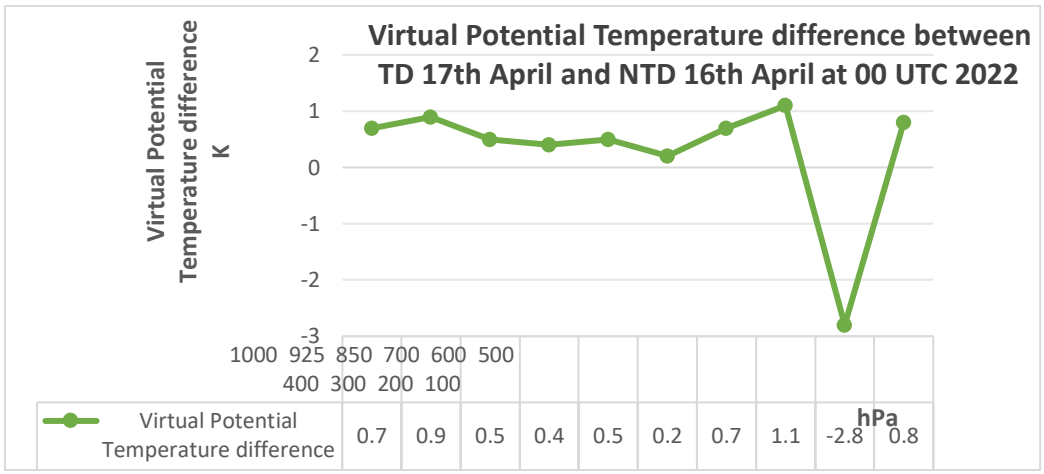

Figure 7.5 f Difference in virtual potential temperature (K) between the dates of occurrence (17th April 2022) and non-occurrence (16th April 2022) at 00 UTC over Kolkata

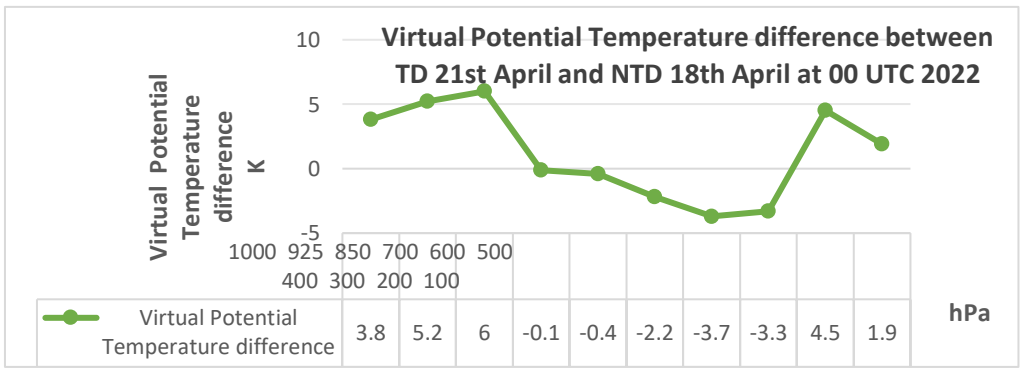

Figure 7.5 g Difference in virtual potential temperature (K) between the dates of occurrence (21st April 2022) and non-occurrence (18th April 2022) at 00 UTC over Kolkata

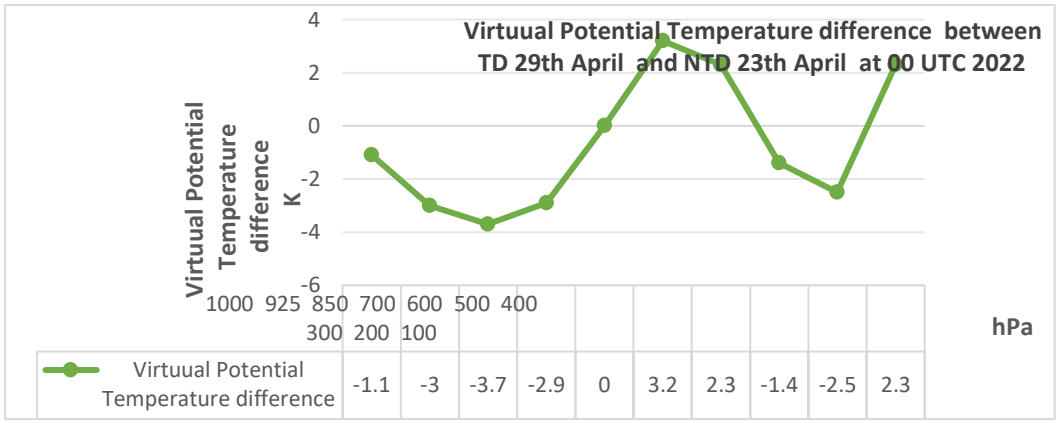

Figure 7.5 h Difference in virtual potential temperature (K) between the dates of occurrence (29th April 2022) and non-occurrence (23rd April 2022) at 00 UTC over Kolkata

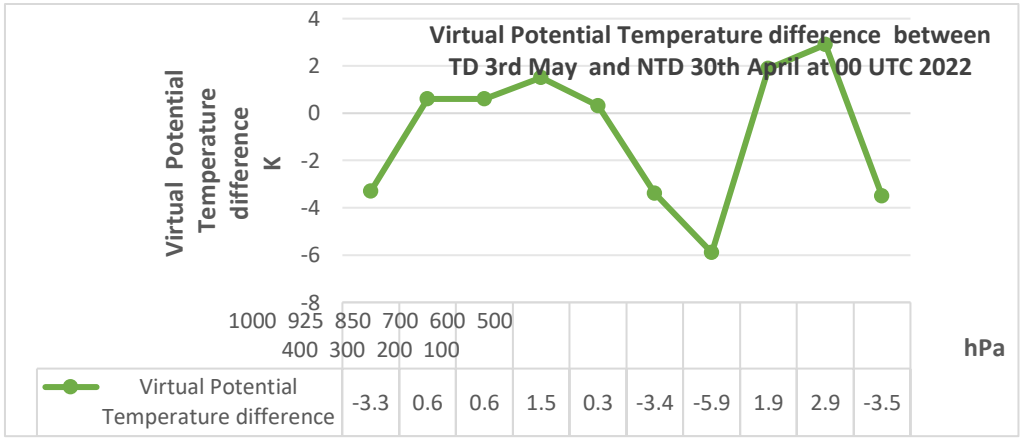

Figure 7.5 i Difference in virtual potential temperature (K) between the dates of occurrence (3rd May 2022) and non-occurrence (30th April 2022) at 00 UTC over Kolkata

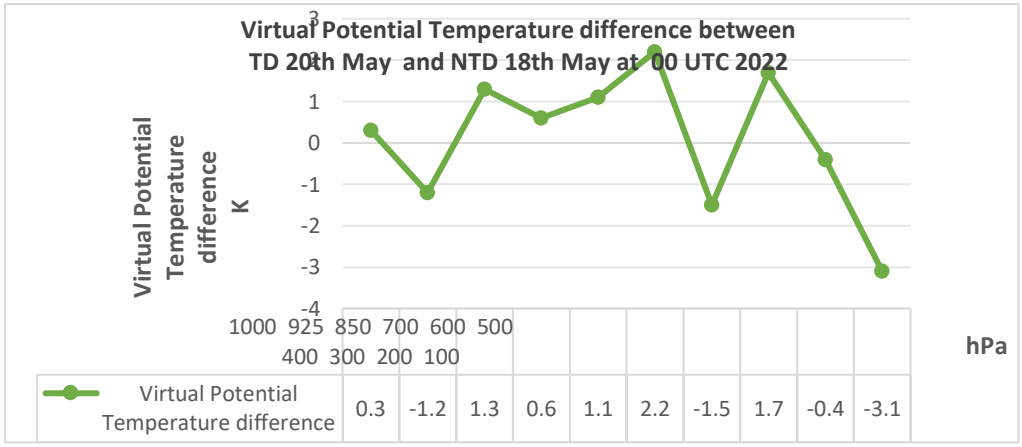

Figure 7.5 j Difference in virtual potential temperature (K) between the dates of occurrence (20th May 2022) and non-occurrence (18th May 2022) at 00 UTC over Kolkata

The vertical profile of difference in virtual potential temperature (K) between the dates of occurrence and non-occurrence at 00 UTC are shown fluctuating in **Figure 7. 5 f, g, h, i, j.**

Conclusions

On the basis of the present study, following conclusions may be drawn:

The potential temperature over Kolkata increases with height, becoming maximum at the top of the troposphere. The potential temperature has a tendency to increase especially from 925 hPa to mid-troposphere on the dates of occurrence of local severe storms in most of the cases as compared to that on the dates of nonoccurrence. The gradient of potential temperature between 1000 hPa and 500 hPa over Kolkata is relatively higher on the dates of occurrence in most cases ranging from 21.1 K to 29.2 K

The equivalent potential temperature over Kolkata decreases with height, becoming minimum at the mid-troposphere (500 hPa), indicating conditional instability in the troposphere, which is favourable for the occurrence of local severe storms. The equivalent temperature then increases significantly beyond 500 hPa. The equivalent potential temperature has the tendency to increase in the lower troposphere on the dates of occurrence with some exceptions. The difference in potential temperature i.e. gradient of equivalent temperature between 1000 hPa and 500 hPa over Kolkata ranges from -17.3 K to -39.6 K.

The virtual potential temperature increases with height, becoming maximum at the top of the troposphere. The difference in virtual potential temperature between 1000 hPa and 500 hPa over Kolkata on the dates of occurrence of local storms is more than 17.8 K ranging from 17.8 K to 26.4 K.

Chapter – 8

Investigation Turbulent Characteristics on Thunderstorms

Introduction

Turbulence

Turbulence is one of the most unpredictable of all the weather phenomena that are of significance to scientist. Turbulence is an irregular motion of the air resulting from eddies and vertical currents. It may be as insignificant as a few annoying bumps or severe enough to momentarily throw an airplane out of control or to cause structural damage. Turbulence is associated with fronts, wind shear, thunderstorms, etc.

CAUSES OF TURBULENCE

There are four causes of turbulence.

1. Mechanical Turbulence- Friction between the air and the ground, especially irregular terrain and man-made obstacles, causes eddies and therefore turbulence in the lower levels. The intensity of this eddy motion depends on the strength of the surface wind, the nature of the surface and the stability of the air. The stronger the wind speed (generally, a surface wind of 20 knots or higher is required for significant turbulence), the rougher the terrain and the more unstable the air, the greater will be the turbulence. Of these factors that affect the formation of turbulence, stability is the most important. If the air is being heated from below, the vertical motion will be more vigorous and extensive and the choppiness more pronounced. In unstable air, eddies tend to grow in size; in stable air, they tend not to grow in size but do dissipate more slowly.
In strong winds, even hangars and large buildings cause eddies that can be carried some distance downwind. Strong winds are usually quite gusty; that is, they fluctuate rapidly in speed. Sudden increases in speed that last several minutes are known as squalls and they are responsible for quite severe turbulence. Below **figures 8.1** and **8.2** shows Mechanical Turbulence.

Figure 8.1 Mechanical Turbulence

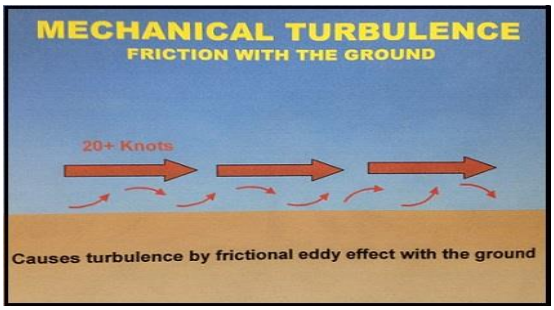

Figure 8.2 Mechanical Turbulence

Mountain waves are turbulent eddies that are found downwind from mountain ridges. They are caused by and are therefore stationary with respect to the mountain ridges. Mountain waves produce some of the most severe turbulence associated with mechanical agencies.

NOTE: Stability of the lower troposphere above and to the lee of the mountain is critical (i.e., the most intense turbulence is associated with stable air above and to the lee of the mountain barrier).

Favourable conditions for mountain waves include:

a. Winds 25 knots or greater, blowing perpendicular to the top of the mountain ridge.
b. Little change of wind direction with height
c. Wind speeds increasing with height
d. Stable atmosphere (there should be some cold air advection across or along the mountain range, a layer of low stability near the ground, a very stable layer at mountain top level above the surface layer, and finally, a less stable layer above the stable layer)

- This requires air parcels forced to rise over the mountain crest to sink toward their initial altitude (or equilibrium level)
- Parcels then rise and fall in a damped oscillatory pattern, much like a weighted spring

1. Often extends from the surface to slightly above the tropopause
2. May extend 100 miles or more downstream from mountain crests
3. Main updraft and downdraft of the wave can displace an aircraft up to 5,000 feet per minute
4. Downdrafts may extend to surface on lee side of mountain
5. The most intense turbulence is usually located at low-levels, leeward of the mountains in or near the rotor cloud, if present
6. Mountain waves may be denoted by mountain wave clouds
   - Cirrocumulus Standing Lenticular (CCSL)
   - Altocumulus Standing Lenticular (ACSL)
   - Rotor clouds (often associated with the most intense turbulence)

Below **figures 8.3** and **8.4** shows Mechanical Turbulence.

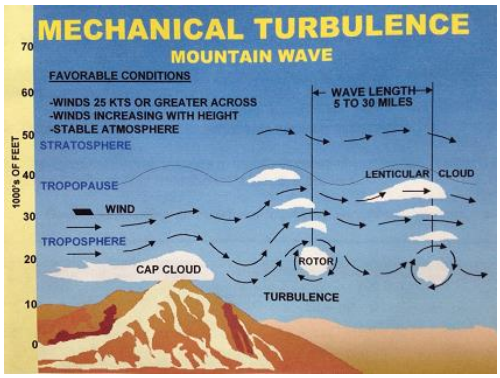

Figure 8.3 Mechanical Turbulence

Figure 8.4 Mechanical Turbulence

3. **Thermal (Convective) Turbulence-** Turbulence can also be expected on warm summer days when the sun heats the earth's surface unevenly. Certain surfaces, such as barren ground, rocky and sandy areas, are heated more rapidly than are grass covered fields and much more rapidly than is water. Isolated convective currents are therefore set in motion with warm air rising and cooler air descending, which are responsible for bumpy conditions as an airplane

flies in and out of them. Turbulence extends from the base to the top of the convection layer, with smooth conditions found above. if cumulus, towering cumulus or cumulonimbus clouds are present, the turbulent layer extends from the surface to cloud tops. Turbulence intensity increases as convective updraft intensity increases. In weather conditions when thermal activity can be expected, many pilots prefer to fly in the early morning or in the evening when the thermal activity is not as severe.

Convective currents may not be made visible by cumuli form clouds, resulting in "dry thermals". Favourable conditions for dry convection include warm surface temperatures, uneven surface hearing, and steep surface-based lapse rates.
Convective currents are often strong enough to produce air mass thunderstorms with which severe turbulence is associated. Turbulence can also be expected in the lower levels of a cold air mass that is moving over a warm surface. Heating from below creates unstable conditions, gusty winds and bumpy flying conditions.

Thermal turbulence will have a pronounced-effect on the flight path of an airplane approaching a landing area. The airplane is subject to convective currents of varying intensity set in motion over the ground along the approach path. These thermals may displace the airplane from its normal glide path with the result that it will either overshoot or undershoot the runway. Below **figure 8.5** shows Thermal (Convective) Turbulence.

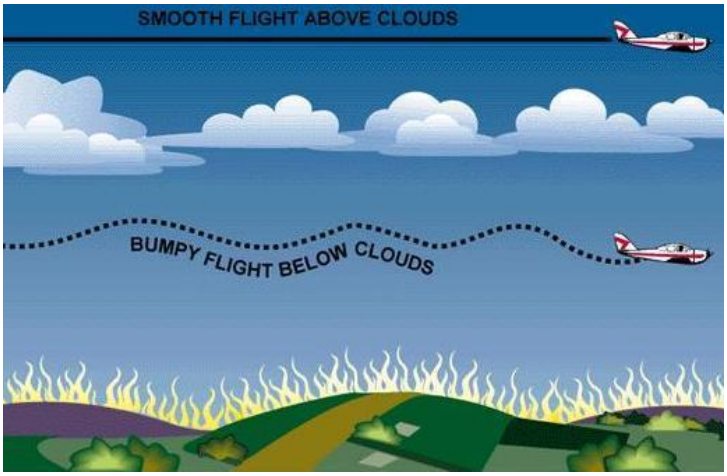

Figure 8.5 Thermal (Convective) Turbulence

3. **Frontal Turbulence**- The lifting of the warm air by the sloping frontal surface and friction between the two opposing air masses produce turbulence in the frontal zone. This turbulence is most marked when the warm air is moist and unstable and will be extremely severe if thunderstorms develop. Turbulence is more commonly associated with cold fronts but can be present, to a lesser degree, in a warm front as well. Below **figure 8.6** shows Frontal Turbulence.

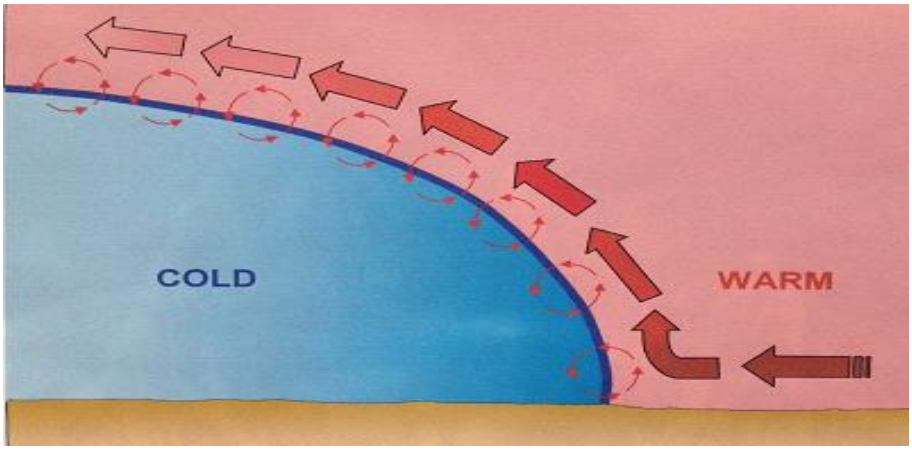

Figure 8.6 Frontal Turbulence

4. Wind Shear- Wind shear is the change in wind direction and/or wind speed over a specific horizontal or vertical distance. Atmospheric conditions where wind shear exists include: areas of temperature inversions, along troughs and lows, and around jet stream. When the change in wind speed and direction is pronounced, quite severe turbulence can be expected. Clear air turbulence is associated at high altitudes (i.e., above 15,000 feet AGL) with the jet stream.
Temperature inversions are zones with vertical wind shear potential. Strong stability prevents mixing of the stable low layer with the warmer layer above. The greatest shear, and thus the greatest turbulence, is found at the tops of the inversion layer. Turbulence associated with temperature inversions often occur due to radiational cooling, which is night time cooling of the Earth's surface, creating a surface-based inversion.
Turbulence associated with lows and troughs is due mainly to horizontal directional and speed shear. Turbulence is generally found along troughs at any altitude, within lows at any altitude, and pole ward of lows in the mid and upper altitudes.
A jet stream is core of strong horizontal winds that follows a wavelike pattern as a part of the general wind flow. It is located where there are large horizontal differences in temperature between warm and cold air masses. Turbulence is located along strong isotach gradient zones. Most often, turbulence is located on pole ward side of cyclonic jet stream. Conversely, turbulence is often located on equator ward side of the anti-cyclonic jet stream. Turbulence is enhanced by an "arching" (amplified) jet stream around troughs and ridges. Below **figures 8.7 and 8.8** shows Wind Shear.

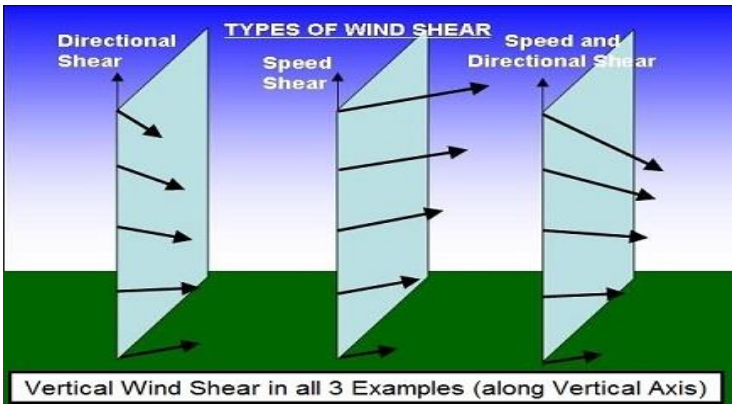

Figure 8.7 Wind Shear

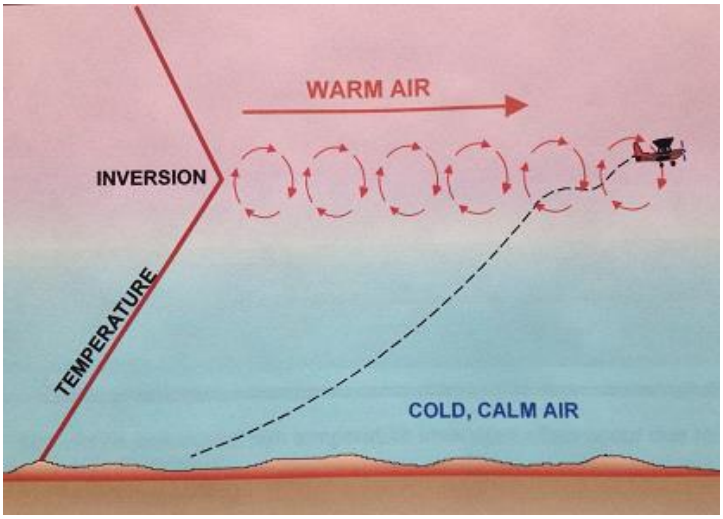

Figure 8.8 Wind Shear

CLEAR AIR TURBULENCE

Clear air turbulence is turbulence not associated with cumuli form clouds, including thunderstorms, occurring at or above 15,000 feet. Clear air turbulence is not restricted to cloud-free air (75% of all CAT encounters are in clear air).

General characteristics of clear air turbulence include:

1. Occurs in patches
2. Area is elongated with the wind
3. Usually found above 15,000 feet
4. In association with a marked change in speeds:
   » with height (vertical shear)
   » or in the horizontal (horizontal shear)
5. 2,000 feet deep
6. 20 miles wide
7. 50 miles long
8. Transitory
9. Most frequent during winter
10. Least frequent during summer

CAT areas at high-levels are usually patchy, and these patches have variable dimensions which have been known to be as much as 10,000 feet thick, 500 miles wide, and 1,000 miles long.

Below **figures 8.9 and 8.10** shows clear air turbulence.

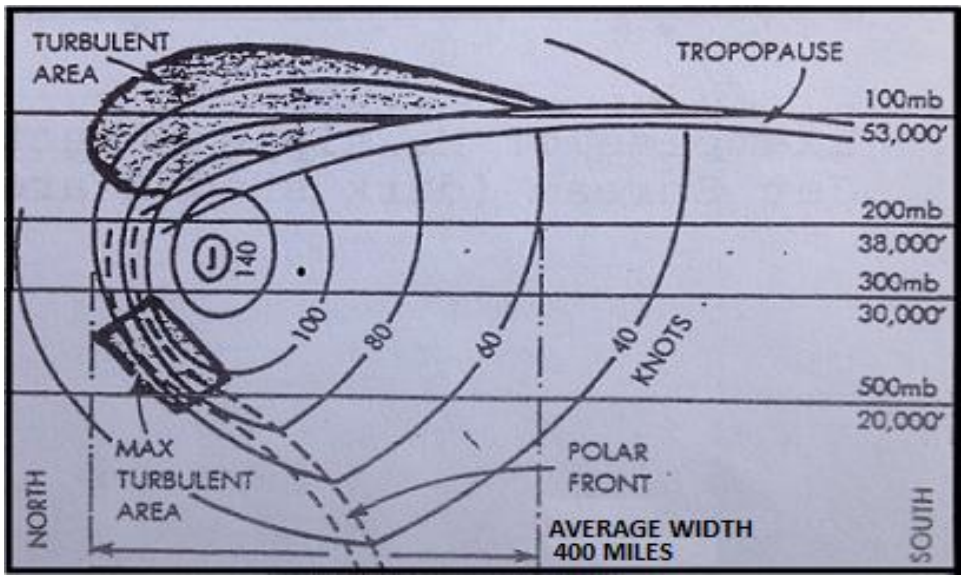

Figure 8.9 Clear air turbulence.

The occurrence of CAT can extend to very high levels and can be associated with other wind flow patterns which produce shears:
a. A sharp upper level trough, especially one moving at speeds greater than 10 knots. (See Figure A. below)
b. A closed low aloft, particularly if the flow is merging or splitting (See Figure B. below)
c. To the northeast of a cut off low aloft as shown in Figure C. below

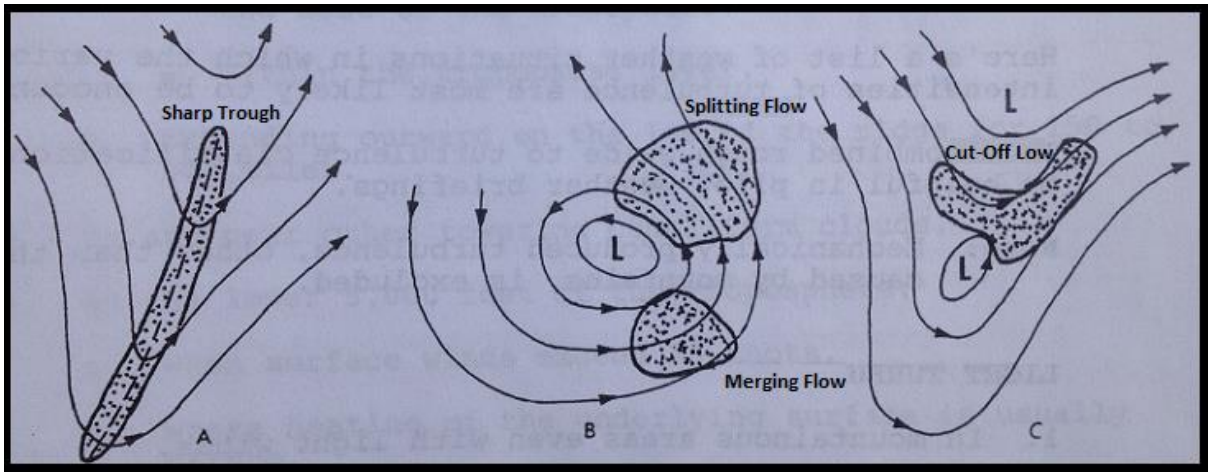

Figure 8.10 Clear air turbulence.

TURBULENCE AND THUNDERSTORMS

Turbulence, associated with thunderstorms, can be extremely hazardous, having the potential to cause over stressing of the aircraft or loss of control. Thunderstorm vertical currents may be

strong enough to displace an aircraft up or down vertically as much as 2000 to 6000 feet. The greatest turbulence occurs in the vicinity of adjacent rising and descending drafts. Gust loads can be severe enough to stall an aircraft flying at rough air (man-euvering) speed or to cripple it at design cruising speed. Maximum turbulence usually occurs near the mid-level of the storm, between 12,000 and 20,000 feet and is most severe in clouds of the greatest vertical development.

Severe turbulence is present not just within the cloud. It can be expected up to 20 miles from severe thunderstorms and will be greater downwind than into wind. Severe turbulence and strong out-flowing winds may also be present beneath a thunderstorm. Micro bursts can be especially hazardous because of the severe wind shear associated with them. Below **figure 8.11** shows turbulence and thunderstorms.

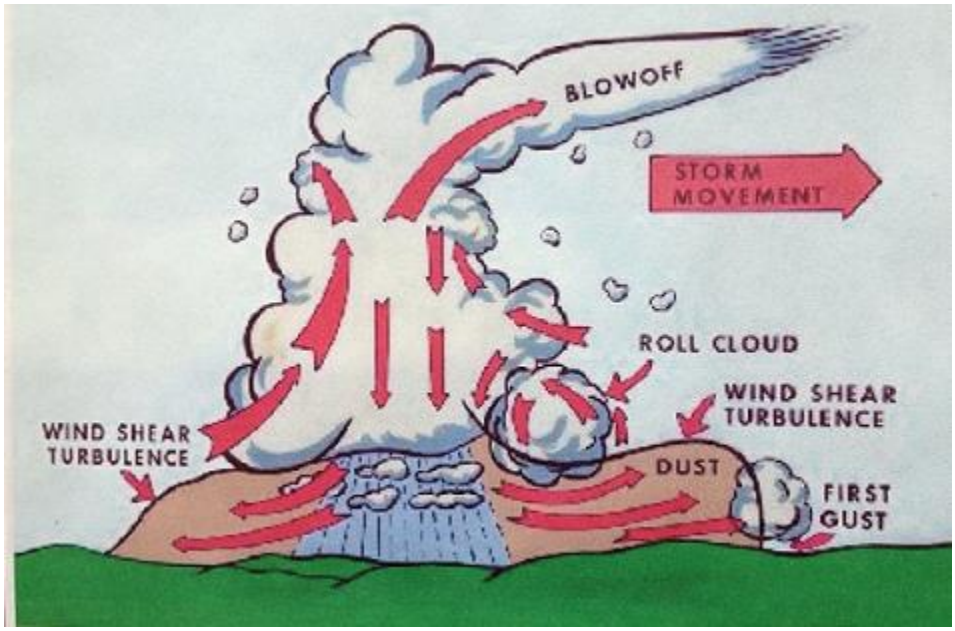

Figure 8.11 turbulence and thunderstorms

Impacts from Turbulence and Friction on Winds

Below **figure 8.12** shows that Lee waves cause updrafts and downdrafts .

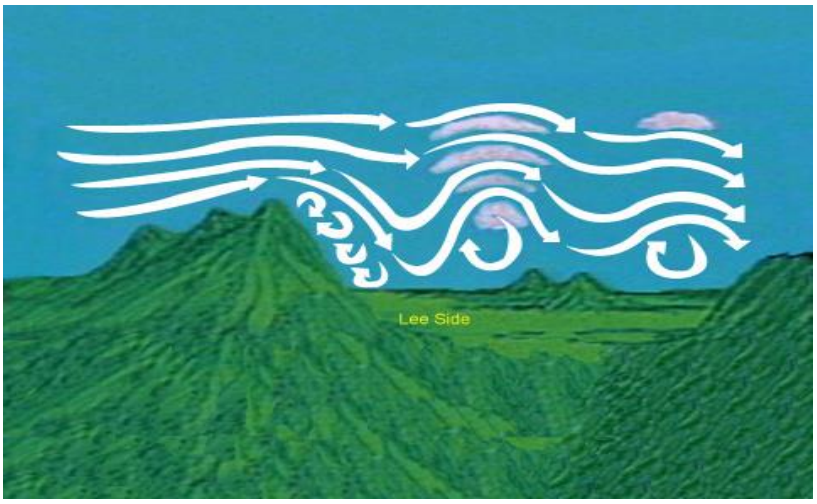

Figure 8.12 Lee waves cause updrafts and downdrafts

We'll give you a series of illustrations on how general winds are modified to help produce surface winds. The figure above illustrates the lee slope, eddy effects on a much larger scale. Tall mountain ranges can modify strong winds aloft to create waves and large eddies on the lee side of the mountains. Winds dip down due to the difference in pressure on the lee side, thus initiating wave actions in those strong winds. Lens-shaped clouds (altocumulus lenticulars) may develop in the tops of these waves. These clouds can easily be formed on the lee side of mountain ranges that are perpendicular to winds of 40 knots or more. The clouds are usually high, and the resulting winds may not be felt at the surface. However, occasionally these strong winds aloft may dip to the surface, or eddy winds may reverse the direction of usual winds. Depending on your location, surface winds can be significantly modified by this process.
Friction and air turbulence generated at the surface slow low level winds. There are two sources of turbulence--mechanical and thermal. The roughness of surfaces, usually due to vegetative cover, causes friction and results in mechanical turbulence. Surface heating during the day causes thermal turbulence as heat convection currents rise from the surface and mix with the air flowing over the surface.
Let's look at some effects of channelling and mechanical turbulence. Imagine a general wind blowing through a pass or saddle in a mountain range. Wind velocities might increase as they pass through the constricted area; then the air spreads out on the lee side with probable eddy actions.
Winds on the lee sides of ridges can shift in direction and speed, making them difficult to predict. We usually term eddy winds as gusty and erratic. Below **figure 8.13 and 8.14** shows that Lee waves cause updrafts and downdrafts .

Figure 8.13

Vegetation may also cause updrafts and downdrafts

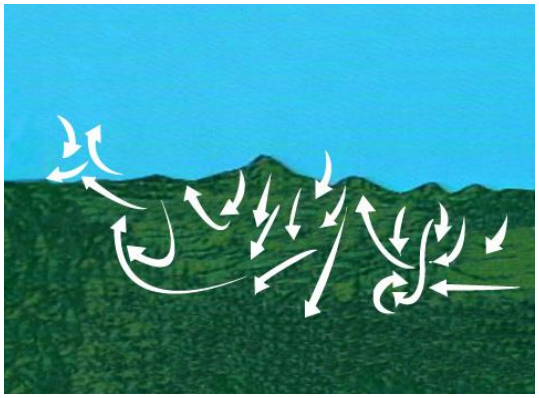

Figure 8.14

Thermal turbulence caused by surface heating

Another factor which has a great deal of effect on low level wind is thermal turbulence caused by surface heating. (See figure above) Different land surfaces absorb, reflect, and radiate varying amounts of heat. Warm air rises and mixes with other air moving across the terrain. This mixing action has differing effects on surface winds, but often makes them gusty and erratic. Below **figure 8.15** shows that relationship between mechanical and thermal turbulence with modifies winds at the surface.

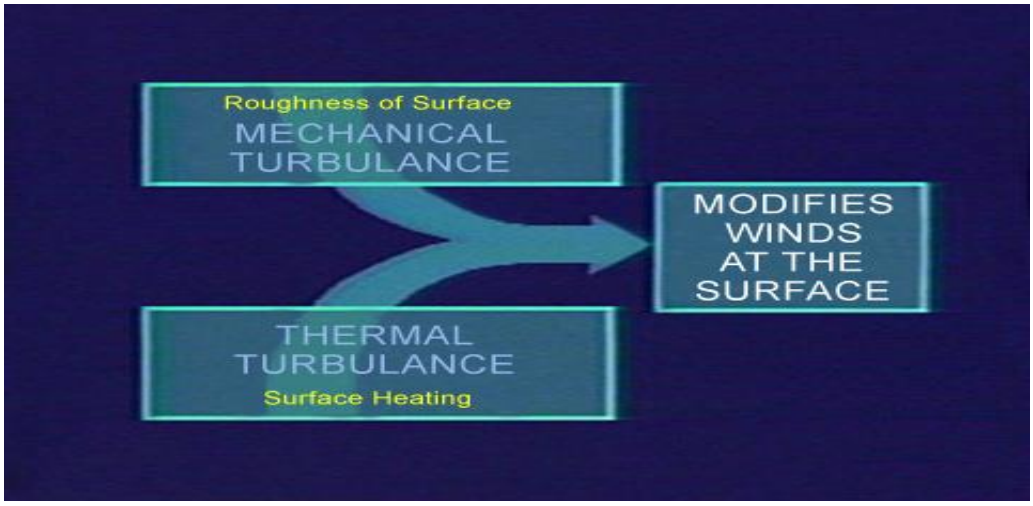

Figure 8.15 Relationship between mechanical and thermal turbulence with modifies winds at the surface.

Source
(https://www.weather.gov/source/zhu/ZHU_Training_Page/turbulence_stuff/turbulence/Wind_Shear.png)

Methodology

Viscosity and Laminar Flow

The precise definition of viscosity is based on laminar, or non-turbulent, flow. **Figure 8.16 (a) , (b)** shows schematically how laminar and turbulent flow differ. When flow is laminar, layers flow without mixing. When flow is turbulent, the layers mix, and significant velocities occur in directions other than the overall direction of flow.

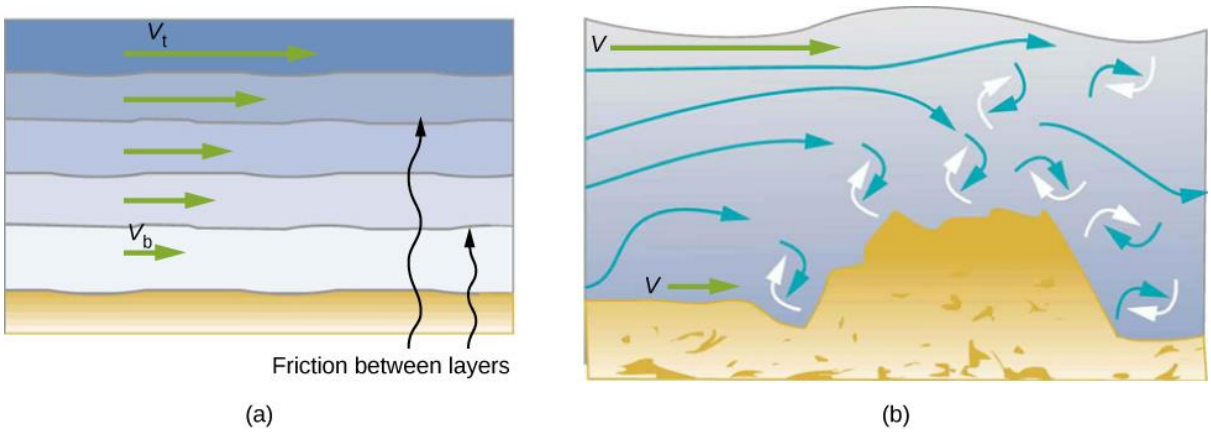

Figure 8.16 (a) Laminar flow occurs in layers without mixing. Notice that viscosity causes drag between layers as well as with the fixed surface. The speed near the bottom of the flow (v_b) is less than speed near the top (v_t) because in this case, the surface of the containing vessel

is at the bottom **(b)** An obstruction in the vessel causes turbulent flow. Turbulent flow mixes the fluid. There is more interaction, greater heating, and more resistance than in laminar flow.

Source (https://courses.lumenlearning.com/suny-osuniversityphysics/chapter/14-7-viscosity-andturbulence/#:~:text=The%20pressure%20drop%20caused%20by,2%20%CF%81%20v%20r%20%CE%B7%20)

Measuring Turbulence

An indicator called the Reynolds number N_R can reveal whether flow is laminar or turbulent. For air flow in the atmosphere with unit radius, the Reynolds number is defined as

$N_R = 2\rho vr / \eta$ (flow in air)

Where, ρ is the air density, v its wind speed of air, η its viscosity of air, and r the radius of air. The Reynolds number is a dimensionless quantity. Experiments have revealed that N_R is related to the onset of turbulence. For N_R below about 2000, flow is laminar. For N_R above about 3000, flow is turbulent.

For values of N_R between about 2000 and 3000, flow is unstable—that is, it can be laminar, but small obstructions and surface roughness can make it turbulent, and it may oscillate randomly between being laminar and turbulent. In fact, the flow of a air with a Reynolds number between 2000 and 3000 is a good example of chaotic behavior. A system is defined to be chaotic when its behavior is so sensitive to some factor that it is extremely difficult to predict. It is difficult, but not impossible, to predict whether flow is turbulent or not when a fluid's Reynolds number falls in this range due to extremely sensitive dependence on factors like roughness and obstructions on the nature of the flow. A tiny variation in one factor has an exaggerated (or nonlinear) effect on the flow.

Source (https://courses.lumenlearning.com/suny-osuniversityphysics/chapter/14-7-viscosity-andturbulence/#:~:text=The%20pressure%20drop%20caused%20by,2%20%CF%81%20v%20r%20%CE%B7%20)

Calculation

Let the flow of the air taken vertical direction. Assume that,

ρ is the air density = 1 Kg / m^3, v its wind speed = 1 Knot = 0.514 m / s.

η its viscosity of air = 1.8 x 10^{-5} Kg / m.s, r the radius of air = 1 m.

N_R = 57,111

N_R > 4000

It indicates turbulent flow of the air due to high Reynolds number.

Result and Discussion

Below **Tables 8.1** and **8.2** shows that, at 00 UTC and 12 UTC on 17th April 2022 over Kolkata region of wind speed data of the air and also shows that Reynolds number of the thunderstorm day.

Table 8.1 Thunderstorm day on 17th April 2022 at 12 UTC over Kolkata region

hPa (Atmospheric Pressure)	Knot (Wind speed)	N_R (Reynolds number)
1000	6	342666
925	10	571110
850	8	456888
700	13	742443
600	15	856665
500	29	1656219
400	38	2170218
300	66	3769326
200	58	3312438
100	31	1770441

Table 8.2 Thunderstorm day on 17th April 2022 at 00 UTC over Kolkata region

hPa (Atmospheric Pressure)	Knot (Wind speed)	N_R (Reynolds number)
1000	4	228444
925	15	856665
850	21	1199331
700	14	799554
600	19	1085109
500	27	1541997
400	41	2341551
300	68	3883548
200	58	3312438
100	31	1770441

The above results show that high value of Reynolds number during thunderstorm day. The Reynolds number value is very high at different atmospheric pressure level. It indicate that high turbulent characteristics exist at different atmospheric pressure level. In atmosphere high turbulent exist during thunderstorm day.

Figures 8.17 and **8.18** shows that, at 00 UTC and 12 UTC on 17th April 2022 over Kolkata region of wind speed graph of the air during thunderstorm day. **Figures 8.19** and **8.20** shows that, at 00 UTC and 12 UTC on 30th April 2022 over Kolkata region of wind speed graph of the air during non- thunderstorm day. **Tables 8.3** and **8.4** shows that, at 00 UTC and 12 UTC on 30th April 2022 over Kolkata region of wind speed data of the air and also shows that Reynolds number of the non-thunderstorm day. Figures 8.17 to 8.20 show that wind speed increase 1000 hPa to 300 hPa, after 300 hPa to 100 hPa wind speed decreases.

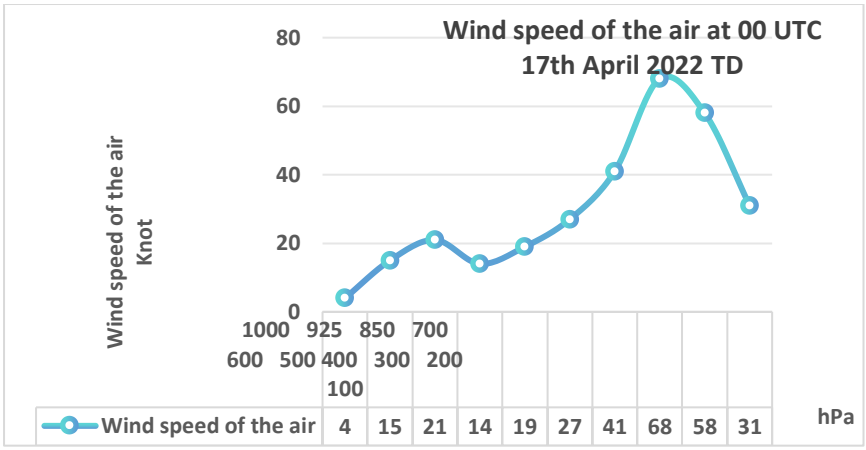

Figure 8.17 Wind speed of the air at 00 UTC over Kolkata region on 17th April 2022 during thunderstorm day.

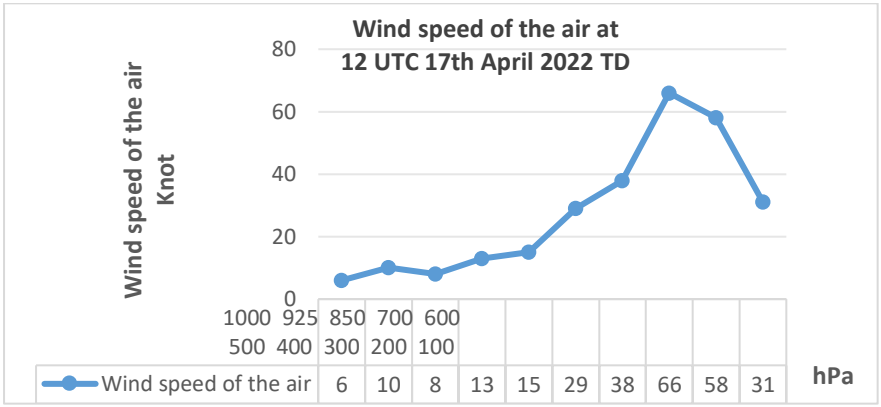

Figure 8.18 Wind speed of the air at 12 UTC over Kolkata region on 17th April 2022 during thunderstorm day.

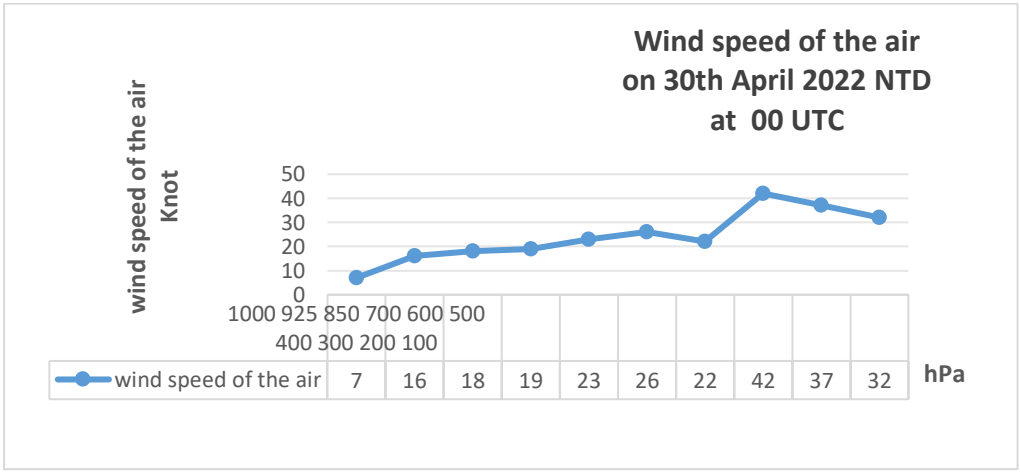

Figure 8.19 Wind speed of the air at 00 UTC over Kolkata region on 30th April 2022 during

Non- thunderstorm day.

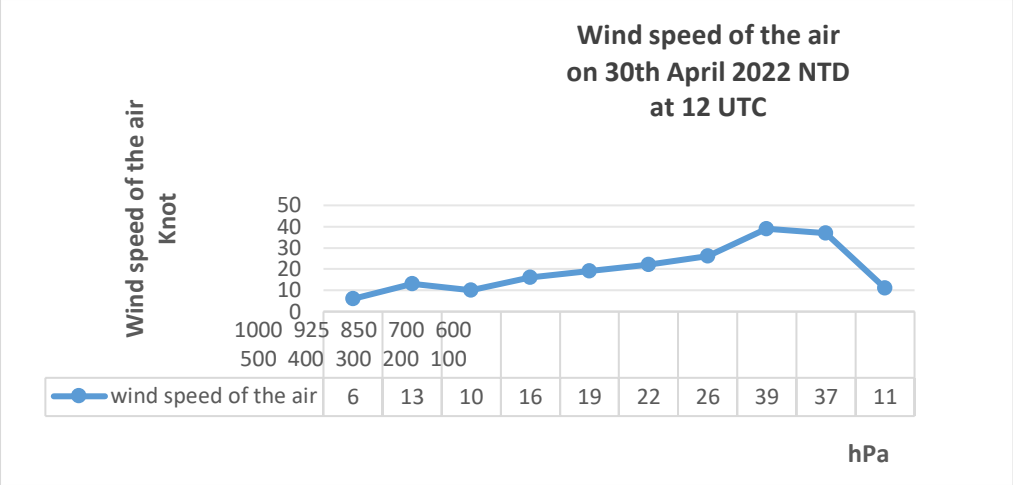

Figure 8.20 Wind speed of the air at 12 UTC over Kolkata region on 30th April 2022 during Non- thunderstorm day.

Table 8.3 Non - Thunderstorm day on 30th April 2022 at 12 UTC over Kolkata Region

hPa (Atmospheric Pressure)	Knot (Wind speed)	N_R (Reynolds number)
1000	6	342666
925	13	742443
850	10	571110
700	16	913776
600	19	1085109
500	22	1256442
400	26	1484886
300	39	2227329
200	37	2113107
100	11	628221

Table 8.5 shows that temperature, relative humidity, dew-point temperature and mixing ratio on 17th April 2022 at 00 UTC during thunderstorm day. **Figure 8.21, 8.22** and **8.23** shows that relative humidity, mixing ratio and dew-point temperature vs temperature on 17th April 2022 at 00 UTC during thunderstorm day.

Table 8.4 Non -Thunderstorm day on 30th April 2022 at 00 UTC Kolkata Region

hPa (Atmospheric Pressure)	Knot (Wind speed)	N_R (Reynolds number)
1000	7	399777
925	16	913776
850	18	1027998
700	19	1085109
600	23	1313553
500	26	1484886
400	22	1256442
300	42	2398662
200	37	2113107
100	32	1827552

The above results show that high value of Reynolds number during non-thunderstorm day. The Reynolds number value is very high at different atmospheric pressure level. It indicate that high turbulent characteristics exist at different atmospheric pressure level. In atmosphere high turbulent exist during non-thunderstorm day.

Table 8.5 Thunderstorm day on 17th April 2022 at 00 UTC over Kolkata Region

PRES hPa	TEMP C	DWPT C	RELH %	MIXR g/kg
1000	27.6	23.8	80	18.98
925	31.4	14.4	36	11.27
850	25.2	11.2	41	9.92
700	10.8	2.8	58	6.73
600	-0.9	-5.4	72	4.29
500	-8.1	-32.1	13	0.52
400	-18.7	-47.7	6	0.13
300	-32.7	-37.4	63	0.51
200	-49.7	-69.7	8	0.02
100	-77.1	-89.1	13	0

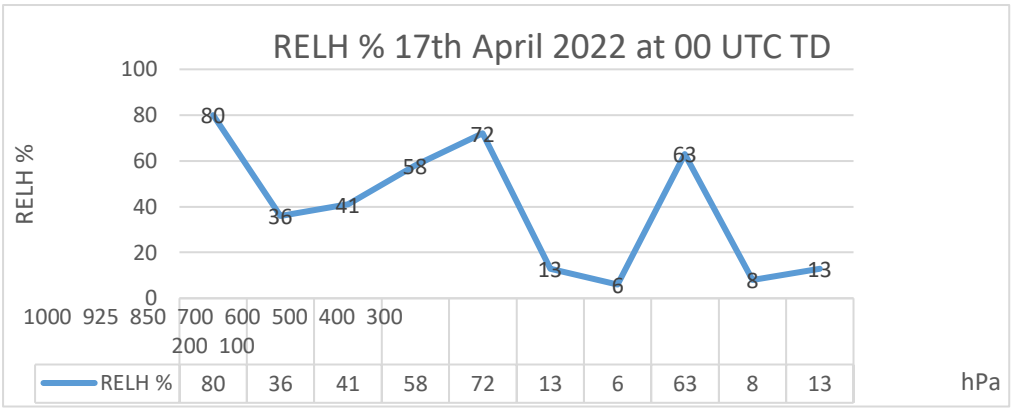

Figure 8.21 Relative humidity of the air at 00 UTC over Kolkata region on 17th April 2022 during thunderstorm day.

The above **figure 8.21** shows that relative humidity values fluctuate at different atmospheric pressure level.

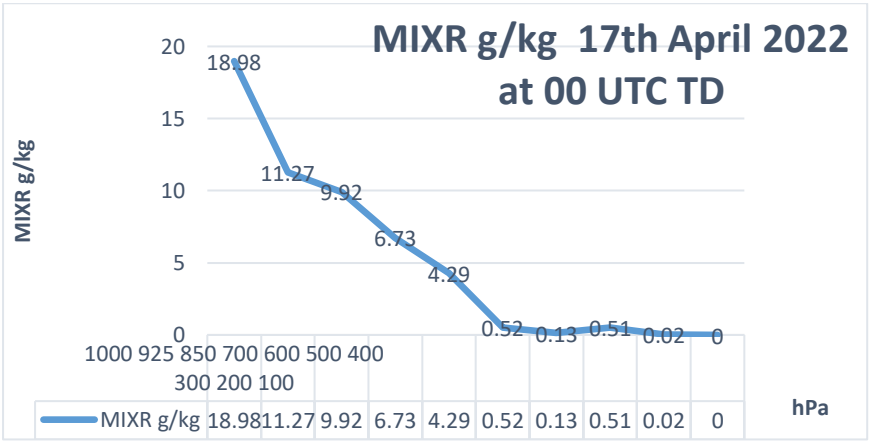

Figure 8.22 Mixing ratio of the air at 00 UTC over Kolkata region on 17th April 2022 during thunderstorm day.

The above **figure 8.22** shows that mixing ratio decreases from 1000 hPa to 500 hPa, after that it becomes tends to zero.

The **figure 8.23** shows that temperature and dew-point temperature decreases from 1000 hPa to 100 hPa and from 700 hPa to 100 hPa that values become negative.

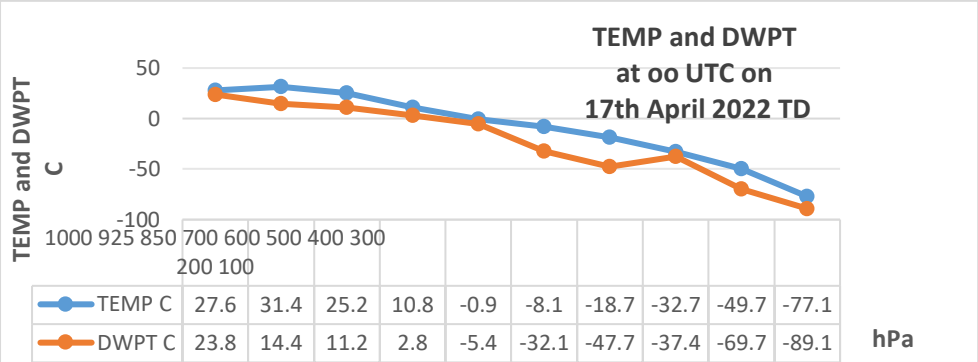

Figure 8.23 Temperature vs Dew-point Temperature of the air at 00 UTC over Kolkata region on 17th April 2022 during thunderstorm day.

CONCLUSIONS

On the basis of this study, following conclusions can be drawn.

1. In the atmosphere, during thunderstorm and non-thunderstorm days high turbulent observed. It means that all time turbulent characteristics exist in the atmosphere.

2. The relative humidity values fluctuate at different atmospheric pressure level.

3. The mixing ratio decreases from 1000 hPa to 500 hPa, after that it becomes tends to zero.

4. The temperature and dew-point temperature decreases from 1000 hPa to 100 hPa and from 700 hPa to 100 hPa that values become negative.

Chapter – 9

Conclusion

Conclusions and Recommendations

Conclusions On the basis of the present study, following conclusions can be drawn:

1. Nor'westers occur when there is low-level moist air flow from the south and cold and dry air flow from the northwest in the middle troposphere.

2. Instability indices in the troposphere were favourable for the occurrence of severe Nor'westers / thunderstorms.

3. CAPE increases significantly during the formation of Nor'westers and becomes insignificant after the occurrence of Nor'westers. The values of CAPE at 1200 UTC over Kolkata were 4175.20 J kg-1, 4067.39 J kg-1, and 3846.89 J kg-1 on 17th April, 19th May and 2oth May 2022 respectively and the value was 2558.06 J kg-1, 2717.73 J kg-1 and 2479.43 J kg-1 at 0000 UTC on 17th April, 19th May and 2oth May 2022 respectively over Kolkata.

4. Bulk Richardson Number (BRN) increases significantly during the formation of Nor'westers and becomes insignificant after the occurrence of Nor'westers. The BRN values indicate that the Nor'westers were associated with super cells and higher turbulence.

5. The mixing ratios are higher in the lower troposphere and decrease with height extending up to 400 hPa and become zero at the top of the troposphere. There exists a variation in mixing ratio between 0000 UTC and 1200 UTC, but mixing ratio is found to increase specially in the lower troposphere either at 0000 UTC or 1200 UTC on the dates of occurrence of Nor'westers. It decreases after the occurrence of the storms. During thunderstorms day high Reynolds number observed. It indicate high turbulent in the atmosphere.

6. The Precipitable water content of the troposphere varies from one Nor'westers to another. But it is found that Precipitable water contents of the troposphere are 40.59 mm, 54.34 mm, 56.58 mm and 55.92 mm at 1200 UTC on 17th April 2022, 1200 UTC on 3rd May 2022, 1200 UTC on 17th May 2022 and 1200 UTC on 19th May 2022. But it is found that Precipitable water contents of the troposphere are 55.93 mm and 61.15 mm 0000 UTC on 22nd April 2022, 0000 UTC on 13th May 2022 respectively.

7. The model is able to simulate the physical and dynamical parameters well with sufficient lead time but about 4-7 hours before the actual time of occurrence of Nor'westers.

8. NCMRWF model is able to simulate rainfall associated with Nor'westers quite well but not at the specific location where the rainfall occurs. The convection is found to move in the east-southeast or east-northeast, differing from one storm to another.

9. Low pressure is simulated in the West Bengal is found to intensify during the formation and occurrence of Nor'westers.

10. The model has simulated strong south-south-westerly flow and circulation at 4 m as well as at 950 hPa level on the dates of occurrence of Nor'westers over Kolkata. In most cases, the

model is able to capture maximum wind speed at 4m level but the values are not location specific.

11. A zone of minimum relative humidity simulated by NCMRWF model is found to exist at 4 m level over West Bengal and adjoining western Bangladesh and high relative humidity exists over north-eastern /eastern Bangladesh on the dates of occurrence of Nor'westers.

12. The vertical time cross-section of relative humidity simulated by NCMRWF model reveals that the lower atmosphere up to about 600 hPa remains very humid on the dates of occurrence of Nor'westers. In most of the cases, an atmospheric window is found through which moisture rises upwards up to about 200 hPa level or more near the time of occurrence of Nor'westers in Kolkata.

13. The surface Vorticity (Level Vorticity > 15 x 10-5 /s) simulated by NCMRWF model (based on 00 UTC) (4 Km) is found to be positive and increases during the time of occurrence of Nor'westers over Kolkata.

14. The surface Convergence at 850 hPa (Level Convergence > 15 x 10-5/s) simulated by NCMRWF model (based on 00 UTC) (4 Km) is found to be positive and increases during the time of occurrence of Nor'westers over Kolkata.

15. On the dates of occurrence of Nor'westers, pockets of positive vertical velocity simulated by NCMRWF model are found to exist in the morning and this vertical velocity becomes prominent with progress of the day and the time of occurrence of the storms. The updrafts and downdrafts are present in the atmosphere on the dates of occurrence of nor'westers.

16.The local people informed that Nor'westers, in addition to causing loss of the ecosystem of the area, causes lots of economic sufferings due to damages of the houses, plants, fruit gardens, forests and agricultural crops. It was further informed that this area is usually vulnerable to thunderstorms and hailstorms, which cause economic loss. During FGD, awareness points regarding the impact of thunderstorms/nor'westers were discussed for saving the lives of people and livestock.

17. All respondents mentioned that the intensity of Nor'westers has increased tremendously and as a result a number of people are being killed due to lightning and thunder of Nor'westers. Because of the increase in intensity, trees are broken, tops of trees are twisted off, trees and electric poles are uprooted, crops and fruits are damaged due to large hails associated with nor'westers. Livestock are also killed.

18. According to the respondents, there is climate change in the form of increase of temperature, precipitation and the frequency of natural disasters. The changes have been perceivable for the last 10-20 years. It is seen that the agriculture sector is most vulnerable to climate change and ensuing disasters.

19. During thunderstorm day at 00 Z , Wet Microburst Sounding shaped observed on 17th April 2022, 29th April 2022 and 17th May 2022 , Lower Level Zet Sounding observed on 21st April 2022 and 20th May 2022, Wet bulb Sounding observed on 22nd April 2022 and 13th May 2022, on 21st April 2022 elevated convection sounding observed.

20. During thunderstorm day at 12 Z , Wet Microburst Sounding shaped observed on 17th April 2022, 22nd April 2022 and 13th May 2022 , Lower Level Zet Sounding observed on 21st April 2022, 17th May 2022 and 20th May 2022, elevated convection sounding observed 19th May 2022.

21. During non-thunderstorm day at 00 Z , Wet Microburst Sounding shaped observed on 20th April 2022, 2nd May 2022, 12th May 2022, 18th May 2022, 22nd May 2022 and 23rd May 2022, Lower Level Zet Sounding observed on 16th April 2022, 28th April 2022 and 16th May 2022, Morning inversion Sounding observed on 19th April 2022, 23rd April 2022 and 30th April 2022, Wet bulb Sounding observed on 2nd May 2022 and Loaded Gun Sounding observed on 4th May 2022.

22. During non-thunderstorm day at 12 Z , Wet Microburst Sounding shaped observed on 16th April 2022, 19th April 2022, 20th April 2022, 12th May 2022, 16th May 2022, 22nd May 2022 and 23rd May 2022, Dry Sounding observed on 18th April 2022 and 23rd April 2022, Lower Level Zet Sounding observed on 28th April 2022, 30th April 2022, 2nd May 2022 and 4th May 2022 and Elevated Convection Sounding observed on 18th May 2022.

Recommendations

• More investigations should be made on thunderstorms/Nor'westers to remove the time lag and location error in forecasting the physical and dynamical characteristics of thunderstorms/Nor'westers.

• Proper awareness campaign should be made among the people in different parts of Kolkata regarding the impact of Nor'westers and climate change, and to save the lives of people.

• Now casting of Nor'westers is essential during the time of formation and their movement from IMD, for which a TV studio is necessary in IMD so that the Meteorologists cast the instantaneous forecast of Nor'westers/thunderstorms with their intensity, movement, areas of impact, squalls and gusty winds, which can surely save the lives of the people under storm threats.

Chapter - 10

REFERENCES

Akram, M.H. and Karmakar, S., 1998. Some meteorological aspects of the Saturia tornado, 1989 - A case study. Journal of Bangladesh Academy of Sciences, 22, 1, pp. 109-122.

Ananthakrishnan R., Marry Selvan M., and Chellappa R., 1965. Seasonal variation of precipitable water vapor in the atmosphere over India. Indian J. Met. & Geophysics., 16, 3, pp. 371-384.

Awdesh et al., 1992. A Climatological Study Of Thunder Storms At Lucknow Airport, Mausam - mausamjournal.imd.gov.in

Barlow, W., 1993. A new index for the prediction of deep convection. In: 17th conference on severe local storms, St., Louis, MO. Amer. Meteorol. Soc., pp., 129-132.

Barros, A. P., Joshi, M., Putkonen, J., & Burbank, D. W., 2000. A study of the 1999 monsoon rainfall in a mountainous region in central Nepal using TRMM products and rain gauge observations. Geophysical research letters, 27(22), 3683-3686.

Barros, A. P., & Lang, T. J., 2003. Monitoring the monsoon in the Himalayas: Observations in central Nepal, June 2001. Monthly Weather Review, 131(7), 1408-1427.

Barros, A. P., 2004. On the space-time patterns of precipitation in the Himalayan range: a synthesis. GAME CD ROM Publ, (11), T8APB19Oct04100318.

Barros, A.P., Kim, G., Williams, E., and Nesbitt, S.W., 2004. Probing orographic controls in the Himalayas during the monsoon using satellite imagery: Natural Hazards and Earth Systems Science, v. 4, p. 1–23.

Basu, S., Basu, S., Rich, F. J., Groves, K. M., MacKenzie, E., Coker, C., & Becker-Guedes, F., 2007. Response of the equatorial ionosphere at dusk to penetration electric fields during intense magnetic storms. Journal of Geophysical Research: Space Physics, 112(A8).

Basu, B.K., 2007. Diurnal variation in precipitation over India during the summer

monsoon season: Observed and model predicted. Monthly weather review, 135(6), pp.2155-2167.

Bechtold, P., Chaboureau, J. P., Beljaars, A., Betts, A. K., Köhler, M., Miller, M., & Redelsperger, J. L., 2004. The simulation of the diurnal cycle of convective precipitation over land in a global model. Quarterly Journal of the Royal Meteorological Society: A journal of the atmospheric sciences, applied meteorology and physical oceanography, 130(604), 3119-3137.

Bera, S., 2017. Trend analysis of rainfall in Ganga Basin, India during 1901-2000. American Journal of Climate Change, 6(01), p.116.

Bhattacharya, A. B., Datta, B. K., & Bhattacharya, R., 1994. Some distinct effects of tropical monsoon clouds as derived from atmospherics. Theoretical and applied climatology, 50, 83-92.

Bidner, A., 1970. The Air Force Global Weather Central Severe Weather Threat (SWEAT) index - A preliminary report. Air Weather Service Aerospace Sciences Review, AWS RP 105-2, No 70-3, 2-5.

Bidner, A., 1970. The Air Force Global Weather Central Severe Weather Threat (SWEAT) index - A preliminary report. Air Weather Service Aerospace Sciences Review, AWS RP 105-2, No 70-3, 2-5.

Bissolli, P., Grieser, J., Dotzek, N., & Welsch, M., 2007. Tornadoes in Germany 1950–2003 and their relation to particular weather conditions. Global and Planetary Change, 57(1-2), 124-138.

Bhatt, B.C. and Nakamura, K., 2005. Characteristics of monsoon rainfall around the Himalayas revealed by TRMM precipitation radar. Monthly Weather Review, 133(1), pp.149 - 165.

Bhatt, B.C. and Nakamura, K., 2006. A climatological-dynamical analysis associated with precipitation around the southern part of the Himalayas. Journal of Geophysical Research: Atmospheres, 111(D2).

Boyden, C., 1963. A simple instability index for use as a synoptic parameter. Meteorol. Mag., 92, 198-210.

Bright, D. R., & Mullen, S. L., 2002. The sensitivity of the numerical simulation of the southwest monsoon boundary layer to the choice of PBL turbulence parameterization in MM5. Weather and Forecasting, 17(1), 99-114.

Browning, K. A., Collier, C. G., Larke, P. R., Menmuir, P., Monk, G. A., & Owens, R. G., 1982. On the forecasting of frontal rain using a weather radar net work. Monthly Weather Review, 110(6), 534-552.

Buytaert et al., 2006**.** Spatial and temporal rainfall variability in mountainous areas: in mountainous areas: **A** case study from the south Ecuadorian Andes - Elsevier

Brier, G., W. and Allen, R., A., 1952. Verification of weather forecasts. Compendium of Meteorology. Amer. Meteor. Soc., pp. 841-848.

Cecil, D. J., & Blankenship, C. B., 2012. Toward a global climatology of severe hailstorms as estimated by satellite passive microwave imagers. Journal of Climate, 25(2), 687-703.

Chakraborty, A., Nanjundiah, R. S., & Srinivasan, J., 2014. Local and remote impacts of direct aerosol forcing on Asian monsoon. International journal of climatology, 34(6), 2108 - 2121.

Chakraborty, H., & Bhattacharya, S., 2015. Application of K-nearest neighbor technique to predict severe thunderstorms. International Journal of Computer Applications, 110 (10), 1 - 4.

Chan, P. W., 2009. Performance and application of a multi-wavelength, ground-based microwave radiometer in intense convective weather. Meteorologische Zeitschrift, 18(3), 253.

Chan, P. W. and Lee, Y. F., 2011. Application of a ground-based, multichannel microwave radiometer to the alerting of low-level windshear at an airport, Meteorol. Z., 20, 423–429.

Chakraborty, T., Pattnaik, S., Vishwakarma, V. and Baisya, H., 2021. Spatio-temporal Variability of pre-monsoon convective events and associated rainfall Over the State of Odisha (India) in the recent decade. Pure and Applied

Geophysics, 178(11), pp.4633 - 4649.

Choudhury, B. A., Konwar, M., Hazra, A., Mohan, G. M., Pithani, P., Ghude, S. D., ... & Barth, M. C., 2020. A diagnostic study of cloud physics and lightning flash rates in a severe pre-monsoon thunderstorm over northeast India. Quarterly Journal of the Royal Meteorological Society, 146(729), 1901-1922.

Chatterjee, P., De, U.K. and Pradhan, D., 2015. Simulation of severe local storm by Mesoscale model MM5 and validation using data from different platforms. International Journal of Atmospheric Sciences, 2015.

Chaudhury, A. K., 1961. Premonsoon thunderstorms in Assam, Tripura and Manipur. Indian J. Meteorol. Geophys., 12, 1, 33–36.

Chowdhury, M. H. K. and Karmakar, S., 1986. Pre-monsoon Nor'westers in Bangladesh with case studies, Proceedings of the SAARC Seminar on Local Severe Storms, held in 1985 at Dhaka, Bangladesh, published by Bangladesh Meteorological Department, pp. 147 - 166.

Chowdhury, M.H.K., Karmakar, S. and Khatun, A., 1991. A diagnostic study on some aspects of tropospheric energy in relation to nor'westers over Bangladesh. Proceedings of the SAARC Seminar on Severe Local Storms, held in Colombo, Sri Lanka, 7-11 October, 1991, pp. 19 - 33.

Chaudhuri, S. and Middey, A., 2011. Adaptive neuro-fuzzy inference system to forecast peak gust speed during thunderstorms. Meteorology and Atmospheric Physics, 114, pp. 139 - 149.

Chaudhuri, S., Dutta, D., Goswami, S., & Middey, A., 2013. Intensity forecast of tropical cyclones over North Indian Ocean using multilayer perceptron model: Skill and performance verification. Natural Hazards, 65, 97-113.

Chaudhuri, S. and Middey, A., 2013. Disparity in the characteristic of thunderstorms And associated lightning activities over dissimilar terrains. Meteorology and Atmospheric Physics, 119, pp.151-161.

Choudhury, B. A., Konwar, M., Hazra, A., Mohan, G. M., Pithani, P., Ghude, S. D., & Barth,

M. C., 2020. A diagnostic study of cloud physics and lightning flash rates in a severe pre-monsoon thunderstorm over northeast India. Quarterly Journal of the Royal Meteorological Society, 146(729), 1901-1922.

Clifford, D., Gurney, R., & Haines, K. , 2009. Effect of ENSO phase on large-scale snow water equivalent distribution in a GCM. Journal of climate, 22(23), 6153 - 6167.

Cluckie, I. D., Tilford, K. A., & Shepherd, G. W., 1991. Radar signal quantization and its Influence on rainfall-runoff models. Hydrological Applications of Weather Radar, edts. ID Cluckie, CG Collier, Ellis Horwood, 440 - 451.

Collier, J.C. and Bowman, K.P., 2004. Diurnal cycle of tropical precipitation in a general Circulation model. Journal of Geophysical Research: Atmospheres, 109(D17).

Collins, W. G., & Tissot, P., 2016. Thunderstorm predictions using artificial neural networks. Artificial Neural Networks-Models and Applications, 252 - 287.

Dai, A., 2001. Global precipitation and thunderstorm frequencies. Part I: Seasonal and interannual variations. Journal of climate, 14(6), pp. 1092 - 1111.

Darkow, G. L., 1968. The total energy environment of severe storms. Journal of Applied Meteorology and Climatology, 7(2), 199 - 205.

Dasgupta, S., & De, U. K., 2007. Binary logistic regression models for short term prediction of premonsoon convective developments over Kolkata (India). International Journal of Climatology: A Journal of the Royal Meteorological Society, 27(6), 831-836.

Das, R. C., Munim A. A., Begum, Q. N. and Karmakar, S., 1994. A Diagnostic study on some local severe storms over Bangladesh. Journal of Bangladesh Academy of Sciences, 18, 1, pp. 81 - 92.

Das, L., Annan, J. D., Hargreaves, J. C., & Emori, S., 2012. Improvements over three Generations of climate model simulations for eastern India. Climate Research, 51(3), 201 - 216.

Das, A. K., Bhowmick, M., Kundu, P. K., & Bhowmik, S. R., 2014. Verification of WRF rainfall forecasts over India during monsoon 2010: CRA method. G eofizika,

31(2), 105-126.

Das, S., Mohanty, U.C., Tyagi, A., Sikka, D. R., Joseph, P.V., Rathore, L.S., Habib, A., Baidya, S. K., Sonam, K. and Sarkar, A., 2014. The SAARC STORM: a coordinated field experiment on severe thunderstorm observations and regional modeling over the South Asian Region. Bulletin of the American Meteorological Society, 95(4), pp. 603 - 617.

Das, S. K., Deb, S. K., Kishtawal, C. M., & Pal, P. K., 2015. Validation of seasonal forecast of Indian summer monsoon rainfall. Pure and Applied Geophysics, 172, 1699 -1716.

Dawn, S. and Mandal, M., 2014. Surface mesoscale features associated with leading convective line - trailing stratiform squall lines over the Gangetic West Bengal. Meteorology and Atmospheric Physics, 125, pp. 119 - 133.

De Coning, E., & Adam, B. F., 2000. The tornadic thunderstorm events during the 1998 - 1999 South African summer. Water SA- Pretoria -, 26(3), 361 - 376.

Desai, B. N., 1950. Mechanism of Nor'wester of Bengal. Indian J. Meteorol. Geophys., 1, 74 - 76.

Deshpande, N.R. and Goswami, B. N., 2014. Modulation of the diurnal cycle of rainfall over India by intraseasonal variations of Indian summer monsoon. International journal of climatology, 34 (3), pp. 793 - 807.

Dhawan, VB., Tyagi, A. and Bansal, MC., 2008. Forecasting of thunderstorms in Pre - monsoon season over northwest India. Mausam, 59(4) , 433-444.

Dinesh Kumar, A., Karthika, R., & Soman, K. P., 2020. Stereo camera and LIDAR sensor Fusion - based collision warning system for autonomous vehicles. Advances In computational intelligence techniques, 239 - 252.

Donaldson, R., Dyer, R . and Kraus, M., 1975. An objective evaluator of techniques for prediction of severe weather events, Preprints, ninth Conf. On severe Local Storms, Norman, OK, Am. Metear. Soc., 321-326.

Doswell, C. A. III, Davies-Jones R. and Keller. D. L., 1990. On summary measures

of skill in rare event forecasting based on contingency tables. Weather Forecast 5, 576-585.

Dotzek, N., & Forster, C., 2011. Quantitative comparison of METEOSAT thunderstorm detection and nowcasting with in situ reports in the European Severe Weather Database (ESWD). Atmospheric research, 100(4), 511 - 522.

Dotzek, N., 2003. An updated estimate of tornado occurrence in Europe. Atmospheric Research, 67, 153 - 161.

Dvorak, M. J., Stoutenburg, E. D., Archer, C. L., Kempton, W., & Jacobson, M. Z., 2012. Where is the ideal location for a US East Coast offshore grid?. Geophysical Research Letters, 39(6).

Emmanuel, K.A., 1994. Atmospheric Convection. Oxford University Press (580 pp).

Faubush, E. J., Miller, R. C. and Starrett, L. G., 1951. An empirical method for forecasting Tornado development. Bull. Amer. Meteor. Soc., 32, p19.

Kalsi, S. R., 2002. Satellite based weather forecasting. Satellite remote sensing and GIS applications in agricultural meteorology, 331.

Kuleshov, Y., De Hoedt, G., Wright, W. and Brewster, A., 2002. Thunderstorm distribution and frequency in Australia. Australian Meteorological Magazine, 51(3), p. 145.

Galway, J. G., and J. T. Lee, Progress report on upper-level jets and their relationship to severe weather, 1956. Inter-office Memo, U. S. Weather Bureau, SELS, Kansas City, Mo.

Gao, Y., Nelson, E.D., Field, M.P., Ding, Q., Li, H., Sherrell, R.M., Gigliotti, C.L., Van Ry, D.A., Glenn, T.R. and Eisenreich, S.J., 2002. Characterization of atmospheric trace elements on PM2. 5 particulate matter over the New York–New Jersey harbor estuary. Atmospheric environment, 36(6), pp. 1077 - 1086.

Gascón, E., Merino, A., Sánchez, J.L., Fernández-González, S., García-Ortega, E., López, L. and Hermida, L., 2015. Spatial distribution of thermodynamic conditions of severe Storms in southwestern Europe. Atmospheric Research, 164, pp. 194 - 209.

Geerts, B., 2001. Estimating Downburst-related maximum surface wind speeds by means of proximity soundings in New South Wales, Australia. Weather and forecasting, 16(2), pp. 261 - 269.

George, JJ., 1960. Weather forecasting for aeronautics. Academic press, 411pp.

Ghosh, A., Lohar, D. and Das, J., 2008. Initiation of Nor'wester in relation to Mid - upper and low-level water vapor patterns on METEOSAT-5 images. Atmos. Res., 87, 116-135.

Ghosh, T. and Krishnamurti, T.N., 2018. Improvements in hurricane intensity forecasts from a multimodel superensemble utilizing a generalized neural network technique. Weather And Forecasting, 33(3), pp. 873 - 885.

Goliger, A. M. and Milford, R. V., 1998. A review of worldwide occurrence Of tornadoes. Journal of Wind Engineering and Industrial Aerodynamics, 74, pp. 111 - 121.

Gray, W. M. and Jacobson Jr, R. W., 1977. Diurnal variation of deep cumulus convection. Monthly Weather Review, 105(9), pp. 1171 - 1188.

Grosh, R., C. and Morgan, Jr., G., M., 1975. Radar - thermodynamic hail day determination, Ninth Conf. On Severe Local Storms, Norman, OK, Amer. Meteor. Soc., 454 - 459.

Güldner, J. and Spänkuch, D., 1999. Results of year-round remotely sensed integrated water vapor by ground-based microwave radiometry. Journal of Applied Meteorology and Climatology, 38(7), pp. 981 - 988.

Gupta, P.K.S., 1952, June. The genesis and movement of the Nor'westers of Bengal. In Proceedings of the Indian Academy of Sciences - Section A (Vol. 35, No. 6, pp. 303 - 309). New Delhi: Springer India.

Haklander, AJ. and Delden, AV., 2003. Thunderstorm predictors and their forecast skill for The Netherlands. Atmos. Res., 67 – 68, 273 - 299.

Halder, P., Dey, R.K. and Mandal, S., 2023. Long - period trend analysis of annual and

seasonal rainfall in West Bengal, India (1901–2020). Theoretical and Applied Climatology, 154(1), pp. 685 - 703.

Hanssen, A. W. and Kuippers, W. J. A., 1965. On the relationship between the frequency of rain and various meteorological parameters, Staatsdrukkerij - en Uitgeverijbedrijf

Hara, K., Nakazawa, F., Fujita, S., Fukui, K., Enomoto, H. and Sugiyama, S., 2014. Horizontal distributions of aerosol constituents and their mixing states in Antarctica during the JASE traverse. Atmospheric Chemistry and Physics, 14(18), pp. 10211 - 10230.

Hariprasad, K. B. R. R., Srinivas, C. V., Singh, A. B., Rao, S. V. B., Baskaran, R. And Venkatraman, B., 2014. Numerical simulation and intercomparison of boundary layer structure with different PBL schemes in WRF using experimental observations at a tropical site. Atmospheric Research, 145, pp.27-44.

Haydu K. J. and Krishnamurthy T. N., 1981. Moisture analysis from radiosonde and Microwave spectrometer data. J. Appl. Met., 20, 10, pp. 1177 – 1191.

Hermida, L., Sánchez, J.L., López, L., Berthet, C., Dessens, J., García - Ortega, E. and Merino, A., 2013. Climatic trends in hail precipitation in France: spatial, altitudinal, and temporal variability. The Scientific World Journal, 2013.

Hirose, M., Oki, R., Short, D.A. and Nakamura, K., 2009. Regional characteristics of scale-based precipitation systems from ten years of TRMM PR data. 気象集誌. 第 2 輯, 87, pp. 353 - 368.

Hu, H. and Timothy Liu, W., 2003. Oceanic thermal and biological responses to Santa Ana winds. Geophysical Research Letters, 30(11).

Hu, X.M., Fuentes, J.D. and Zhang, F., 2010. Downward transport and modification of Tropospheric ozone through moist convection. Journal of atmospheric chemistry,

65, pp. 13 - 35.

Hu, X. M., Nielsen - Gammon, J. W. and Zhang, F., 2010. Evaluation of three planetary boundary layer schemes in the WRF model. Journal of Applied Meteorology and Climatology, 49(9), pp. 1831 - 1844.

Huang, A., Lu, G., Zhang, H., Liu, F., Fan, Y., Zhu, B., Yang, J. and Wang, Z., 2018. Locating parent lightning strokes of sprites observed over a mesoscale Convective system in Shandong Province, China. Advances in Atmospheric Sciences, 35, pp. 1396 - 1414.

Huang, K., Xiao, Q., Meng, X., Geng, G., Wang, Y., Lyapustin, A., Gu, D. and Liu, Y., 2018. Predicting monthly high- resolution PM2. 5 concentrations with random forest model in the North China Plain. Environmental pollution, 242, pp. 675 - 683.

Ivanova, A. R., 2019. International practices of thunderstorm nowcasting. Russian Meteorology and Hydrology, 44, pp. 756 - 763.

Jayakrishnan P, Babu C (2014) Assessment of convective activity using stability Indices as inferred from Radiosonde and MODIS data. Atmos Clim Sci 4(1): 122–130. doi:10.4236/acs.2014.41014

Jergensen, G.E., McGovern, A., Lagerquist, R. and Smith, T., 2020. Classifying convective storms using machine learning. Weather and Forecasting, 35(2), pp. 537 - 559.

Jergensen, G.E; McGovern, A.; Lagerquist, R.; and Smith, T., 2019. Classifying convective storms using machine learning. Wea Forecasting 35:537–559. https://doi.org/10.1175/waf-d-19-0170.1

Jiang, F., Zhang, M., Li, Y., Zhang, J., Qin, J. and Wu, L., 2021. Field measurement study of

Wind characteristics in mountain terrain: Focusing on sudden intense winds. Journal of Wind Engineering and Industrial Aerodynamics, 218, p.104781.

Karmakar, S., 2005. Study of nor'westers and development of prediction techniques in Bangladesh during the pre-monsoon season . Ph. D. Thesis, Department of Physics, Khulna University of Engineering and Technology (KUET).

Karmakar, S. and Alam, M. M., 2005. On the probabilistic extremes of thunderstorm frequency over Bangladesh during the pre-monsoon season. Journal of Hydrology and Meteorology (SOHAM-Nepal), 2, 1, pp. 41 - 47

Karmakar, S. and Alam, M. M, 2005. On the sensible energy, latent heat energy and potential energy of the troposphere over Dhaka before the occurrence of nor'westers in Bangladesh during the pre-monsoon season. Mausam, 56, 3, pp. 671 - 680.

Karmakar, S. and Alam, M. M., 2006. Instability of the troposphere associated with thunderstorms/nor'westers over Bangladesh during the pre-monsoon season. Mausam, 57, 4, pp. 629 - 638.

Karmakar, S. and Alam, M. M., 2007. Tropospheric moisture and its relation with rainfall due to nor'westers in Bangladesh. Mausam, 58, 2, pp. 153 - 160.

Karmakar and Alam, M.M., 2007. Interrelation among different instability indices of the troposphere over Dhaka associated with thunderstorms/nor'westers over Bangladesh During the pre-monsoon season. Mausam, 58, 3, pp. 361 - 368.

Karmakar, S. and Alam, M. M., 2011. Modified instability index of the troposphere associated with thunderstorms/nor'westers over Bangladesh during the pre-monsoon season. Mausam, 62, 2, pp. 205 - 214.

Karmakar, S. and Quadir, D. A., 2014. Variability of local severe storms and associated Moisture and precipitable water content of the troposphere over Bangladesh and neighhood during the pre-monsoon season. Journal of NOAMI, Vol. 31, No. 1 & 2, pp. 1 - 25.

Karmakar S. and Quadir D. A., 2014. Study on the potential temperatures of the Tropospher associated with local severe storms and their distribution over

Bangladesh and neibourhood during the pre-monsoon season . Journal of Engineering Sciences, Vol. 05, No. 1, 13 - 3

Kamangir, H., Collins, W., Tissot, P. and King, S.A., 2020. A deep-learning model to predict thunderstorms within 400 km2 South Texas domains. Meteorological Applications, 27(2), p.e1905.

Kessler, E., 1982. Thunderstorm morphology and dynamics, U.S. Department of commerce. National Oceanic and Atmospheric Administration, Environmental Research Laboratories, Vol. 2.

Kiran Prasad, S., Mohanty, U.C., Routray, A., Osuri, K. K., Ramakrishna, S. S. V. S. and Niyogi, D., 2014. Impact of Doppler weather radar data on thunderstorm simulation during STORM pilot phase—2009. Natural hazards, 74, pp. 1403 - 1427.

Kobler, K., and Tafferner, A., 2009. Tracking and nowcasting of convective cells using remote sensing data from radar and satellite. Meteorol. Z. 1, 75–84.

Koffi, E., 2007. The use of radiometer derived convective indices in thunderstorm nowcasting, Res. Rep. 2007-02-MW, 31 pp., Inst. of Appl. Phys., Univ. of Bern, Bern.

Kohn, M., Galanti, E., Price, C., Lagouvardos, K. and Kotroni, V., 2011. Nowcasting thunderstorms in the Mediterranean region using lightning data. Atmospheric Research, 100(4), pp. 489 - 502.

Kuleshov, Y., De Hoedt, G., Wright, W. and Brewster, A., 2002. Thunderstorm Distribution and frequency in Australia. Australian Meteorological Magazine, 51(3), p.145.

Kumar, G. and Mohapatra, M., 2006. Some climatological aspects of thunderstorms and squalls over Guwahati Airport. Mausam, 57(2), pp. 231 - 240.

Kumar, P., Kishtawal, C.M. and Pal, P.K., 2017. Impact of ECMWF, NCEP, and NCMRWF global model analysis on the WRF model forecast over Indian

Region. Theoretical and Applied Climatology, 127, pp. 143 - 151.

Kumar, N., Jaswal, A. K., Mohapatra, M. and Kore, P. A., 2017. Spatial and temporal variation in daily temperature indices in summer and winter seasons over India (1969 – 2012). Theoretical and Applied Climatology, 129, pp. 1227 - 1239.

Kunz, M., 2007. The skill of convective parameters and indices to predict isolated and severe thunderstorms. Nat. Hazards Earth Syst. Sci., 7, 327 – 342.

Kursinski, E.R., Bennett, R.A., Gochis, D., Gutman, S.I., Holub, K.L., Mastaler, R., Minjarez Sosa, C., Minjarez Sosa, I. and van Hove, T., 2008. Water vapor and surface observations in northwestern Mexico during the 2004 NAME Enhanced Observing Period. Geophysical Research Letters, 35(3).

Kursinski, A. L. and Mullen, S.L., 2008. Spatiotemporal variability of hourly precipitation over the eastern contiguous United States from stage IV multisensor analyses. Journal of Hydrometeorology, 9(1), pp.3 - 21.

Kursinski, E.R. and Ward, D., 2008, December. A Radio Occultation System Optimized for Observing Climate Change: the Active Temperature, Ozone and Moisture Microwave Spectrometer (ATOMMS). In AGU Fall Meeting Abstracts (Vol. 2008, pp. GC23A - 0748).

Kuwagata, T., Numaguti, A. and Endo, N., 2001. Diurnal variation of water vapor over the central Tibetan Plateau during summer. Journal of the Meteorological Society of Japan. Ser. II, 79(1B), pp . 401 - 418.

Lang, T. J., & Barros, A. P., 2002. An investigation of the onsets of the 1999 and 2000 monsoons in central Nepal. Monthly weather review, 130(5), 1299 - 1316.

Lang, T. J., & Barros, A. P., 2004. Winter storms in the central Himalayas. Journal of The Meteorological Society of Japan. Ser. II, 82(3), 829 - 844.

Lee, K., Kim, H.S. and Choi, Y.S., 2019. Effects of high-resolution geostationary Satellite imagery on the predictability of tropical thunderstorms over Southeast Asia. Natural Hazards and Earth System Sciences, 19(10), pp.2241 - 2248.

Lee, K., Kim, H.S. and Choi, Y.S., 2019. Effects of high-resolution geostationary satellite imagery on the predictability of tropical thunderstorms over Southeast Asia. Natural Hazards and Earth System Sciences, 19(10), pp.2241 - 2248.

Lee, J.G., Min, K.H., Park, H., Kim, Y., Chung, C.Y. and Chang, E.C., 2020. Improvement of the rapid-development thunderstorm (RDT) algorithm for use with the GK2A satellite. Asia-Pacific Journal of Atmospheric Sciences, 56, pp.307-319.

Leena, P.P., Pandithurai, G., Gayatri, K., Murugavel, P., Ruchith, R.D., Sakharam, S., Dani, K.K., Patil, C., Dharmaraj, T., Patil, M.N. and Prabhakaran, T., 2019. Analysing the characteristic features of a pre-monsoon thunderstorm event over Pune, India, using ground-based observations and WRF model. Journal of Earth System Science, 128, pp.1-15.

Leinonen, J., Hamann, U., Germann, U. and Mecikalski, J.R., 2022. Nowcasting thunderstorm hazards using machine learning: the impact of data sources on performance. Natural Hazards and Earth System Sciences, 22(2), pp.577-597.

Li, X. and Pu, Z., 2008. Sensitivity of numerical simulation of early rapid intensification of Hurricane Emily (2005) to cloud microphysical and planetary Boundary layer parameterizations. Monthly Weather Review, 136(12), pp. 4819 - 4838.

Li, P.W. and Lai, E.S., 2004. Short-range quantitative precipitation forecasting In Hong Kong. Journal of Hydrology, 288(1-2), pp. 189 - 209.

Litta, AJ. and Mohanty, U.C., 2008. Simulation of a severe thunderstorm event during the field experiment of STORM programme 2006 using WRF-NMM model. Curr. Sci., 95(2), 204-215.

Litta, A.J., Mohanty, U.C. and Idicula, S.M., 2012 a. The diagnosis of severe thunderstorms with high-resolution WRF model. Journal of earth system science, 121(2), pp.297 - 316.

Litta, A.J., Mohanty, U.C., Das, S. and Idicula, S.M., 2012 b. Numerical simulation of severe local storms over east India using WRF-NMM mesoscale model. Atmospheric research, 116, pp.161 - 184.

Litta, A.J., Mary Ididcula, S., Mohanty, U.C. and Kiran Prasad, S., 2012 a, b. Comparison of thunderstorm simulations from WRF-NMM and WRF - ARW Models over east Indian region. The Scientific World Journal, 2012.

Litta, A.J. and Sumam Mary, I., 2013. Computational models for the prediction of severe thunderstorms over east Indian region (Doctoral dissertation, Cochin University of Science And Technology).

Litynska, Z., Parfiniewicz, J. and Pinkowski, H., 1976. The prediction of air mass thunderstorms and hails. WMO Bull., 450, 128 - 130.

Lohar, D. and Pal, B., 1995. The effect of irrigation on pre-monsoon season precipitation over South West Bengal, India. J. Climate, 8(10), 2567 - 2570.

Lundberg, S.M. and Lee, S.I., 2017. A unified approach to interpreting model predictions. Advances in neural information processing systems, 30.

Maddalena, L., Gori, M. and Pal, S.K., 2020. Pattern recognition and beyond: Alfredo Petrosino's scientific results. Pattern Recognition Letters, 138, pp . 659 - 669.

Madala, S., Satyanarayana, A.N.V. and Rao, T.N., 2014. Performance evaluation of PBL and cumulus parameterization schemes of WRF ARW model in simulating Severe thunderstorm events over Gadanki MST radar facility— case study. Atmospheric Research, 139, pp. 1 -17.

Madala, S., Satyanarayana, A.N.V., Srinivas, C.V. and Tyagi, B., 2016. Performance evaluation of PBL schemes of ARW model in simulating thermo-dynamical structure of pre-monsoon convective episodes over Kharagpur using STORM data sets. Pure and Applied Geophysics, 173, pp. 1803 - 1827.

Madhulatha, A.; Rajeevan, M.; Venkat Ratnam, M.; Bhate, J. and Naidu, C.V., Nowcasting severe convective activity over southeast India using ground-based microwave radiometer observations. Journal of Geophysical Research: Atmospheres, 118(1), pp.1 - 13.

Mahanta, R. and Yamane, Y., 2020. Climatology of local severe convective storms in Assam, India. International Journal of Climatology, 40(2), pp.957-978.

Maitra, A., Jana, S., Chakraborty, R. and Majumder, S., 2014, August. Multi-technique observations of convective rain events at a tropical location. In 2014 XXXIth URSI General Assembly and Scientific Symposium (URSI GASS) (pp. 1-4). IEEE.

Majumder A. and Das S., 2021. Geospatial Analysis of the Dynamics of Climate in Kolkata Metropolitan Area. Journal of Physics: Conference Series. https://doi.org/10.1088/1742-6596/1964/4/042038

Manzato, A., 2003. A climatology of instability indices derived from Friuli Venezia Giulia soundings, using three different methods. Atmospheric research, 67, pp. 417 - 454.

McCann, D.W., 1992. A neural network short-term forecast of significant thunderstorms. Weather and Forecasting, 7(3), pp. 525 - 534.

McCann, D.W., 1994. WINDEX—A new index for forecasting microburst potential. Weather and forecasting, 9(4), pp. 532 - 541.

McClave, J. T. and Dietrich II, F., H., 1988. Statistics, Dellen Publishing Company, 1014pp.

MCCULLAGH, P. & NELDER, J. A. (1989). Generalized Linear Models, 2nd ed. London: Chapman and Hall. ROYALL, R. M. (1986). Model robust confidence intervals using maximum likelihood estimates. Int. Statist. Rev. 54, 221 - 6.

McGovern, A; Elmore, K.; Gagne, D.J.; Haupt, S; Karstens, C.; Lagerquist, R.; Smith,

T.; Williams, J., 2017. Using Artificial Intelligence to Improve Real-Time Decision-making for High-Impact Weather.Bulletin of the American Meteorological Society, 98(10):2073–2090, https://doi.org/10.1175/BAMS-D-16-0123.1

McIntosh P. H. and Thom A. S., 1973. Essentials of Meteorology. Wykeham Publications (London) Ltd., pp. 68 - 69

Mecklenburg, S.M., 2000. Nowcasting precipitation in an Alpine region with a radar echo tracking algorithm (Doctoral dissertation, ETH Zurich).

Merino, A., Wu, X., Gascón, E., Berthet, C., García-Ortega, E. and Dessens, J., 2014. Hailstorms in southwestern France: Incidence and atmospheric characterization. Atmospheric research, 140, pp. 61 - 75.

Miao, S., Chen, F., LeMone, M.A., Tewari, M., Li, Q. and Wang, Y., 2009. An observational and modeling study of characteristics of urban heat island and boundary layer structures in Beijing. Journal of Applied Meteorology and Climatology, 48(3), pp.484 - 501.

Midya, S.K., Sarkar, H. and Saha, U., 2011. Sharp depletion of atmospheric refractive index associated with Nor'wester over Gangetic West Bengal: a possible method of forecasting Nor'wester. Meteorology and atmospheric physics, 111, pp.149-152.

Means, L.L., 1952. Stability index computation graph for surface data. 2pp, Unpublished manuscript available from F. Sanders, 9 Flint St., Marblehead, MA, 01945.

Miller, R., C., 1967. Notes on analysis and severe storm forecasting procedures of the Military Weather Warning Centre, AWS Tech. Rep., 200, USAF, 170p.

Mitra C. and Jordon T. R., 2011. On the relationship between the pre-monsoonal rainfall Climatology and urban land cover dynamics in Kolkata city, India. International Journal of Climatology. https://doi.org/10.1002/joc.2366

Mohanty U C, Sikka D R, Madan O P, Kiran Prasad S, Litta A J et al 2009. Weather Summary Pilot Experiment of Severe Thunderstorms – Observational and Regional Modeling (STORM) Programme – 2009

Moncrieff, M. and Miller, M., 1976. The dynamics and simulation of tropical cumulonimbus and squall lines. Q. J. Meteorol. Soc., 102, 373-394.

Mostajabi, A., Finney, D.L., Rubinstein, M. and Rachidi, F., 2019. Nowcasting lightning occurrence from commonly available meteorological parameters using machine learning techniques. Npj Climate and Atmospheric Science, 2(1), p.41.

Mowla, K.G., 1986. A scientific note on the nor'wester of 14th April, 1969 in Bangladesh. Proceedings of the Seminar (SAARC) on Local Severe Storms, pp. 10 - 19.

Mukherjee, A. K. and Bhattacharya, P. B., 1972. An early morning tornado at Diamond Harbour on 21 March, 1969. Indian J. Met. Geophys., 23, 2, pp. 223 - 226.

Mukherjee, A. K., Kumar, S. and Krishnamurty, G., 1977. A radar study of growth and decay of thunderstorms around Bombay during pre-monsoon season . Indian J. Met. Geophys., 28, 4, pp. 475 - 478

Mukhopadhyay, P., Sanjay, J. and Singh, SS., 2003. Objective forecast of thundery / non thundery days using conventional indices over three northeast Indian stations. Mausam, 54(4), 867 - 880.

Mukhopadhyay, P., Mahakur, M. and Singh, H. A. K., 2009. The interaction of large scale and mesoscale environment leading to formation of intense thunderstorms over Kolkata Part I: Doppler radar and satellite observations. Journal of Earth System Science, 118, pp. 441 - 466.

Murthy, B.S., Latha, R. and Madhuparna, H., 2018. WRF simulation of a severe hailstorm over Baramati: a study into the space–time evolution. Meteorology And Atmospheric Physics, 130, pp. 153 - 167.

Nesbitt S, Zipser E. 2003. The diurnal cycle of rainfall and convective intensity According to three years of TRMM measurements. Journal of Climate 16: 1456 — 1475.

Niall, S. and Walsh, K., 2005. The impact of change on hailstorms in

southeastern Australia. International Journal of Climatology: A Journal of the Royal Meteorological Society, 25(14), pp. 1933 - 1952.

Nie, J., Sobel, A.H., Shaevitz, D.A. and Wang, S., 2018. Dynamic amplification of extreme precipitation sensitivity. Proceedings of the National Academy of Sciences, 115(38), pp. 9467 - 9472.

Nischitha, V., Ahmed, S. A., Varikoden, H., Revadekar, J. V. and Srinivasa Reddy, G. S., 2013. Spatial and temporal variability of daily monsoon rainfall in Tunga and Bhadra River basins, Karnataka. Annals of GIS, 19(4), pp.219 - 230.

Ochoa-Rodriguez, S., Wang, L.P., Gires, A., Pina, R.D., Reinoso-Rondinel, R., Bruni, G., Ichiba, A., Gaitan, S., Cristiano, E., van Assel, J. and Kroll, S., 2015. Impact of spatial and temporal resolution of rainfall inputs on urban hydrodynamic Modelling outputs: A multi-catchment investigation. Journal of Hydrology, 531, pp. 389 - 407.

Pal, A. and Pal, SK., 2017 . Pattern recognition: evolution, mining and big data. In: Pal A, Pal SK (eds) Pattern recognition and big data. World Scientifc, Singapore, pp 1 – 36

Pal, SK., Meher, SK., Skowron, A., 2015. Data science, big data and granular mining. Pattern Recognit Lett 67: 109 – 112. https://doi. org/10.1016/j.patrec.2015.08.001

Pathak, A., and Pal, SK., 1986. Fuzzy grammars in syntactic recognition of skeletal maturity from X-rays. IEEE Trans Syst Man Cybern 16:657 – 667. https://doi.org/10.1109/tsmc.1986.289310

Patra, A.K., De, U.K. and Lohar, D., 1998. Existence of low-level jet during Pre-monsoon period over eastern India and its role in the initiation of nocturnal thunderstorms, Atmosfera, 12, 15-26

Peppier, R.A., 1988. A review of static stability indices and related thermodynamic parameters. SWS Miscellaneous Publication, 104.

Pramanik, S.K., 1939. Forecasting of Nor'westers in Bengal. roc. Nat. Inst. Sc. (India), 5, 43.

PURDOM, J.F., 2003. Local severe storm monitoring and prediction using satellite data. Mausam, 54(1), pp. 141 - 154.

Rajeevan, M., Unnikrishnan, C.K., Bhate, J., Niranjan Kumar, K. and Sreekala, P. P., 2012. Northeast monsoon over India: variability and prediction. Meteorological Applications, 19(2), pp.226 - 236.

Ramakrishna, S. S. V. S., Vijaya Saradhi, N. and Srinivas, C.V., 2012. On the role of the Planetary Boundary Layer in the numerical simulation of a severe cyclonic Storm Nargis using a mesoscale model. Natural hazards, 63, pp. 1471 - 1496.

Rao, A. D., Upadhaya, P., Ali, H., Pandey, S. and Warrier, V., 2020. Coastal inundation due to tropical cyclones along the east coast of India: an influence of climate change impact. Natural Hazards, 101, pp. 39 - 57.

Rasp, S., and S. Lerch, 2018: Neural networks for postprocessing ensemble Weather forecasts. Mon. Wea. Rev., 146(11), 3885 –3900, https://doi.org/10.1175/MWR-D-18-0187.1.

Rasmussen, E. N., and R. B. Wilhelmson, 1983: Relationships between storm characteristics and 1200 GMT hodographs, low level shear and stability. Preprints, 13th Conf. on Severe Local Storms, Tulsa, OK, Amer. Meteor. Soc., 55 - 58.

Rasmussen, K.L. and Houze, R.A., 2011. Orogenic convection in subtropical South America as seen by the TRMM satellite. Monthly Weather Review, 139(8), pp. 2399 - 2420.

Ravi, N., Mohanty, UC., Madan, OP. and Paliwal, RK., 1999. Forecasting of thunderstorms in the pre-monsoon season at Delhi. Meteorol. Appl., 6, 29-38 Revering A (on line documentation) MAP / variable / parameter explanation. http://www.aprweather.com/forum/viewtopic.php?p=11

Risanto, C.B., Castro, C.L., Moker Jr, J.M., Arellano Jr, A.F., Adams, D.K., Fierro,

L.M. and Minjarez Sosa, C.M., 2019. Evaluating forecast skills of moisture from convective-permitting WRF-ARW model during 2017 North American monsoon season. Atmosphere, 10(11), p.694.

Roy, SC. and Chatterji, G., 1929. Origin of Nor'westers. Nature 124 : 481. https://doi.org/10.1038/124481a0

Roy, S. S. and Roy, S. S., 2011. Regional variability of convection over northern India during the pre-monsoon season. Theoretical and Applied Climatology, 103, pp.145 - 158.

Roy, A., 2019. Making India's coastal infrastructure climate-resilient: challenges and Opportunities. Observer Research Foundation.

Różycki, M. and Wypych, A., 2018. Atmospheric Moisture Content over Europe and the Northern Atlantic. Atmosphere. https://doi.org/10.3390/atmos9010018

Sadhukhan, I., Lohar, D. and Pal, D. K., 2000. Premonsoon season rainfall Variability over Gangetic West Bengal and its neighbourhood, India. International Journal of Climatology. A Journal of the Royal Meteorological Society, 20(12), pp. 1485 - 1493.

Saha, U., Midya, S.K., Sarkar, H. and Das, G.K., 2012. Sharp depletion of absolute humidity associated with squall over Kolkata (22 34′ N, 88 26′ E): a possible Method of forecasting squall. Pacific J. Sci. Technol, 13(1), pp.683 - 688.

Saha, U., Maitra, A., Midya, S.K. and Das, G.K., 2014. Association of thunderstorm frequency with rainfall occurrences over an Indian urban metropolis. Atmospheric research, 138, pp. 240 - 252.

Saha, A., Guha, A. and De, B.K., 2015. Sunrise effect on 40 kHz signal amplitude and its characteristic variation with respect to geomagnetic storms. Canadian Journal of Physics, 93(12), pp. 1574 - 1582.

Sahu, R.K., Dadich, J., Tyagi, B., Vissa, N. K. and Singh, J., 2020 a. Evaluating

The impact of climate change in threshold values of thermodynamic indices during pre-monsoon thunderstorm season over Eastern India. Natural Hazards, 102, pp. 1541 - 1569.

Sahu, R.K., Dadich, J., Tyagi, B. and Vissa, N.K., 2020 b. Trends of thermodynamic indices thresholds over two tropical stations of north-east India during pre-monsoon thunderstorms. Journal of Atmospheric and Solar-Terrestrial Physics, 211, p.105472.

Samanta, S., Tyagi, B., Vissa, N.K. and Sahu, R.K., 2020. A new thermodynamic index for thunderstorm detection based on cloud base height and equivalent potential temperature. Journal of Atmospheric and Solar- Terrestrial Physics, 207, p.105367.

Santhosh, K., Sarasakumari, R., Gangadharan, V. K. and Sasidharan, N. V., 2001. Some climatological features of thunderstorms at Thiruvananthapuram, Kochi and Kozhikode airports. Mausam, 52, 2, 357 - 364.

Sahany, S., Venugopal, V. and Nanjundiah, R.S., 2010. Diurnal-scale signatures of monsoon rainfall over the Indian region from TRMM satellite observations. Journal of Geophysical Research: Atmospheres, 115(D2).

Sarkar, T., Das, S. and Maitra, A., 2015. Assessment of different raindrop size measuring techniques: Inter-comparison of Doppler radar, impact and optical disdrometer. Atmospheric Research, 160, pp.15 - 27.

Sarkar, A., Das, S. and Dutta, D., 2019. Computation of skill of a mesoscale model in forecasting thunderstorm using radar reflectivity. Modeling Earth Systems and Environment, 5, pp.443 - 454.

Sánchez, J. L., Fraile, R., De la Fuente, M. T. and Marcos, J.D.L., 1998. Discriminant analysis applied to the forecasting of thunderstorms. Meteorology And Atmospheric Physics, 68, pp. 187 - 195.

Sánchez, J. L., J. L. Marcos, M. T. De La Fuente, and A. Castro, 1998: A logistic

regression model applied to short term forecast of hail risk. Phys. Chem. Earth, 23, 645–648, https:// doi.org/10.1016/S0079-1946(98)00102-5.

Sa´nchez, J.L., Lo´pez, L., Bustos, C., Marcos, JL. And Garcı´a, O.E., 2008. Short-term forecast of thunderstorms in Argentina. Atmos. Res., 88, 36-45.

Sánchez, J.L., Posada, R., García-Ortega, E., López, L. and Marcos, J.L., 2013. A method to improve the accuracy of continuous measuring of vertical profiles of temperature and water vapor density by means of a ground-based microwave radiometer. Atmospheric Research, 122, pp.43 - 54.

Sandeep, A. and Prasad, V.S., 2020. On the variability of cold wave episodes over Northwest India using an NGFS retrospective analysis. Pure and Applied Geophysics, 177, pp.1157 - 1166.

Santanello, J. A. and Welty J., 2020. Increased likelihood of Appreciable Afternoon Rainfall Over Wetter or Drier Soils Dependent Upon Atmospheric Dynamic Influence. Geophysical Research Letters. https://doi.org/10.1029/2020g1087779

Sarraf , M. and Dasgupta S., 2011. India – Vulnerability of Kolkata metropolitan area to increased precipitation in a changing climate. https://doi.org/10.11588/xarep.00003747

Scheafer, J. T., 1990. The Critical Success Index as an indicator of warning skill. Weath. Forecasting. 5, 570 - 575.

Schultz, M. G., Betancourt, C., Gong, B., Kleinert, F., Langguth, M., Leufen, L. H., Mozaffari, A. and Stadtler, S., 2021. Can deep learning beat numerical weather prediction?. Philosophical Transactions of the Royal Society A, 379(2194), p.20200097.

Shapley, L. S., 1953. A value for n-person games. In H. W. Kuhn and A. W. Tucker (Eds.), Contributions to the Theory of Games, pp. 307 – 317. Princeton University Press.

Shrestha, D., Singh, P. and Nakamura, K., 2012. Spatiotemporal variation of rainfall

over the central Himalayan region revealed by TRMM Precipitation Radar. Journal of geophysical research: atmospheres, 117(D22).

Shrestha, Y., Zhang, Y., Doviak, R. and Chan, P.W., 2021. Lightning flash rate Nowcasting based on polarimetric radar data and machine learning. International Journal of Remote Sensing, 42(17), pp. 6762 - 6780.

Shrestha, P., Mendrok, J. and Brunner, D., 2022. Aerosol characteristics and polarimetric signatures for a deep convective storm over the northwestern part of Europe – modeling and observations. Atmospheric Chemistry and Physics, 22(21), pp.14095 - 14117.

Showalter, A. K.., 1953. A stability index for thunderstorm forecasting. Bulletin of the American Meteorological Society, 34(6), pp. 250 - 252.

Singh, P. and Kumar, N., 1997. Effect of orography on precipitation in the western Himalayan region. Journal of Hydrology, 199(1-2), pp.183 - 206.

Singh, D., Ganju, A. and Singh, A., 2005. Weather prediction using nearest-neighbour model. Current science, pp. 1283 - 1289.

Singh, P. and Nakamura, K., 2009. Diurnal variation in summer precipitation over The central Tibetan Plateau. Journal of Geophysical Research: Atmospheres, 114(D20).

Singh, P. and Nakamura, K., 2010. Diurnal variation in summer monsoon Precipitation during active and break periods over central India and southern Himalayan foothills. Journal of Geophysical Research: Atmospheres, 115(D12).

Someshwar Das, M.N.I. and Das, M. K., 2014. Simulation of severe storm of Tornadic intensity over Indo-Bangla region. Simulation, 551(3), pp. 549 - 3.

Srinivasan, V., Ramamuthy, K. and Nene, Y.R., 1973. Summer—Nor'westers and Andhis and large-scale convective activity over peninsula and central parts of the country. India Meteorological Department, Forecasting Manual: Part III STORM (Severe

Thunderstorms—Observations and Regional Modeling) Programme (2005) Science plan. Department of Science and Technology, Government of India.

Srinivas, C. V., Venkatesan, R. and Singh, A. B., 2007. Sensitivity of mesoscale simulations of land–sea breeze to boundary layer turbulence parameterization. Atmospheric Environment, 41(12), pp.2534 - 2548.

Srinivas , C. V., Venkatesan, R., Bhaskar Rao, D. V. and Hari Prasad, D., 2007. Numerical simulation of Andhra severe cyclone (2003): Model sensitivity to the boundary layer and convection parameterization. Atmospheric and Oceanic: Mesoscale Processes, pp.1465-1487.

Srinivas, C. V., BhaskarRao, D. V., V. Yesubabu, Baskaran, R., and Venkatraman, B., 2013. Tropical cyclone predictions over the Bay of Bengal using the high-resolution Advanced Research Weather Research and Forecasting model, *Q. J. R. Meteorol. Soc.*, 139(676), 1810–1825, doi:10.1002/qj.2064.

Srinivas, C.V., Hariprasad, D., Bhaskar Rao, D.V., Anjaneyulu, Y., Baskaran, R. and Venkatraman, B., 2013 a. Simulation of the Indian summer monsoon regional Climate using advanced research WRF model. International Journal of Climatology, 33(5), pp.1195 - 1210.

Srinivas, C.V., Bhaskar Rao, D., Yesubabu, V., Baskaran, R. and Venkatraman, B., 2013b. Tropical cyclone predictions over the Bay of Bengal using the high-resolution Advanced Research Weather Research and Forecasting (ARW) model. Quarterly Journal of the Royal Meteorological Society, 139(676), pp. 1810 - 1825.

Srinivas, C.V., Bhaskar Rao, D.V., Hari Prasad, D., Hari Prasad, K.B.R.R., Baskaran, R. and Venkatraman, B., 2015 a. A study on the influence of the land surface Processes on the southwest monsoon simulations using a regional climate model. Pure and Applied Geophysics, 172, pp.2791 - 2811.

Srinivas, C.V., Hari Prasad, D., Bhaskar Rao, D.V., Baskaran, R. and Venkatraman,

B., 2015 b, September. Simulation of the Indian summer monsoon onset-phase Rainfall using a regional model. In Annales Geophysicae (Vol. 33, No. 9, pp. 1097-1115). Göttingen, Germany: Copernicus GmbH.

Srikanth, M., Satyanarayana, A.N.V., Srinivas, C.V. and Kumar, M., 2015. Mesoscale Atmospheric flow-field simulations for air quality modelling over complex terrain region of Ranchi in eastern India using WRF. Atmos. Environ, 107, pp.315 - 328.

Stankova, E., Tokareva, I.O. and Dyachenko, N.V., 2021. On the possibility of using neural networks for the thunderstorm forecasting. In Computational Science and Its Applications–ICCSA 2021: 21st International Conference, Cagliari, Italy, September 13–16, 2021, Proceedings, Part VIII 21 (pp. 350-359). Springer International Publishing.

STORM (2005). Science Plan. Deptartment of Science and Technology, Government Of India (118 pp. ((http://www.coral.iitkgp.ernet.in/storm/index.htm)).

Strumbelj, E. and Kononenko, I., 2010. An efficient explanation of individual classifications using game theory. The Journal of Machine Learning Research, 11, pp. 1 -18.

Stull, R.B., 1988. Mean boundary layer characteristics. In An introduction to Boundary layer meteorology (pp. 1-27). Dordrecht: Springer Netherlands.

Subrahmanyam, K. V., Kumar, K. K. and Narendra Babu, A., 2015. Phase relation Between CAPE and precipitation at diurnal scales over the Indian summer Monsoon region. Atmospheric Science Letters, 16(3), pp.346 - 354.

Tabari, H. and Hosseinzadeh Talaee, P., 2011. Recent trends of mean maximum and minimum air temperatures in the western half of Iran. Meteorology And atmospheric physics, 111, pp. 121 - 131.

Tyagi, A., 2007. Thunderstorm climatology over Indian region. Mausam 58(2): 189 – 212

Tyagi, B. N. Krishna, V. and Satyanarayan, A. N. V., 2011. Study of thermodynamic indices in forecasting pre-monsoon thunderstorms over Kolkata during STORM pilot phase 2006- 2008, Nat. Hazards, 56, 681-698.

Tyagi, A., Sikka, D.R., Goyal, S. and Bhowmick, M., 2012. A satellite based study of pre-monsoon thunderstorms (Nor'westers) over eastern India and their organization into mesoscale convective complexes. Mausam, 63(1), pp. 29 - 54.

Tyagi, B., Satyanarayana, A. N. V. and Vissa, N.K., 2013. Thermodynamical structure Of atmosphere during pre-monsoon thunderstorm season over Kharagpur As revealed by STORM data. Pure and Applied Geophysics, 170, pp.675-687.

Tyagi, B., Satyanarayana, A. N. V., 2014a. Coherent structures contribution to fluxes of momentum and heat during stable conditions for pre-monsoon Thunderstorm season. Agric For Meteorol, 186:43 – 47

Tyagi, B., Satyanarayana, A. N. V., 2014b. Coherent Structures contributions in fluxes of momentum and heat at two tropical stations during Pre-Monsoon Thunderstorm season. Int J Climatol 34(5): 1575 – 1584. https://doi.org/10.1002/joc.3785

Tyagi, B., Satyanarayana, A. N. V., 2015. Delineation of surface energy exchanges variations during thunderstorm and non-thunderstorm days during pre-monsoon season. J Atmos Sol Terr Phys 122: 138 – 144. https://doi.org/10.1016/j.jastp.2014.11.010

Tomassetti, N. and AMS collaboration., 2015. Nuclear and Particle Physics. Elsevier, August – September 2015, Pages 245 - 247

Umakanth, N., Satyanarayana, G.C., Simon, B., Rao, M. C. and Babu, N.R., 2020. Long-term analysis of thunderstorm-related parameters over Visakhapatnam and Machilipatnam, India. Acta Geophysica, 68, pp. 921 - 932.

Umakanth, N., Satyanarayana, G.C., Simon, B., Rao, M.C., Kumar, M.T. and Babu, N.R., 2020. Analysis of various thermodynamic instability parameters and their association with the rainfall during thunderstorm events over Anakapalle

(Visakhapatnam district), India. Acta Geophysica, 68, pp. 1549 - 1564.

Umakanth, N., Satyanarayana, G. C., Simon, B., Kumar, P. and Rao, M. C., 2020. Impact of convection and stability parameters on lightning activity over Andhra Pradesh, India. Acta Geophysica, 68, pp. 1845 - 1866.

Ueno, K., 1998: Characteristics of Plateau-scale precipitation in Tibet estimated by satellite data during 1993 monsoon season. J. Meteor. Soc. Japan, 76, 533 − 548.

Ueno, K., H. Fujii, H. Yamada, and L. Liu, 2001a: Weak and frequent monsoon Precipitation over the TP. J. Meteor. Soc. Japan, 79, 429 − 434.

Ueno, K., R.B. Kayastha, H. M. R. Chitrakar, O. R. Bajracharya, A. P. Pokhrel, H. Fujinami, T. Kadota, H. Iida, D. P. Manandhar, M. Hattori, T. Yasunari, and M. Nakawo, 2001b: Meteorological observations during 1994 − 2000 at the automatic weather station (GEN-AWS) in Khumbu region, Nepal Himalayas. Bulletin of Glacier Research, 18, 23 − 30.

Ueno, K., K. Toyotsu, L. Bertolani, and G. Taritari, 2008: Stepwise onset of monsoon weather observed in the Nepal Himalayas. Mon. Wea. Rev., 136, 2507 − 2522.

Varikoden, H., Kumar, K. K. and Babu, C. A., 2013. Long term trends of seasonal and monthly rainfall in different intensity ranges over Indian subcontinent. Mausam 64: 481 – 488.

Vivekanandan J. and Sahoo S., 2011. Trade-off between vertical resolution and accuracy in water vapor retrievals from ground-based microwave brightness temperature measurements. https://doi.org/10.1109/ursigass.2011.6050842

Wang, B., Lee, J. Y., Kang, I. S., Shukla, J., Park, C. K., Kumar, A., Schemm, J., Cocke, S., Kug, J.S., Luo, J.J. and Zhou, T., 2009. Advance and prospectus of seasonal prediction: assessment of the APCC/CliPAS 14-model ensemble retrospective seasonal prediction (1980 – 2004). Climate Dynamics, 33, pp.93 - 117.

Wakimizu K. and Jinno K., 2002. A Numerical Study on Variation of Water Vapor in

Lower Layers Connected with Precipitable Water. Proceedings of Hydraulic Engineering. https://doi.org/10.2208/prohe.46.19

Weissman, M. L. and Klemp, J., B., 1982. The dependence of numerically simulated convective storms on vertical wind shear and buoyancy. Mon. Weather Rev., 110, 504 - 520.

Won, H.Y., Kim, Y.H. and Lee, H.S., 2009. An application of brightness temperature received from a ground-based microwave radiometer to estimation of Precipitation occurrences and rainfall intensity. Asia-Pacific Journal of Atmospheric Sciences, 45(1), pp.55 - 69.

Weston, KJ., 1972. The dryline of northern India and its role in cumulonimbus convection. Q., J., R., Meteorol. Soc., 98, 519-531.

Williams, E.R. and Sátori, G., 2004. Lightning, thermodynamic and hydrological Comparison of the two tropical continental chimneys. Journal of Atmospheric and Solar-Terrestrial Physics, 66(13 - 14), pp. 1213 - 1231.

Williams, E. R., 2005. Lightning and climate: A review. Atmospheric research, 76(1 - 4), pp.272 - 287.

Wilson, D.I., Agarwal, M. and Rippin, D. W. T., 1998. Experiences implementing the extended Kalman filter on an industrial batch reactor. Computers & chemical engineering, 22(11), pp. 1653 - 1672.

Xie, B., Fung, J.C., Chan, A. and Lau, A., 2012. Evaluation of nonlocal and local Planetary boundary layer schemes in the WRF model. Journal of Geophysical Research: Atmospheres, 117(D12).

Xu, G., Zhang, W., Feng, G., Liao, K. and Liu, Y., 2014. Effect of off-zenith Observations on reducing the impact of precipitation on ground-based Microwave radiometer measurement accuracy. Atmospheric Research, 140, pp. 85 - 94.

Yadava, P.K., Soni, M., Verma, S., Kumar, H., Sharma, A. and Payra, S., 2020. The Major lightning regions and associated casualties over India. Natural

Hazards, 101, pp. 217 - 229.

Zhao, J., Deng, F., Cai, Y. and Chen, J., 2019. Long short-term memory-Fully connected (LSTM-FC) neural network for PM2. 5 concentration prediction. Chemosphere, 220, pp.486 - 492.

Yu, L., Jin, X. and Weller, R.A., 2007. Annual, seasonal, and interannual variability of air–sea heat fluxes in the Indian Ocean. Journal of climate, 20(13), pp.3190 - 3209.

Zhou Y. and Liu J., 2016. Role of Water Vapor Content in the Effects of Aerosol on The Electrification of Thunderstorms: A Numerical Study. Atmosphere.

Zhou, K., Zheng, Y., Li, B., Dong, W. and Zhang, X., 2019. Forecasting different types of convective weather: A deep learning approach. Journal Of Meteorological Research, 33, pp.797 - 809.

Zhou, C., Fang, Z., Xu, X., Zhang, X., Ding, Y. and Jiang, X., 2020. Using long short-term memory networks to predict energy consumption of air-conditioning systems. Sustainable Cities and Society, 55, p.102000.

Zhou, X., Zhu, Y., Hou, D., Fu, B., Li, W., Guan, H., Sinsky, E., Kolczynski, W., Xue, X., Luo, Y. and Peng, J., 2022. The development of the NCEP global Ensemble forecast system version 12. Weather and Forecasting, 37(6), pp.1069 - 1084.

11. Source link

1. (www.theweatherprediction.com)

2. (http://en.wikipedia.org/wiki/Virtual_temperature)

3. (JEFF HABY “Potential temperature and equivalent potential temperature”, http://www.theweatherprediction.com/habyhints/162/)

4. NCUM-Writeup.pdf (Source - https://www.ncmrwf.gov.in)

5. (http://www.aprweather.com/forum/viewtopic.php?p=11)

6. (https://en.m.wikipedia.org/wiki/Turbulence)

7. (https://courses.lumenlearning.com/suny-osuniversityphysics/chapter/14-7-viscosity-and-turbulence/#:~:text=The%20pressure%20drop%20caused%20by,2%20%CF%81%20v%20r%20%CE%B7%20)

8.(https://www.weather.gov/source/zhu/ZHU_Training_Page/turbulence_stuff/turbulence/Wind_Shear.png)

9.(https://world-weather.info/forecast/india/kolkata/april-2023

10.weather.uwyo.edu

12. Abbreviations

ANN : Artificial Neural Network

AWS : Automatic Weather Station

BOYD : Boyden Index

BPI : Bordoichila Prediction Index

BRN : Bulk Richardson Number

CAPE : Convective Available Potential Energy

CBHT : Cloud Base Height

CIN : Convective Inhibition

CMIP5 : Coupled Model Intercomparison Project Phase 5

C-NON : Correct Non-occurrence

CSI : Critical Success Index

CTI : Cross Totals Index

DCI : Deep Convective Index

DPT : Dew Point Temperature

DPT 850: Dew Point Temperature at 850 hPa

DWR : Doppler Weather Radar

FAR : False Alarm Ratio

GPS : Global Positioning System

HI : Humidity Index

hPa : Hectopascal

HSS : Heidke Skill Scores

IMD : India Meteorological Department

KI : K Index

LCL : Lifting Condensation Level

LFC : Level of Free Convection

LI : Lifted Index

LIDAR : Light Detection and Ranging

MCT : Modified CTI

MEI : Modified Energy Index

MKI : Modified KI

MODIS : Moderate Resolution Spectral Radiometer

MPI : MODIS Profile Index

MR : Miss Rate

MSWI : Modified SWEAT

MTT: Modified TTI

MVT : Modified VTI

NCAPE : Normalised Convective Available Potential Energy

NSS : Normalised Skill Score

NTD : Non-Thunderstorm Day

POD : Probability of Detection

RADAR : Radio Detection and Ranging

RAMS : Regional Atmospheric Modelling System

RH700 : Relative Humidity at 700 hPa

RINO : Bulk Richardson Number

RSS : Rank Sum Score

STORM : Severe Thunderstorm Observations and Regional Modelling

SAARC-STORM:South Asian Association for Regional Cooperation- STORM

SHEAR : Vertical Wind Shear

SHOW: Showalter Index

SODAR : Sound Detection and Ranging

SWEAT: Severe Weather Threat Index

SWISS: Combined Stability and Wind Shear Index for Thunderstorms in Switzerland

TD : Thunderstorm Day

TPI : Composite Stability Index

TSS : True Skill Statistic

TTI : Total Totals Index

VTI : Vertical Total Index

WRF-ARW: Advanced Research Weather Research and Forecasting model

WRF- NMM :Weather Research and Forecasting-Non-hydrostatic Mesoscale Model

13. List of Publications based on this thesis

1. Sinha , T. B., Sarkar , R., Sen, G. K., and Mukhopadhyay, P., 2024. A study on thunderstorm prediction prior to the monsoon over Kolkata region, West Bengal (India). J. Ind. Geophys. Union, 28(3) (2024), 207 - 221.

2. Sinha , T. B., 2024. Predictability of local Thunderstorms and associated moisture and Precipitable water content prior to the monsoon over Kolkata region, West Bengal (India). IJARESM, Volume 12, Issue 5, May - 2024, page 1568 - 1581.

14. Corrigendum

Q. 1. What is the scope of the study of thunderstorms?

Ans. Scope of the Study

The scope of the study of thunderstorms, as various aspects including the **analysis** of **movement directions**, v**ertical wind shear effects**, **spatial and temporal characteristics**, and the **application of object methods** for characterizing thunderstorm properties.

Studies have focused on specific regions such as Gangetic Bengal, where thunderstorm were **predominantly** from the **northwest** but also included **rare cases** from the **southeast, south**, and **southwest**. Additionally, the role of **vertical wind shear** in the **longevity** and **strength** of thunderstorms was investigated, revealing that moderate to high vertical wind shear combined with **instability** is significant for t**hunderstorm persistence.**

The scope of thunderstorm studies is broad and interdisciplinary, ranging from movement and wind shear analysis to the application of **advanced tracking algorithms** and the examination of thunderstorms' contribution to atmospheric processes. The literature reflects a diverse array of methodologies and regional focuses, which collectively enhance the understanding of thunderstorm dynamics and characteristics.

This study focuses on the meteorological, geographical, and environmental aspects of thunderstorms. It includes the analysis of the causes, development stages, and types of thunderstorms, with an emphasis on their occurrence in [specific region or country, if any]. The study covers:

- The atmospheric conditions that lead to thunderstorm formation.
- Classification of thunderstorms (e.g., single-cell, multi-cell, supercell).
- Seasonal and geographical patterns in thunderstorm activity.
- Associated weather phenomena such as lightning, hail, strong winds, and heavy rainfall.
- Data from satellite imagery, weather radar, and ground-based observations over a defined time period.
- The effects of thunderstorms on human life, infrastructure, and the environment.

However, the study does **not** cover long-term climate change impacts on thunderstorms or global-scale modelling, unless directly relevant to the region of interest.

Q.2. What are the future scopes of the study of thunderstorms?

Ans. Future Scope of the Study

States Prone to Thunderstorms

- **East India**:
- **Bihar**: Moderate to severe thunderstorms with lightning are likely, especially during the next 24 hours.
- **Jharkhand:** Similar to Bihar, thunderstorms with lightning are expected.
- **West Bengal**: Gangetic West Bengal is prone to thunderstorms, especially during May.
- **Odisha**: Thunderstorms and strong winds are possible.

- Northeast India:

- **Assam**: Thunderstorms and heavy rainfall are expected, particularly during the monsoon season.
- **Meghalaya**: Similar to Assam, thunderstorms and heavy rainfall are likely.
- **Arunachal Pradesh**: Thunderstorms, lightning, and rain can occur, especially during the pre-monsoon season.
- **Nagaland:** Thunderstorms and strong winds are possible.
- **Manipur**: Thunderstorms and strong winds are likely.
- **Tripura**: Similar to Manipur, thunderstorms and strong winds are expected.

- **Central India:**
- - **Madhya Pradesh:** Thunderstorms and lightning are possible, especially during April and May.
- **Chhattisgarh:** Thunderstorms and strong winds are likely.

- South India:

- **Tamil Nadu:** Thunderstorms and heavy rainfall are expected, particularly during the pre-monsoon season.
- **Kerala:** Thunderstorms and lightning are possible.
- **Karnataka**: Thunderstorms and heavy rainfall are likely.

- **North India**:

- **Uttarakhand**: Thunderstorms, strong winds, and hailstorms are possible.

- **Himachal Pradesh**: Similar to Uttarakhand, thunderstorms, strong winds, and hailstorms are likely.

- **Punjab**: Thunderstorms and strong winds are possible.

- **Haryana**: Thunderstorms and strong winds are likely.

Time of Year-

Pre-monsoon season (April-May): Thunderstorms are common in many parts of India, especially in the eastern and north-eastern regions.

- **Monsoon season (June-September):** Thunderstorms and heavy rainfall are expected in various states, particularly in the western and central regions.
-

- **Post-monsoon season (October-November):** Thunderstorms can occur in some parts of India, especially in the southern region.

The **future scope** of a study highlights potential directions for further research, technological development, or applications based on the current findings. In the context of **thunderstorms**, here are several important **future scopes**:

Future Scope of the Study on Thunderstorms:

1. **Advanced Forecasting Technologies:**
   - Development and integration of machine learning and AI models to improve thunderstorm prediction accuracy.
   - Enhancement of real-time satellite and radar systems for earlier and more precise warnings.
2. **Climate Change Impact Analysis:**
   - Investigating how global warming and shifting climate patterns affect the frequency, intensity, and distribution of thunderstorms.
   - Long-term modelling of future thunderstorm trends under various climate scenarios.

3. **Urban Planning and Infrastructure Resilience:**
    - Studying the impact of thunderstorms on growing urban areas and proposing resilient infrastructure designs to withstand extreme weather events.
    - Integration of thunderstorm risk assessments into city planning and construction codes.
4. **Lightning and Electrical Activity Research:**
    - Exploring the physics and dynamics of lightning formation in greater detail.
    - Developing better lightning protection systems for buildings, aircraft, and power grids.
5. **Public Safety and Education Programs:**
    - Designing effective public education campaigns to increase awareness and preparedness.
    - Research on community response and risk perception to improve emergency communication strategies.
6. **Environmental and Ecological Effects:**
    - Studying the ecological impacts of frequent thunderstorms on forests, soil erosion, and biodiversity.
    - Examining the role of thunderstorms in atmospheric chemistry, especially their role in nitrogen fixation and ozone formation.

Q.3. What is the objective of the study of thunderstorms?

Ans. The objectives of the study of thunderstorms in Kolkata, as gleaned from the provided papers, are multifaceted and include understanding the **meteorological parameters** that differentiate between thunderstorms days and non-thunderstorm days, examining the role of generalized **potential temperature** in describing the **humid state of the atmosphere** and its impact on weather systems, and enhancing the predictability of severe thunderstorms using decision-making techniques.

These studies reveal interesting contradictions and facts, such as the prevalence of multicell thunderstorms over supercell thunderstorms in Kolkata, and the high

accuracy of nowcasting models for predicting thunderstorm categories. Moreover, the potential for thunderstorm predictability based on the history of thunderstorm and non-thunderstorm days and the identification of only a **few significant parameters** out of many for thunderstorm prediction highlight the complexity and challenges in forecasting such weather phenomena.

The collective aim of these studies is to improve the understanding and forecasting of thunderstorms in Kolkata by identifying key meteorological parameters, developing predictive models, and assessing the implications for urban development and climate change mitigation.

In the context of thunderstorms, the **objective of the study** generally refers to the main goal or purpose behind conducting the research. A well-defined objective helps guide the research questions, methodology, and analysis. Here's a sample version of a study objective on the topic of thunderstorms:

Objective of the Study:

The objective of this study is to investigate the formation, characteristics, and impacts of thunderstorms. Specifically, the study aims to:

- Understand the meteorological conditions that lead to thunderstorm development.
- Analyse the frequency, intensity, and seasonal patterns of thunderstorms in a specific region.
- Assess the potential hazards associated with thunderstorms, including lightning, hail, strong winds, and flash flooding.
- Evaluate current forecasting techniques and propose improvements for early warning systems to mitigate risks.

Q.4. Can you provide a five-year analysis of thunderstorm data?

Ans. <u>Thunderstorm data analysis (2020-2024)</u>

Table A: Indices' mean and standard deviation based on 0000 UTC data from Kolkata stations (2020 – 2024)

Index	Thundery day (Mean)	Thundery day Standard deviation	Non-Thundery day(Mean)	Non-Thundery day Standard deviation
K	30.73	6.198	27.96	7.48
TT	46.38	4.744	45.49	4.896
SLI	-4.42	3.454	-3.22	3.498
DCI	31.78	5.92	29.2	6.832
HI	38.7	18.104	44.91	17.266
BI	-158.39	25.65	-171.7	12.94
SWEAT	222.68	97.93	197.5	70.39
CAPE	1733.9	1127.43	1791.82	1072.65
CIN	-218.74	168.45	-233.65	171.6
BRN	143.62	193.17	270.36	393.83
SI	0.32	2.98	0.81	2.84

For the year 2020, the total number of 8 days with thunder and 9 days without thunder is taken into account. For the year 2021, the total number of 9 days with thunder and 11 days without thunder is taken into account. For the year 2022, the total number of 11 days with thunder and 14 days without thunder is taken into account. For the year 2023, the total number of 14 days with thunder and 10 days without thunder is taken into account. For the year 2024, the total number of 10 days with thunder and 11 days without thunder is taken into account. For the year **2020 - 2024**, the total number of **52** days with thunder and **55** days without thunder is taken into account.

Table B: Indices' mean and standard deviation based on 1200 UTC data from Kolkata stations (2022 – 2024)

Index	Thundery day (Mean)	Thundery day Standard deviation	Non-Thundery day(Mean)	Non-Thundery day Standard deviation
K	28.34	8.34	29.11	7.58
TT	46.58	5.4	53.25	28.77
SLI	-3.98	4.73	-4.07	4.48
DCI	33.52	8.36	35.36	9.59
HI	44.09	22.77	52.59	23.84
BI	-102.14	18.19	-104.07	17.57
SWEAT	205.86	104.52	232.01	174.15
CAPE	2174.53	1394.1	2302.51	1563.69
CIN	-62.56	87.4	-903.13	2404.77
BRN	88.34	62.02	98.62	112.44
SI	-0.069	3.97	-0.77	5.38

For the year 2022, the total number of 10 days with thunder and 14 days without thunder is taken into account. For the year 2023, the total number of 14 days with thunder and 10 days without thunder is taken into account. For the year 2024, the total number of 10 days with thunder and 11 days without thunder is taken into account. For the year **2022-2024**, the total number of **34** days with thunder and **35** days without thunder is taken into account. We were unable to access or download 1200 UTC data for 2020 and 2021, limiting our analysis to **2022 to 2024**.

Q.5. What are the best skill indices for evaluating thunderstorms Prediction / forecasting (on five years data)?

Ans.

Table C: Test statistics (Z_{xy}) for eleven indices at the Kolkata station at 0000 UTC (2020 – 2024)

Index	Values of Z_{xy}	Significance level (%)
K	1.577418	94
TT	1.004578	85
SLI	-2.60261	99
DCI	1.66496	95.5
HI	-0.51856	70
BI	0.821459	79.5
SWEAT	0.089325	47
CAPE	-0.00125	50
CIN	0.013519	50
BRN	-0.03554	51.5
SI	-1.51116	93.5

To select those indices that will pass the significance test, Z statistics (Z_{xy}) is calculated for all the eleven indices as shown in Table B. So far as statistical significance (Table B) **DCI, SLI, SI and KI** appeared to have the highest Z_{xy} value and thus signifies that these four indices are having the best potential to differentiate the thundery and nonthundery days. The rest of the seven indices do not have the desired level of significance to be designed as predictors of thundery and nonthundery days and hence denied. In order to quantify the accuracy of forecasts different skill scores are calculated for the four indices namely **DCI, SLI, SI and KI** which have shown at least a **93.5%** significant level or more.

SLI value has **99%** significant level. **DCI 95.5%** significant level. While **KI** value, **94%** significant level. **SI** value has **93.5%** significant level. For best possible forecast, we have considered above mention indices. We have considered best threshold value for

calculating skill score of thundery and non-thundery days with the help of iteration process for perfect result.

SLI value has 99% significant level, DCI 95.5% significant level, KI 94% significant level. SI value has 93.5% significant level.

For best possible forecast, we have considered above mention indices. We have considered best threshold value for calculating skill score of thundery and non-thundery days with the help of iteration process for perfect result.

Table D: Test statistics (Z_{xy}) for eleven indices at the Kolkata station at 1200 UTC (2022 – 2024)

Index	**Values of Z_{xy}**	**Significance level (%)**
K	-0.20882	58
TT	-0.42729	67
SLI	0.113184	54.5
DCI	-0.61004	73
HI	-0.41863	66.5
BI	0.161158	56.5
SWEAT	-0.03434	51.5
CAPE	-0.00156	50
CIN	0.007983	50
BRN	-0.03383	51.5
SI	0.845234	80

To select those indices that will pass the significance test, Z statistics (Z_{xy}) is calculated for all the eleven indices as shown in Table E. So far as statistical significance (Table E) DCI and SI appeared to have the highest Z_{xy} value and thus signifies that these four indices are having the best potential to differentiate the thundery and nonthundery days. The rest of the seven indices do not have the desired level of significance to be designed as predictors of thundery and nonthundery days and hence denied. In order to quantify the accuracy of forecasts different skill scores are calculated for the four

indices namely **DCI and SI** which have shown at least a **73%** significant level or more.

SI value has **80%** significant level. **DCI 73%** significant level. For best possible forecast, we have considered above mention indices. We have considered best threshold value for calculating skill score of thundery and non-thundery days with the help of iteration process for perfect result.

For best possible forecast, we have considered above mention indices. We have considered best threshold value for calculating skill score of thundery and non-thundery days with the help of iteration process for perfect result.

Q.6. Can you explain the values of POD, FAR, CSI, TSS and HSS in the context of thunderstorm prediction/forecasting (on five years data)?

Table E : Skill ratings and specified threshold values of chosen metrics for the Kolkata station at 0000 UTC (2020 – 2024)

Indices	**POD**	**FAR**	**CSI**	**TSS**	**HSS**
SLI ≤ -0.2 **A=46, B=6** **C=49, D=6**	0.8846	0.516	0.455	-.0063	-0.0062
DCI ≥ 24 **A=45, B=7** **C =48, D=7**	0.8654	0.516	0.45	-0.0073	-0.0072
KI ≥ 24 **A = 46, B = 6** **C = 46, D = 9**	0.8846	0.5	0.4694	0.0482	0.0473
SI ≤ 2 **A=34, B=18** **C=36, D=19**	0.6538	0.5143	0.3864	- 0.0007	- 0.00069

Table E gives the recommended threshold and corresponding skill scores for these identified indices. The best skill is obtained from DCI and SLI with threshold values 24^0 C and -0.2 respectively. This means that thundery (nonthundery) days will be forecast when DCI is greater (less) than 24^0 C and for KI the forecast will be thundery (nonthundery) when its value will be greater (less) than 24. From the skill score point of view, POD score of 0.8846 for DCI and KI is highest.

Table F: Kolkata station at 0000 UTC (2020 – 2024)

Total number of thundery days (TD) observed - 48.6%
Total number of non-thunderstorm days observed - 51.4%

Index	**Observation**	**Prediction TD (%)**	**Prediction NTD (%)**
SLI ≤ -0.2 POD=0.8846, FAR=0.516, CSI=0.455, TSS= -.0063, HSS = -0.0062	TD (%) NTD (%)	**42.9** **45.8**	**5.7** **5.6**
DCI ≥ 24 POD=0.8654, FAR=0.516, CSI=0.45, TSS= - .0073, HSS = -0.0072	TD (%) NTD (%)	**42.1** **44.9**	**6.5** **6.5**
KI ≥ 24 POD=0.8846, FAR=0.5, CSI=0.4694, TSS= 0.0482, HSS = 0.0473	TD (%) NTD (%)	**42.9** **43**	**5.7** **8.4**
SI ≤ 2 POD=0.6538, FAR=0.5143, CSI=0.3864, TSS= - 0.0007, HSS = - 0.00069	TD (%) NTD (%)	**31.8** **33.6**	**16.8** **17.8**

Table G: Skill ratings and specified threshold values of chosen metrics for the Kolkata station at 1200 UTC (2022 – 2024)

Indices	**POD**	**FAR**	**CSI**	**TSS**	**HSS**
SI ≤ 2 **A=24, B=10** **C=22, D=13**	0.706	0.478	0.393	0.077	0.077
DCI ≥ 25 **A=27, B=7** **C =30, D=5**	0.794	0.526	0.422	-0.0631	-0.056

Table H : Kolkata station at 1200 UTC (2022 – 2024)

Total number of thundery days (TD) observed - 49.3%
Total number of non-thunderstorm days observed - 50.7%

Index	Observation	Prediction TD (%)	Prediction NTD (%)
SI ≤ 2 POD=0.706, FAR=0.478, CSI=0.393, TSS= 0.077, HSS = 0.077	TD (%) NTD (%)	**34..8** **31.9**	**14.5** **18.8**
DCI ≥ 25 POD=0.794, FAR=0.526, CSI=0.422, TSS= - .0631 HSS = -0.056	TD (%) NTD (%)	**39.15** **43.5**	**10.15** **7.2**

Table G gives the recommended threshold and corresponding skill scores for these identified indices. The best skill is obtained from **DCI and SI** with threshold values 25^0 C and 2 respectively. This means that thundery (nonthundery) days will be forecast when DCI is greater (less) than 25^0 C and for SI the forecast will be thundery (nonthundery) when its value will be less (greater) than 2. From the skill score point of view, POD score of 0.794 for DCI is highest.